# GELS AND ELECTROSPUN FIBERS FOR BIO-MEDICAL APPLICATIONS

A THESIS SUBMITTED TO

SAVITRIBAI PHULE PUNE UNIVERSITY

FOR AWARD OF DEGREE OF

**DOCTOR OF PHILOSOPHY (Ph.D)**

IN

**CHEMICAL ENGINEERING**

SUBMITTED BY

**ASHWINI WALI**

UNDER THE GUIDANCE OF

**Dr. SATISH R. INAMDAR**          **Dr. MANOHAR V. BADIGER**
(*Research Guide*)          (*Research Co-Guide*)
VIT, PUNE          CSIR-NCL, PUNE

RESEARCH CENTRE

**DEPARTMENT OF CHEMICAL ENGINEERING**

VISHWAKARMA INSTITUTE OF TECHNOLOGY

BIBWEWADI, PUNE - 411037

**NOVEMBER 2020**

## Certificate by Research Center

I, **Dr. R. M. Jalnekar**, Director of Vishwakarma Institute of Technology, Pune, which is Research Center under the subject Chemical Engineering hereby declare that **Ms. Ashwini Wali** is a registered Ph.D. student of the centre and has worked under **Dr. Satish R. Inamdar**. I declare that **Ms. Ashwini Wali** has me t all the norms and requirements of thesis submission as per provision of Ph.D. Rules vide University Circular No.217/2014 dated 28/11/2014 and Circular No. 14/2017 dated 09/01/2017

Date: 25-11-20

Director

Director
Vishwakarma Institute
of Technology
Pune-411 037.

## Certificate of Research Supervisor (Guide)

Certified that the work incorporated in the dissertation /thesis **"Gels and Electrospun Fibers for Biomedical Applications"** submitted by **Ms. Ashwini Wali** , was carried out by the candidate under my supervision / guidance. Such material has been obtained from other sources has been duly acknowledged in the dissertation /thesis.

Date: 25/11/2020

Place: Pune

**Dr. Satish R. Inamdar**

Research Supervisor (Guide)

## Certificate of Research Supervisor (Co-Guide)

Certified that the work incorporated in the dissertation /thesis **"Gels and Electrospun Fibers for Biomedical Applications"** submitted by **Ms. Ashwini Wali** , was carried out by the candidate under my supervision / guidance. Such material has been obtained from other sources has been duly acknowledged in the dissertation /thesis.

Date: 26|11|2020

**Dr. Manohar V. Badiger**

Research Supervisor (Co-Guide)

Place: Pune

# Declaration by the Student

I declare that the thesis entitled **"Gels and Electrospun Fibers for Biomedical Applications"** submitted by me for the degree of Doctor of Philosophy in Chemical Engineering, is the record of work carried out by me during the period from 2016 to 2020, under the guidance of **Dr Satish R. Inamdar (Research Guide), VIT Pune,** and **Dr Manohar V. Badiger (Research Co-Guide), CSIR-NCL Pune,** and has not formed the basis for the award of any degree, diploma, associateship, fellowship, titles in this or any other University or other institution of Higher learning.

I further declare that the material obtained from other sources has been duly acknowledged in the thesis.

Date: 26 - 11 - 2020

Place: Pune

**Ms. Ashwini Wali**

(Signature of the Student)

# Dedicated To……


# "MY MOTHER"

## Mrs JAYASHREE C WALI

# ACKNOWLEDGEMENT

*accomplished. Thanks to my sister- in- law **Mrs Bhuvaneshwari Wali,** who tirelessly helped me to pack my luggage and other stuff, every time I returned to Pune from home.*

*Thanks to my two little stars, **Shrinkila and Viraj** who eagerly wait for me to return from Pune.*

*I heartily thank my husband **Santosh Kumar Kaddi,** my in- laws and my lovely little boy, my son **Vrishank** who sacrificed his childhood by patiently waiting for me all these years to complete my PhD.*

*I would fail in my duties if I don't thank SERB (Science and Engineering Research Board, Delhi) for giving me the travel grant to attend International Conference at AGH University of Science and Technology, Poland in 2018.*

*Special thanks to my **Activa Scooter**, first ever self owned bike which tremendously supported all throughout my journey without ever giving slightest of troubles.*

*I wish to mention my sincere thanks to **Dr Ravindra Gudi**, Professor at IIT Bombay, for the remarkable statement, he made once. It was, "Your PhD is complete in real sense only when you are able to give one to your student".*

*I will always remember his kind words and continue to work further by contributing to science in the best of my ability.*

*Last but not the least with all due respects, I thank the "**ALMIGHTY**" for without the blessings of the Omnipotent, even the best of science can fail sometimes.*

*HE gave me all the necessary strength and courage to move on, inspite of the difficulties and struggles, encountered in this journey by never losing my self-confidence. I am also greatly indebted to HIM for keeping all my family members healthy and safe during this period to help me achieve my biggest dream of life. **"My PhD"***

*Awali*

**ASHWINI WALI**

# Abstract

## GELS AND ELECTROSPUN FIBERS FOR BIOMEDICAL APPLICATIONS

The objective of the thesis was to design and develop newer novel biomaterials in the form of gels and electrospun fibers from polysaccharides which are biocompatible and biodegradable in nature. The polysaccharides (e.g., celluloses and proteins) which form the basic building blocks of life, are gaining increased interest in recent times for researchers to develop newer health care products from renewable bio-polymers which are cheaper and easily available with different desirable properties. Gels are highly swollen three dimensional networks of hydrophilic polymers cross-linked by physical or chemical interactions. The unique property of using the bio-polymeric gels and fibers is their high swelling ability, they mimic the extra cellular matrix (ECM) and also closely resemble the living tissues in our body which are most suited for human health applications. Smart polymeric gels and electrospun fibers constitute a new generation of biomaterials that are now being developed at a prolific pace for their use as biosensors, actuators, templates in biomedical devices, drug delivery, wound healing, scaffolds and implants for tissue regeneration, pharmaceutical and cosmetic industry. However, the major drawback of using the bio-polymers used for biomedical applications is the lack good mechanical properties and since they are biodegradable in nature, it is important to control the rate of degradation for certain specific applications which requires long time applications.

In this context, our focus was to design and develop a novel microgel system which would effectively deliver the anti-cancer drug to the targeted site by slow and sustained release for longer times. The water soluble Hydrophobically modified Ethyl Hydroxy Ethyl Cellulose (HM-EHEC) biopolymer was used in the synthesis of microgels by Michael-type addition reaction between the primary hydroxyl groups of HM-EHEC and Divinyl sulphone (DVS) crosslinker using water-in-oil emulsion technique. The microgels obtained were spherical in shape having flower type morphology

with average size of 5 to 8 µm. The anti-cancer drug 5-Flurouracil (5-FU) drug was successfully incorporated and around 56% of the 5-FU was released in 72 hours with a loading efficiency of 95%. The cell viability (MTT assay) studies confirmed the cycto-toxicity on the MDA-MB 231 breast cancer cell line. There was increase in the cell death with increase in the concentration of microgel containing drug concentration. The HM-EHEC microgels could be effectively used in the form of a topical cream in the skin and breast cancer for on-site slow and targeted delivery.

Next, we designed and fabricated novel electrospun nanofiber mats using the Ethyl Hydroxy Ethyl Cellulose (EHEC) and hydrophobically modified Ethyl Hydroxy Ethyl Cellulose (HM-EHEC) bio-polymers. We report for the first time electrospinning of these polymers for biomedical applications. These speciality polymers are used as rheology modifiers in paint industry and for oil recovery applications. The morphology of spin-coated films and electrospun fibers of ethyl hydroxy ethyl cellulose (EHEC), hydrophobically modified ethyl hydroxy ethyl cellulose (HM-EHEC) and their blends with Poly (vinyl alcohol) (PVA) were examined by Atomic Force Microscopy (AFM), SEM and contact angle measurements. These polysaccharides upon blending with PVA exhibited smooth surface which was evidenced by AFM observation. The oriented fibers could be obtained using a rotating disc collector. Contact angles of spin-coated films and electrospun fibers were discussed in terms of hydrophobicity and wetting characteristics. Further, the nanofibers of EHEC/PVA were in-situ crosslinked using natural and non-toxic citric acid and were used for controlled release of Chlorhexidine Digluconate (ChD), an antibacterial drug. In-vitro studies of cyto-toxicity, cell growth and cell proliferation were performed using L929 mouse fibroblast cells. These nanofiber mats show potential in drug delivery and as scaffolds in tissue engineering applications.

In continuation of the above work, we further studied the EHEC/PVA electrospun mats by incorporating nano-materials namely Halloysite nanoclay (HNT) and Silver nanoparticles (AgNPs), to understand their morphology, effect on the mechanical properties, *in-vitro* and *in-vivo* characteristics and release behaviour of an antibacterial drug for drug delivery and as scaffolds

for tissue regeneration. The Halloysite (HNT) loaded EHEC/PVA nanofiber mats exhibited very good mechanical properties and proved a potential in wound healing activity by slow and sustained release of the Gentamicin (GS) drug. The mechanical properties also increased with the addition of silver nanoparticles. The AgNPs embedded EHEC/PVA nanofiber mats having lower concentration of $AgNO_3$ (0.5% AgNPs) were found to enhance the wound healing with no scar formation in the wistar rat studies. The biological *in-vitro* and *in-vivo* studies in both the cases (nanoclay and nanoparticles) supported the study for making the EHEC based nanofibers an excellent healing biomaterial in case of severe burns and wounds.

The bio-polymer based electrospun fibers have tremendous applications in bio-separations. In order to explore further, for the separation of impurities from blood like uremic toxins and smaller sized molecules, we designed a novel filter media from gelatin which is a cost effective and biodegradable resource. The gelatin fibers obtained from electrospinning process were incorporated with the Halloysite nanoclay (HNT) and crosslinked with glutaraldehyde for improvement in the mechanical properties. The morphology was studied by SEM and fiber diameter ranged from 1 to 3 µm. The porosity and pore size distribution, pressure drop were studied using the 3D-Microtomography experiments. The *in-vitro* MTT assay for cell viability of the L929 fibroblast cells showed no toxicity and the same was confirmed by the haemolysis study which showed that the gelatin filter media could be used as filtration/purification system. This filter media could possibly find a replacement for synthetic membranes which are used in the dialysis treatment for patients with kidney failures and disorders.

Thus, in this thesis we report for the first time the use of bio-polymers namely EHEC and HM-EHEC polysaccharides for the design and development of novel polymeric gels and electrospun fibers which have a great potential in biomedical applications like drug delivery, scaffolds in tissue regeneration for wound healing and in blood purification applications.

| Table of Contents | | | Page No |
|---|---|---|---|
| ∗ | Abstract | | i |
| ∗ | List of Tables | | ix |
| ∗ | List of Figures | | x |
| ∗ | Abbreviations and Symbols | | xv |
| **Chapter I : Introduction and Literature Survey** | | | |
| **1.1** | **Biomaterials** | | 1 |
| **1.2** | **Classification of Biomaterials** | | 2 |
| | 1.2.1 | Metallic | 2 |
| | 1.2.2 | Ceramic | 2 |
| | 1.2.3 | Polymeric | 2 |
| | 1.2.4 | Composites | 3 |
| | 1.2.5 | Natural | 3 |
| **1.3** | **Biomaterials in Health Care** | | 3 |
| **1.4** | **Gels** | | 5 |
| | 1.4.1 | Gel Properties | 6 |
| | 1.4.2 | Gels/Hydrogels from Natural and Synthetic Polymers | 7 |
| **1.5** | **Microgels** | | 8 |
| | 1.5.1 | Microgel Synthesis | 9 |
| | 1.5.2 | Microgel Applications | 10 |
| **1.6** | **Nanofibers** | | 11 |
| | 1.6.1 | Fabrication Techniques for Nanofiber Production | 12 |
| | | 1.6.1.1 Electrospinning Technique | 12 |
| | 1.6.2 | Nanofiber Applications | 14 |
| **1.7** | **Special Characterization Techniques Used in Thesis** | | 15 |
| | 1.7.1 | Atomic Force Microscopy (AFM)) | 15 |
| | 1.7.2 | Micro Computed Tomography (µ-CT) | 16 |
| **1.8** | **Summary** | | 17 |
| **1.9** | **References** | | 17 |
| **Chapter II : Scope and Objectives** | | | |
| **2.1** | **Microgels and Nanofibers from Natural Polysaccharides** | | 25 |
| **2.2** | **Rationale and Significance of the study** | | 26 |
| **2.3** | **Objectives of the Thesis** | | 26 |
| **2.4** | **References** | | 27 |
| **Chapter III : Synthesis and Characterization of Hydrophobically Modified Ethyl Hydroxy Ethyl Cellulose (HM-EHEC) Microgels for Drug Delivery Applications** | | | |
| **3.1** | **Introduction** | | 28 |
| **3.2** | **Materials and Methods** | | 29 |
| **3.3** | **Experimental Section** | | 30 |
| **3.4** | **Characterization Techniques** | | 32 |
| | 3.4.1 | Scanning Electron Microscopy (SEM) | 32 |
| | 3.4.2 | Fourier Transform Infra red Spectroscopy (FTIR) | 33 |
| **3.5** | **Biological Studies** | | 33 |
| | 3.5.1 | *In-vitro* 5-FU drug release | 33 |

# LIST OF TABLES

# LIST OF FIGURES

# ABBREVIATIONS AND SYMBOLS

| | |
|---|---|
| Å | Angstrom |
| AR | Analytical Reagent |
| AgNPs | Silver nanoparticles |
| AGU | Anhydroglucose Units |
| AFM | Atomic Force Microscopy |
| API | Active Pharmaceutical Ingredients |
| ATR | Attenuated Total Reflectance |
| BSA | Bovine Serum Albumin |
| CA | Contact Angle |
| ChD | Chlorhexidine Digluconate |
| $CO_2$ | Carbon dioxide |
| DAPI | 4,'6 diamidino-2-phenylidole |
| DLS | Dynamic Light Scattering |
| DMA | Dynamic Mechanical Analyser |
| DMEM | Dulbecco's Modified Eagle Medium |
| DVS | Divinyl Sulphone |
| *E.coli* | *Escherichia coli* |
| ECM | Extra Cellular Matrix |
| EHEC | Ethyl Hydroxy Ehyl Cellulose |
| ES | Electrospinning |
| FBS | Fetal Bovine Serum |
| FTIR | Fourier Transform Infra Red |
| GFM | Gelatin filter media |
| GS | Gentamicin |
| HM-EHEC | Hydrophobically Modified Ethyl Hydroxy Ethyl Cellulose |
| HNT | Halloysite nanotubes/nanoclay |
| $H_2O$ | Water |
| KBr | Potassium Bromide |
| M | Molar |
| MW | Molecular Weight |
| MWCO | Molecular Weight Cut off |
| Micro-CT | Micro-Computed Tomography |
| PBS | Phosphate Bovine Serum |
| MTT | 3-(4,5-Dimethylthiazol-2-yl)-2,5-Diphenyltetrazolium Bromide |
| NPs | Nanoparticles |
| NIPAM | N-Isopropylacrylamide |
| PCL | Polycaprolactone |
| PVA | Poly Vinyl Alcohol |
| Pvt Ltd | Private Limited |
| *S. auereus* | Staphylococcus aureus |
| SEM | Scanning Electron Microscopy |
| STP | Standard Temperature Pressure |
| TEM | Transmission Electron Microscopy |

| TFE | Trifluroethanol |
|---|---|
| THF | Tetrahydrofuran |
| TGA | Thermogravimetric Analysis |
| 5-FU | 5-flurouracil |
| UV-Vis | UV-Visible |
| XRD | X-Ray Diffraction |
| fig | Figure |
| rpm | revolutions per minute |
| nm | nanometer |
| cm | centimeter |
| μm | micrometer |
| μL | microlitre |
| ml | millilitre |
| ml/min | millilitre per minute |
| h | hour |
| kV | kiloVolt |
| ºC | degree Centigrade |
| μM | microMolar |
| g/mol | gram per mole |
| g/ml | gram per millilitre |
| Nm | Newton metre |
| N/m | Newton per metre |
| mN/m | milli Newton per metre |
| Hz | Hertz |
| KHz | KiloHertz |
| Pa | Pascal |
| MPa | Mega Pascal |
| s | second |
| $s^{-1}$ | per second |
| & | and |
| min | minutes |
| % | percent |
| mA | milliampere |
| □ | theta |
| $\lambda_{max}$ | lambda maximum |
| K | Kelvin |
| w/w | weight by weight |

# CHAPTER I

---

## Introduction and Literature Survey

---

*The first step to knowledge is to know that we are ignorant.*

*Socrates*

## 1.1 Biomaterials

The area of Biomaterials is an exciting field of science that has been significantly and steadily developed over the last fifty years and encompasses aspects of medicine, biology, chemistry and materials science. In 600 BC, Indian surgeon *"Susruta"* in his book has written on repairing the torn ear lobes from the cheek skin and reconstruction of the nose using the forehead skin[1] as shown in **fig 1.1(a)**. Egyptians in much earlier times knew about the linen sutures. The artificial teeth, ear, nose, eyes were found on the bodies of the mummies in the Egyptian civilization.[2] In olden days, apart from glue, wax materials like gold, zinc, and glass were also used as biomaterials.[3] Over the last fifty years there has been considerable understanding in the interactions between tissues and materials with tremendous improvements in the use of surgical materials, implants and devices in biomedical applications primarily in the field of tissue engineering scaffolds, drug delivery and regenerative medicine.



**Figure 1.1(a):** Susruta performing surgery on the patient's ear.**(600 BC)**
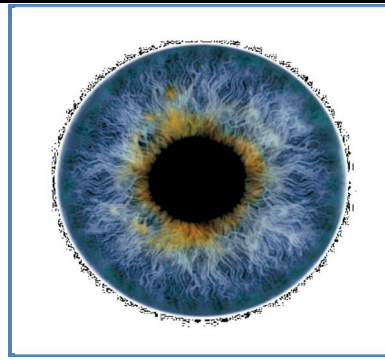
**Figure 1.1(b):** "Holoclar" contact lens made from patient's stem cells.**(2015)**

*Adapted with permission from Springer Nature; Regrowing the body; Willyard, C. Timeline; 2016. © Macmillan Publishers Limited.[1]*

*"Holoclar"* is a recent development by researchers shown in **fig 1.1(b)** where the contact lens is made up of limbal stem cells, which helps in restoring the eyesight by repairing the cornea after an injury.

**"Biomaterial"** is therefore, defined as a material which intends to interface with the biological system in order to evaluate, treat, and replace any tissue/organ or functions of the body.[4] They are widely used to improve the

quality of patient's life in the form of dental implants, heart valves, vascular grafts, intraocular lenses, pacemakers and biosensors.

The biomaterials market is projected to reach USD 206.64 billion by 2024 and expected to increase tremendously in the future. The Journal of Bone and Joint Surgery, has reported that the demand for knee arthroplasties is estimated to grow and reach 3.48 million by 2030. The demand for total hip arthroplasties is anticipated to rise upto 5,72000 people by the year 2030.[5] The future of biomaterials is expected to enhance greatly through the development of newer and advanced functional materials in the medical and other fields of applications.[6]

## 1.2 Classification of Biomaterials

Biomaterials available today are developed either singly or in combination of the materials. The materials have different atomic arrangement which present the diversified structural, physical, chemical, and mechanical properties for various applications in the body. They are bio-inert, bio-stable, bio-active and bio-degradable in nature and basically classified as metallic, ceramic, natural, polymeric, and composite materials.[7]

**1.2.1** **Metallic**: Metals are the most widely for load-bearing implants as screws and fracture plates. Stainless steel, titanium and its alloys, cobalt alloys along with nickel, chromium, iron, molybdenum, and tungsten are also used in maxillofacial surgery, cardiovascular surgery, and for dental applications.[8]

**1.2.2** **Ceramic:** They are generally hard, and biodegradable. Alumina, zirconium, silicone nitrides and carbon are inert bio ceramics. Certain glass ceramics, hydroxyapatites are semi-inert and calcium phosphates and calcium aluminates are resorbable ceramics.[8]

**1.2.3** **Polymeric:** The polymeric biomaterials are very advantageous over the metal or ceramic materials because they possess desired physical and mechanical properties and are easily available at low cost. The polymers poly methyl methacrylate (PMMA), polyethylene, polyester, polyvinyl chloride, silicone rubber, nylon, poly lactic acid, poly glycolic acid, and poly (lactide-co-glycolide) are frequently used. [8]

**1.2.4 Composites:** Some applications of composites in biomaterial applications are in dental filling composites, orthopaedic implants with porous surfaces. Flexible composite bone plates are effective in promoting healing. The carbon reinforced polymer composites are of great interest for bone repair and joint replacement because of their low elastic modulus properties.[8]

**1.2.5 Natural:** Biomaterials made from natural polymers are often advantageous as they do not elicit any toxic or chronic reactions in the body and are capable of regenerating new tissues. They include collagen, chitosan, alginate, hyaluronic acid, gelatin, fibrin, silk and cellulose.[8]

## 1.3 Biomaterials in Health care

The medical implants including heart valves, stents, grafts, artificial joints, hearing loss implants, dental implants, hip implants are biomaterials used to repair the damaged parts of the human body. One of the most outstanding and remarkable application of biomaterials in recent times is deep brain stimulation to treat Parkinson disease where a thin electrode is inserted in the brain and the other end is connected to the stimulator causing uncontrolled tremor, rigidity, slowness which gradually disappear thereby improving the patients health.[9] The joint replacement orthopaedic surgery is generally conducted to relieve arthritis pain and hip fractures.
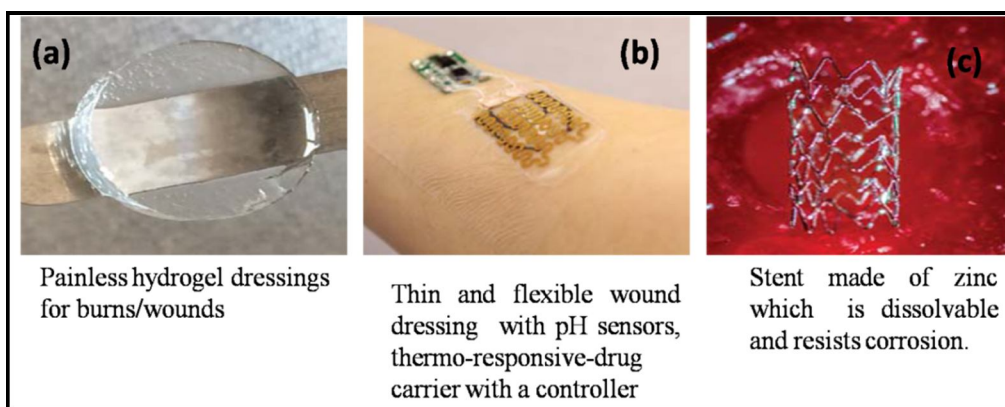


**Figure 1.2:** Biomaterials in human health.

*Adapted from National Institute of Biological Imaging and Bioengineering, US Department of Health and Human Services, National Institutes of Health.*[11]

**Figure 1.3:** Biomaterial based non-woven nanofiber face masks.
*Adapted from website of Azonano,* Image *credit: Inovenso.*[13]

Researchers are working on to regenerate the ailing heart with a tissue patch which is pre-seeded with bone marrow cells or mesenchyme stem cells.[10] The painless and responsive hydrogels are being studied as wound dressing materials and also for on demand drug delivery technologies which will enable the patient's having chronic diseases to control the dosage and frequency of drug as shown in **fig 1.2 (a) and (b).** The bio-absorbable zinc stent developed by researchers as seen in **fig 1.2 (c)**, eventually erodes away by itself with time without causing any chronic risk or damage to the patient's health.[11] Polymeric micro and nano fibers have gained much popularity as potential substrates for the immobilization of bio molecules which can have tremendous applications in cancer diagnostics, theronostics, in air and water filtration and also as membranes in bio-separations. The porous fibrous membranes of micro/nano size, work as an artificial kidney dialyzer are developed for the rapid dialysis.[12] The nanofiber polymeric face masks are in great demand these days due to the dreadful covid-19 pandemic. These nanofiber masks are flexible and comfortable to use, which helps to inhibit the virus/bacteria owing to their high filtering efficiencies[13] as shown in the **fig 1.3**. Recyclable disposable face masks offer protection against the deadly corona virus to a great extent. Nanofiber masks along with antibacterial coatings are also efficient in filtering air pollutants and particulate matter of 0.3μm thereby protecting against invisible bacteria, viruses, volatile chemicals, dust and exhaust fumes.

## 1.4 Gels

Pierre-Gilles de Gennes in the year 1991 named gels under the broad category of *"soft matter"*.[14] Polymeric gels are three-dimensional networks which are swollen by a large amount of solvent. Peppas defined Hydrogels as "hydrophilic, three-dimensional networks, which are able to imbibe large amounts of water or biological fluids and resembles a biological tissue."[15] The first polymeric biomaterial developed in 1960 was in the form of a hydrogel using Poly hydroxy ethyl methacrylate (PHEMA) as contact lenses for human use.[16, 17] Gels are basically classified as chemical gels and physical gels, depending on their nature of crosslinking as shown in **fig 1.4**. In the case of chemical gels, a three-dimensional network is formed by crosslinking through covalent bonds. The physical gels are physically connected in form of aggregates and depending on the nature of the interactions, the junctions may be hydrogen bonds, crystalline regions, ionic clusters, or phase-separated microdomains.[18, 19]
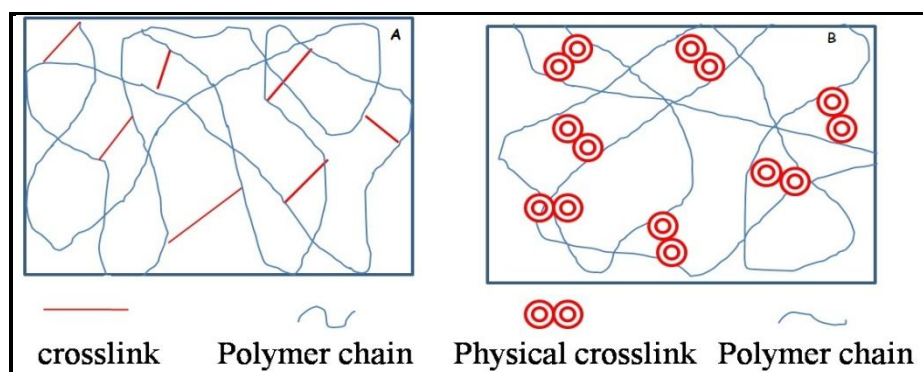


**Figure 1.4:** (A) Chemical gels generated by chemical crosslinking (B) Physical gels via non-covalent interactions in polymer chains.

Gels are also categorized depending on their size as macrogels, microgels, or nanogels. The microgel particles are in the size range range of 100 nm to 1 µm. The gels are referred to as nanogels, when their overall sizes are below 100 nm. The unique properties of functional microgels/nanogels are mainly related to their dynamic, permeable, network like architecture, their capability to swell in different solvents, and their deformability. These gels combine typical characteristics of macromolecules, colloids, and surfactants.[20] Like macromolecules, they are soft and respond extremely fast to changes in solvent quality by changes in their local conformation[21, 22] like colloids, they

can crystallize at high volume fractions[23-25] and as surfactants; they adsorb to interfaces and reduce the interfacial tension.[26, 27]

### 1.4.1 Gel Properties

In the design of any gel system, it is important to know the molecular structure of the gel and how the interactions between the gel phase and the surrounding liquid phase occur. The most desirable properties of the gel for biomaterial applications are given below:

### 1.4.1.1 Biodegradability

Biodegradable materials are most frequently desirable in case of implants into the human body. After the purpose is served, the gels must be capable of breaking down into catabolites and should be excreted from the body. The rate of degradation should be comparable to the rate of tissue regeneration.[28]

### 1.4.1.2 Biocompatibility

Hydrogels are biocompatible in nature and due to their high water content, they mimic the extra cellular matrix (ECM) of the body and therefore, demonstrate high tissue compatibility.[29, 30]

### 1.4.1.3 Mechanical strength and stability

Gels are soft and fragile materials and are prone to erosion. If the rate of erosion is too fast then the hydrogel may disappear, before it has successfully accomplished its desired therapeutic effect. The mechanical strength of the gel can be tuned depending on the application by varying the chemical structure of the gel. It is possible to obtain a gel with higher stiffness increasing the crosslinking degree. [31, 32]

### 1.4.1.4 Porosity/ porous structure

Porosity is a morphological feature of a material that can be simply described as the presence of void cavity inside the bulk. Pores may be formed in gels by phase separation during synthesis, or they may exist as smaller pores within the network. The interconnected porous structure within the polymeric hydrogel improves their performance. The accurate design of pore structure in

hydrogels, in terms of the porosity and pore size distribution, is strongly required for tissue engineering applications, to allow for the three-dimensional cell and tissue infiltration.[33]

### 1.4.1.5 Swelling

The volume fraction of the polymers in the swollen state describes how much fluid can be absorbed and retained. The equilibrium state of the hydrogel swollen in a fluid is determined by two forces. The thermo dynamical force of mixing favours the swelling, while the other is the stored energy in the stretched polymer chains hinders the swelling.[34]

### 1.4.2 Gels/Hydrogels from Natural and Synthetic Polymers

The natural polymers used in preparation of scaffolds/materials for biomedical applications are either from plant or animal origin. The polymers from animal origin are chitosan, keratin, silk, collagen, chitin, and elastin, which are usually derived from animal's body. The natural polymers which are obtained from plant origin are cellulose, cellulose derivates, hyaluronic acid, chondroitin sulfate**,** starch and pectin.[35] The polysaccharides based gels have attracted great deal of attention due to their properties like biodegradable, biocompatible, non toxic, easy to prepare and easily available at  low  costs. The natural polymers are not very stable and often lack the required optimum mechanical properties for the functioning of the product/device in the medical field and therefore, the use of synthetic biodegradable polymers is often blended with natural polymers. Poly hydroxy ethyl methacrylate (PHEMA) was the first synthetic hydrogel shown for applications in contact lenses, burn wound dressings, artificial skin, drug delivery and tissue engineering scaffolds for promoting cell adhesion and in artificial cartilage production for bone marrow and spinal cord cell regeneration.[36,37] Hydrogels based on polyethylene glycol methacrylate (PEGMA), poly ethylene glycol dimethacrylate (PEGDMA) and poly ethylene glycol diacrylate (PEGDA) most widely used for hydrogels in medicine. They possess high biocompatibility, non-toxic  on surrounding tissue which makes them good candidates for drug delivery system applications.[38,39] Polyvinyl Alcohol(PVA) hydrogels are mostly used in contact lens production, cartilage reconstruction,

artificial organs regeneration, drugs delivery systems and wound dressings by providing the skin with a moist environment, favour epithelial cell and tissue reconstruction for faster wound healing.[40,41] PVA based hydrogels are also used for injectable implants, endoprostheses ,soft tissue fillers in plastic, reconstructive and aesthetic surgery.[42,43] Polyvinylpyrrolidone (PVP) is also used in drug delivery systems and wound dressings and are usually obtained with the radiation technique[44], an apparently simple, efficient, clean and environmentally friendly process. They are advantageous due to softness and elasticity and their ability to store large amounts of liquid while retaining quite good mechanical properties. Agar, cellulose or PEG are the usual polymers added to PVP hydrogels.[45] Wang *et al* reported that the blending poly vinyl pyrrolidone (PVP) and carboxy methyl cellulose(CMC) yields a hydrogel with good mechanical properties, high water uptake, enhanced biodegradability.[46] Polyacrylate (PA) hydrogels, mainly poly acryl amide (PAA), are used mostly as agricultural gels. They also play an important role in biomedical applications in lip enhancement, chest deformities aesthetic corrections, as soft tissue fillers and augmentation materials for breast implants.[47] Polyurathene (PU) hydrogels serve as drug carriers, in drug delivery, wound dressing manufacture, artificial kidney membranes, catheter coating materials and contact lenses.[48,49]

## 1.5 Microgels

"Microgels" are colloidal dispersions of gel particles. Staudinger and Husemann were the first to prepare microgels in 1935 by suspension polymerisation of Poly (divinyl benzene) (DVB) using organic solvents.[50]
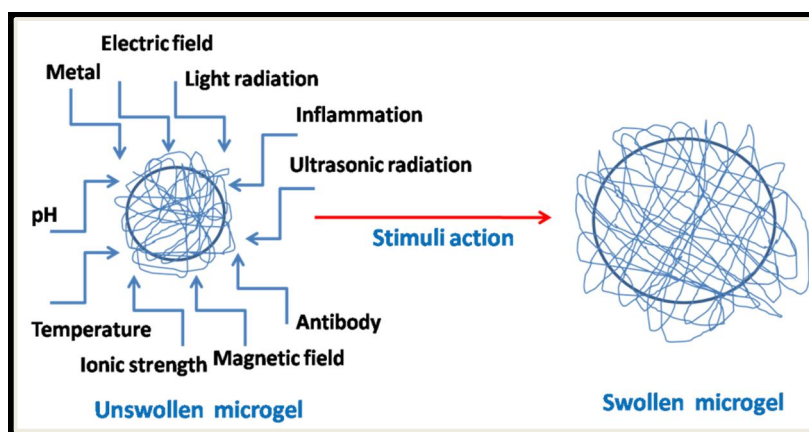


**Figure 1.5:** Stimuli action of Microgel.

Baker in this publication, *"Microgel-A new Macromolecule"* in 1949, used the word microgel to describe the cross linked poly butadiene latex particles.[51] Pelton and Chibante were the first to synthesize the poly N-isopropyl acryl amide (PNIPAM) based microgels.[52] The swelling behaviour of microgels is governed by the nature of the microgel (hydrophilic/hydrophobic balance), degree of cross linking, gel-solvent interaction, temperature, pH, magnetic field, etc. The stimuli like pH, temperature, ionic strength, magnetic field, electric field etc as shown in the above **fig 1.5,** influence the volume transitions in gels.

## 1.5.1 Microgel Synthesis

Various synthetic strategies for the preparation of microgels can be divided into three groups: (1) physical self-assembly or cross linking of pre polymers in homogeneous phase or in micro droplets (2) polymerization of monomers in homogeneous phase or in micro droplets and (3) photolithographic techniques. The physical or chemical cross linking of polymers can be realized in both water and water in- oil (W/O) emulsion systems. In water in-oil, aqueous droplets of pre polymers are stabilized by oil-soluble surfactants in a continuous oil phase. Membrane emulsification techniques allow preparation of highly mono disperse microgel particles. Microgels can be prepared by hetero phase polymerization (free radical or controlled radical) of monomers in the presence of a crosslinking agent in aqueous phase. Microgel preparation by polymerization of monomers can be also realized in aqueous droplets prepared by use of membrane emulsification or micro fluidic devices. Alternatively, microgel formation in Water/Oil systems can also be done by poly addition reactions between reactive multifunctional pre polymers. In this case, the use of crosslinker is not required.[53] The precipitation polymerization is a versatile technique and offers several advantages for the preparation of aqueous microgels. The polymerization process can be carried out as a batch, semi batch, or continuous process. This offers the possibility to optimize reaction conditions and obtain microgels with desired properties. Microgel size can be controlled over a broad range (from 100nm to 3μm) by the use of surfactants or co-monomers. Microgel particles with narrow size distribution can be obtained. Different co-monomers can be integrated into the microgel

network during the polymerization process. Hybrid colloids can be prepared by encapsulation of nanoparticles (NPs) during microgel formation.

## 1.5.2 Microgel Applications

Microgels have a wide variety of applications in cement, paints, ink-jet printing, oil recovery, molecular separation, biosensors, water purification, waste water treatment, drug delivery, and enzyme immobilization etc.[54] Snowden *et al*, reported thermo sensitive microgel dispersions of poly(NIPAM) with cationic or anionic surface charges which absorb/adsorb good amount of chemical ions like lead, cadmium, ammonium and nitrates from aqueous solution at room temperature.[55] Another application of microgels is in photonic crystals, which are periodic dielectric materials on a nano scale. Photonic crystals have applications in many photonic devices due to their ability to control the flow of light as in the case of chemical sensors and micro lasers. The colloidal crystals are simple to produce and cost effective. Furthermore, the colour of the colloidal crystal can be changed through the microgel swelling by infiltrating the particles with different organic solvents like methanol, ethanol etc.[56,57] Peng and Wu studied the chemical interactions between metal cations ($Hg^{2+}$, $Cu^{2+}$, $Ca^{2+}$ and $Na^+$) and thermo sensitive poly(N-vinylcaprolactam-co-AA) microgels, which could be used for the immobilization of proteins and drugs.[58] Freemont and Saunders demonstrated microgel dispersions containing methacrylic acid which were capable of providing structural support for damaged soft tissue such as inter vertebral disc and help in the tissue regeneration.[59] Gan *et al* investigated the potential of poly(NIPAM-co-2-hydroxyethyl methacrylate-co-acrylic acid) microgels to act as injectable cell scaffolds which demonstrated successful culture and proliferation of HepG2 cells with a low degree of syneresis.[60] Panda *et al* fabricated large numbers of cell-laden microgel particles using stop-flow lithography, for drug delivery and tissue engineering.[61] Magnetic fluid hyperthermia where the magnetic nanoparticles are injected into a tumour and which is subjected to an alternating magnetic field that induces heat destroying the tumour, shows a promising future in treatment of cancer.[62] Microgels are also used in wound dressings where controlled release of an antibiotic drug for trans dermal drug delivery has been reported.[63,64]

Microgels may play a role in the development of a viable implantable glucose sensor to assist in the management of diabetes mellitus, by continuously monitoring glucose levels. Boronic acid-based optical glucose sensors operate under physiological conditions and give a reproducible signal in vitro by utilizing fluorescence as a detection method have been developed.[65,66] Extensive studies have been reported on microgels and their applications in various fields. However, we have discussed only a few studies relevant to the biomedical field have been discussed here.

## 1.6 Nanofibers

The replacement for diseased or damaged tissues, which mimic the physiological conditions and simultaneously promote cell growth and regeneration by patients own cells still remains a major challenge in the area of biomedicine. Recently, nanofibers have attracted a major attention in the health care systems. It is estimated that the global nanofiber market was worth around $400 million in 2016, growing to over $1 billion in 2020. This is owing to the use of relatively low-cost materials and the development of efficient nanofiber mass production technologies. The cylindrical kind of structures that originate from polymers, are described as solid fibers that possess high mechanical properties compared to other forms, made from the same polymers.[67] Nanofibers are interesting class of nanomaterials with the size of less than 100 nm.[68] They can be prepared from polymers of both synthetic and natural origin, but usually those being biocompatible and biodegradable are preferred. Nanofibers can be synthesized from natural polymers like chitosan, collagen, silk, fibronectin, gelatin, and cellulose derivatives and also from synthetic polymers like poly lactic acid (PLA), poly glycolic acid (PGA), poly lactic-co-glycolic acid (PLGA), poly ε-caprolactone (PCL), polyurethane (PU), polyvinyl pyrrolidone (PVP), poly vinyl alcohol (PVA), tyrosine-derived polycarbonates. The polymer selection is of paramount importance for the production of fibers. Polymeric nanofibers have attracted attention mainly because of their enormous specific surface area, high flexibility, large surface-to-volume ratio, high porosity which are suitable for various applications.

### 1.6.1 Fabrication Techniques for Nanofiber Production

Polymeric nanofibers obtained from natural and synthetic polymers can be synthesized using techniques like drawing, phase separation, template synthesis, self assembly and electrospinning. The drawing is a process similar to dry spinning in fiber industry, which can make one-by-one very long single nanofibers. However, only a visco-elastic material that can undergo strong deformations while being cohesive enough to support the stresses developed during pulling can be made into nanofibers through drawing. The template synthesis uses a nanoporous membrane as a template to make nanofibers of solid or hollow shape which are in the nanometer range. The phase separation consists of dissolution, gelation, and extraction using different solvents which results in nanosize porous foam. The self-assembly process in which the atomic and molecular aggregates arrange themselves by bonding into stable and structurally well-defined entities at meso or nano dimensions gives rise to nanofibers. However, the self-assembly is time-consuming in processing continuous polymer nanofibers. Thus, the electrospinning process seems to be the only method which can be further developed for mass production of one-by-one continuous nanofibers from various polymers. Melt blown method is based on melt blowing fiber spinning technology. Here, the polymer blend is extruded though a small orifice in combination with high velocity streams of heated air. This method yields fibers in the range of 150 to 1000 nm. Electrospinning is the most acceptable method for preparing nanofiber. The fibers produced by this process are in the range of nano meters to micrometers. Nano-spider is another modified electrospinning and commercial method that has a high productive ability to fabricate polymeric nanofibers in diameter range of 50 to 300 nm into nonwovens. Airbrush Spray is another low-cost, fast and easily adaptable technique to manufacture nonwoven micro/nanofibrous membranes.[69]

### 1.6.1.1 Electrospinning Technique

The electrospinning technique is well known since 1897 and is based on Rayleigh's principle.[70] It is also a cost effective and scalable method/technique to produce large volumes of nanofibers using different natural and synthetic polymers. Electrospinning process utilizes the electrostatic forces to draw the

fibers from the droplet formed at the tip of spinneret. In the fabrication process the electrical voltage is applied to the polymer solution when it extrudes out from the needle tip and the fibers are collected on an aluminium plate owing to the attractive forces that are generated due to oppositely charged polymers.[71]
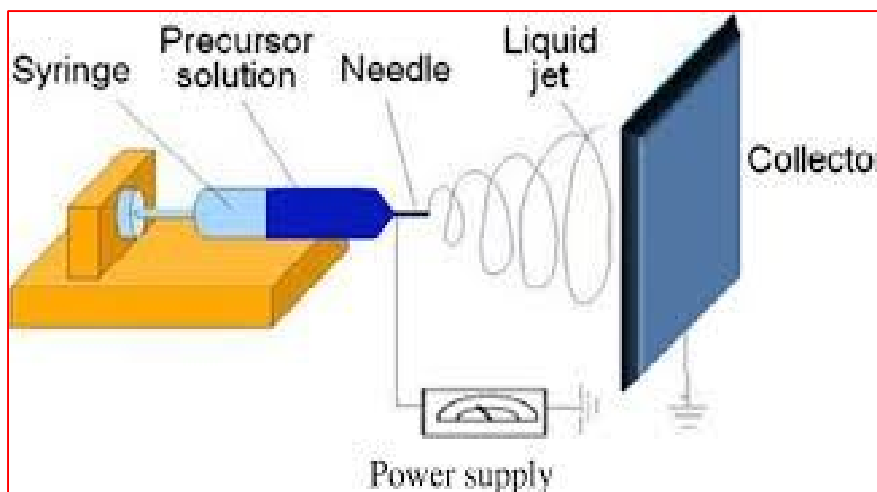


**Figure 1.6:** Electrospinning set-up.

*Adapted with permission from Springer Nature, Copyright © 2014, Gupta et al.; licensee Bio Med Central Ltd.*[72]

As the electric field intensity increases, the hemispherical surface of the fluid at the tip of the capillary tube elongates to form a conical shape known as the Taylor cone. Further increasing the electric field, a critical value is attained with which the repulsive electrostatic force overcomes the surface tension and the charged jet of the fluid is ejected from the tip of the Taylor cone. The discharged polymer solution jet undergoes an instability and elongation process, followed by long and this fiber formation on the collector. One electrode is placed into the spinning solution/melt and the other attached to the collector. In most cases, the collector is simply grounded, as indicated in **fig 1.6.** The formation of nanofibers is mainly grouped in following parameters which are grouped as solution parameters which includes conductivity, surface tension and viscosity of solution. The process parameters include applied voltage, distance between tip to collector, flow rate, and electric field induced by the collector. The ambient parameters include temperature and humidity.[72]

## 1.6.2 Nanofiber Applications

The electrospun nanofibrous scaffolds based drug delivery systems (DDS) provide better control on drug dosages when compared to other methods of drug delivery systems.[73] The electrospun nanofibrous scaffolds have been developed for the treatment of Tinea Pedis and other fungal infections and the drug itraconazole is widely developed and study of release.[74] The scaffolds having electrospun nanofibers with low diameters was found to be more effective in dual drug delivery.[75-77] Polysaccharides such as chitosan, cellulose, and hyaluronic acid (HA) as well as proteins, such as collagen and silk have been electrospun for localized drug delivery applications.[78] Many of these polymers have specific properties that promote wound healing, chitosan exhibits both antibacterial and hemostatic activities. To reduce the post-surgical infections and increase the wound healing rates, two different drugs are released. The poly(ethylene-co-vinyl alcohol) (EVOH) electrospun nanofibrous scaffolds loaded with silver (Ag) nanoparticles have been used as dressing material in skin wound healings to prevent the inflammation.[79] The electrospun nanofibers for bone tissue culturing and regeneration utilize a range of biopolymers with synthetic origin, which include poly($\alpha$-hydroxyl acid) and poly(hydroxyl alkanoate), such as poly(hydroxyl butyrate) (PHB). The PHB and poly (hydroxyl butyrate-co-hydroxy valerate) (PHBV) electrospun nanofibers have shown enhanced osteoblastic activity.[80] The electrospun nanofibrous scaffolds have also been used successfully in controlled delivery of genes[81], proteins[82-84], enzymes.[85] and also in post-surgical treatment of Glioma cells.[86] These investigations have clearly indicated that electrospinning could also be used in fabrication of vascular grafts and scaffolds for biomedical applications. Apart from biomedical field, nanofibers also find wide applications in lithium ion batteries, air filtration, bio-sensing, optical sensors, oil-water separations, protective clothing, cosmetics, textiles.

.

## 1.7 Special Characterization Techniques Used in Thesis

### 1.7.1   Atomic Force Microscopy (AFM)

Atomic force microscopy (AFM) is a high-resolution form of scanning probe microscopy, also known as scanning force microscopy (SFM). In force microscopy the probing tip is attached to a cantilever-type spring. In response to the force between tip and sample, the cantilever also called as lever, is deflected. Images are taken by scanning the sample relative to the probing tip and digitizing the deflection of the lever or the z-movement of the piezo as a function of the lateral position x, y.
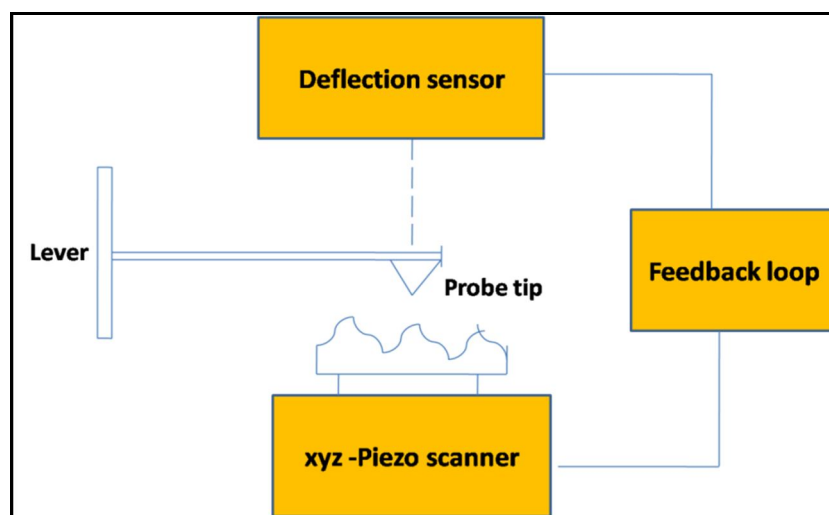


**Figure 1.7:**  Basic principles of Atomic Force Microscopy.

*Adapted with permission from Elsevier, Atomic Force Microscopy, E. Meyer;*
*Progress in Surface Science, Copyright © 1992 Published by Elsevier B.V.*[87]
.

Typical spring constants are between 0.001 to 100 N/m and motions from microns to ≈ 0.1Å are measured by the deflection sensor as shown in the **fig 1.7**. There are two force regimes namely the contact and the non-contact mode. When the microscope is operated in non-contact mode at tip-sample separations of 10 to l00nm, forces, such as Vander Waals, electrostatic, magnetic or capillary forces, can be sensed and give information about surface topography, distributions of charges, magnetic domain wall structure or liquid film distribution. At smaller separations of the order of Å the probing tip is in contact with the sample. In this mode, ionic repulsion forces allow the surface topography to be traced with high resolution.[88, 89]

### 1.7.2 Micro-Computed Tomography (µ-CT)

Micro-computed tomography (µ-CT) is a non-invasive, high resolution X-ray scanning technique that allows unique possibilities for precise 3-dimentional imaging. The µ-CT units consists of an X-ray source, a specimen that is to be imaged, an X-ray to – electronic signal – converting imaging array, and a device that either rotates the specimen or rotates the scanner around the stationary specimens.[90] The method of providing high resolution images falls into one of the three approaches: (i) cone-beam (ii) optical magnification and (iii) Bragg's diffraction.
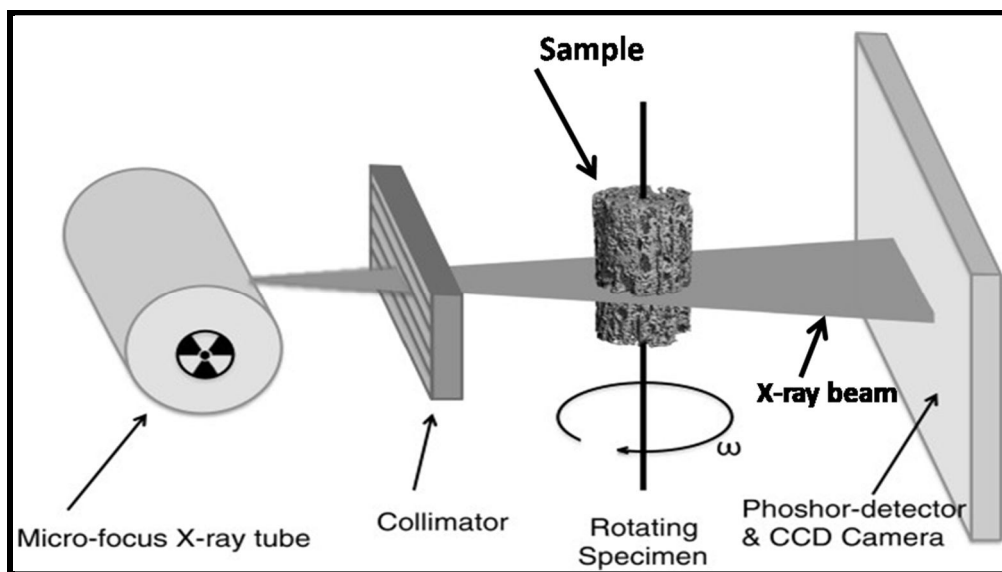


**Figure 1.8:** Components of micro-Computed Tomography.

*Adapted with permission from Boerckel et al. Micro computed tomography: approaches and applications in bioengineering; Stem Cell Research & Therapy. Copyright © licensee BioMed Central. 2014.*[91]

µ-CT combines micro-focal spot X-ray projections rotated through multiple viewing directions to produce 3-D reconstructed images of materials. The topographic reconstruction can be based on a cone-beam convolution-back projection algorithm. Combined with 3-D simulations and analyses that are capable of handling the complexity of microstructures in materials, µ-CT has emerged as a powerful tool that provides clear insights into the link between materials processing and properties. µ-CT can be used to investigate micro-

structural characterization of wide range of materials which includes cellular metallic heterogeneous structure, electronic components, dental materials, polymer scaffolds for tissue engineering and drug delivery, trabecular bone, bio-ceramics etc.[92]

## 1.8 Summary

To summarize, natural polymers due to their unique characteristics of biocompatibility, biodegradability, non-toxicity, sustainability, resemblance to the extra cellular matrix (ECM) in the body, are easily available. They find an array of applications as biomaterials in the form of gels and nanofibers in the biomedical and pharmaceutical fields. In this thesis, we have made a sincere attempt to explore the unexplored natural polysaccharides and their modified derivatives in the synthesis of microgels and fabrication of electrospun nano and micro fibers which show great promise as future biomaterials in human health care applications.

## 1.9 References

**1.** Willyard, C. Timeline.; Regrowing the body. *Nature*. 2016, 540**,** 50–51.

**2.** Williams, D. F.; Cunningham, J. *Materials in Clinical Dentistry*; Oxford medical publications; Oxford University Press, 1979.

**3.** Ramakrishna, S.; Mayer, J.; Wintermantel, E.; Leong, K. W. Biomedical Applications of Polymer-Composite Materials: A Review. *Composites Science and Technology*. 2001, 61, (9), 1189-1224.

**4.** Grainger, D. W. The Williams Dictionary of Biomaterials. Liverpool University Press ,1999.

**5.** https://www.industryarc.com/Report/18210/biomaterials-market.html; 2020.

**6.** Hench, L. L. Biomaterials: A Forecast for the Future. *Biomaterials*. 1998, 19 (16), 1419–1423.

**7.** Hench, L. L. Bioceramics: From Concept to Clinic. *J. Am. Ceram. Soc.* 1991, *74* (7), 1487–1510.

**8.** Schindhelm, K.; Milthorpe, B.K. An overview of biomaterials. *Australas Phys Eng Sci Med*. 1986; 9(1), 29-32.

**9.** Benabid, AL.; Koudsie A.; Benazzouz A, et al. Deep brain stimulation for Parkinson's disease. *Adv Neurol*. 2001, 86, 405-412.

**10.** Martinez, E C.; Kofidis, T. Adult stem cells for cardiac tissue engineering. *J Mol Cell Cardiol*. 2011, 50(2):312-319.

**11.** https://www.nibib.nih.gov/science-education/science-topics/biomaterials

**12.** Humes, H. D.; Fissell, W. H.; Tiranathanagul, K. The Future of Hemodialysis Membranes. *Kidney Int.* 2006, 69 (7), 1115–1119.

**13.** https://www.azonano.com/equipment-details.aspx?EquipID=1811

**14.** Carretti, E.; Dei, L.; Weiss, R. G. Soft Matter and Art Conservation. Rheoreversible Gels and Beyond. *Soft Matter.* 2005, 1 (1), 17–22.

**15.** Peppas, N. A.; Merrill, E. W. Poly(Vinyl Alcohol) Hydrogels: Reinforcement of Radiation-Crosslinked Networks by Crystallization. *J. Polym. Sci. Polym. Chem. Ed.* 1976, 14 (2), 441–457.

**16.** Lee, S.C.; Kwon I K.; Park K. Hydrogels for delivery of bioactive agents: a historical perspective. *Adv Drug Deliv Rev*. 2013, 65(1):17-20.

**17.** Kopecek, J.; Hydrogel biomaterials: a smart future? *Biomaterials.* 2007, 28(34):5185-5192.

**18.** Li, L.; Aoki, Y. Rheological Images of Poly(Vinyl Chloride) Gels. 1. The Dependence of Sol−Gel Transition on Concentation. *Macromolecules.* 1997, 30 (25), 7835–7841.

**19.** Knoben, W.; Besseling, N. A. M.; Cohen Stuart, M. A. Rheology of a Reversible Supramolecular Polymer Studied by Comparison of the Effects of Temperature and Chain Stoppers. *J. Chem. Phys*. 2007, 126 (2), 24907.

**20.** Plamper, F. A.; Richtering, W. Functional Microgels and Microgel Systems. *Acc. Chem. Res.* 2017, 50 (2), 131–140.

**21.** Keidel, R.; Ghavami, A.; Lugo, D. M.; Lotze, G.; Virtanen, O.; Beumers, P.; Pedersen, J. S.; Bardow, A.; Winkler, R. G.; Richtering, W. Time-Resolved Structural Evolution during the Collapse of Responsive Hydrogels: The Microgel-to-Particle Transition. *Sci. Adv.* 2018, 4 (4), 1-8.

**22.** Wrede, O.; Reimann Y,; Lülsdorf S, et al. Volume phase transition kinetics of smart N-n-propylacrylamide microgels studied by time-resolved pressure jump small angle neutron scattering. *Scientific Reports*. 2018, 8(1): 13781.

**23.** Senff, H.; Richtering, W. Temperature Sensitive Microgel Suspensions: Colloidal Phase Behavior and Rheology of Soft Spheres. *J. Chem. Phys.* 1999, 111 (4), 1705–1711.

**24.** Debord, J. D.; Lyon, L. A. Thermoresponsive Photonic Crystals. *J. Phys. Chem B*. 2000, 104 (27), 6327–6331.

**25.** Brijitta, J.; Tata, B. V. R.; Joshi, R. G.; Kaliyappan, T. Random Hcp and Fcc Structures in Thermoresponsive Microgel Crystals. *J. Chem. Phys.* 2009, 131 (7), 74904.

**26.** Ngai, T.; Behrens, S. H.; Auweter, H. Novel Emulsions Stabilized by PH and Temperature Sensitive Microgels. *Chem. Commun.* 2005, 3, 331–333.

**27.** Destribats, M.; Lapeyre, V.; Wolfs, M.; Sellier, E.; Leal-Calderon, F.; Ravaine, V.; Schmitt, V. Soft Microgels as Pickering Emulsion Stabilisers: Role of Particle Deformability. *Soft Matter.* 2011, 7 (17), 7689–7698.

**28.** Li, J.; Mooney, D. J. Designing Hydrogels for Controlled Drug Delivery. *Nat. Rev. Mater.* 2016, 1 (12), 16071.

**29.** Naahidi S, Jafari M, Logan M, et al. Biocompatibility of hydrogel-based scaffolds for tissue engineering applications. *Biotechnol Adv*. 2017, 35(5): 530-544.

**30.** Li, Z.; Loh, X. J. Water Soluble Polyhydroxyalkanoates: Future Materials for Therapeutic Applications. *Chem. Soc. Rev.* 2015, 44 (10), 2865–2879.

**31.** Lei, K.; Chen, Y.; Wang, J.; Peng, X.; Yu, L.; Ding, J. Non-Invasive Monitoring of in Vivo Degradation of a Radiopaque Thermoreversible Hydrogel and Its Efficacy in Preventing Post-Operative Adhesions. *Acta Biomater.* 2017, 55, 396–409.

**32.** Drury J.L, Mooney DJ. Hydrogels for tissue engineering: scaffold design variables and applications. *Biomaterials*. 2003, 24(24):4337-4351.

**33.** Sannino, A.; Netti, P. A.; Madaghiele, M.; Coccoli, V.; Luciani, A.; Maffezzoli, A.; Nicolais, L. Synthesis and Characterization of Macroporous Poly(Ethylene Glycol)-Based Hydrogels for Tissue Engineering Application. *J. Biomed. Mater. Res. Part A*. 2006, 79A (2), 229–236.

**34.** De, S. K.; Aluru, N. R.; Johnson, B.; Crone, W. C.; Beebe, D. J.; Moore, J. Equilibrium Swelling and Kinetics of PH-Responsive Hydrogels: Models, Experiments, and Simulations. *J. Microelectromechanical Syst.* 2002, 11 (5), 544–555.

**35.** Sionkowska, A. Current Research on the Blends of Natural and Synthetic Polymers as New Biomaterials: Review. *Prog. Polym. Sci.* 2011, 36 (9), 1254–1276.

**36.** Kumar, N. A.; Hullathy Subban Ganapathy.; J. Kim and Y. Jeong. Preparation of poly 2-hydroxyethyl methacrylate functionalized carbon nanotubes as novel biomaterial nanocomposites. *European Polymer Journal*. 2008, 44, 579-586.

**37.** Bavaresco, V. P.; Zavaglia, C. A. C.; Reis, M. C.; Gomes, J. R. Study on the Tribological Properties of PHEMA Hydrogels for Use in Artificial Articular Cartilage. *Wear* 2008,265 (3), 269–277.

**38.** Zhao, X.; Mllton Harris, J. Novel Degradable Polyethylene Glycol Hydrogels for Controlled Release of Protein. *J. Pharm. Sci.* 1998, 87 (11), 1450–1458.

**39.** Underhill, G. H.; Chen, A. A.; Albrecht, D. R.; Bhatia, S. N. Assessment of Hepatocellular Function within PEG Hydrogels. *Biomaterials.* 2007, 28 (2), 256–270.

**40.** Riley, S. L.; Dutt, S.; De la Torre, R.; Chen, A. C.; Sah, R. L.; Ratcliffe, A. Formulation of PEG-Based Hydrogels Affects Tissue-Engineered Cartilage Construct Characteristics. *J. Mater. Sci. Mater. Med.* 2001, 12 (10–12), 983–990.

**41.** Jandera, V.; Hudson, D. A.; de Wet, P. M.; Innes, P. M.; Rode, H. Cooling the Burn Wound: Evaluation of Different Modalites. *Burns.* 2000, *26* (3), 265–270.

**42.** Dini, L.; Panzarini, E.; Miccoli, M. A.; Miceli, V.; Protopapa, C.; Ramires, P. A. In Vitro Study of the Interaction of Polyalkilimide and Polyvinyl Alcohol Hydrogels with Cells. *Tissue Cell.* 2005, 37 (6), 479–487.

**43.** Li, J. K.; Wang, N.; Wu, X. S. Poly(Vinyl Alcohol) Nanoparticles Prepared by Freezing–Thawing Process for Protein/Peptide Drug Delivery. *J. Control Release.* 1998, 56 (1), 117–126.

**44.** Ajji, Z.; Othman, I.; Rosiak, J. M. Production of Hydrogel Wound Dressings Using Gamma Radiation. *Nucl. Instruments Methods Phys. Res. Sect. B Beam Interact. with Mater. Atoms.* 2005, 229 (3), 375–380.

**45.** Benamer, S.; Mahlous, M.; Boukrif, A.; Mansouri, B.; Youcef, S. L. Synthesis and Characterisation of Hydrogels Based on Poly(Vinyl Pyrrolidone). *Nucl. Instruments Methods Phys. Res. Sect. B Beam Interact. with Mater. Atoms.*2006, 248 (2), 284–290.

**46.** Wang, M.; Xu, L.; Hu, H.; Zhai, M.; Peng, J.; Nho, Y.; Li, J.; Wei, G. Radiation Synthesis of PVP/CMC Hydrogels as Wound Dressing. *Nucl. Instruments Methods Phys. Res. Sect. B Beam Interact. with Mater. Atoms.* 2007, 265 (1), 385–389.

**47.** Cheng, N. xin; Wang, Y. lu; Wang, J. huang; Zhang, X. man; Zhong, H. Complications of Breast Augmentation with Injected Hydrophilic Polyacrylamide Gel. *Aesthetic Plast. Surg.* 2002, 26 (5), 375–382.

**48.** Abraham, G. A.; de Queiroz, A. A. A.; Román, J. S. Hydrophilic Hybrid IPNs of Segmented Polyurethanes and Copolymers of Vinylpyrrolidone for Applications in Medicine. *Biomaterials.* 2001, 22 (14), 1971–1985.

**49.** Akita, S.; Akino, K.; Imaizumi, T.; Tanaka, K.; Anraku, K.; Yano, H.; Hirano, A. A Polyurethane Dressing Is Beneficial for Split-Thickness Skin-Graft Donor Wound Healing. *Burns.* 2006, 32 (4), 447–451.

**50.** Bonham, J. A.; Faers, M. A.; Van Duijneveldt, J. S. Non-Aqueous Microgel Particles: Synthesis, Properties and Applications. *Soft Matter.* 2014, 10 (47), 9384–9398.

**51.** Baker, W. O. Microgel, A New Macromolecule. *Ind. Eng. Chem.* 1949, 41 (3), 511–520.

**52.** Zhang, J.; Pelton, R. Poly(N-Isopropylacrylamide) Microgels at the Air−Water Interface. *Langmuir.* 1999, 15 (23), 8032–8036.

**53.** Walter Richtering, Andrij Pich, Chemical Design of Responsive Microgels (Ebook)

**54.** Kausar, N Chowdhry, B Z.; Snowden, M J. Microgels from smart polymers. In: Galaev I, Mattiasson B (eds) Smart polymers: applications in biotechnology and biomedicine (2nd).CRC, Boca Raton, 2008, pp 137–175.

**55.** De, S. K.; Aluru, N. R.; Johnson, B.; Crone, W. C.; Beebe, D. J.; Moore, J. Equilibrium Swelling and Kinetics of PH-Responsive Hydrogels: Models, Experiments, and Simulations. *J. Microelectromechanical Syst.* 2002, *11* (5), 544–555.

**56.** Kim, S.; Seo, Y. G.; Cho, Y.; Shin, J.; Gil, S. C.; Lee, W. Optimization of Emulsion Polymerization for Submicron-Sized Polymer Colloids towards Tunable Synthetic Opals. *Bull. Korean Chem. Soc.* 2010, 31 (7), 1891–1896.

**57.** Biffis, A.; Graham, N. B.; Siedlaczek, G.; Stalberg, S.; Wulff, G. The Synthesis, Characterization and Molecular Recognition Properties of Imprinted Microgels. *Macromol. Chem. Phys.* 2001, 202 (1), 163–171.

**58.** Peng, S.; Wu, C. Controllable Interaction between Cations and Thermally Sensitive Poly(N-Vinylcaprolactam-Co-Sodium Acrylate) Microgels in Water. *Polymer.* 2001, 42 (16), 6871–6876.

**59.** Freemont, T. J.; Saunders, B. R. PH-Responsive Microgel Dispersions for Repairing Damaged Load-Bearing Soft Tissue. *Soft Matter.* 2008, *4* (5), 919–924.

**60.** Gan, T.; Guan, Y.; Zhang, Y. Thermogelable PNIPAM Microgel Dispersion as 3D Cell Scaffold: Effect of Syneresis. *J. Mater. Chem.* 2010, 20 (28), 5937–5944.

**61.** Panda, P.; Ali, S.; Lo, E.; Chung, B. G.; Hatton, T. A.; Khademhosseini, A.; Doyle, P. S. Stop-Flow Lithography to Generate Cell-Laden Microgel Particles. *Lab Chip.* 2008, *8* (7), 1056–1061.

**62.** Phillips, J. L. A Topical Review of Magnetic Fluid Hyperthermia. *Am. Inst. Chem. Eng. Conf.* 2005, 14–18.

**63.** Nur H.; Snowden M J.; Cornelius V J.; Mitchell J C.; Harvey P J.; Benee L S. Colloidal microgel in removal of water from biodiesel. *Colloids and Surfaces A: Physicochem Eng. Aspects.* 2009, 335:133-137.

**64.** Antonietti, M.; Bremser, W.; Mainz, D.; Germany, W.; Schmidt, M.; Polymerforschung, M.; Germany, W. Microgels : Model Polymers for the Cross-Linked State. *Macromolecules.*1990, 3796–3805.

**65.** Lopez, V. C.; Raghavan, S. L.; Snowden, M. J. Colloidal Microgels as Transdermal Delivery Systems. *React. Funct. Polym.* 2004, 58 (3), 175–185.

**66.** Lopez, V. C.; Hadgraft, J.; Snowden, M. J. The Use of Colloidal Microgels as a (Trans)Dermal Drug Delivery System. *Int. J. Pharm.* 2005, *292* (1), 137–147.

**67.** Repanas, A.; Andriopoulou, S.; Glasmacher, B. The Significance of Electrospinning as a Method to Create Fibrous Scaffolds for Biomedical Engineering and Drug Delivery Applications. *J. Drug Deliv. Sci. Technol.* 2016, *31*, 137–146.

**68.** Rošic, R.; Kocbek, P.; Pelipenko, J.; Kristl, J.; Baumgartner, S. Nanofibers and Their Biomedical Use. *Acta Pharm.* 2013, *63* (3), 295–304.

**69.** Kamble, P.; Sadarani, B.; Majumdar, A.; Bhullar, S. Nanofiber Based Drug Delivery Systems for Skin: A Promising Therapeutic Approach. *J. Drug Deliv. Sci. Technol.* 2017, *41*, 124–133.

**70.** Last I, Levy Y, Jortner J: Beyond the Rayleigh instability limit for multicharged finite systems: from fission to Coulomb explosion. PNAS. 2002, 99: 9107-10.1073/pnas.142253999.

**71.** Reneker, D. H.; Chun, I. Nanometre Diameter FIbres of.Pdf. 1996, 7, 216–223.

**72.** Gupta, K.C., Haider, A., Choi, Y. et al. Nanofibrous scaffolds in biomedical applications. *Biomater Res.* 2014, 18, 5.

**73.** Verreck, G., Chun, I., Peeters, J. *et al.* Preparation and Characterization of Nanofibers Containing Amorphous Drug Dispersions Generated by Electrostatic Spinning. *Pharm Res.* 2003, 20, 810–817.

**74.** Zong, X.; Kim, K.; Fang, D.; Ran, S.; Hsiao, B. S.; Chu, B. Structure and Process Relationship of Electrospun Bioabsorbable Nanofiber Membranes. *Polymer.* 2002, 43, (16), 4403–4412.

**75.** Song, B.; Wu, C.; Chang, J. Dual Drug Release from Electrospun Poly(Lactic-Co-Glycolic Acid)/Mesoporous Silica Nanoparticles Composite Mats with Distinct Release Profiles. *Acta Biomater.* 2012, 8, (5), 1901–1907.

**76.** Xiang, Q.; Ma, Y.-M.; Yu, D.-G.; Jin, M.; Williams, G. R. Electrospinning Using a Teflon-Coated Spinneret. *Appl. Surf. Sci.* 2013, 284, 889–893.

**77.** Joung, Y K.; Heo, J H.; Park, K M.; Park K D. Controlled release of growth factors from core-shell structured PLGS microfibers for tissue engineering. *Biomaterial Research.* 2011, 15: 78.

**78.** Kim, A R.; Park, H S.; Kim, S S.; Noh I. Biological evaluation of cellulose hydrogel with temperature responsive particles. *Biomaterial Research.* 2013, 17: 181.

**79.** Xu, C.; Xu, F.; Wang, B.; Lu, T. Electrospinning of Poly(Ethylene-Co-Vinyl Alcohol) Nanofibres Encapsulated with Ag Nanoparticles for Skin Wound Healing. *J. Nanomater.* 2011, 201834.

**80.** Sombatmankhong, K.; Sanchavanakit, N.; Pavasant, P.; Supaphol, P. Bone Scaffolds from Electrospun Fiber Mats of Poly(3-Hydroxybutyrate), Poly(3-Hydroxybutyrate-Co-3-Hydroxyvalerate) and Their Blend. *Polymer.* 2007, 48, (5), 1419–1427.

**81.** Saraf, A.; Baggett, L. S.; Raphael, R. M.; Kasper, F. K.; Mikos, A. G. Regulated Non-Viral Gene Delivery from Coaxial Electrospun Fiber Mesh Scaffolds. *J. Control Release.* 2010, 143, (1), 95–103.

**82.** Ji, W.; Yang, F.; van den Beucken, J. J. J. P.; Bian, Z.; Fan, M.; Chen, Z.; Jansen, J. A. Fibrous Scaffolds Loaded with Protein Prepared by Blend or Coaxial Electrospinning. *Acta Biomater.* 2010, 6, (11), 4199–4207.

**83.** Meng, Z. X.; Xu, X. X.; Zheng, W.; Zhou, H. M.; Li, L.; Zheng, Y. F.; Lou, X. Preparation and Characterization of Electrospun PLGA/Gelatin Nanofibers as a Potential Drug Delivery System. *Colloids Surfaces B Biointerfaces.* 2011, 84, (1), 97–102.

**84.** Noh, H. K.; Lee, S. W.; Kim, J.-M.; Oh, J.-E.; Kim, K.-H.; Chung, C.-P.; Choi, S.-C.; Park, W. H.; Min, B.-M. Electrospinning of Chitin Nanofibers: Degradation Behavior and Cellular Response to Normal Human Keratinocytes and Fibroblasts. *Biomaterials.* 2006, 27 , (21), 3934–3944.

**85.** Maleki, M.; Latifi, M.; Amani-Tehran, M.; Mathur, S. Electrospun Core–Shell Nanofibers for Drug Encapsulation and Sustained Release. *Polym. Eng. Sci.* 2013, 53 , (8), 1770–1779.

**86.** Ranganath, S. H.; Wang, C.-H. Biodegradable Microfiber Implants Delivering Paclitaxel for Post-Surgical Chemotherapy against Malignant Glioma. *Biomaterials.* 2008, 29, (20), 2996–3003.

**87.** Meyer, E. Atomic Force Microscopy. *Prog. Surf. Sci.* 1992, 41 (1), 3–49.

**88**. Sheng, S.; Shao, Z. Cryo-Atomic Force Microscopy. *Methods Cell Biol.* 2002, (68), 243–256.

**89.** S. H. Cohen and M. L. Lightbody. *Atomic Force Microscopy/Scanning Tunneling Microscopy 2*. Plenum, New York 1997.

**90.** Stock, S. R., MicroComputed Tomography: Methodology and Applications. CRC Press: 2008.

**91.** Boerckel, J. D.; Mason, D. E.; McDermott, A. M.; Alsberg, E. Microcomputed Tomography: Approaches and Applications in Bioengineering. *Stem Cell Res. Ther.* 2014, 5, (6), 1–12.

**92.** Ho, S. T.; Hutmacher, D. W. A Comparison of Micro CT with Other Techniques Used in the Characterization of Scaffolds. *Biomaterials.* 2006, 27 (8), 1362–1376.

# CHAPTER II

## Scope and Objectives

*The next best thing of knowing something is knowing where to find it.*

*Sameul Johnson*

Globally several surgical procedures are performed everyday to replace or repair tissues that have been damaged by diseases, accidents or trauma. Millions of people would benefit immensely if tissues and organs can be replaced on demand[1]. However, the cost and shortage of tissues is hampering the treatment of patients enormously. In this context, polymeric gels/hydrogels have become extremely important. Gels/Hydrogels are three dimensionally crosslinked polymers and due to their hydrophilic nature can absorb large amount of water[2]. Gels are soft and resilient and mimic the extra cellular matrix (ECM) of the body tissues and find wide applications in tissue engineering as scaffolds, implants, controlled drug delivery and a variety of other applications[3].

Numerous synthetic polymeric gels such as polystyrene, poly-l-lactic acid (PLLA), poly-glycolic acid (PGA) and poly-l-lactic-co-glycolic acid (PLGA) have been used to make injectables, scaffolds and implants. Biological materials such as collagen, proteoglycans, alginate-based substrates and chitosan have also been looked at in designing of scaffolds for tissue engineering[4]. Unlike synthetic polymers, natural polymers are biocompatible, promote excellent cell adhesion and growth and are also biodegradable which the most desirable properties for biomedical applications are. Natural polymers such as silk, wool, deoxyribonucleic acid (DNA), cellulose, collagen and proteins[5] have also been used for biomedical applications. Gels, upon reduction in their size to the colloidal regime, are often referred to as nanogels (typically < 100 nm) and microgels with the size in the micron range. Microgels/Nanogels have shown great promise scientifically as well as for technological developments in biomedical applications.

## 2.1 Microgels and Nanofibers from Natural Polysaccharides

Polysaccharides based microgels/nanogels have recently attracted a great deal of interest in tissue engineering and drug delivery applications as they are renewable, non-toxic, biodegradable and relatively cheap. In addition, they also possess a large number of functional groups such as hydroxyl, amino, and carboxylic acid, which can be utilized for cross-linking or further modification.[6] The typical examples of naturally occurring polysaccharides are : Chitosan (CS), Hyaluronan (HA), Dextran (Dex), Cellulose (CeL),

Pullulan (PuL), Chondroitin Sulfate (ChS), Alginate (Alg) etc. Further, the nanofibers fabricated from these polysachharides are also gaining lot of importance in biomedical fields due to their very high surface area, controllable porosity, appreciable mechanical strength and good flexibility.

Many of these nanofibers are obtained using the electrospinning technique.[7] Electro-spinning (ES) is the most commonly used technique to generate ultra thin nanofibers with controllable diameters, compositions, and orientations.[8] This flexibility allows for controlling the shape and arrangement of the fibers so that different structures (*i.e.* hollow, flat and ribbon shaped) can be fabricated depending on intended applications such as tissue engineering, drug delivery, cancer diagnosis, lithium-air battery, optical sensors, air filtration and bio-separations[9] etc.

## 2.2 Rationale and Significance of the study

In this thesis, focus is given on design and synthesis of new microgels and electrospun nanofibers for biomedical applications. The novelty in this work is that, the microgels and nanofibers are synthesised and fabricated using the unexplored polysaccharides which are not reported earlier. There is a great scope in designing and synthesizing new functional microgels made from available natural polymers. Similarly, there is a wide scope in designing newer nanofibers in combination with clays and active pharmaceutical ingredients (API) for making devices for wound healing applications.

## 2.3 Objectives of the Thesis

1. To synthesize biodegradable microgels using hydrophobically modified Ethyl hydroxy ethyl cellulose (HM-EHEC) by emulsion technique and to study the loading of an anticancer drug and its release kinetics under physiological conditions.

2. To design and fabricate electrospun nanofibers from Ethyl hydroxyl ethyl cellulose (EHEC) and Poly vinyl alcohol (PVA) for applications as scaffolds in tissue engineering and regenerative medicine.

3. To incorporate inorganic fillers like nanoclay and nanoparticles namely, Halloysite nanotubes and silver nanoparticles in polymer mats for enhanced wound healing property.

4. To design and fabricate a porous filter media from Gelatin electrospun fibers for separation of impurities and uremic toxins from the blood plasma.

## 2.4 References

**1.** Giwa S, Lewis JK, Alvarez L, et al. The promise of organ and tissue preservation to transform medicine. *Nat Biotechnol*. 2017, 35(6):530-542.

**2.** Chai, Q.; Jiao, Y.; Yu, X. Hydrogels for Biomedical Applications: Their Characteristics and the Mechanisms behind Them. *Gels.* 2017, *3*, 6-10.

**3.** Mantha S, Pillai S, Khayambashi P, et al. Smart Hydrogels in Tissue Engineering and Regenerative Medicine. *Material (Basel)*. 2019, 12(20):3323.

**4.** O'Brien, F. J. Biomaterials & Scaffolds for Tissue Engineering. *Mater Today.* 2011, 14(3), 88–95.

**5.** Tchobanian, A.; Van Oosterwyck, H.; Fardim, P. Polysaccharides for Tissue Engineering: Current Landscape and Future Prospects. *Carbohydr. Polym.* 2019, 205, 601–625.

**6.** Liu, Z.; Jiao, Y.; Wang, Y.; Zhou, C.; Zhang, Z. Polysaccharides-Based Nanoparticles as Drug Delivery Systems. *Adv. Drug Deliv. Rev.* 2008, 60 (15), 1650–1662.

**7.** Sill TJ, von Recum HA. Electrospinning: applications in drug delivery and tissue engineering. *Biomaterials*. 2008, 29(13):1989-2006.

**8.** Frenot, A.; Henriksson, M. W.; Walkenström, P. Electrospinning of Cellulose-Based Nanofibers. *J. Appl. Polym. Sci.* 2007, 103 (3), 1473–1482.

**9.** Liang D, Hsiao BS, Chu B. Functional electrospun nanofibrous scaffolds for biomedical applications. *Adv Drug Deliv Rev*. 2007, 59(14):1392-1412.

# CHAPTER III

## Synthesis and Characterization of Hydrophobically Modified-Ethyl Hydroxy Ethyl Cellulose (HM-EHEC) Microgels for Drug Delivery Applications

*Nothing in life is to be feared, it's only to be understood.*

*Marie Curie*

## 3.1 Introduction

According to the World Health Organisation (WHO), Cancer is a major cause of deaths in more than 50% of the countries worldwide and a cure for it is one of the biggest challenges of the 21st century. It is a disease which involves the abnormal cells to divide in an uncontrolled manner and destroy the various tissues of the body. The most common type of cancer, with the highest number of cases is the lung cancer which is followed by breast, skin, prostate and colon cancer.[1] Deaths caused due to cancer are estimated to rise rapidly, with an estimated number of more than 20 million by the end of 2025.[2] The diagnosis of cancer must be made in the early stages and must be accurate and requires great healthcare facilities and newer advanced technologies. The advancement in nanotechnology for cancer treatment offers a versatile platform for biodegradable and biocompatible systems to deliver conventional chemotherapeutic drugs by increasing their bioavailability and improving the release profiles. Chemotherapy, radiation therapy, gene therapy, magnetic hyperthermia and targeted therapies are more frequently used for the cancer treatment. However, these treatments have some limitations. Chemotherapy has toxic side effects, by developing resistance to the chemical agents and other forms of treatment are required to be given in combination with chemotherapy. Researchers also report that the various forms of chemo, radiation therapy cause early aging at cellular and genetic level, and the cells start to die sooner than normal. Therefore, in this regard, nanogels, microgels/ micro-particles are more frequently being explored as drug carriers for various applications right from diagnosis to therapy.[3]

Microgels/nanogels present exciting opportunities with their peculiar physicochemical properties being small in size and possessing high surface to volume ratios. Biopolymer based microgels/nanogels have become an important field in bio-nanotechnology, tissue engineering, medical implants and particularly in drug delivery applications.[4] Microgels are three dimensional hydrophilic polymeric networks that are capable of absorbing water and other biological fluids and also help in improving the efficacy of the therapeutic agents and also minimizing the side effects.[5] Polysaccharides based

biopolymers like chitosan, alginates, starch and cellulose are commonly used for controlled and targeted drug delivery due to the fact that they are biocompatible, biodegradable, low immunogenicity, also capable of multitude chemical modifications and therefore biopolymers are a major point of focus in anti-cancer drug delivery applications for diagnostics and chemotherapeutics.[6]

The biopolymer reported in this chapter for the synthesis and characterizations of microgels is based on hydrophobically modified ethyl hydroxy ethyl cellulose (HM-EHEC). It is a non-ionic amphiphilic water soluble polymer with hydrophilic and hydrophobic micro-domains distributed randomly on the polymer backbone, along with low amount of nonyl phenol groups onto the backbone. This polymer is of interest due the fact that it is biocompatible and biodegradable and suitable for biomedical applications like transdermal/topical drug delivery.

We have made an attempt here to synthesize for the first time the HM-EHEC based microgels for releasing the anti cancer drug for site specific/targeted delivery at the tumor site.

## 3.2 Materials and Methods

Hydrophobically Modified Ethyl Hydroxy Ethyl Cellulose (HM-EHEC, MW 1200KDa, Akzonobel, Sweden under the trade name of Bermocoll (EHM-500) was used for the preparation of the microgels. Divinyl Sulphone (DVS) was used as a cross linker having molecular weight of 118.16 g/mol was purchased from Sigma Aldrich, India. The hydrophilic anti-cancer drug,5-Flurouracil (5-FU) having a molecular weight of 130.07g/mol was purchased from Sigma Aldrich with CAS number 51-21-8, and was used in the controlled release studies in the phosphate buffer saline (PBS) solution. The obtained HM-EHEC was extracted with acetone for 1 day at room temperature to remove any organic soluble fat. The polymer was then dried and 1.0 wt% aqueous solutions was made. These solutions were centrifuged at 8000 rpm for 40 minutes and the supernatant clear liquid was dialyzed against water using a dialysis bag of 12000 MW cut off (MWCO). The dialysis was carried out for

24 h by frequently changing the external water. The dialyzed solutions were freeze dried to get pure polymer of HM-EHEC.



$$EHEC: R = H$$
$$HM\text{-}EHEC: R = -\left(CH_2-CH_2-O\right)_x C_6H_4-C_9H_{19}$$
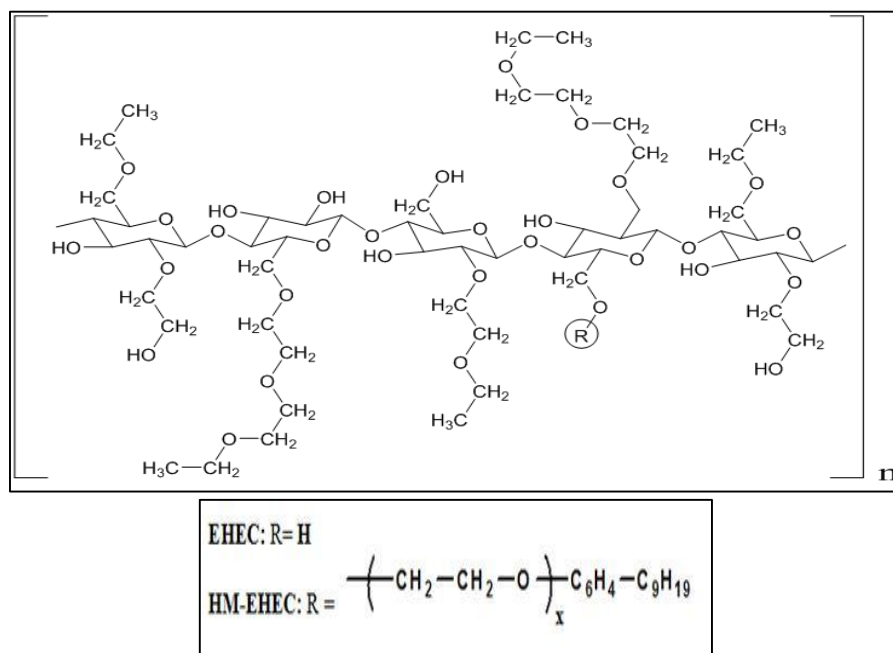
**Figure 3.1:** Chemical structure of HM-EHEC.

Toluene, having molecular weight of 92.141 g/mol was the solvent used for microgel synthesis. All the chemicals used were of analytical grade. The cell viability studies were done using the MDA MB 231 human breast cancer cell lines to check the efficacy of 5-FU anti cancer drug on cancer cells. Distilled water was used throughout the experiment.

## 3.3 Experimental Section

The hydrophobically modified ethyl hydroxy ethyl cellulose (HM-EHEC) microgels were synthesized using water in oil (W/O) emulsion polymerization technique. The HM-EHEC polymer (0.5%) was dissolved in 0.1 M NaOH solution. The toluene/water mixtures taken were in the ratio of 3:1, i.e. 30 ml of toluene + 10 ml water. The 10 ml HM-EHEC polymer solution was added slowly to the three neck jar containing toluene-water mixture connected to a water bath. The stirring speed was maintained at 1000 rpm. Within a few minutes of stirring, the toluene water mixture containing polymeric solution turned milky white in colour.[7, 8] The initial temperature of the water bath was

25 $^0$C. When the bath temperature reached 15 $^0$C, then 30% (w/w) of divinyl sulphone (DVS) crosslinker was added slowly during the continous stirring. The Micheal addition reaction of crosslinking takes place between divinyl sulphone (DVS) and the cellulose polysaccharide is shown in **fig 3.2.** The reaction of divinyl sulfone (DVS) with polysaccharides usually lead to cross linked products due to nucleophilic hydroxyl/amino groups attacking the electrophilic double bond of DVS by Michael-type addition.[9] The reaction mixture was kept for 24 hours for complete polymerization and then the reaction mixture was cooled at room temperature. A thick white precipitate was observed. The precipitate was further washed several times with distilled water and centrifuged and the microgels obtained were kept in vacuum oven for overnight drying. The microgel particles re-suspended in aqueous media and were later freeze dried and the obtained microgel powder used for the further studies.
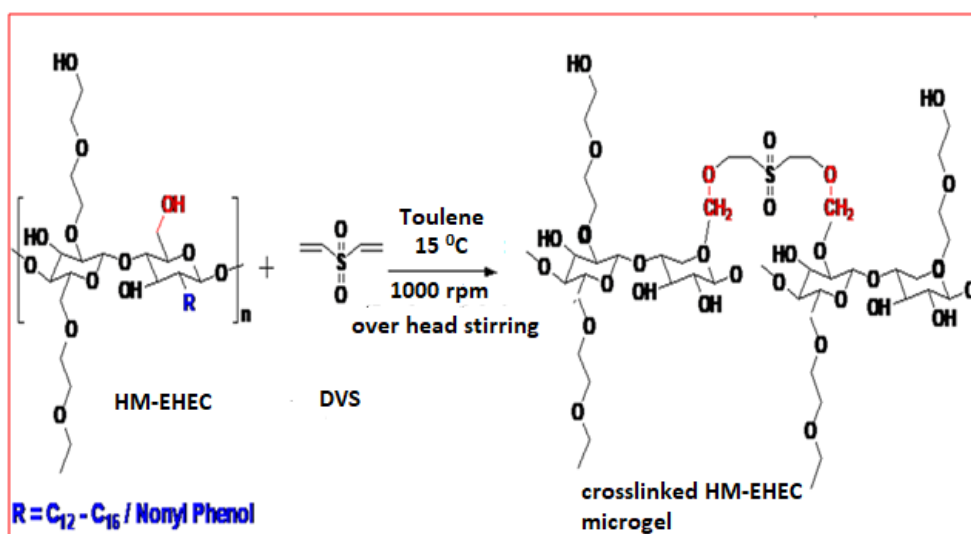


**Figure 3.2:** Reaction scheme for formation of microgels.

The reaction scheme for the synthesis of HM-EHEC microgels is shown in the **fig 3.2** and the experimental cartoon is shown in **fig 3.3**. Microgels are obtained at lower polymer concentration and at higher concentrations we observe bulk gels or macrogels and not microgels. We observed at higher polymer concentrations of 1, 1.5 and 2 % (w/v), microgel paticles were in micron size (micro-beads) and ranged from 20 to 30 μm. Therefore, the

polymer concentration was fixed at 0.5% (w/v) for the synthesis of microgel particles as our aim was to obtain f 2 to 10 micron sized particles. The DVS crosslinking density was fixed at (30% w/w). The effect of different crosslinking densities on the size of the micro particles were not studied since it was our first attempt and we focused on the preparation and synthesis of microgels in the first place.
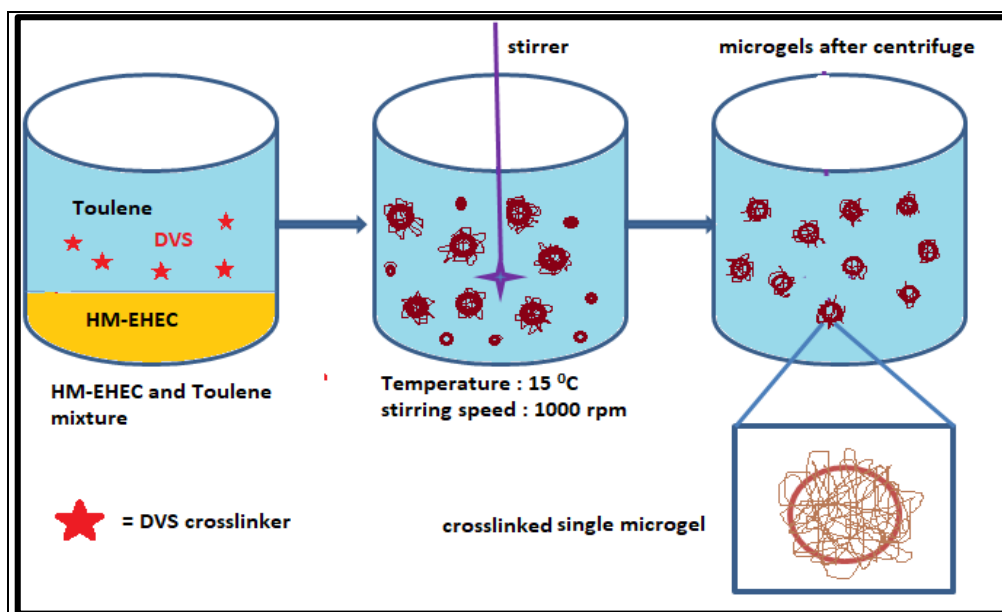


**Figure 3.3:** Water in Oil (W/O) emulsion technique for microgel synthesis.

The increase in the crosslinking density would produce rather hard and rigid microgels which would not be so effective for our application and moreover the drug loading and the swelling capacity would be varied. However lower concentrations of 5, 10 and 20% (w/w) of DVS crosslinker were tried but from the SEM images we it was clear that there was no uniform formation of the microgels, rather coagulation and aggregation of the particles was observed.

## 3.4 Characterization Techniques

### 3.4.1 Scanning Electron Microscopy (SEM)

The morphology of the nanofibers was studied using Scanning Electron Microscopy quanta 200 3D dual beam ESEM (FEI, Finland). The electron source was tungsten (W) filament with thermionic emission at 15 kV in high

vacuum. Before SEM imaging, the microgels were sputter coated with a thin layer of gold.

### 3.4.2 Fourier Transform Infra-red spectrometer (FT-IR)

The IR spectra of the nanofiber mats were recorded on Perkin Elmer Instruments, Spectrum One, FT-IR spectrometer. The recording was done in a diffused reflectance mode in the wavelength range of 400 to 4000 cm$^{-1}$. The samples were mulled with KBr powder and the background scan was done with pure KBr (Potassium Bromide) disc for recording the spectra.

## 3.5 Biological Studies

### 3.5.1 In-Vitro 5-FU Drug Release

The 5-Flurouracil drug release from the microgels was studied in phosphate buffer saline (PBS). A 15 ml phosphate buffer solution (PBS) was taken, in test tube which was covered with an aluminium foil and kept in a shaker bath (Julabo SW 23) with gentle shaking at 37$^0$C. Known quantities of microgel particles(5mg) containing 5-FU were placed into the test tube. At predetermined time intervals, 1 ml of PBS was taken and replenished with an equal volume of fresh PBS into the test tube. The amount of 5-FU released was determined by UV-Vis spectrometer (UV-160 PC Shimadzu) at a maximum absorbance wavelength $\lambda_{max}$ of 266 nm.[10] The percentage drug release was calculated in PBS at 7.4 pH. The release experiments of each sample were performed in triplicates and the average values were reported. The encapsulation efficiency was calculated using equation.

$$\text{Encapsulation efficiency } (\%) = \frac{\text{mass of maximum drug released}}{\text{mass of total drug released}} * 100$$

### 3.5.2 In-Vitro cyto-toxicity study

The cyto-toxicity study of the HM-EHEC microgels were performed on the MD-MBA 231 human breast cancer cell line, using MTT 3-(4,5-dimethylthiazol-2-yl)-2,5-diphenyltetrazolium bromide) assay. The cancer cells were obtained from National Centre for Cell Science (NCCS), Pune, India. The cells ($4\times10^4$) were seeded in 24-well, flat bottom culture plate and

incubated for 24 h. After incubation, the MTT solution (10 mg/ml of stock solution of which 20μl of MTT solution was added in 100μl of DMEM media) was added to each well followed by further incubation at $37^0$C for 4 h. The formazan crystals formed were dissolved by addition of acidified isopropanol. After 15 min, the amount of coloured formazan derivative formed was determined by measuring the optical density (OD) using a microplate reader (Spectra Max, MS; Molecular Devices, LCC) at 570 nm. Microscopic images of the well plates were obtained at 0 and 24h as control and treated samples. All the experiments were done in triplicates. The percentage cell viability was calculated by the equation as given below:

$$\% \text{ Cell viability} = \frac{(OD)\text{sample} - (OD)\text{blank}}{(OD)\text{control} - (OD)\text{blank}} * 100$$

## 3.6 Result and Discussion

### 3.6.1 Scanning Electron Microscopy (SEM)

The SEM images of the HM-EHEC microgels are shown in **fig 3.4**. The SEM micrographs shows that the microgels are spherical in shape having a coarse surface.
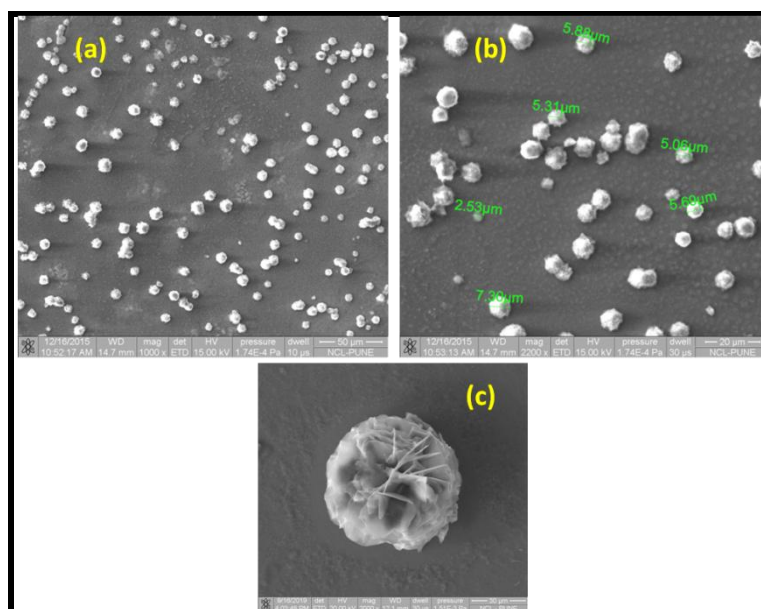


**Figure 3.4:** SEM images of HM-EHEC microgels.
(a) Scale bar: 50μm; magnification 1000 X (b) Scale bar: 20μm;
magnification 2200 X (c) Scale bar: 30μm; magnification 2000 X.

The microgels are seen well dispersed and the average diameters of the microgels are in the range of 5 to 8 µm. The images show a spherical flower like morphology using the HM-EHEC polymer. This morphology was checked and repeated several times and the same flower like morphology was obtained each time. The emulsion technique used for microgel synthesis using the natural water soluble biopolymer namely HM-EHEC connects the hydroxyl groups in the cellulose by forming a 3D hydrophilic network via a covalent bond by crosslinking with di vinyl sulphone (DVS) which might have helped in obtaining flower-like morphology.

### 3.6.2 Fourier Transform Infra-red Analysis (FT-IR)

The structural changes in the microgels were confirmed by the FT-IR analysis after the incorporation of 5 FU anti-cancer drug. The prominent peaks of 5-FU were quite diminished due to the fact that encapsulated drug existed in the amorphous state into the microgel matrix. The figure 3.5 below shows the spectra, where a broad band between the 3136 cm$^{-1}$, is attributed to the N-H stretching vibrations of 5-FU.
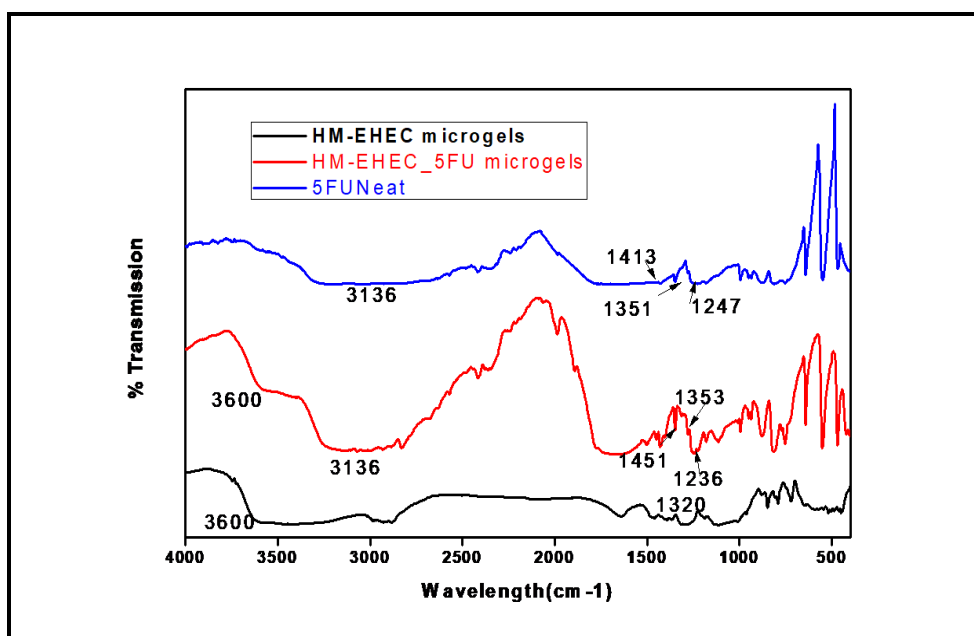


**Figure 3.5:** FT-IR spectrum of HM-EHEC microgels along with 5-FU.

The peak at 1413 cm$^{-1}$ was belong to C-F stretching band in the spectrum of 5-FU. The peak at 1247 cm$^{-1}$ is due to C-N stretching vibrations of 5-FU. The

peak at 1351 cm$^{-1}$ refers to vibration of pyrimidine compound confirming 5-fluorouracil. The peak at 1320 cm$^{-1}$ refers to the stretching vibration of S=O and which is merged with 1351 cm$^{-1}$ with the 5-FU drug.[11, 12]

### 3.6.3 Drug release of 5-Flurouracil (5-FU)

Microgels have been used as drug delivery vehicles for low molecular-weight to bio-macromolecules. The binding of these drugs is greatly influenced by the local crosslink density and the functional group distribution within the microgel.[13] The in-vitro release profile of the drug 5-FU is shown below in figure 3.6. The 5-FU drug release studies were carried out at 37 $^{0}$C. The microgel samples (5 mg) were incubated in a PBS solution in an incubator with a shaking speed of 200±10 rpm. The encapsulation efficiency was found to be 95% (passive loading). The initial burst release was accounted for 20% ±2 during the first 2 hour of the release study. The total amount of the drug released in the next 72 hours was found to be around 56%.
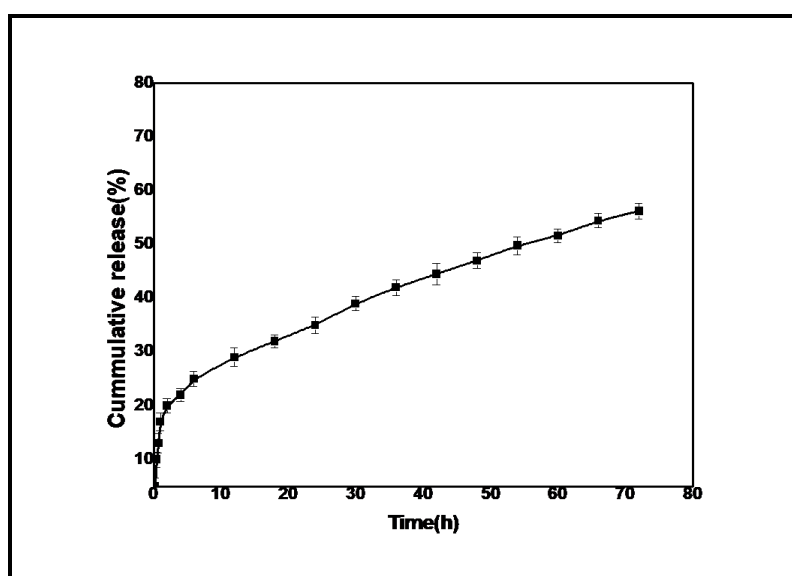


**Figure 3.6:** Drug release of 5-FU from the HM-EHEC microgels.

In the process of loading the drug into the microgel system, there could have been some losses and therefore the real encapsulation efficiency could have been higher than the actual percentage of the drug loaded. Never the less, a slow and controlled release of 5-FU was observed over the time. The uneven

distribution of the drug in microgels often results in initial burst effect for few minutes and then exhibiting slow and sustained release for several days to weeks.[14]

### 3.6.4 Cell viability studies (MTT Assay)

The cell viability of human breast cancer cell line was studied for the toxicity effect by the 5-FU drug. The MDA MB 231 cells ($4 \times 10^4$) were seeded into 96-well plate and incubated further at 37ºC. These cells were either treated or untreated with microgels containing the 5-FU for 24 hours. After 24 hours the cells were incubated with MTT (0.5mg/ml) for 4 hours to form the formazan crystals. The formazan crystals formed were dissolved in isopropanol and the absorbance was measured at 570 nm in ELISA reader (Thermo Scientific).
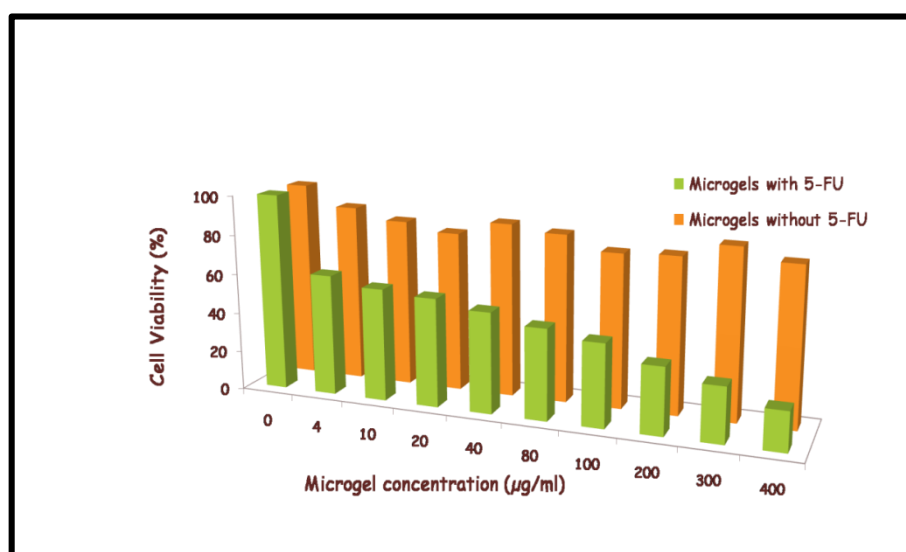


**Figure 3.7:** MTT Assay for HM-EHEC microgels with and without 5-FU.

| a) **Untreated with 5-FU** | b) **Treated with 5-FU** |
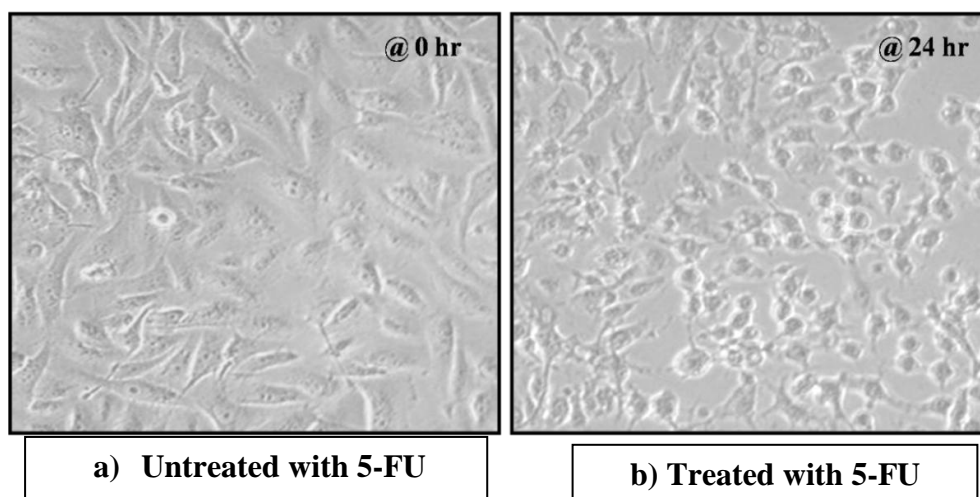
**Figure 3.8:** Confocal Microscopy images of MDA-MB 231 cancer cells.

All the experiments were performed in triplicates, analyzed statistically and represented graphically in the form of bar chart as shown in the **fig 3.7**. The cancer cell line photographs before and after treatment were taken using Image Pro plus 6.0 software under phase contrast microscope (Nikon) with magnification 20 X  and shown in  **fig 3.8**. The images reveal that before the treatment, the cells maintained their morphology and after the treatment with 10μg/ml microgels containing 5-FU, the cells lost their elongated spindle shape morphology and were seen round in shape after 24 hours which indicates the cell death.[15] The cell proliferation was inhibited and cell death occurred due to the anti-cancer drug. More cell deaths were observed with increase in time and concentration of the microgel loaded 5-FU.

## 3.7 Conclusions

In this chapter, we aimed at synthesizing polymeric based microgels for topical drug delivery of an anti-cancer drug for a site specific application on the skin. We could successfully synthesize the HM-EHEC microgels by using water in oil emulsion technique. The average size of the microgles was found to be in the range of 5 to 8 μm. The microgels were spherical in shape and uniformly distributed with a flower-like morphology. The 5-Flurouracil drug was incorporated into the microgel matrix which was confirmed by FT-IR analysis. The anti-cancer drug loading efficiency was 95% for the 5% drug incorporation.  The study revealed the initial burst release for 2 hours where

20% of the total drug loaded was released and then there was a slow and controlled release of 56% drug observed upto the next 72 hours. The MTT assay was done using the MDA-MB 231 breast cancer cell line to check for the cell viability and cyto-toxicity of 5-FU on the cell lines. The cell death increased with the microgel concentration and it was observed that 50% cell death occurred when 100μg/ml of microgel concentration which contained around 12μg/ml of 5-FU. The microscopic images of the treated and untreated microgels also exhibited the cell death of the cancer cells.

## 3.8 References

**1.** Bray, F.; Ferlay, J.; Soerjomataram L.; Siegel R.L.; Torre L. A.; Jemal A. Global cancer statistics 2018: GLOBACAN estimates of incidence and mortality worldwide for 36 cancers in 185 countries. *CA Cancer J. Clinc.* 2018, 68: 394–424.

**2.** Cancer Incidence and Mortality Worldwide. International Agency for Research on Cancer; Lyon, France: 2011.

**3.** Oh, J. K.; Lee, D.; Park, J. Biopolymer-Based Microgels/Nanogels for Drug Delivery Applications. *Prog. Polym. Sci.* 2009, 34, 1261–1282

**4.** Jacob, Joby; Haponiuk, Józef; Thomas, Sabu; Gopi, Sreeraj. Biopolymer Based Nanomaterials In Drug Delivery Systems: A Review. *Materials Today.* 2018, 9, 43-55.

**5**. Khanal, A.; Bui, M P.; Seo, S S. Microgel-encapsulated methylene blue for the treatment of breast cancer cells by photodynamic therapy. *J Breast Cancer.* 2014, 17(1):18-24. 18–24.

**6.** Martinelli, C.; Pucci, C.; & Ciofani, G. Nanostructured carriers as innovative tools for cancer diagnosis and therapy. *APL bioengineering.* 2019, 3(1), 011502.

**7.** Bonham, J. A.; Faers, M. A.; Van Duijneveldt, J. S. Non-Aqueous Microgel Particles: Synthesis, Properties and Applications. *Soft Matter.* 2014, 10 (47), 9384–9398.

**8.** Brugger, B.; A. Rosen, B.; Richtering, W. Microgels as Stimuli-Responsive Stabilizers for Emulsions. *Langmuir.* 2008, 24 (21), 12202–12208.

**9.** Hahn, S. K.; Jelacic, S.; Maier, R. V; Stayton, P. S.; Hoffman, A. S. Anti-Inflammatory Drug Delivery from Hyaluronic Acid Hydrogels. *J. Biomater. Sci. Polym. Ed.* 2004, 15 (9), 1111–1119

**10.** Ortiz, R.; Prados, J.; Melguizo, C.; Arias, J. L.; Adolfina Ruiz, M.; Álvarez, P. J.; Caba, O.; Luque, R.; Segura, A.; Aránega, A. 5-Fluorouracil-Loaded Poly(ε-Caprolactone) Nanoparticles Combined with Phage E Gene Therapy as a New Strategy against Colon Cancer. *Int. J. Nanomedicine.* 2012, 7, 95–107.

**11.** Olukman, M.; Şanlı, O.; Solak, E. K. Release of Anticancer Drug 5-Fluorouracil from Different Ionically Crosslinked Alginate Beads. *J. Biomater. Nanobiotechnol.* 2012, 03 (04), 469–479.

**12.** Kanth, V. R.; Kajjari, P. B.; Madalageri, P. M.; Ravindra, S.; Manjeshwar, L. S.; Aminabhavi, T. M.; Vallabhapurapu, V. S. Blend Hydrogel Microspheres of Carboxymethyl Chitosan and Gelatin for the Controlled Release of 5-Fluorouracil. *Pharmaceutics.* 2017, 9 (2), 1–13.

**13.** Smeets, N. M. B.; Hoare, T. Designing Responsive Microgels for Drug Delivery Applications. *J. Polym. Sci. Part A Polym. Chem.* 2013, 51 (14), 3027–3043.

**14.** Klinger, D.; Landfester, K. Stimuli-Responsive Microgels for the Loading and Release of Functional Compounds: Fundamental Concepts and Applications. *Polymer.* 2012, 53 (23), 5209–5231.

**15.** Razak, N. A.; Abu, N.; Ho, W. Y.; Zamberi, N. R.; Tan, S. W.; Alitheen, N. B.; Long, K.; Yeap, S. K. Cytotoxicity of Eupatorin in MCF-7 and MDA-MB-231 Human Breast Cancer Cells via Cell Cycle Arrest, Anti-Angiogenesis and Induction of Apoptosis. *Sci. Rep.* 2019, 9 (1), 1–12.

# CHAPTER IV

# Design and Fabrication of Ethyl Hydroxy Ethyl Cellulose (EHEC) Nanofibers for Tissue Engineering Applications

*Research is to see what everybody else see's and to think what nobody has thought.*

*Albert Szent Gyorgyi*

## 4.1 Introduction

Electrospinning (ES) has emerged as an excellent technique to prepare very fine (in the range of micrometer to nanometer) continuous polymer fibers with different morphologies by subjecting polymer solutions to an external electric field. These electrospun nanofibers exhibit high surface to volume ratio, high porosity compared to conventional fibers, and find wide range of applications in tissue engineering scaffolds, drug delivery[1,2], sensors[3] , nanocomposites[4] , energy storage[5] etc. Large numbers of synthetic polymers have been electrospun for the above applications. For the medical applications, biopolymer based fibers are particularly important due to their inherent nature of biocompatibility and biodegradability.[6,7,2] In this context, the feasibility of electrospinning of polysaccharides such as chitosan[8], cellulose[9], hyaluronic acid[10], dextran[11], pullulan[12], starch[13] etc, have been reported in the literature. Although electrospinning appears to be a simple and versatile technique, the parameters such as conductivity, surface tension, and flow rate, concentration of the polymer solution, applied voltage, distance between syringe tip and the collector plate play an important role in nanofiber spinning.[14]

Non-ionic cellulose ethers namely ethyl hydroxy ethyl cellulose (EHEC) and hydrophobically modified ethyl hydroxy ethyl cellulose (HM-EHEC) are important polysaccharides and find wide applications as thickening/rheology control agents in paints, cosmetics, detergents and oil recovery.[15] Extensive work on rheology of these polymers has been reported.[16] They are non-toxic, biocompatible and biodegradable, and hence also find applications in biomedical field. These polymers cause neither irritation to the skin nor any allergic reaction.[17] Therefore, they have been used in nasal and ophthalmic drug delivery systems.[18] Ethyl hydroxy ethyl cellulose (EHEC), based thermo-responsive hydrogels in combination with lysine surfactants enhance the biocompatibility of hydrogels.[19] To the best of our knowledge, there are no reports on the electrospining of these polysaccharides.

Poly (vinyl alcohol) (PVA) is a highly hydrophilic, non-toxic and biocompatible semi-crystalline polymer with excellent properties such as strength, water solubility, gas permeability and thermal characteristics.[20] It is a synthetic polymer with good mechanical properties as well as biomedical

properties. PVA has good chemical and physical stability[21] and has the ability to form fibers, films and membranes. Further, this polymer can be easily crosslinked[22, 23] to make variety of hydrogels.

In this chapter, we report on the electrospinning of EHEC, HM-EHEC and their blends with PVA. We have chosen PVA as a co-spinning agent due to its good spinnability. The spin-coating of aqueous solutions of EHEC, HM-EHEC and their blends with PVA on silicon wafers was carried out at different rotation speeds. The surface topography of these spin-coated films and electrospun fibers were observed by atomic force microscopy (AFM) and scanning electron microscopy (SEM). Water droplet contact angles were measured to show the wetting nature. The nanofiber mats were in-situ crosslinked using citric acid and thermal treatment. The controlled release of a model drug, Chlorhexidene Digluconate (ChD), from the EHEC nanofiber mats was investigated. The cell viability, growth and proliferation on these nanofiber mats were also studied using L929 mouse fibroblast cells.

## 4.2 Material and Methods

EHEC and HM-EHEC polymers were obtained from Akzo-Nobel Functional Chemicals AB, Sweden with the trade names of Bermocoll E411 FQ and EHM-500, respectively. Their molecular weight (MW) was ~ 1200 Kg/mole with about 7000 anhydro glucose units (AGU). In the HM-EHEC, the hydrophobic modification (0.6 % of glucose units) was performed with nonyl phenol groups and this is as reported by the supplier. The chemical structures of the polymers used are shown below in **fig 4.1**. PVA was obtained from Kurary Co., Ltd., Japan with the trade name of PVA-117. The MW and degree of saponification were 75 Kg/mole and 97-98% respectively. Chlorhexidine Digluconate (ChD) solution (CAS No. 18472-51-0) was purchased from Sigma-Aldrich (India) as 20% in water (solubility: >50% in water at 20°C).
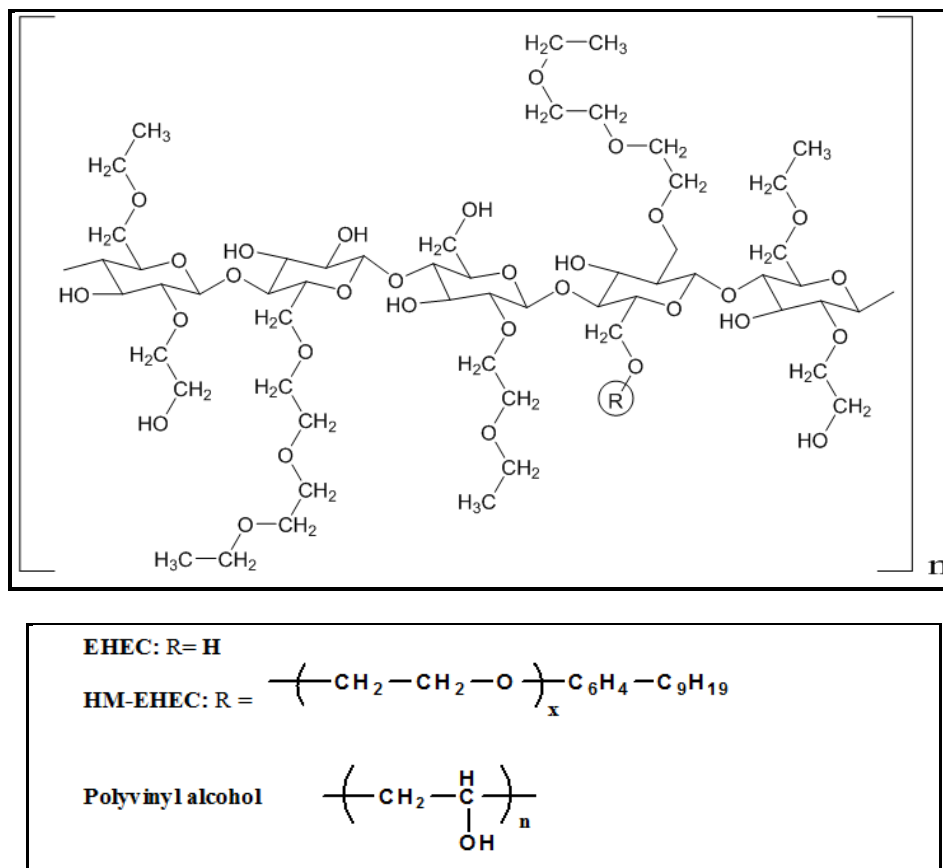
**Figure 4.1:** Chemical structures of EHEC and PVA.

Citric acid, anhydrous pure with molecular weight 192.12 g/mol were purchased from Merck Limited, India. EHEC and HM-EHEC were purified before using and PVA was used as received.

## 4.3 Experimental Section

### 4.3.1 Purification of EHEC and HM-EHEC

EHEC and HM-EHEC (dry powders) were extracted with acetone for 1 day at room temperature to remove any organic soluble fat. The polymers were then dried and 1.0 wt% aqueous solutions were made. These solutions were centrifuged at 8000 rpm for 40 minutes and the supernatant clear liquid was dialyzed against water using a dialysis bag of 12000 MW cut off (MWCO). The dialysis was carried out for 24 h by frequently changing the external water. The dialyzed solutions were freeze dried to get pure polymers.[24]

## 4.3.2 Solution preparation

The EHEC and HM-EHEC solutions of 1.0 % (w/v) were prepared in Tetrahydrofuran (THF) and water mixture in THF/water = 2/1 ratios. Solutions of EHEC/PVA and HM-EHEC/PVA of 1.0 %( w/v) having 1:1 ratio in THF/water were also prepared in the same way. For the in-situ crosslinking of nanofibers, citric acid (20 wt% based on the polymer) was added into the polymer solutions before electrospinning.

## 4.3.3 Spin-coating

The spin-coating of aqueous solutions of 1.0 % (w/v) of EHEC, HM-EHEC and blends of EHEC and HM-EHEC/PVA was performed on silicon wafer of 10 mm x 10 mm square. 80 µL solution was used and spin-coating was carried out for 90 seconds at a rotation rate of 4500 rpm. The spin-coated films were dried at $45^{\circ}$C under vacuum for 1 day before taking them for contact angle measurement and AFM observation.

## 4.3.4 Electrospinning

Electrospinning of solutions of EHEC, HM-EHEC and their blends with PVA in THF/water mixture [2/1(v/v)] at the polymer concentration of 1.0 % (w/v) was carried using a NANON-01A (MECC Co., Ltd., Japan) electrospinning device. Both plate collector (static) and disc collector (rotating at 1000 rpm) were used to collect the fibers. The polymer solution was loaded into a syringe and discharged from the spinneret (0.5mm diameter) at a flow rate of 0.2 ml/hr. The applied voltage was 27 kV and the distance between the spinneret and the plate collector was 15 cm. All the electrospinning experiments were performed at ambient temperature. The nanofibers were collected on an aluminium foil attached to the plate collector. The electrospinning was also performed using aqueous solutions with high concentrations of EHEC polymer. The nanofiber mats of EHEC/PVA [10 % (w/v)] prepared using citric acid, were thermally treated at $90^{\circ}$C for 3 h to induce crosslinking.

## 4.4 Characterization Techniques

### 4.4.1 Scanning Electron Microscopy (SEM)

SEM images of the electrospun fibers of EHEC, HM-EHEC, EHEC/PVA and HM-EHEC/PVA using 1.0% (w/v) prepared in THF/water, were obtained using a Real Surface View VE 7800 (Keyence Co., Ltd., Osaka, Japan) with an applied voltage of 5 kV. A small piece of aluminium foil on which the electro-spun fibers were collected was cut and mounted on a SEM sample holder. It was then coated with a thin osmium layer using HPC-1SW Hollow Cathode Plasma CVD (Shinkuu Device Co., Ltd., Mito, Japan) to prevent sample from charging. The electrospun fibers of EHEC/PVA using 10 % (w/v) prepared in aqueous medium were coated with gold layer for the SEM analysis using Quanta 200 3D (FEI, Finland), dual beam having electron source of tungsten (W) filament with emission at resolution of 20 kV in high vacuum.

### 4.4.2 Atomic Force Microscopy (AFM)

AFM images were obtained on a scanning force microscopy (SPA400, Hitachi High-Tech Science Corporation, Tokyo, Japan) in the intermittent tapping mode with 20 µm x 20 µm scanner. A back-side aluminium-coated rectangular cantilever with a force constant of 35-40 N/m and a resonance frequency of 320-400 kHz (SI-DF40, Hitachi High-Tech Science Corporation, Tokyo, Japan) were used.

### 4.4.3 Contact Angle measurements (CA)

The static contact angles were measured with a drop-shape analysis system, Theta T-200 Auto3 (Biolin Scientific, Stockholm, Sweden), equipped with a video camera. A 2 µL water droplet was placed on the surfaces and the static contact angles were recorded.

### 4.4.4 Viscosity, surface tension and conductivity measurements

The zero-shear viscosity of EHEC, HM-EHEC, EHEC/PVA and HM-EHEC/PVA solutions were measured on Anton Paar MCR-301 rheometer with a cup-and-bob geometry, CC17, Sr. No. 28342 (cup internal diameter = 18 mm, bob diameter = 16 mm, gap length of bob = 25 mm). In the steady

state mode, the shear rate was varied from 0.01 to 100 s$^{-1}$ at 25 $^0$C. The data was analyzed using Carrau fit model.

### 4.4.5 Fourier Transform Infra-Red spectrometer (FT-IR)

The IR spectrum was recorded on Perkin Elmer Instruments, Spectrum One, FT-IR spectrometer. The recording was done in the wavelength range of 400 to 4000 cm$^{-1}$. The background scan with air was used for recording the spectra. The pristine EHEC was mixed with KBr and a pellet was prepared. The EHEC/PVA nanofiber mat was scanned in ATR mode in the same wavelength range.

## 4.5 Drug release study

Chlorhexidine Digluconate (ChD) was incorporated in the EHEC/PVA nanofibers to study the drug release profile in a 7.4 pH phosphate buffered solution (PBS). EHEC/PVA nanofiber mats with 5, 10 and 15% loading of ChD were immersed in 15 mL PBS at 37°C in test tubes and covered with aluminium foils and placed in a shaker bath (Julabo SW 23) with gentle shaking. At predetermined time intervals, 1 ml of PBS was taken by a micropipette and replaced with an equal volume of fresh PBS into the test tubes. The amount of Chlorhexidine Digluconate released in the supernatant solution was measured by a UV–Vis spectrophotometer (UV-1601 PC, SHIMADZU) at a wavelength of 256 nm.[25] All the UV experiments were done in triplicates and the average values were taken.

## 4.6 Biological Studies

### 4.6.1 Cell Viability study

The nanofiber mats were sterilized for 20 minutes by autoclaving. Samples were carefully transferred to a sterile untreated 24 well plate. Healthy L929 fibroblast cell lines (passage number 54) were maintained and 40,000 cells were placed in each well of the 24 well plate. The cells were incubated in 5% $CO_2$ at 37°C for 1, 2, 3 days respectively. On each day to the samples in the well plate, 100 μl of 600 μM resazurin solution (in complete DMEM media) was added. It was incubated for 6 hours in 5% $CO_2$ at 37°C. From each well 100 μl media was taken out and read in a plate reader (excitation 530 to 560

nm and emission at 590 nm). The % mitochondrial activity was calculated using the formula (E570 of cells on mat/E570 of only cells)*100, where E is the emission and 570 is the wavelength. Data shown are mean ±standard error of n=3. While calculating the emission, a correction of 100 µM resazurin in complete DMEM solution was incorporated.

### 4.6.2 Fluorescence microscopy and SEM Imaging

Healthy murine fibroblasts L929 were maintained using 10% FBS/DMEM. Nanofiber mats after UV sterilization for 15 minutes inside a biosafety cabinet were placed in 24 well plates. 50,000 cells were seeded in the each well plate. After 48 hours incubation in 5% $CO_2$ at 37°C, the cells were washed twice with PBS and fixed with 4% paraformaldehyde. The nanofiber mats were then treated with 5% Bovine Serum Albumin (BSA) along with 0.1% Triton-X in PBS for 1h, and further washed with PBS again. Cells were sequentially treated with DAPI (4', 6-diamidino-2-phenylindole) and 6-Carboxyfluorescein for 10 minutes in dark at room temperature along with a thorough washing with PBS after each treatment. The nanofiber mat was then placed 'face down' on clean slides with the help of mounting media (Fluoroshield, SigmaAldrich). Cells were visualized using an epifluorescence microscope from Carl Zeiss, AX10 Observer Z1, S.No. 3851000678. An objective of 10X was used to visualize the cells under microscope. Nucleus and cytoplasm were observed using blue and green filters at 358 nm and 495 nm absorption wavelength respectively.

For the SEM imaging of the fibroblast L929 cells, another $5x10^4$ cells were incubated. After 48 hours of incubation at cell culture conditions, the cells were washed twice with PBS. The mats were incubated with 3% glutaraldehyde in PBS for overnight at 4°C. The mats were washed with PBS followed by sequential washing for 10 minutes with different ethanol/water solutions namely 10/90, 30/70, 50/50, 70/30, 90/10 and 100/0 which was followed by air-drying overnight at room temperature. The nanofiber mats were then gold sputtered and taken for imaging.

## 4.7 Results and Discussion

### 4.7.1 Spin-coating of polymer solutions onto silicon wafers

The spin-coating of EHEC, HM-EHEC and EHEC/PVA, HM-EHEC/PVA solutions 1.0 % (w/v) in THF/ water mixture [2/1(v/v)] was done on silicon wafers at 3-different rotation speeds (1500, 3000 and 4500 rpm). The thickness and surface roughness were measured by AFM topographic images and are shown in **table 4.1**.

**Table 4.1:** Thickness and surface roughness of EHEC spin-coated films[a].
[a] Solution of EHEC in THF/water (2/1 (v/v))
1.0 % (w/v) was spin-coated on silicon wafer substrate.

| Parameters | Rotation speed (rpm) | | |
|---|---|---|---|
| | 1500 | 3000 | 4500 |
| Thickness (nm) | 83 | 103 | 75 |
| Surface roughness (nm) | 3.6 | 2.8 | 1.7 |

Although the thickness was independent on the rotation speeds, the surface roughness decreased with increasing rotation speed. Therefore, the spin-coating films prepared at 4500 rpm rotation speed were used in all the subsequent experiments to get the uniform roughness of the coatings.

### 4.7.2 Electrospinning of EHEC/PVA solution

Electrospinning of polymer solutions strongly depends on the concentration, viscosity, conductivity and the surface tension of the polymer solution. These parameters need to be optimized in order to get stable charged jet and uniform fiber geometry. Further, the operational conditions such as, applied voltage, flow rate and the distance between the tip and the collector have to be carefully adjusted to produce uniform fibers. The mixture of THF and water (THF/water = 2/1 (v/v)) was used as solvent to balance the surface tension and solubility, and the optimum operating conditions were explored by figuring out the fiber geometry through SEM and AFM observations.
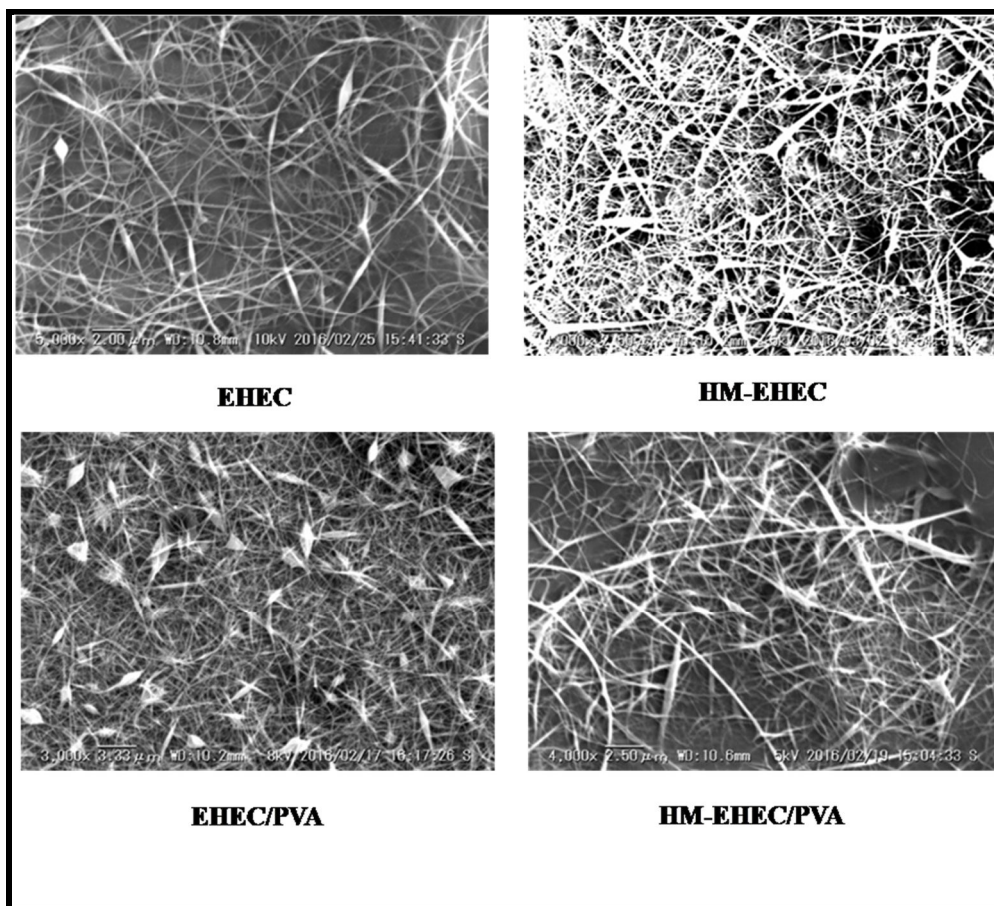
**Figure 4.2:** SEM images of electrospun nanofibers of EHEC,
HM-EHEC, EHEC/PVA & HM-EHEC/PVA.

SEM images of EHEC, HM-EHEC, EHEC/PVA and HM-EHEC/PVA fibers are shown in **fig 4.2**. All the polymers showed the spinnability into fibers. EHEC showed long, uniform fibers with a diameter in the range of 0.5-1.0 µm. While HM-EHEC produced short, interconnected fibers with a small number of beads in the fibers. HM-EHEC required a slightly higher voltage and lower feed rate for the stable electrospinning. Upon blending EHEC and HM-EHEC with PVA, the spinnability was improved, and a dense fiber network with fine fibers was produced. However, significant number of beads were observed in the case of 1.0% (w/v) EHEC/PVA fibers. The solution properties namely viscosity, conductivity and surface tension of these solutions were measured and summarized in **table 4.2**

**Table 4.2:** Zero Shear viscosity, Surface tension and Conductivity measurements of EHEC, HM-EHEC, EHEC/PVA, and HM-EHEC/PVA in THF/Water.

| Sample name | Zero shear viscocity ($\eta_0$) ( Pa.s) | Surface Tension (mN/m) | Conductivity (mS/cm) |
|---|---|---|---|
| EHEC (1%) | 2.43 | 43.86 | 0.30 |
| EHEC (1.5%) | 13.47 | 47.98 | 0.36 |
| HM-EHEC 1% | 4.45 | 38.85 | 0.34 |
| HM-EHEC (1.5%) | 37.46 | 57.55 | 0.50 |
| EHEC-PVA (1%) | 0.13 | 34.29 | 0.21 |
| EHEC/PVA (1.5%) | 0.59 | 36.73 | 0.30 |
| HMEHEC/PVA (1%) | 0.17 | 33.62 | 0.21 |
| HMEHEC/PVA (1.5%) | 1.51 | 39.37 | 0.32 |

The viscosity, surface tension and conductivity of the solution play an important role and can influence the ability to electrospin the nanofibers. From the above table, the zero shear viscosity for 1% EHEC was 2.43 Pa.s and by the addition of PVA was decreased to 0.13 Pa.s. In case of 1.5% EHEC the viscosity recorded was 13.47 Pa.s and later decreased to 0.59 Pa.s when PVA was added. In case of HM-EHEC, the viscosity was found to be 1.45 Pa.s for 1% and decreased to 0.17 Pa.s by PVA addition. We observed in case of 1.5% HM-EHEC, the viscosity was 37.46 Pa.s and eventually decreased to 1.51 Pa.s with PVA addition. The decrease in the viscosities by the addition of PVA was due to its hydrophilic nature. The surface tension and the conductivities also decreased with the increase in the concentration of EHEC and HM-EHEC from 1% to 1.5%. From the above data, we could conclude that due to the lower concentration of EHEC and HM-EHEC, the viscosities weren't enough to get beadless nanofibers as indicated in the **fig 4.2**, because a critical solution viscosity is needed to maintain molecular chain entanglement to form fibers during the electrospinning process. Although the solution viscosity will

depend on the polymer used for spinning and other factors and typical values of viscosity are reported in the range of 0.5-2 Pa·s. In order to check the spinnability of EHEC into oriented fibers, we performed electrospinning of EHEC solution (1.0 wt %) in THF/water mixture [2/1 (v/v)] using rotating disc collector. SEM images of electrospun fibers obtained using static plate

collector and rotating disc collector are shown in **fig 4.3 (a)** and **(b)**. The electrospun fibers were well aligned in rotational direction to give uniaxially aligned nanofibers.
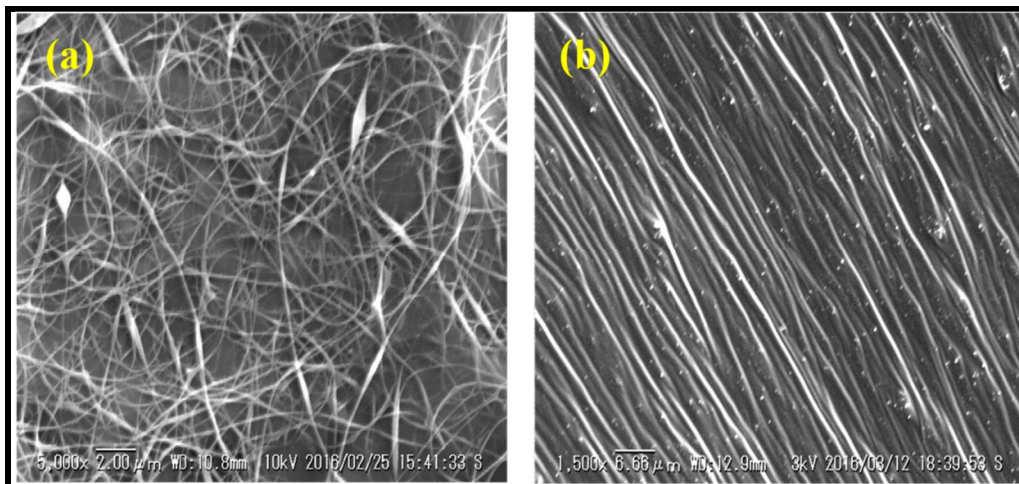


**Figure 4.3:** SEM images of **(a)** EHEC non-woven electrospun fiber mats on plate collector at 5000X magnification and scale bar: 2µm **(b)** Oriented fibers on rotating disc collector, 1500X magnification and scale bar:6.66µm.

From the above images and data, it was observed that EHEC and HM-EHEC polymers were spinnable in THF/water system but with bead formation. To overcome the beaded structure in the electrospun fibers obtained, we tried to carry out electrospinning using water as a solvent instead of a mixed solvent of THF and water [THF/water = 2/1 (v/v)]. The polymer concentration was increased to 10% (w/v), and the EHEC/PVA ratio was varied. The optimization of EHEC/PVA for the electrospinning process was done with a series of experiments as shown in **table 4.4**. Further, another set of experiments were conducted to optimize the voltage and flowrate keeping the distance from spinneret to collector constant which are as shown in the **table 4.5**. Finally EHEC/PVA ratio was optimized to 4/6 that is total of 10% (w/v) and electrospinning parameters like flowrate were optimized to 0.5ml/hr, and voltage to 25kV. The distance between spinneret to collector plate was kept constant at 15 cm. The needle diameter was 0.8 mm. The optimized parameters further exhibited nanofibers without any bead formation.

**Table 4.3:** Conductivity, Surface tension and average diameters aqueous solutions EHEC/PVA electrospun fibers.

| EHEC/PVA (w/w) | Conductivity (mS/cm) | Surface Tension (mN/m) | Spinnability | Average diameter(nm) |
|---|---|---|---|---|
| 1/9 | 1.51 | 45.35 | spinnable/ bead free | 283±5 |
| 2/8 | 2.02 | 45.65 | spinnable/ bead free | 261±5 |
| 3/4 | 2.51 | 45.11 | Spinnable with beads | 318±10 |
| 3/7 | 2.83 | 45.98 | spinnable/ bead free | 255±5 |
| **4/6** | **3.68** | **45.84** | **spinnable/ bead free** | **321±8** |
| 5/5 | 2.78 | 45.44 | unstable spinning | 294±6 |
| 6/4 | - | - | Viscous gel | - |
| 8/2 | - | - | Viscous gel | - |

**Table 4.4:** Parameters for the electrospinning of EHEC/PVA nanofibers for optimization.

| EHEC/PVA (w/w) | Flowrate (ml/hr) | Voltage (kV) | Spinneret to collector (cm) | Spinnability | Range of diameter (nm) |
|---|---|---|---|---|---|
| 2/4 | 0.3 | 30 | 15 | Fibers with beads | 183±15 |
| 3/4 | 0.3 | 30 | 15 | Fibers with beads | 318±10 |
| 3/5 | 0.3 | 30 | 15 | Beadless fibers | 300±18 |
| 4/5 | 0.3 | 30 | 15 | Beadless fibers | 467±25 |
| 4/6 | 0.3 | 25 | 15 | Beadless fibers | 320±6 |
| 4/6 | 0.3 | 30 | 15 | Beadless fibers | 450±15 |
| 4/6 | 0.3 | 35 | 15 | Beadless fibers | 220±10 |
| **4/6** | **0.5** | **25** | **15** | **Beadless fibers** | **321±8** |
| 4/6 | 0.5 | 30 | 15 | Beadless fibers | 283±8 |

| 4/6 | 0.5 | 35 | 15 | Beadless fibers | $405 \pm 10$ |
|-----|-----|-----|-----|-----|-----|
| 4/6 | 0.8 | 25 | 15 | Beadless fibers | $235 \pm 10$ |
| 4/6 | 0.8 | 30 | 15 | Beadless fibers | $250 \pm 10$ |
| 4/6 | 0.8 | 35 | 15 | Beadless fibers | $310 \pm 7$ |



**Figure 4.4:** Photograph of EHEC/PVA (4/6) as spun nanofiber mat.
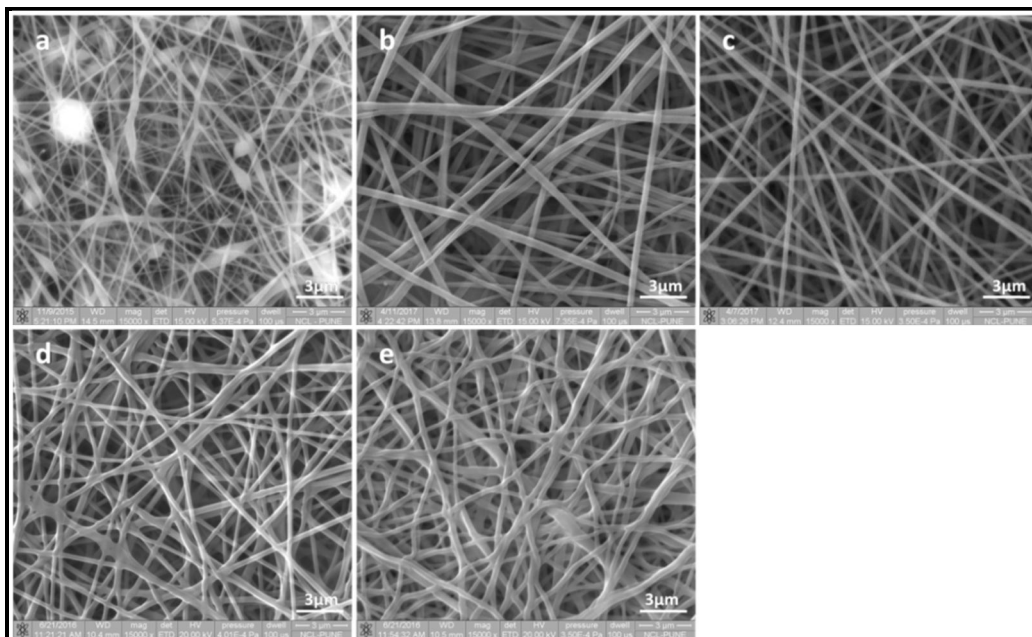


**Figure 4.5:** SEM images of electrospun fibers with different EHEC/PVA **(a)**3/4 **(b)** 4/6 **(c)** 3/7 **(d)** citric acid crosslinked fibers before thermal treatment, **(e)** after thermal treatment. [All scale bars**:** 3µm]
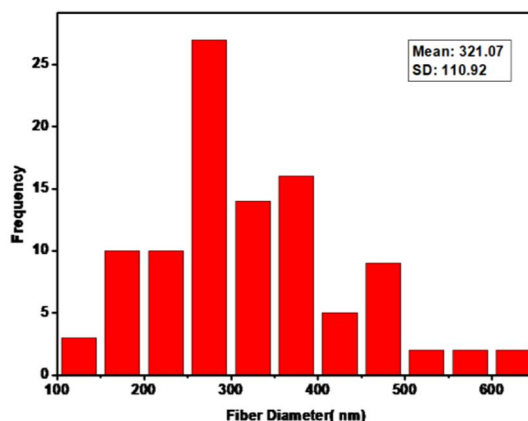
**Figure 4.6:** Bar graph showing average fiber diameter of EHEC/PVA (4/6) nanofiber mat by Image J.

Although the surface tension was almost independent of the polymer composition, the conductivity decreased with increasing PVA composition. The spinnabilty got better with increasing PVA composition, indicating that the low conducting solutions are preferable for spinning stabilization. The electrospun fibers exhibited beads if the PVA composition was insufficient as shown in **fig 4.5(a)**, whereas the spinnability got improved and the fiber geometry got uniform without any beads with the increasing PVA composition are seen in **fig 4.5(b) & (c)**. SEM images of the EHEC/PVA electrospun fibers prepared from the aqueous solutions including 20% (w/w) citric acid before and after treatment are shown in **fig 4.5(d) & (e)**. The presence of citric acid in the polymer solutions enhanced the spinnability of the polymer solutions probably because of the reduction in the surface tension of the polymer solution.The *in-situ* crosslinked electrospun fiber mats were obtained by thermal treatment of the citric acid incorporated electrospun fiber mats at 90°C for 3 h. The EHEC/PVA (4/6) fibers with citric acid exhibited the average diameter of the nanofibers in the range of 250-450 nm as shown in **table 4.5** The crosslinked fiber mat showed interconnected structure that the fibers coalesced at the contact points. The fiber geometry was almost maintained even after thermal treatment, although the fiber diameter slightly increased as compared to the uncrosslinked fibers. The uncrosslinked 10 % (w/v) [i.e 4/6] , of EHEC/PVA fiber mat was soluble in phosphate buffer (PBS) solution,

whereas the same when crosslinked with 20 % (w/w) citric acid were insoluble in the PBS and were used for further drug release and cell viability studies.

### 4.7.3 Atomic Force Microscopy (AFM) Observations

The high-resolution geometry of the spin-coated films and electrospun fibers were further elaborated by AFM observation. AFM topographic and phase images of EHEC, HM-EHEC, EHEC/PVA and HM-EHEC/PVA spin-coated films are shown in **fig 4.7**. The blend ratio of EHEC/PVA and HM-EHEC/PVA is 1:1 (w/w). The surface morphology of the EHEC and HM-EHEC films are slightly different. The hydrophobic modification of EHEC induces cohesive aggregation of the polymers in aqueous solutions resulting in viscosity augmentation at the same polymer concentrations. The aggregation of the hydrophobic parts of the nonyl phenol groups in the HM-EHEC causes granular surface geometry. Upon blending with PVA, the surface topography became smoother in both EHEC and HM-EHEC.
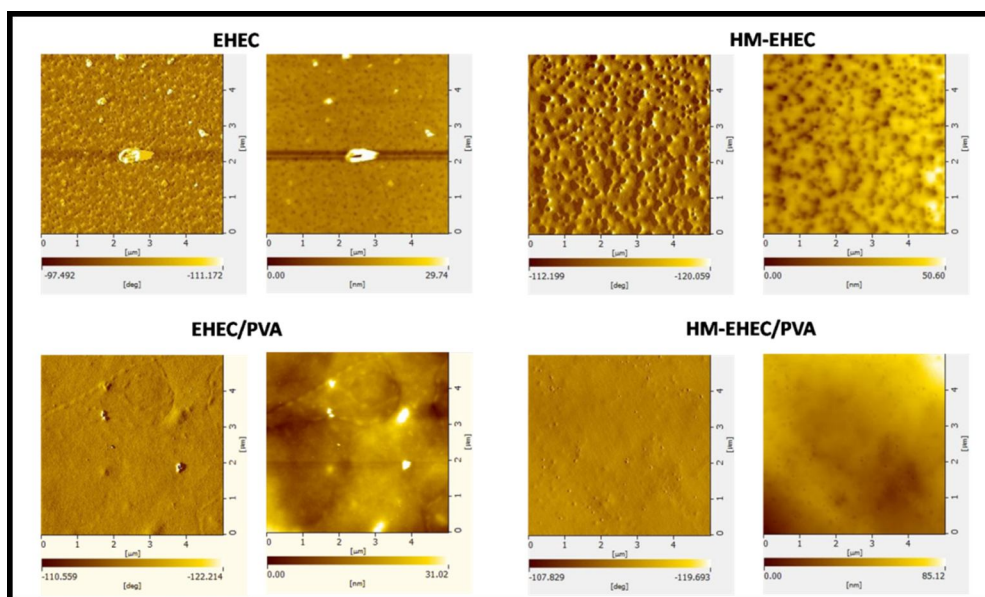


**Figure 4.7:** AFM topographic images of the spin-coated EHEC, HM-EHEC, EHEC/PVA and HM- EHEC/PVA films.
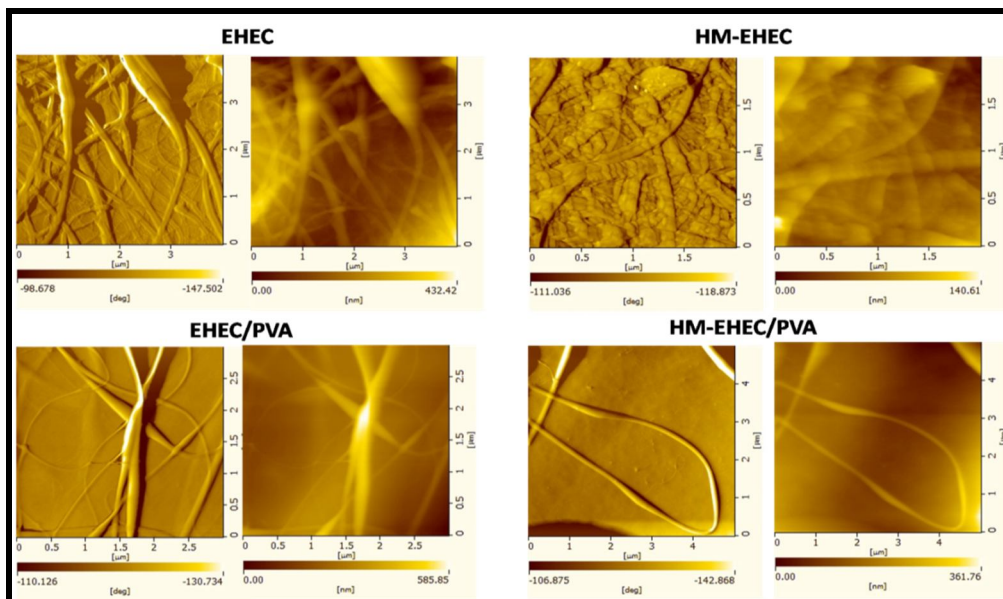
**Figure 4.8:** AFM topographic images (left side) and phase images (right side) of EHEC, HM- EHEC, EHEC/PVA and HM-EHEC/PVA electrospun fibers.

The PVA would promote the homogeneous dissolution of EHEC and HM-EHEC to prevent aggregation of hydrophobic parts in the polymers to give smoothening of the surface geometry. AFM topographic and phase images of the electrospun fibers are shown in **Fig. 4.8**. The EHEC produced smooth fibers, whereas the HM-EHEC exhibited a wrinkled surface geometry with an uneven texture. Blending of PVA promoted smoothening of the electrospun fibers, which is consistent with the spin-coated films. The smoothening effect is attributed to the compatibility of PVA with the non-ionic cellulose ethers as well as the stabilization of the spinning.

### 4.7.4 Contact angles of spin-coated films and electrospun non-woven fiber mats

The side view of water droplets on spin-coated films and electrospun non-woven fiber mats are shown in **fig 4.9**. The contact angles of spin-coated EHEC and HM-EHEC films are slightly higher than the respective electro-spun non-woven fiber mats. The water repellency is attributed to the segregation of hydrophobic groups (nonyl phenol) at the surface.
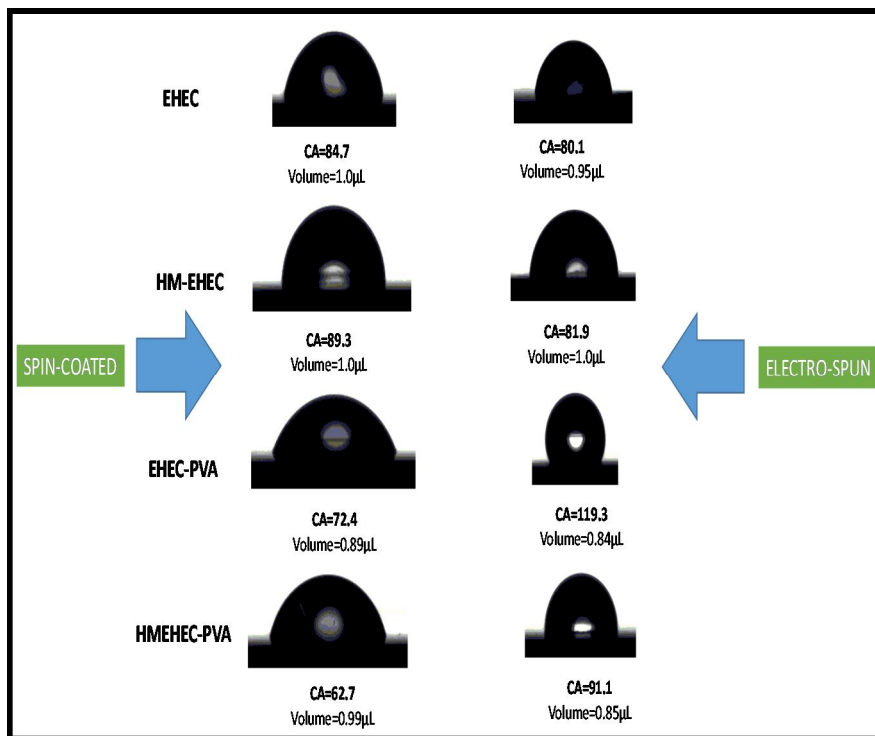
**Figure 4.9:** Contact angles of spin-coated films and electrospun non-woven fiber mats of EHEC, HM-EHEC, EHEC/PVA and HM EHEC/PVA.

The hydrophobic modification of EHEC is favourable for the segregation of hydrophobic groups to make the surface more hydrophobic than unmodified EHEC.The water droplet contact angles on the electrospun fiber mats of 1.0% (w/v) EHEC and HM-EHEC were lower than the spin-coated films indicating the surface geometry of non-woven fiber mats promote water wetting. The contact angle reduction may be due to the Wenzel mode of wetting on the heterogeneous surface geometry. Blending of PVA into the non-ionic cellulose ethers reduced the water droplet contact angles on the spin-coated films, whereas the electrospun fibers of EHEC/PVA and HM-EHEC/PVA [blend ratio is 1.0% (w/v)] showed significantly higher contact angles compared to the spin-coated films. Due to more hydrophilic nature of PVA, one would have expected a decrease in contact angles upon blending with PVA. This was indeed observed in the spin-coated films. However, the electrospun non-woven fiber mats after blending with PVA exhibited contact angles higher than 90° that is much higher than the electrospun fiber mats of EHEC and HM-EHEC. The wetting characteristics are attributed to both the

hydrophobicity of the fiber surface and fiber mat geometry. The unusual observation may be attributable to the fact that the -OH groups of the cellulose backbone and PVA can strongly interact during the electrospinning process and cause a favourable segregation of the hydrophobic groups at the surface since EHEC and HM-EHEC are both amphiphilic polymers. Further, the electrospun fibers of EHEC/PVA and HM-EHEC/PVA exhibit more rough surface geometry than those of EHEC and HM-EHEC and result into more hydrophobic surface with higher contact angles compared to the spin coated films. The appropriate cavity size and the uniformity and lack of defects would induce the wetting mode transition from Wenzel mode to Cassie-Baxter mode as well as the hydrophobicity of fiber surface.

### 4.7.5 Fourier Transform Infra Red Spectroscopy (FT-IR)

The FT-IR spectra of pristine EHEC and EHEC/PVA nanofiber mat are shown in **fig 4.10**. The broad peak at 3358-3428 cm$^{-1}$ is presented by O-H stretching. Saturated aliphatic C-H group from cellulose chain appears at 2900- 3000 cm$^{-1}$ [26]. The band around 1084 cm$^{-1}$ is due to C-O-C stretching[27].
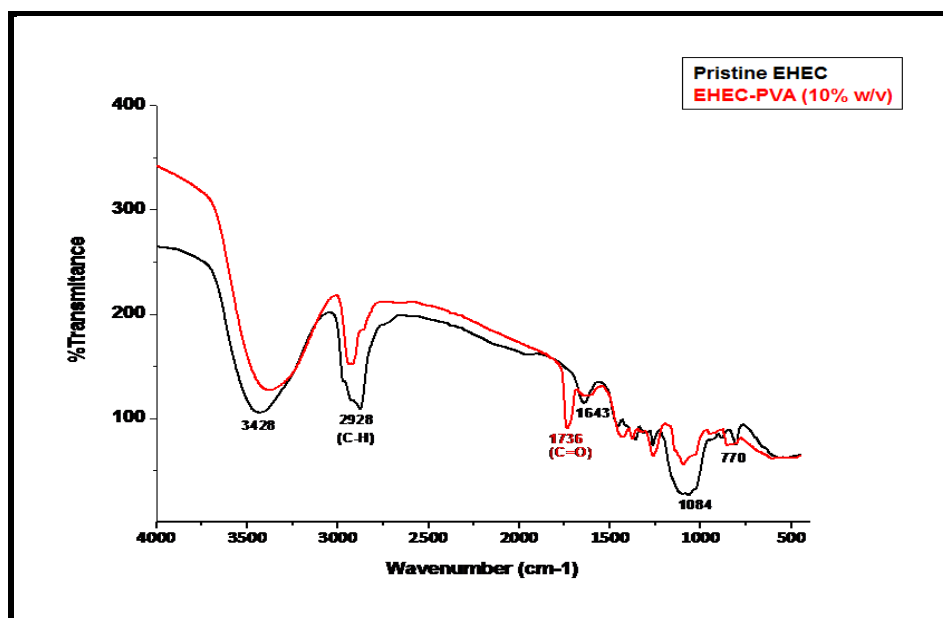


**Figure 4.10:** The FT-IR of pristine EHEC and EHEC/PVA nanofiber mat.

In the EHEC spectra, the band around 1643 cm$^{-1}$ is related to O-H bond of cellulose structure. The spectrum of EHEC/PVA also presented characteristic broad band's for hydroxyl groups at 3387 cm$^{-1}$, for the stretching vibration of

C-H bonds at 2939 cm$^{-1}$ and the stretching vibration of C-O bonds at 1419 and 1096 cm$^{-1}$(not shown in figure). Other small peak at 770 cm$^{-1}$ are related to the existence of –CH bending of β 1-4 glycoside bonds confirm crosslink of cellulose. The chemical reaction with citric acid forms ester bonds and that was observed at 1736 cm$^{-1}$. According to Azeredo *et al*, these were described to C=O of ester bonds that was formed as a product of the crosslinking reaction.[28]

### 4.7.6 Release of Chlorhexidine Digluconate (ChD) from EHEC/PVA nanofiber mats

The antimicrobial drug, Chlorhexidine Digluconate (ChD) was incorporated into the 10% (w/v) EHEC/PVA nanofiber mat during the electrospinning process. Different amounts of ChD viz 5, 10, 15 wt% on the basis of EHEC/PVA was incorporated in the electrospinning solution. Several studies have been reported that there is no remarkable change in the drug and polymer in terms of degradation and hydrolysis during the electrospinning process.[29] The release studies were carried out in PBS at 7.4 pH and 37 $^0$C. Prior to release studies, a calibration curve was generated by measuring the absorbance of ChD solution in PBS at different concentrations of ChD at 256 nm. Least square linear fitting was performed on the data and the $R^2$ =0.9985 was obtained as shown in **fig 4.11**.
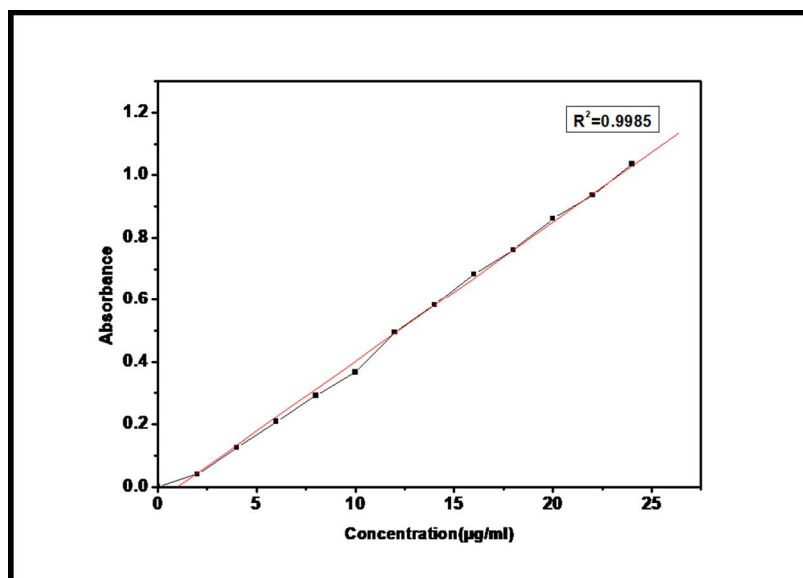


**Figure 4.11:** Calibration curve for Chlorhexidene Digluconate (Antibacterial drug).
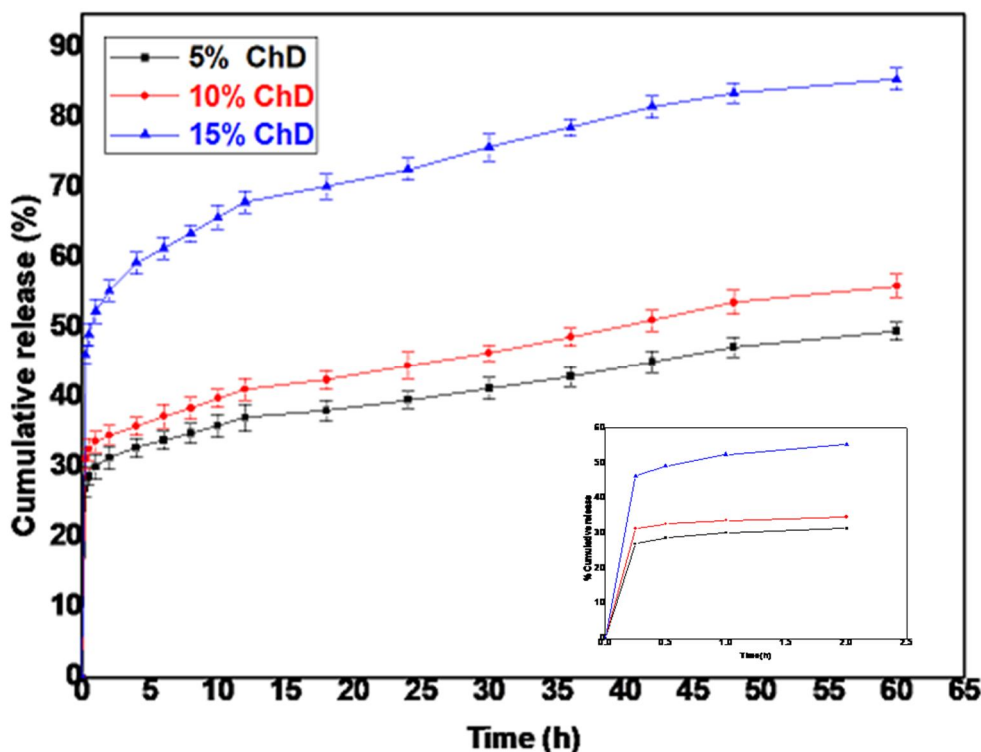
**Figure 4.12:** In-vitro drug release of the EHEC-PVA nanofiber mats at different concentration of Chlorhexidine Digluconate (ChD).

We show in **fig 4.11**, the in-vitro release profiles of ChD in PBS from EHEC/PVA nanofiber mat containing different loadings of ChD as a function of time. It can be readily seen from the figure that in all the cases there was an initial burst release of ChD for the first 4-5 hours. This could be due to the surface adsorbed ChD which could diffuse rapidly into the PBS. The burst release was higher with higher drug loading due to higher amount of drug associated on the surface and high surface area of the nanofiber mat. However, after 5 hours the release of ChD was almost constant with time upto the next 60 hours. The swelling of the citric acid crosslinked EHEC/PVA nanofiber mat in the PBS caused the slow/constant release of ChD into the PBS. The drug encapsulation efficiency was calculated using the formula,

*Encapsulation efficiency (%) =*

Final weight of the drug in the nanofiber mat / initial weight loaded in the blend solution before electrospinning the nanofiber * 100
Encapsulation efficiency is defined as the percentage of drug that is successfully loaded or entrapped into the nanofiber mat. It depends on the

process of polymer solution preparation and other physicochemical properties of drug. The encapsulation efficiencies were found to be 83.3 %, 71.1 % and 53.6 % respectively for 5, 10 and 15% of Chlorhexidine digluconate (ChD). The cumulative release was 45% for 5% ChD, 56% for 10% ChD and 86% for 15% ChD. There was an increase in the release with increase in the drug concentration. The cumulative release for initial 2 hours was 30, 35 and 55% as shown in the inset of **fig 4.12**. The "$n$" values were found to be between 0.5 and 0.89 indicating that the mechanism of drug release was non-Fickian diffusion.

### 4.7.7 Cell Viability Study (MTT Assay)

The toxicity of 10% (w/v) of EHEC/PVA nanofiber mats was characterized by an in-vitro cell viability test. The nanofiber mats and control group as a pure medium without the cells were cultured simultaneously under the same conditions.
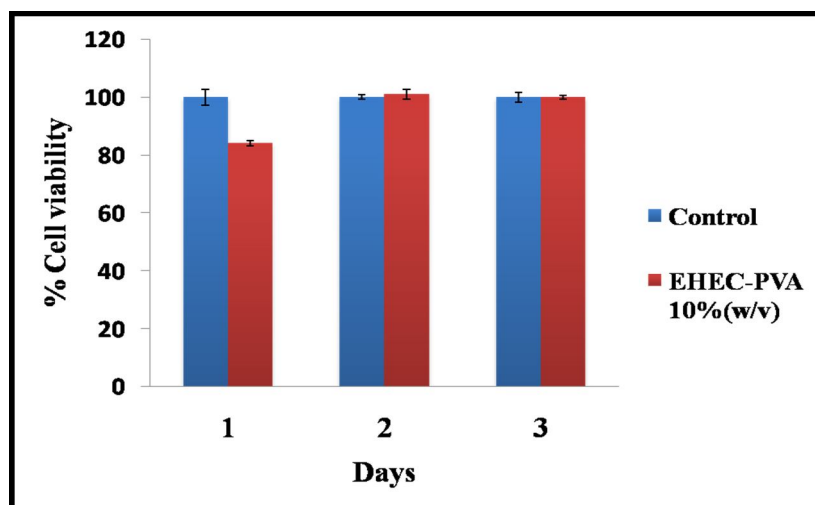


**Figure 4.13:** Cyto-toxicity test of EHEC/PVA 10%(w/v) nanofiber mats.

The values for samples cultured for day 1, 2 and 3 are presented in **fig.4.13.** The bar chart values reflect the number of viable cells, which are associated to their survival rate and activity. The cell viability values of L929 cells cultured for 48 and 72 hours in the cell culture medium with the extract of nanofiber mats showed no significant difference compared to the control group, indicating that the nanofiber mats have no toxic effects on the L929 cells. The

results illustrate that the crosslinked EHEC/PVA nanofiber mats have good cytocompatibility and no toxicity, which are the most desired properties for biomedical applications.

### 4.7.8 Fluorescence and SEM morphology of L929 mouse fibroblast cells

**Fig 4.14(a) & (b)** shows the fluorescence and the corresponding SEM images of L929 cells cultured for 48 hours in the EHEC/PVA of 10 % (w/v) nanofiber mats. The cells exhibited a good growth state (indicated by the marked oval shape of the nuclei) and an evenly dispersed nuclear chromatin was observed.
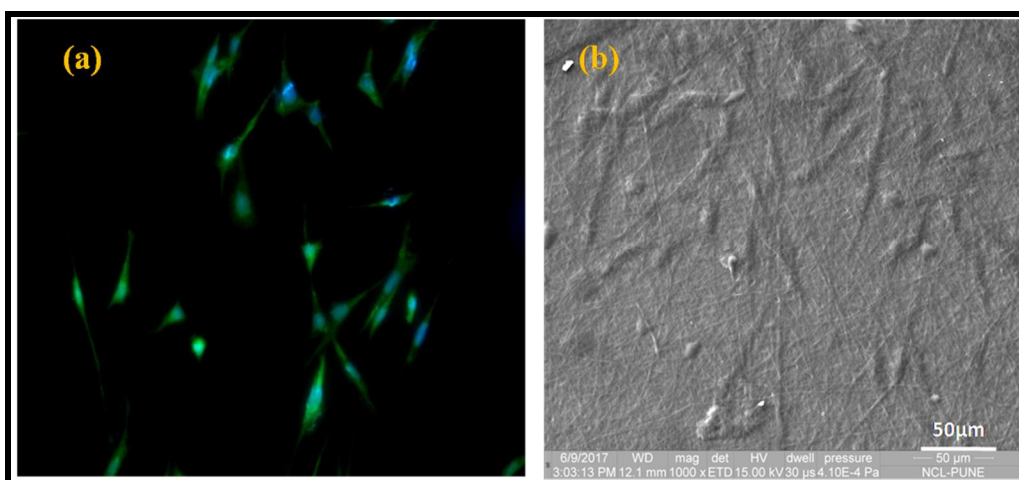


**Figure 4.14 (a)** Fluorescence image **(b)** SEM image of EHEC/PVA mats used for L929 cell growth.  Scale bar: 50µm; 1000X magnification.

The cells showed even distribution and good adhesion to the nanofiber mat. The fibroblast cells were seen tightly attached to the nanofiber mats because of the large specific surface area and the three dimensional structure of the mats.[30] This finding thus indicates that the EHEC/PVA nanofiber mats are suitable for the adhesive growth of biological cells.

## 4.8 Conclusions

The surface morphology of EHEC and HM-EHEC polymers and their blends with PVA was studied by Atomic Force Microscopy (AFM), Scanning Electron Microscopy (SEM) and Contact Angle measurements. The spin coating at 4500 rpm gave minimum surface roughness at moderate thickness. In the AFM images, it was observed that the surface roughness of HM-EHEC

is higher than the EHEC. Upon blending with PVA, the surfaces of both EHEC and HM-EHEC became much smoother and finer. The contact angles for the spin coated EHEC and HM-EHEC samples were higher than electro-spun fibers. Upon blending of these polymers by PVA the electro-spun fibers showed significantly higher contact angles compared to spin coated samples. This was attributed to the fact that, upon electrospinning there could be more interaction between PVA and -OH groups of the cellulose backbone chain resulting into more bare cellulose on the surface of the fiber which can make the surface more hydrophobic in nature and exhibit higher contact angles. Also, the electrospun fibers of EHEC/PVA and HM-EHEC/PVA exhibited more rough surface geometry and could contribute to the increase in hydrophobicity and contact angles. Electro-spinning of EHEC solution of 1.0 % (w/v) in THF/water [2/1 (v/v)] gave fine oriented fibers by using the disc collector. The zero shear viscosities, conductivities and surface tension decreased when the EHEC solution was blended with PVA. The citric acid crosslinked nanofiber mats showed good strength in PBS solutions and these mats were utilized for controlled release of an antimicrobial drug, Chlorhexidine Digluconate (ChD). Furthermore, the in vitro cytotoxicity tests against fibroblast cell cultures demonstrated that the nanofiber mats are biocompatible and non-toxic in nature. These mats successfully attached to the cells and stimulated cell growth and proliferation. All the above studies reveal that these polymers could be electro-spun into nanofibers and can have a potential in drug delivery and tissue engineering applications.

## 4.9 References

**1.** Liang, D.; Hsiao, B. S.; & Chu, B. Functional electrospun nanofibrous scaffolds for biomedical applications. *Advanced Drug Delivery Reviews.* 2007, 59(14), 1392–1412.

**2.** Venugopal, J.; & Ramakrishna, S. Applications of polymer nanofibers in biomedicine and biotechnology. *Applied Biochemistry and Biotechnology.* 2005, 125(3), 147–158.

**3.** Jiang, Z.; Yin, M.; & Wang, C. Facile synthesis of Ca2+ /Au co-doped $SnO_2$ nanofibers and their application in acetone sensor. *Materials Letters.* 2017,194, 209-212.

**4.** Guan, Y.; Li, W.; Zhang, Y.; Shi, Z.; Tan, J.; Wang, F.; & Wang, Y. Aramid nanofibers and poly (vinyl alcohol) nanocomposites for ideal combination of strength and toughness via hydrogen bonding interactions. *Composites Science and Technology*. 2017, 144, 193–201.

**5.** Qiao, H.; Xia, Z.; Fei, Y.; Cai, L.; Cui, R.; Cai, Y.; Wei, Q.; & Yao, Q. Electrospinning combined with hydrothermal synthesis and lithium storage properties of $ZnFe_2O_4$-graphene composite nanofibers.*Ceramics International*. 2017, 43(2), 2136-2142.

**6.** Lee, K. Y.; Jeong, L.; Kang, Y. O.; Lee, S. J.; & Park, W. H. Electrospinning of polysaccharides for regenerative medicine. *Advanced Drug Delivery Reviews*. 2009, 61(12), 1020–1032.

**7.** Sill, T. J.; & von Recum, H. A. Electrospinning: Applications in drug delivery and tissue engineering. *Biomaterials*. 2008, 29(13), 1989–2006.

**8.** Guerra Nista, S.V.; Bettini, J.; & Innocentini Mei, L.H. Coaxial nanofibers of chitosan-alginate-PEO poly complex obtained by electrospinning. *Carbohydrate Polymers*. 2015,127, 222–228.

**9.** Frenot, A.; Henriksson, M. W.; & Walkenstrom, P. Electrospinning of cellulose-based nanofibers. *Journal of Applied Polymer Science*. 2007, 103(3), 1473–1482.

**10.** Entekhabi, E.; Nazarpak, M. H.; Moztarzadeh, F.; & Sadeghi, A. Design and manufacture of neural tissue engineering scaffolds using hyaluronic acid and polycaprolactone nanofibers with controlled porosity. *Materials Science and Engineering C*. 2016, 69, 380–387.

**11.** Zhou, T.; Zhu, B.; Chen, F.; Liu, Y.; Ren, N.; Tang, J.; Ma, X.; Su, Y.; & Zhu, X. Micro-/nanofibers prepared via co-assembly of paclitaxel and dextran. *Carbohydrate Polymers*. 2017,157, 613–619.

**12.** Amrita., Arora, A.; Sharma, P.; & Katti, D.S. Pullulan-based composite scaffolds for bone tissue engineering: Improved osteoconductivity by pore wall mineralization. *Carbohydrate Polymers*. 2015, 123, 180–189.

**13.** Liu, G.; Gu, Z.; Hong, Y.; Cheng, L.; & Li, C. Electrospun starch nanofibers: Recent advances, challenges, and strategies for potential pharmaceutical applications. *Journal of Controlled Release*. 2017,252, 95-107.

**14.** Okutan, N.; Terzi, P.; & Altay, F. Affecting parameters on electrospinning process and characterization of electrospun gelatin nanofibers. *Food Hydrocolloids*. 2014, 39, 19-26.

**15.** Ostrovskii, D.; Kjøniksen, A.L.; Nystrom, B.; & Torell, L.M. Association and Thermal Gelation in Aqueous Mixtures of Ethyl (hydroxyethyl) cellulose and Ionic Surfactant: FTIR and Raman Study. *Macromolecules*. 1999, 32, 1534-1540.

**16.** Nystrom, B.; Kjoniksen, A.; & Lindman, B. Effects of Temperature, Surfactant, and Salt on the Rheological Behavior in Semidilute Aqueous Systems of Nonionic Cellulose Ether. *Langmuir.* 1996, 12 (13), 3233–3240.

**17.** Nahringbauer, I. Dynamic Surface Tension of Aqueous Polymer Solutions, I: Ethyl (hydroxyethyl) cellulose (BERMOCOLL cst-103). *Journal of Colloid and Interface Science.* 1995,176, 318 – 328.

**18.** Pereswetoff-Morath, L.; Bjurstrom, S.; Khan, R.; Dahlin, M.; & Edman, P. Toxicological aspects of the use of dextran microspheres and thermogelling ethyl (hydroxyethyl) cellulose (EHEC) as nasal drug delivery systems. *International Journal of Pharmaceutics.* 1996,128, 9-21.

**19.** Calejo, Maria Teresa.; Cardoso, Ana Maria S.; Marques, Eduardo F.; et al. In vitro cytotoxicity of a thermoresponsive gel system combining ethyl (hydroxyethyl) cellulose and lysine-based surfactants. *Colloids and Surfaces B: Biointerfaces.* 2013, 102, 682– 686.

**20.** Park, J-C.; Ito, T.; Kim, K-O.; Kim, K-W.; Kim, B-S.; Khil, M-S.; Kim, H-Y.; & Kim, I-S. Electrospun poly(vinyl alcohol) nanofibers: effects of degree of hydrolysis and enhanced water stability. *Polymer Journal.* 2010, 42, 273–276.

**21.** Shalumon, K. T.; Binulal, N. S.; Selvamurugan, N.; Nair, S. V.; Menon, D.; Furuike, T.; & Jayakumar, R. Electrospinning of carboxymethyl chitin/poly(vinyl alcohol) nanofibrous scaffolds for tissue engineering applications. *Carbohydrate Polymers.* 2009, 77(4), 863–869.

**22.** Ignatova, M.; Starbova, K.; Markova, N.; Manolova, N.; & Rashkov, I. Electrospun nano-fiber mats with antibacterial properties from quaternised chitosan and poly (vinyl alcohol). *Carbohydrate Research.* 2006, 341(12), 2098–2107.

**23.** Tang, C.; Saquing, C. D.; Harding, J. R.; & Khan, S. A. *In Situ* cross-linking of electrospun poly (vinyl alcohol) nanofibers. *Macromolecules.* 2010, 43, 630–637.

**24.** Gupta, N. R.; Torris, A. A. T.; Wadgaonkar, P. P.; Rajamohanan, P. R.; Ducouret, G.; Hourdet, D.; Creton, C.; & Badiger, M.V. Synthesis and characterization of PEPO grafted carboxymethyl guar and carboxymethyl tamarind as new thermo-associating polymers. *Carbohydrate Polymers.* 2015,117, 331–338.

**25.** Senel, S.; Ikinci, G.; Kas, S.; Yousefi-Rad, A.; Sargon, M. F.; & Hincal, A. A. Chitosan films and hydrogels of chlorhexidine gluconate for oral mucosal delivery. *International Journal of Pharmaceutics.* 2000, 193(2), 197–203.

**26.**Soni, B.; Hassan, E. B.; Mahmoud, B. Chemical Isolation and Characterization of Different Cellulose Nanofibers from Cotton Stalks. *Carbohydrate Polymers.* 2015, 134, 581–589.

**27.**A. Salama.; M. Neumann.; C. Günter.; and A. Taubert. Ionic liquid-assisted formation of cellulose/calcium phosphate hybrid materials. *Beilstein Journal of Nanotechnology.* 2014, 5, 1553-1568.

**28.** H.M.C.Azeredo, C. Kontou-Vrettou, G.K. Moates, N. Wellner, K. Cross, P.H.F. Pereira, K.W. Waldron.; Wheat straw hemicellulose films as affected by citric acid. *Food Hydrocolloids.* 2015, 50, 1-6.

**29.** U. Sunil Chandra.; N. B. Sridhar.; Sanganal, Jagadeesh S.; & C. Ravikumar. Nanofibers in drug delivery: An Overview. *World Journal of Pharmaceutical Research.* 2015, 4, (8), 2576-2594.

**30.** Guo, J.; Zhou, H.; Akram, M.Y.; Mu, X.; Nie, J.; & Ma, G. Characterization and application of chondroitin sulfate/polyvinyl alcohol nanofibers prepared by electrospinning. *Carbohydrate Polymers.* 2016, 143, 239-245.

# CHAPTER V(A)

## Design and Fabrication of EHEC Nanofibers with Nano-materials for Wound Healing Applications

### Part A: Halloysite Nanotubes

*Success is a journey, not a destination.*

*Ben Sweetland*

## 5A.1 Introduction

Wound healing is a complex multi step process in which the damaged skin and the tissue at the wound site gets repaired themselves after the injury with their own pace. The cascade of healing process involves four overlapping phases: i) Haemostatic (blood clotting) ii) Inflammatory iii) Proliferation iv) Maturation. Hemostasis, the first phase of healing begins at the onset of the injury with an objective of stopping the bleeding. The inflammatory phase focuses on destroying the bacteria and cleaning the debris which is important for the growth of new tissues. In the proliferative phase, filling of wound followed by contraction of wound margins and wound covering (epithelialisation) takes place. Finally, in the maturation phase, the new tissue formed slowly gains the strength and flexibility.[1]

In order to enhance the wound healing process, fabrication of nanofibrous mat/wound dressing material with an antibiotic and antibacterial property has become extremely important. Recently, electrospun biopolymers have attracted increasing attention as wound dressing materials due to their excellent biocompatibility, biodegradability and structural resemblance to natural extra cellular matrix (ECM) which could support fibroblast growth and repair the damaged tissues.[2] Electrospinning (ES) has emerged as an important technique for fabricating polymeric nanofibers. Nanofibrous scaffolds/mats fabricated using ES holds promising architectural resemblance to the ECM and provides the most desired characteristics of scaffolds/mats which are the large surface to volume ratio with interconnected porous network for oxygen and nutrients permeation/diffusion, tunable mechanical properties, inhibition to pathogenic micro-organism filtration and absorption of wound exudates.[3] Although a variety of polymers/biopolymers such as PVA, PLA, PCL, Polyurethanes (PU), gelatin, chitosan and the blends of these polymers have been electrospun and evaluated for wound dressing applications, still there is a large scope for designing and developing novel, efficient and cost-effective nanofiber scaffolds/mats loaded with antibacterial and antibiotic moieties for rapid wound healing applications. It is also known that, incorporation of

natural inorganic nanofiller into a biodegradable polymer gives a promising hybrid material for biomedical application.[4] For example, halloysite clay can improve the mechanical properties of an electrospun mat for wound healing applications. Halloysite has been incorporated into poly(lactic-co-glycolic)[PLGA] nanofibers to enhance the mechanical property and hemocompatibility of the nanofibers.[5] Halloysite doped poly (caprolactone/gelatin electrospun nanofibrous membranes were investigated for guided tissue regeneration/bone regeneration applications.[6] Halloysite comprises of naturally occurring alumino silicate with Al: Si ratio of 1:1 and having molecular formula $Al_2Si_2O_5(OH)_4 \cdot nH_2O$. Halloysite has a tubular structure with an external diameter of 30-60 nm, lumen diameter of 12-15 nm, and a length of around 1 µm. Due to its cytocompatibility and non-toxic characteristics, it finds wide applications in biomedical area.[7]

Ethyl hydroxy ethyl cellulose (EHEC) is non-ionic cellulose ether which is non-toxic, biocompatible and biodegradable, also finds applications in biomedical field such as ophthalmic and nasal drug delivery.[8] The electrospinning of EHEC solution alone was challenging since it shows a complex solution behaviour with the inherent property of temperature induced phase separation. Therefore, to overcome this limitation, PVA was used as a co-spinning agent in the electrospinning process. PVA is also biodegradable, biocompatible, non-toxic polymer with good mechanical and swelling properties which makes it suitable for wound dressing materials.[9]

In this work, we report on the fabrication and characterization of electro-spun EHEC-PVA nanofiber mat loaded with halloysite and gentamicin sulphate for enhanced wound healing applications. We demonstrate that halloysite clay and gentamicin sulphate, both provide antibacterial and antibiotic properties which result in the rapid wound healing process. The structure and morphology of the nanofibers were examined by scanning electron microscopy (SEM), transmission electron microscopy (TEM), X-ray diffraction (XRD) and Fourier transform infra red spectroscopy (FT-IR). Halloysite incorporated nanofibers were evaluated for mechanical properties, biological tests such as

cytotoxicity, hemocompatibility, cell growth and proliferation and finally, the *in-vivo* wound healing studies were undertaken using wistar rats.

## 5A.2 Material and Methods

Ethyl hydroxyl ethyl cellulose (EHEC) was obtained from Akzo-Nobel Functional Chemicals AB, Sweden with trade name as Bermocoll E411FQ. The molecular weight was 1200Kg/mol with about 7000 anhydro glucose units (AGU). Polyvinyl alcohol (PVA) with degree of hydrolysis of 89% was obtained from S.D Fine Chemicals, Boisar, India. Halloysite nanotubes (HNTs) were purchased from Sigma Aldrich with CAS No: 1332-58-7. Gentamicin sulphate (GS), CAS No. 37636(074810) [1405-41-0] was purchased from Sisco Research Laboratories Pvt. Ltd, India. Citric acid was purchased from Merck Limited, India. Distilled water was used throughout the experiments.

## 5A.3 Experimental Section

### 5A.3.1 Solution preparation

To prepare the electrospinning solution, pure EHEC was taken. The aqueous solution of EHEC and PVA was prepared in the ratio of 4:6 wt% and the total polymer concentration was kept at 10% (w/v). In order to post crosslink the nanofiber mats, citric acid (20 wt% of the total polymer) was added to the above solution. To incorporate the drug gentamicin sulphate (GS) and halloysite nanotubes into the polymer nanofiber mat, the drug (10% of polymer weight) was first mixed with HNTs (3% of the polymer weight) in a glass vial and sonicated for 15 minutes. This mixture (drug and HNTs) was subjected to vacuum for 10 minutes (for three times) to remove the air entrapped in the lumen of HNTs which can otherwise affect the efficient loading of the GS in the HNTs. This drug-HNTs mixture was then mixed with the EHEC-PVA solution containing citric acid and taken for electrospinning.

### 5A.3.2 Electrospinning of EHEC/PVA with Halloysite

Electrospinning of EHEC/PVA solution containing HNTs and GS was carried out on ESPIN NANO, Model No: V2C, S.No: 01062015, India. The polymer solution was loaded into a syringe and discharged from the spinneret (0.8 mm

dia) at a flow rate of 0.5 ml/h. The applied voltage was 25 kV and the distance between the spinneret and the collector plate was 15 cm. All the experiments were performed at ambient temperature. The nanofibers were collected on an aluminium foil attached to the plate collector. The aluminium foils were then removed and kept in a desiccator for drying. The nanofiber mats were peeled off from the aluminium foil and further heated at $90^{0}$C for 3 h to induce crosslinking by citric acid. The nanofiber mats prepared, were denoted as EHEC/PVA as E1, EHEC/PVA/3HNTs (3wt%HNT) as E2, EHEC/PVA/10GS (10 wt% GS) as E3 and EHEC/PVA/3HNT/10GS as E4.

## 5A.4 Characterization Techniques

### 5A.4.1 Conductivity measurements

The electrical conductivities were measured using a conductometer, Toshniwal Instruments Mfg. Pvt Ltd, Ajmer, SR No: 10J694. Conductivity cell: Type: TCC-1, K=0.98. All measurements were done at $25^{0}$C in triplicates and average values reported.

### 5A.4.2 Viscosity measurements

The viscosity measurements were done on Anton Paar Germany Gmbh, Physica MCR 301 rheometer using a cup and bob geometry. All experiments were done at $25^{0}$C in triplicates and mean values reported.

### 5A.4.3 Surface Tension measurements

Surface tension of the electrospinning solutions was carried out on the optical contact angle measurement system, Carl Zeiss, Jena, Japan. All experiments were done at $25^{0}$C in triplicates and mean values reported.

### 5A.4.4 Contact Angle measurements

Contact angle measurements were performed by using an automated optical contact angle goniometer (OCA) equipped with a video streaming system having a high-resolution CCD camera and a high-performance digitizing adapter. The nanofiber mats were fixed on top of a plane solid support and kept flat. The data was analyzed using SCA 20 (Data Physics Instruments, GmbH) software. The water droplet volume was 5.0($\pm$ 0.3) µL. Images were collected 25 times per second starting from the deposition of the drop to 40 s.

Five measurements were carried out on each nanofiber mat sample and average values reported.

### 5A.4.5 Scanning Electron Microscopy (SEM)

The morphology of the nanofibers was studied using Scanning Electron Microscopy quanta 200 3D dual beam ESEM FEI, Finland. The electron source was tungsten (W) filament with thermionic emission at 15 kV in high vacuum. The size and distribution of the electrospun fibers were analyzed using Image J analysis software (Image J, National Institutes of Health, USA). For each electrospun mat, 100 fibers were randomly selected from different regions of the SEM image and size of the fibers was reported as an average diameter.

### 5A.4.6 Transmission Electron Microscopy (TEM)

The size of HNTs in the nanofibers was determined using TEM FEI, TECNAIG2 F30 instrument operated at an accelerated voltage of 200 kV. The electrospun nanofibers were directly mounted on the copper grids and examined under TEM.

### 5A.4.7 Fourier Transform Infra-red spectrometer (FT-IR)

The IR spectra of the nanofiber mats were recorded on Perkin Elmer Instruments, Spectrum One, FT-IR spectrometer. The recording was done in the ATR mode in the wavelength range of 400 to 4000 $cm^{-1}$. The background scan with air was used for recording the spectra.

### 5A. 4.8 X-Ray Diffraction (XRD)

The X-ray diffraction measurements were performed on HNT incorporated nanofiber mats using a Bruker-D8 Advance Diffractometer operating with Cu Kα radiation (λ=0.15406 nm, Ni filter) generated at 40 kV and 30 mA. A small piece of fiber mat was inserted into circular hole of the aluminium plate and XRD spectra were recorded in the $2\theta$ angle scale range $10^0$ to $60^0$ at a rate of $2^0$/min.

### 5A.4.9 Brunauer–Emmett–Teller (BET) Analysis

The surface area, average pore diameter (mesopore) and cumulative pore volume of the electrospun EHEC/PVA and EHEC/PVA/HNT nanofibers were

examined using Brunauer–Emmett–Teller (BET) surface area analyser (Quantachrome, IQ-C model) with low-temperature (77 K). Nitrogen adsorption isotherms measured over a wide range of relative pressures from 0.01 to 1.00. The surface area of the samples was determined with multipoint BET method. On the other hand, density functional theory (DFT) was used to determine cumulative pore volume.

### 5A.4.10 Thermogravimetric Analysis (TGA)

Thermal analysis was performed using Thermal Analyzer, STA-6000 (Perkin-Elmer, USA) in the temperature range from $30^0$ to $600^0$ C at a controlled heating rate of $10^0$ C min$^{-1}$ with the nitrogen flushed at 30 ml/min.

### 5A.4.11 Mechanical Properties

The mechanical strength of the nanofiber mats was measured using a dynamic mechanical strain analyzer, RSA-3 (TA Instruments, USA). The samples were cut into dumble shaped strips with dimensions of 2 cm (length) x 0.5cm (width) and then mounted onto the tensile grips. The rate of pulling was 10mm/min and gauge length of 15 cm at 10 Hz was subjected to tensile force at $25^0$C. Each sample was repeated five times to authenticate its normal stress–strain curves. The material thickness (µm) was determined at five different places using a screw gauge and average values were taken for calculation.

## 5A.5 Swelling Studies

The nanofiber mats of 5 mg each of E1, E2, E3 and E4 were dipped in the phosphate buffer saline (PBS) solution (pH 7.4) at $37^0$C. Excess surface water was blotted out with filter paper before weighing the samples and weights were taken at various time intervals starting from 30 minutes to 30 h. All the experiments were done in triplicates and average value was taken. The percent degree of swelling was calculated from the formula[10] :

Degree of Swelling (%) = [($M_w$-$M_d$)/ $M_d$] ×100, where $M_w$ and $M_d$ are mass of wet and dry samples respectively.

## 5A.6 *In-Vitro* Drug Release Studies

To evaluate the drug release from the electro spun nanofiber mats, the cut piece(1 cm x 1 cm) of nanofiber mat was immersed in 15 ml phosphate buffer solution(PBS) taken in a covered test tube and kept in a shaker bath (Julabo

SW 23) with gentle shaking at 37$^0$C. At predetermined time intervals, 1 ml of PBS was taken and replenished with an equal volume of fresh PBS into the test tube. The amount of gentamicin sulphate (GS) released was determined by UV-Vis spectrometer (UV-160 PC Shimadzu) at a $\lambda_{max}$ of 280 nm. The percentage drug release was calculated using the calibration curve of the drug in PBS at 7.4 pH. The release experiment of each sample was performed in triplicates and the average value is reported. The encapsulation efficiency was calculated as follows:

$$\text{Encapsulation efficiency } (\%) = \frac{\text{mass of maximum drug released}}{\text{mass of total drug released}} * 100$$

## 5A.7 Antibacterial Studies

The antibacterial studies were performed on the nanofiber mats loaded HNTs, GS and combination of HNT and GS using the Kirby Bauer disk diffusion method. The gram-positive, Staphylococcus aureus (*S. aureus)* is a round-shaped bacterium which is a member of the microbiota of the body and is often found in the upper respiratory tract and on the skin. *S. aureus.* The gram negative bacteria Escherichia coli (*E.coli*), is a type of bacteria which is mostly found in the intestines. Both these bacteria's *were* inoculated in 10 ml nutrient broth in culture tubes and kept at 37 $^0$C in an incubator. The nutrient agar petriplates were prepared. After overnight incubation of nutrient broth, 100µl from each (*E. coli* and *S. aureus*) were inoculated on the petriplates in triplets. The cultured broth (100µl) was spread on the nutrient agar plates by sterile spreader. The nanofiber mats E1, E2, E3 and E4 were cut into circular shape of equal size and placed on the agar plates along with positive control (antibiotic discs of kanamycin and tetracycline) at 37 $^0$C in the incubator. After overnight incubation, the zones of inhibition measured and photographs were recorded.

## 5A.8 Biological Studies

### 5A.8.1 Cell Viability Studies (MTT Assay)

The cytotoxicity of nanofiber mats was investigated using MTT assay. The L929 mouse fibroblast cell line used was obtained from National Centre for

Cell Science (NCCS), Pune, India. The cells were cultured in DMEM medium, supplemented with 10% fetal bovine serum, streptomycin (10 g/ml) and penicillin (100 units/ml) and were maintained in a humidified atmosphere at $37^0$C under 5% $CO_2$.[11] Cells ($1\times10^4$) were seeded per well in 24-well, flat bottom culture plate and incubated for 24 h, followed by the treatment using nanofiber mats E1, E2, E3 and E4 were treated for 1, 3 and 5 days. After incubation, the MTT solution (5 mg/ml of stock solution of which 20µl of MTT solution was added in 200µl of DMEM media) was added to each well followed by further incubation in darkness at $37^0$C for 4 h. The formazan crystals formed were dissolved by addition of acidified isopropanol. After 15 min, the amount of colored formazan derivative formed was determined by measuring the optical density (OD) using a microplate reader (Spectra Max, MS; Molecular Devices, LCC) at 570 nm. All the experiments were done in triplicates. The percentage cell viability was calculated as:

$$\% \text{ cell viability} = \frac{(OD)\text{sample} - (OD)\text{blank}}{(OD)\text{control} - (OD)\text{blank}} * 100$$

### 5A.8.2 *In-vitro* Wound Migration Assay

Motility of L929 fibroblast mouse cells in the presence of nanofiber mats E1, E2, E3 and E4 was determined by wound migration/scratch assay using a 24-well, flat bottom plate. Briefly, L929 cells were grown in monolayer and synchronized in serum depleted medium. A sterile tip was used for scrape-wounding to create a denuded zone (gap) of constant width. Cellular debris was removed with sterile PBS followed by addition of various test samples which were then incubated at $37^0$C for 24 h. The migration of L929 fibroblast cells to the wounded region was observed by phase contrast microscope (Nikon) and photographed (10X magnification) at $t = 0$ h and $t = 24$ h.[12] The wound migration was measured by Image-Pro plus software and estimated by the following equation[13]:

Wound migration % = [1-(wound area at $T_t$/wound area at $T_0$) × 100], where $T_t$ is the time after wounding (24 h) and $T_0$ is the time immediately after wounding (0 h).

### 5A.8.3 Hemocompatibility Assay

Hemolysis study of electrospun mats namely E1, E2, E3 and E4 was performed using method of indirect contact according to the requirements of ISO 10993.[14] About 3ml of rat blood was collected in EDTA coated vials and was diluted to 3 times in physiological saline. 1 ml of diluted blood was then centrifuged at 2000 rpm for 15 minutes at $4^0$C. 200µl of this diluted blood was taken in an eppendorf tube and made upto 1 ml. The nanofiber mats were immersed into the diluted blood and incubated for 1 h at $37^0$C and then centrifuged at 2000 rpm for 15 minutes. After centrifugation, the supernatant liquid was collected and absorbance was recorded at 540 nm. Triton-X (0.1%) was used as positive control and saline as negative control for the study. All the experiments were done in triplicates and average value was reported. The percent hemolysis was calculated using the following formula:

$$\% \text{ Hemolysis} = \frac{\text{Sample (OD)} - \text{Negative control (OD)}}{\text{Positive control(OD)} - \text{Negative control(OD)}} * 100$$

### 5A.8.4 Cell growth and Proliferation

The nanofiber mats were sterilized for 15 minutes inside a biosafety cabinet and placed in 24 sized flat bottom well plates. Approximately 4 x $10^4$ of L929 fibroblast cells were seeded equal number in each well plate. After 48 h incubation in 5% $CO_2$ at 37 °C, the cells were washed using PBS and fixed with 4% paraformaldehyde. The nanofiber mats were treated with 5% Bovine Serum Albumin (BSA) along with 0.1% Triton-X in PBS for 1 h, and further washed with PBS. The cells were treated with DAPI (4′, 6-diamidino-2-phenylindole) for 10 minutes and further the nanofiber mats were placed 'face down' on clean slides with the help of mounting media (Fluoroshield, Sigma Aldrich). Cells were then visualized using an epifluorescence microscope from Carl Zeiss, AX10 Observer Z1, and S.No. 3851000678. An objective of 10X was used to visualize the cells under microscope, the nucleus of the cells was observed using a blue filter at 358 nm. After 48 h of incubation, the cells were

washed using PBS. The mats were then incubated with 3% glutaraldehyde in PBS for overnight at $4^0$C. The mats were again washed for 10 minutes using PBS and followed by ethanol at room temperature followed by gold sputtering for obtaining SEM images.

### 5A.8.5 *In-vivo* Wound healing Assay

All the animal experiments were performed in accordance with the guidelines for Institutional Animal Care and Use Committee (IACUC) at National Centre for Cell Science (NCCS), Pune, India, and approved by the Animal Ethics Committee of NCCS with approval number IEAF/2018/B-339, dated 13-03-2018, which follows the guidelines of the committee for the purpose of control and supervision of experimentation on animals (CPCSE, Govt. of India). Female rats (Wistar 200–250 g) were anesthetized by intraperitoneal injection of ketamine and xylazine hydrochloride (4:1).The dorsal hairs of the rats were shaved, depilated on their backs. A surgical wound of 2.5 cm (dia) was created using a surgical scissor there-by removing the skin and subcutaneous tissue. The wounds were then washed with saline water. Six groups with three rats in each group (n=3) were used for the experiments. In group I, the wound was left open without applying any medication on the rats (control). In group II, the wounds were treated with a marketed ointment (povidone iodine). In group III, the nanofiber mats E1 (3cmx3cm) were applied on the wound of the rat and covered with a surgical adhesive tape. Similarly, in group IV, the nanofiber mats E2 (3cmx3cm) were applied and covered. In group V the nanofiber mat E3 and group VI the nanofiber mat E4 were applied and covered using the tape. These nanofibers mats were changed once in two days interval and the reduction in wound size was monitored and measured using a scale. The images of the healing area were taken using a digital camera. The whole experiment was conducted for a period of 21 days and then the rats were euthanized. The wounded area on the 21st day was cut using a scissor and stored in 10% neutral formalin solution for histopathology study. The % wound closure was calculated using the formula[15]**:**

Wound closure (%)$= \frac{A0- At}{A0} * 100$, where $A_0$ and $A_t$ are the wound sizes at day 0 and day $t$ respectively.

### 5A.8.6 Histopathology Study

The blood samples of the wistar rats were collected in tubes coated with EDTA anticoagulant. All the blood samples were analyzed by Beckman Coulter veterinary hematology analyzer. Formalin fixed skin tissue samples were trimmed and processed routinely. Tissue processing was done to dehydrate in ascending grades of alcohol, clearing in xylene and embedded in paraffin wax. Paraffin wax embedded tissue blocks were sectioned at 3 to 4 μm thickness with the Rotary Microtome. Slides of skin were stained with Hematoxylin and Eosin (H & E) and Masson's Trichrome stains for morphological observations and collagen fibers.[16] Gomori's reticulin staining technique was used for demonstration of reticulin fibers and Verhoeff's Van Gieson(EVG) test for elastin fibers.[17,18] The prepared slides were examined under microscope to note histopathological lesions if any. Severity of the observed lesions were recorded as 0= No abnormality detected, +1=Minimal (<1%),+2=Mild (1-25%), +3=Moderate (26-50%), +4=Marked/Moderately Severe (51-75%), +5= Severe (76-100%)and distribution was recorded as focal, multifocal and diffuse.

### 5A.8.7 Statistical Analysis

All the experiments were carried out for n = 3 samples, the data was analyzed using statistical software OriginPro 8 (Origin lab Corporation, USA). The in-vitro, in-vivo experiments are represented in the form of bar graphs respectively using Sigma Plot 10.0 software. The histological observations were done using Nikon E100 microscope along with Olyumpus DC 5 camera and software.

## 5A.9 Results and Discussion

### 5A.9.1 Conductivity, Viscosity, and Surface Tension measurements

The conductivity, viscosity and surface tension experiments were done for EHEC/PVA (10% w/v) polymer solution containing 1, 3 and 5 % (w/w) Halloysite nanotubes (HNT).and 10% Gentamicin drug (GS).

**Table 5A.1:** Conductivity, Viscosity, and Surface Tension of EHEC/PVA with HNT and GS.

| Sample Name | Viscosity (Pa.s) | Conductivity (mS/cm) | Surface Tension (mN/m) |
|---|---|---|---|
| EHEC/PVA/0%HNT | 177 | 4.80 | 46.22 |
| EHEC/PVA/1%HNT | 195 | 5.18 | 45.36 |
| EHEC/PVA/3%HNT | 199 | 4.85 | 52.93 |
| EHEC/PVA/5%HNT | 76.5 | 5.05 | 44.51 |
| EHEC/PVA/10%GS | 184 | 4.92 | 48.10 |
| EHEC/PVA/3%HNT/10%GS | 208 | 5.23 | 53.45 |

The solution parameters, namely surface tension, viscosity, conductivity of the polymer solution are important parameters for successful electrospinning. When there is a balance between surface tension and repulsive electrostatic forces, there is formation of submicron range fibers. Solution viscosity plays a major role in electrospinning. There are bead formations when the solution viscosity reaches a lower range because the Taylor cone shape oscillates and becomes asymmetrical. However when the polymer concentration exceeds a certain limit, the viscosity of the solution becomes exceedingly high, thereby disrupting the flow of the polymer solution through the capillary.[19] In our study, the viscosity increased from 171 to 199 Pa.s with the increase in HNT clay but decreased for 5%HNT and this may be due to the excess HNT aggregation. The viscosity was 184 Pa.s when 10% Gentamicin (GS) drug was added and was 208 Pa.s when 10% GS was incorporated into 3% HNT.

Distilled water is most favourable solvent when nanofibers are required to be used for biomedical applications. It was observed that the conductivity ranged from 4.8 to 5.23 mS/cm as shown in **table 5A.1.** Surface tension is the measure of the cohesive forces between the molecules in solution and depends on the polymer solution and solvent. Surface tension plays an important role in the electrospinning process and it should be in the range of 35 to 55 mN/m for effective spinning of the polymer solution.[20] The surface tension measured in our study was found to be in the range of 44 to 53 mN/m.

**5A.9.2 Contact Angle measurements**

The surface wettability of a material is important for many applications, and the wettability is usually determined using the contact angle method. The contact angle is related to the surface roughness and the chemical composition.
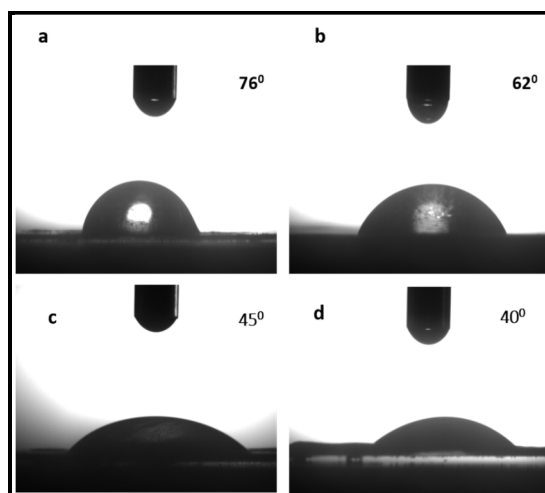


**Figure 5A.1 :** Contact angle of (a) EHEC/PVA nanofiber mat (b) EHEC/PVA nanofiber mat with 3%HNT (c) EHEC/PVA nanofiber mat with 10% GS (d) EHEC/PVA nanofiber mat with 3%HNT/10%GS.

In case of hydrophilic surface, the contact angle between the surface and the water droplet is less than 90°, as a result when the water droplet falls in the surface of material it will be adsorbed on the smooth surface of the nanofiber mat instead of rolling off.[21] The HNTs are also basically hydrophilic in nature and its addition of the nanofibers, we observed decrease in the contact angle from $76^0$ for EHEC/PVA nanofiber mat to $40^0$ in case of 3%HNT10%GS as shown in the **fig 5A.1**. This can be attributed to the formation of strong hydrogen bonds between EHEC/PVA matrix and the nanoclay.

**5A.9.3 Morphology of Nanofibers by SEM and TEM**

**Fig 5A.2 A** shows typical SEM micrographs along with the histograms of size distribution of EHEC/PVA neat nanofibers and HNT and GS. It can be clearly seen that nanofibers exhibited a smooth and bead free surface morphology having a diameter distribution in the range of 250-350 nm with an average diameter of $325 \pm 30$ nm.
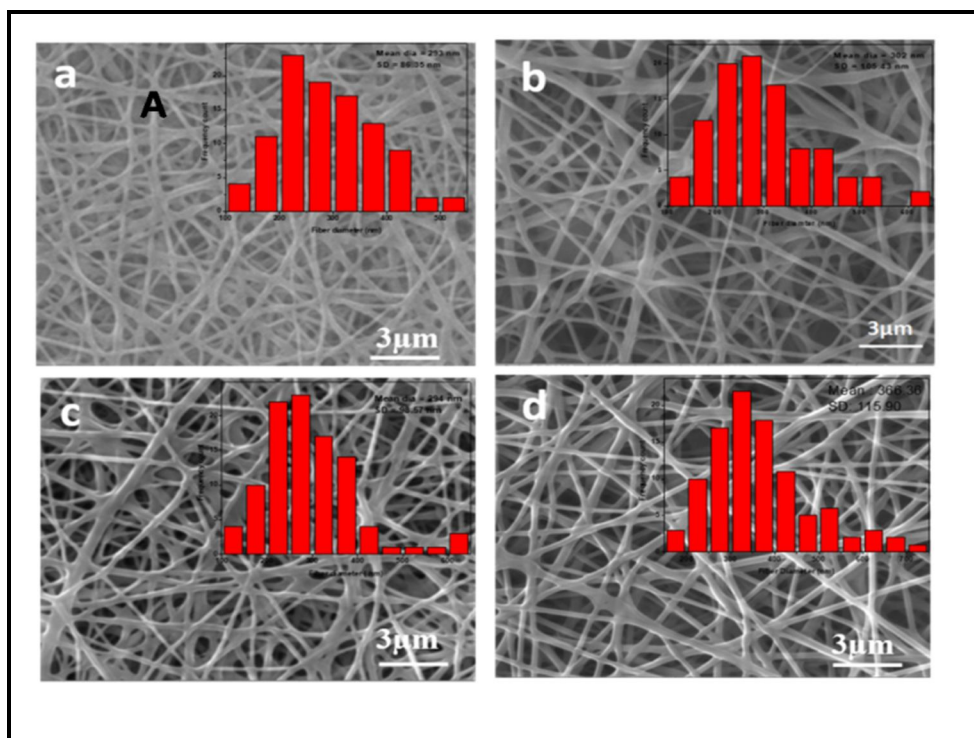
**Figure 5A.2: A)** SEM images of mats of E1 (a), E2 (b), E3 (c), E4 (d)
(All scale bars are 3µm) **B)** TEM image of E2 mat.
Scale bars: 0.5µm and 200 nm)

These fibrous structure results in large surface area to volume ratio and interconnected porosity which are essential for transport of oxygen and nutrients to the cell. The incorporation of HNTs into EHEC/PVA slightly increased the average diameter from 290 nm to 300 nm. This could be attributed to the fact that the negatively charged HNTs incorporated into the electrospinning solution would decrease of surface density of the spinning jet and increase in electrical conductivity and viscosity leading to the formation of

nanofibres with larger diameters.[22,23] The obtained nanofiber mats were opaque with good flexibility and having 10±0.5µm thickness. The thickness of the mat could be adjusted by varying the electrospinning time. The incorporation of HNT's into the nanofiber mat was examined by TEM. **Fig 5A.2B** shows the TEM micrographs of EHEC/PVA nanofiber mat with 3% wt HNTs. The tubular morphology distribution and alignment of HNTs in the nanofiber matrix can be readily seen from the figure. The images show the orientation of HNT's along the fiber axis.

**5A.9.4 Fourier Transform Infrared Spectroscopy (FT-IR)**

The FT-IR spectra of nanofiber mats E1, E2, E3, E4 are shown in **fig 5A.2**. The EHEC-PVA (E1) mat exhibit C-H stretching bands of $CH_2$ groups in the range of 2920-2930 $cm^{-1}$. The bands in the region 1350-1450 $cm^{-1}$ are due to the symmetrical deformations of $CH_2$ and COH groups. The bands due to primary alcohol (-$CH_2OH$-) groups stretching at 1073-1104 $cm^{-1}$ and $CH_2$ twisting vibrations appear in the region of 916-952 $cm^{-1}$. The weak bands around 599-669 are due to the ring stretching and ring deformation of α-D-(1-4) and α-D-(1-6) linkages.[24] The gentamicin peaks at 1104 $cm^{-1}$ was due to the $HSO_4$ groups and the peaks at 536-599 $cm^{-1}$ was due to $SO_2$ bond.[25] The peak at 1104 $cm^{-1}$ was not prominently observed in E4 as it has merged with the Si-OH group present in HNT. The peaks observed between 3352-3347 $cm^{-1}$ were due to the -OH groups. The C=O carbonyl sharp peaks are observed around 1721-1729 $cm^{-1}$ in all the graphs which confirms the presence of PVA (86% hydrolysed). The HNT shows characteristic peaks at 3687-3690 $cm^{-1}$ which is prominent in the graphs of E2 and E4 attributing to the stretching of the inner surface of the hydroxyl groups.[26] The Al-OH and Si-OH bending was observed at 916-922 and 611-614 $cm^{-1}$.
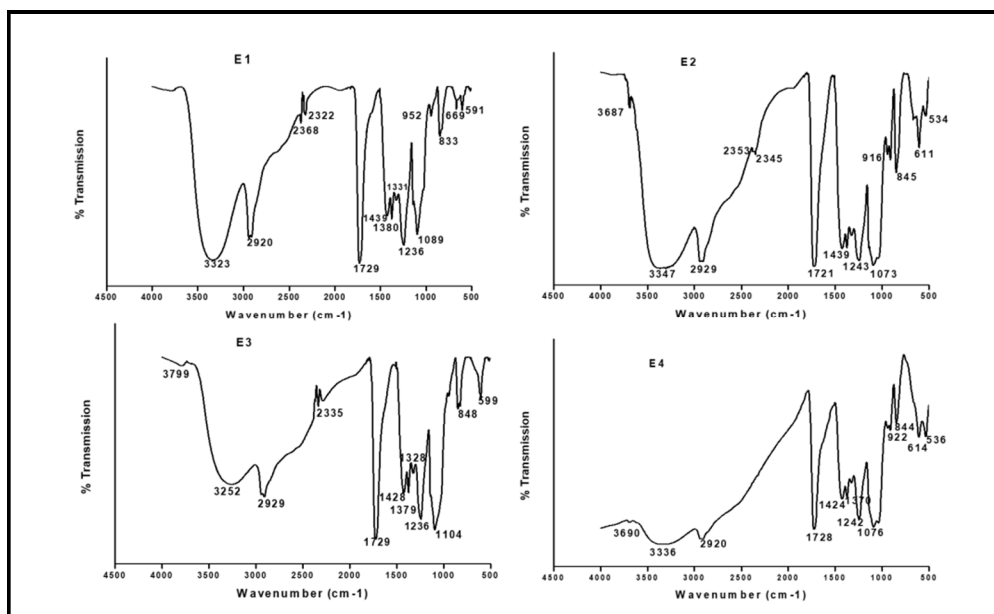
**Figure 5A.3:** FT-IR spectra of E1, E2, E3 and E4 nanofiber mats.

The Si-OH stretching vibration was observed at around 1073-1076 cm$^{-1}$. All the peaks of GS and HNT are observed in the E4 graph which reveals that the drug and nanotubes are successfully incorporated into the nanofibers.

**5A.9.5 X-Ray Diffraction (XRD)**

**Fig 5A.3** shows the XRD patterns of neat EHEC, PVA and HNT and compared with the different diffactograms of nanofiber mats (b). The neat EHEC showed peaks at $2\square$ of $22.2^0$, $33.1^0$, $46.8^0$. The neat PVA showed a broad peak at $19.7^0$ indicating the semi-crystalline nature. The neat HNT showed three distinct peaks at $11.9^0$, $20.3^0$, and $25.1^0$ with d-spacing values of 7.53, 4.4 and 3.5 Å respectively.[27] The nanofiber mats showed broad, smooth and similar XRD patterns with distinct peak at $2\square$ $=19.6^0$ indicating an inherent semi-crystalline nature of PVA present in the nanofiber mats. The distinct peaks of HNT's disappeared in all the nanofiber mats which reveal that the crystalline structure of HNT's could be potentially destroyed resulting into sheet like shapes.
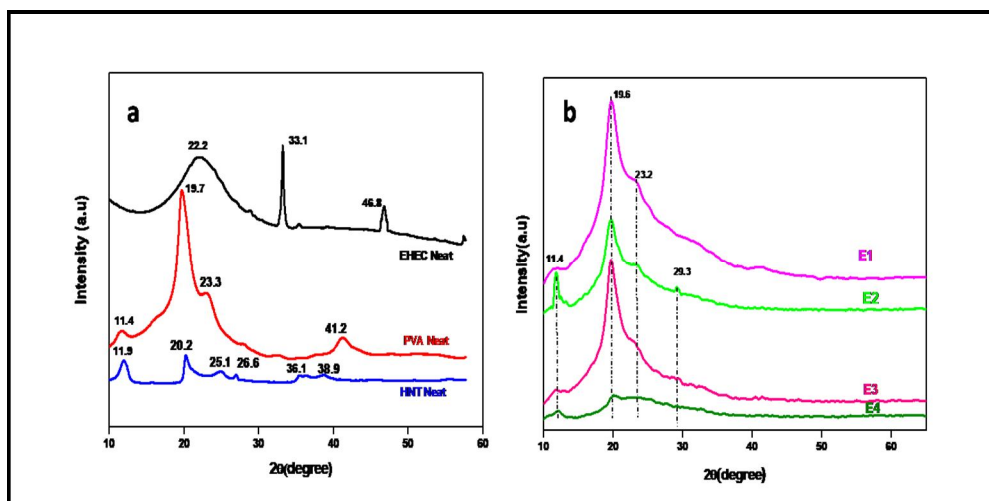
**Figure 5A.4:** XRD spectra of neat EHEC, PVA and HNT (a) Nanofiber mats of E1, E2, E3 and E4 (b).

The nanofiber mat E4 with the content of both HNT and GS showed very broad hump where the characteristic diffraction peak of PVA also disappeared. This clearly indicates that the incorporation of GS reduces the semi-crystalline nature of PVA significantly.

## 5A.9.6 Brunauer−Emmett−Teller (BET) Analysis

The $N_2$ adsorption and desorption isotherms of the EHEC/PVA and EHEC/PVA containing HNT and GS  electrospun nanofibers were degassed at 150 $^0$C  for atleast 12 hours and experiments were conducted at 77 K. The specific surface areas of the nanofibers were calculated using the Braunauer−Emmett−Teller (BET) method and the pore size distribution by Barrett−Joyner− Halenda (BJH) and Density Function Theory (DFT) method. The average pore radius was 1.89 nm for 0%HNT , 1.93 nm for 1%HNT, 1.91 nm for 3%HNT and 2.99 nm for 5%HNT and 9.75 nm for pristine HNT (data not shown in the table ). The multi point BET specific surface area increased from 94.28 $m^2$/g  for EHEC/PVA(0%HNT) nanofiber mat to 187.15 $m^2$/g for 1%HNT. The multi point surface area decreased to 83.56 $m^2$/g for 3%HNT and  40.16 $m^2$/g for 5%HNT  as shown in **table 5A.2.**

**Table 5A.2** Multi point Surface area (BET) and pore size distribution (BJH & DFT) methods of EHEC/PVA nanofiber mats with different loadings of HNT.

| Sample | BJH method pore size distribution | | | DFT method pore size distribution | | | Multipoint BET Surface area ($m^2/g$) |
|---|---|---|---|---|---|---|---|
| | Surface area ($m^2/g$) | Pore volume (cc/g) | Pore radius (Å) | Surface area ($m^2/g$) | Pore volume (cc/g) | Half pore width (Å) | |
| 0%HNT | 46.97 | 0.082 | 16.30 | 31.01 | 0.072 | 15.85 | 94.22 |
| 1%HNT | 49.71 | 0.081 | 15.67 | 32.09 | 0.069 | 25.99 | 187.15 |
| 3%HNT | 49.46 | 0.076 | 16.56 | 31.31 | 0.067 | 23.76 | 83.56 |
| 5%HNT | 29.52 | 0.052 | 15.65 | 21.52 | 0.049 | 15.84 | 40.16 |
| Pure HNT | 91.05 | 0.36 | 18.57 | 55.69 | 0.25 | 179.99 | 73.83 |

The surface area for pure HNT was 73.83 $m^2/g$. The pore size distribution was calculated using BJH and DFT methods. The surface area, pore radius and pore volume values were recorded as shown in table. The half pore width of pristine HNT was highest having 179.99 Å as shown in **fig 5A.5.** The half pore width and BET multi point surface area decreased with increase in the HNT concentration. This may be due to the formation of aggregates with increase in HNT. The **fig. 5A.6** shows the typical nitrogen sorption isotherms of nanofiber mats with pristine HNT and **fig 5A.7** showing isotherms with varying HNT concentrations. They show typical adsorption behaviours for the IV type, with an H3 type hysteresis loop according to the IUPAC classification which is a characteristic of mesoporous structure and indicates the existence of narrow slit-like pores.
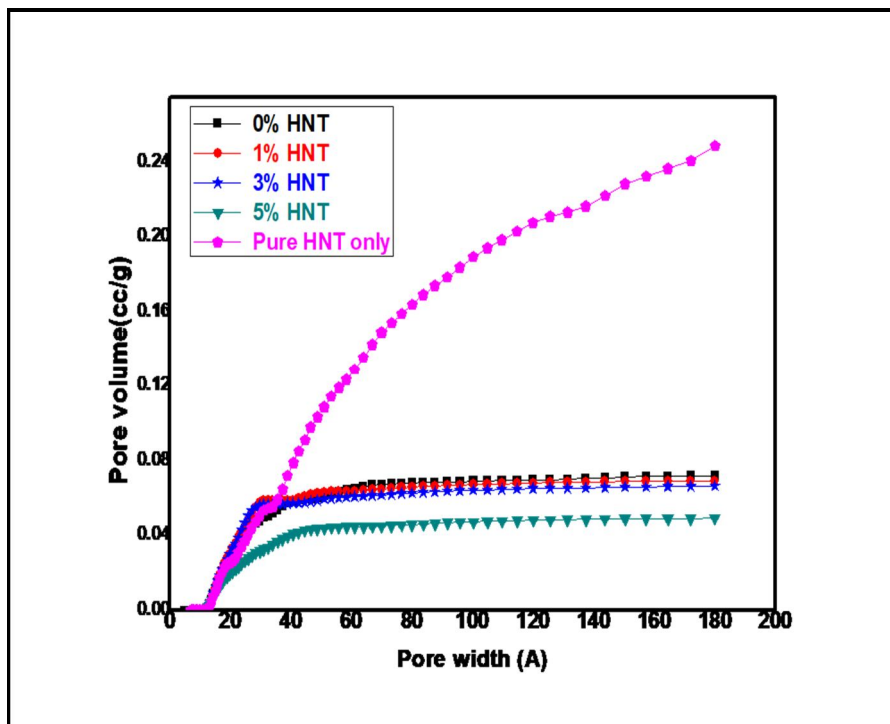
**Figure 5A.5:** DFT method for pore volume Vs pore width of EHEC/PVA nanofiber mats containing different HNT concentrations and Pristine HNT.
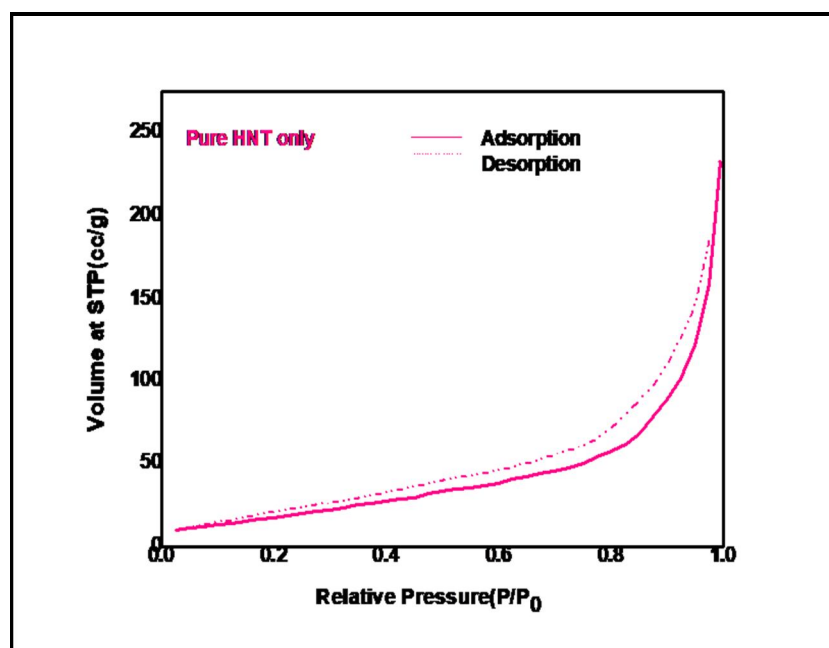


**Figure 5A.6:** Nitrogen sorption isotherms of Pristine HNT.
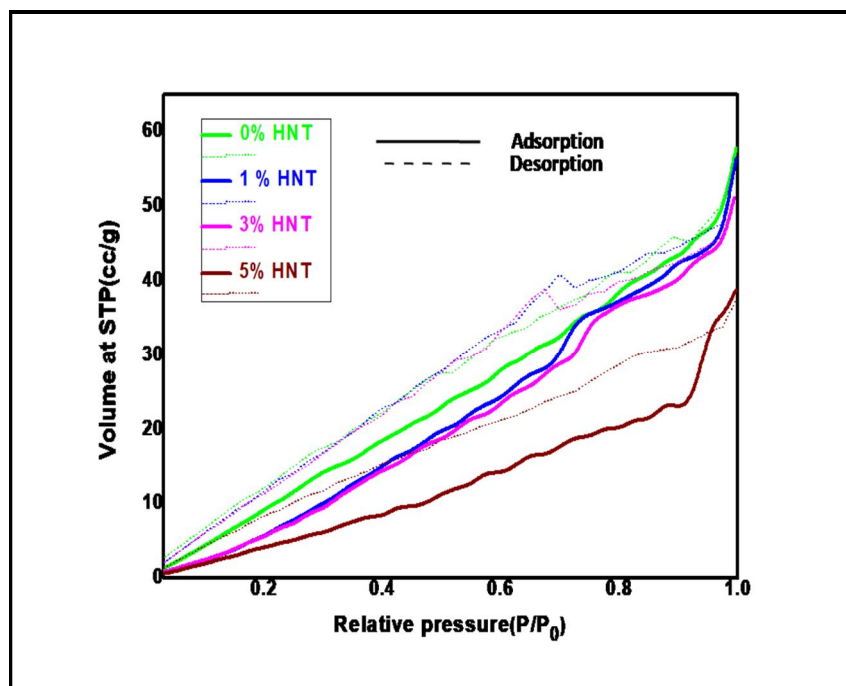
**Figure 5A.7:** Nitrogen sorption isotherms of nanofiber mats with HNT.

It can be seen that electrospun EHEC/PVA mat containing 5% HNT has the lower volume adsorbed and widest desorption branch. This is attributed to increase in content of mesopores of fibers due to incorporation of HNT. Furthermore, during the adsorption and desorption process, existence of pores with complex shapes might trap the meniscus, leading to slower desorption process and wider desorption branch.[28]

**5A.9.7 Thermal stability of nanofiber mats (TGA)**

The thermal stability of the nanofiber mats (E1, E2, E3 and E4) was examined by TGA and the results are as shown in **fig 5A.8**. The thermo grams show the decomposition of neat EHEC around 294 $^0$C (not shown here). The decomposition temperature of neat PVA is known to be around 85-97 $^0$C, depending on the molecular weight. Due to the low decomposition temperature of PVA, the nanofiber mat of EHEC/PVA (E1) showed the decomposition temperature at 250 $^0$C. However, with the incorporation of HNT into EHEC/PVA, the decomposition temperature increased to 270 $^0$C, which was due to to the release of water adsorbed on the surface of the nanotubes. Further, the increase in HNT loading from 1 to 3% showed only

marginal change in the decomposition temperature (data not shown in fig). The increased stability could be attributed to enhanced intermolecular interactions between the HNT's and the polymer matrices.
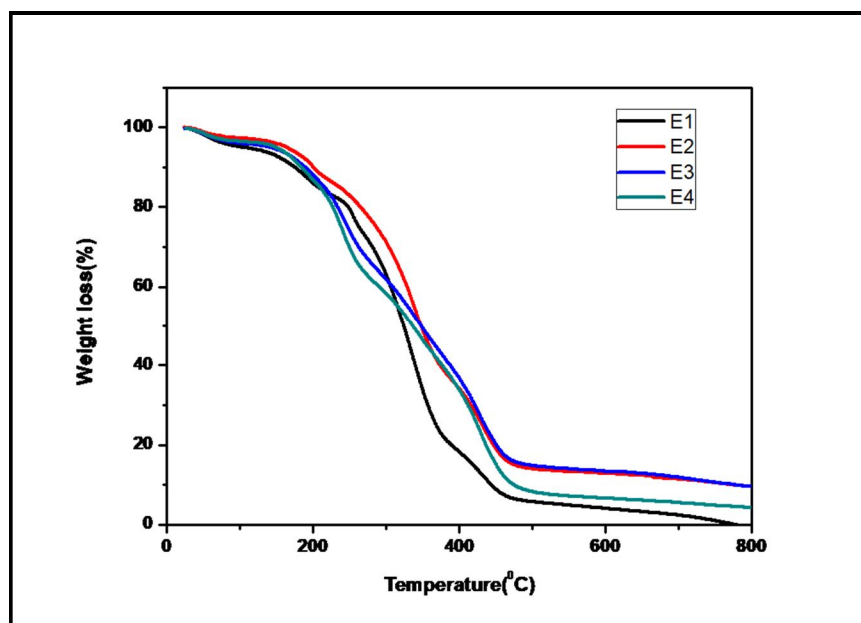


**Figure 5A.8:** Thermo grams of E1, E2, E3 and E4 nanofiber mats.

The thermo grams of HNT nanofibers showed a second decomposition step at 435-440$^0$C indicating two step decomposition behaviour which is attributed to the loss of intercalated water molecules in the interlayer space.[29] This observation indicates that HNT contributes to the thermal stability of EHEC/PVA nanofiber mats. The decomposition of GS incorporated nanofibers (E3) was observed at around 150$^0$C and the thermal stability slightly increased to 200$^0$C for E4 followed by again two step degradation around 400$^0$C due to the presence of HNT. The nanofiber mats E4 exhibits good thermal stability in the range of 200-250$^0$C.

**5A.9.8 Mechanical Studies**

**Fig 5A.9** shows the typical stress-strain curves for EHEC/PVA nanofiber mats with different loadings of HNTs. The results are given in **table 5A.3**.

It can be readily seen from the table that, the incorporation of HNT's into EHEC/PVA nanofibers significantly improved the mechanical properties. The nanofiber mats without HNTs showed the tensile strength of 5.1MPa. Upon

adding of 1 and 3 % HNTs, the tensile strength increased to 7.6 and 18.6 MPa respectively. The improved mechanical strength is due to the efficient transfer of load from polymer matrices to the HNTs. However, with further increase of HNT content to 5 wt%, the tensile strength decreased to 12.5 MPa.
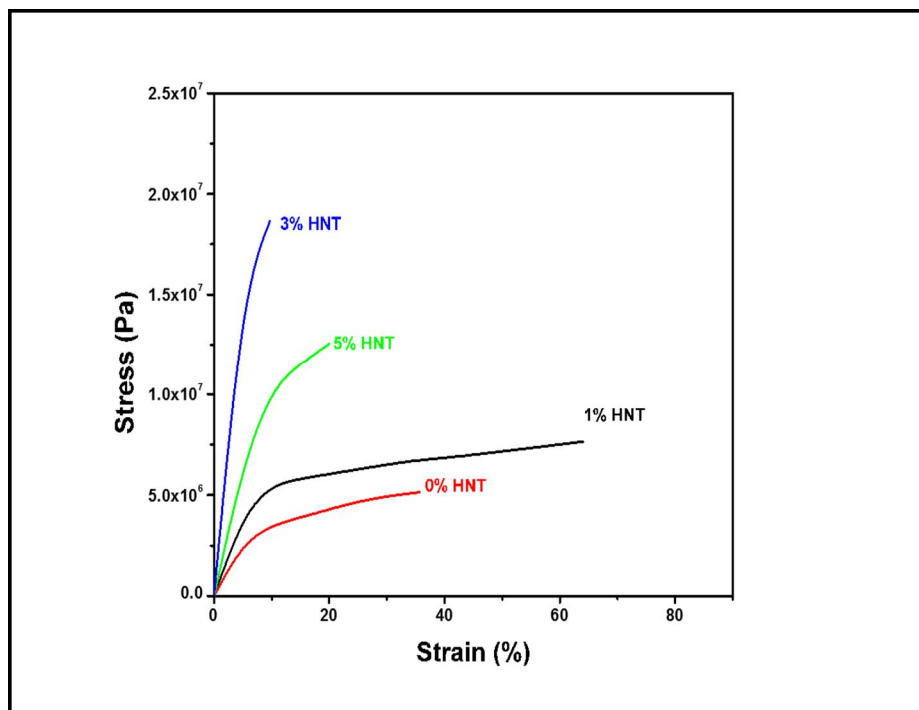


**Figure 5A.9:** Tensile stress-strain curve with different halloysite loading in the EHEC/PVA nanofibers.

**Table: 5A.3:** The tensile strength, elongation at break and Modulus of nanofiber mats.

| Sample Name | Modulus from slope (MPa) | Elongation at break (EB) % | Tensile Strength (MPa) |
|---|---|---|---|
| EHEC/PVA 0%HNT | 0.052 | 83.28 | 5.1 |
| EHEC/PVA 1%HNT | 0.191 | 57.74 | 7.6 |
| EHEC/PVA 3%HNT | 1.928 | 27.98 | 18.6 |
| EHEC/PVA 5%HNT | 0.338 | 39.44 | 12.5 |

It can be due to the fact that, at high HNT content, the interfacial adhesion between the fiber and clay might decrease leading to slippage and the loss of

load transfer resulting to lower tensile strength.[30] The nanofiber mats showed decreased elongation at break with the incorporation of HNT's which is expected since the nanofibers become more rigid in the presence of HNT's. The tensile strength of nanofiber mats did not vary much by the addition of the drug GS and hence not discussed here.

### 5A.9.9 Swelling Studies

The most predominant criteria of wound healing involves not only attachment of the scaffold to the wound bed, but also uptake of wound exudates, support new tissue formation and also transports nutrients in the scaffold during *in vitro* cell culture[31] and therefore the swelling of the nanofiber mats is critical. The equilibrium swelling of the nanofiber mats was measured in PBS buffer at 25°C. All the mats showed equilibrium swelling in the range of 1000-1200% as shown in **fig 5A.10**. The swelling increased with time and the mats attained the equilibrium swelling in ~ 24 h.
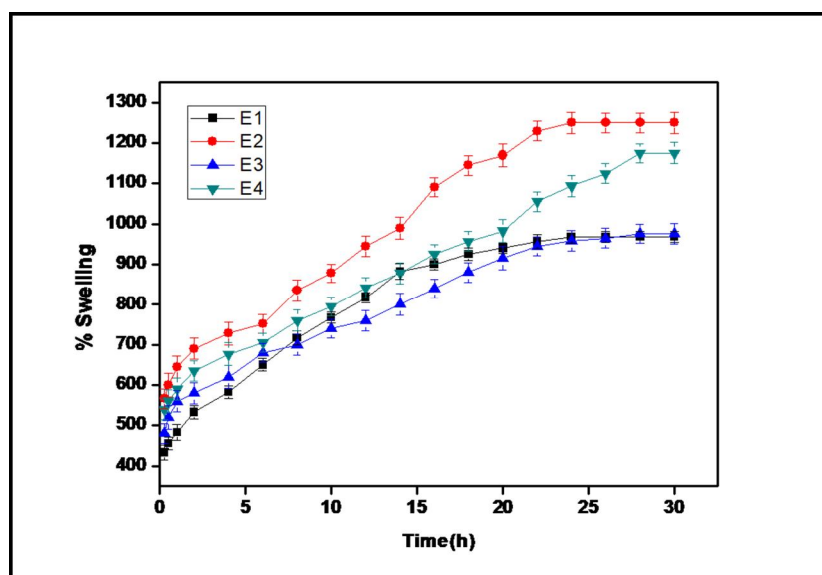


**Figure 5A.10:** Equilibrium swelling (%) of E1, E2, E3 and E4 nanofiber mats.

The presence of HNT in the nanofiber mats increased the hydrophilicity of the mats and showed the higher swelling property and degree of crosslinking is kept constant for all the nanofiber mats. All the equilibrium swollen nanofiber mats E1,E2, E3 and E4 were dried in a vacuum oven at room temperature and SEM images were taken (not shown here) to know if the morphology of the

fibers is affected by swelling in PBS. The nanofiber mats did not show any change and were found to be stable in PBS solution.

**5A.9.10 Drug release from halloysite loaded gentamicin nanofiber mats**

In vitro drug release study as shown in **fig 5A.11** was performed to understand the loading and release performance of GS from the HNT nanotubes and nanofiber loaded HNT and GS. Gentamicin sulphate (GS) was taken as the model drug for the release study in both pure form and embedded within the HNT into the nanofibers. The factors such as presence of HNT, method of loading the drug into the HNT does play an important role in the release. In our study, the entrapment effeciency for EHEC/PVA/10GS nanofibers was found to be 90.21% and that for EHEC/PVA nanofibers, with 10%GS incorporated in 3% HNT was found to be 87.33%. The entrapment efficiency of only 10% GS in 3% HNT was found to be 8.69%.
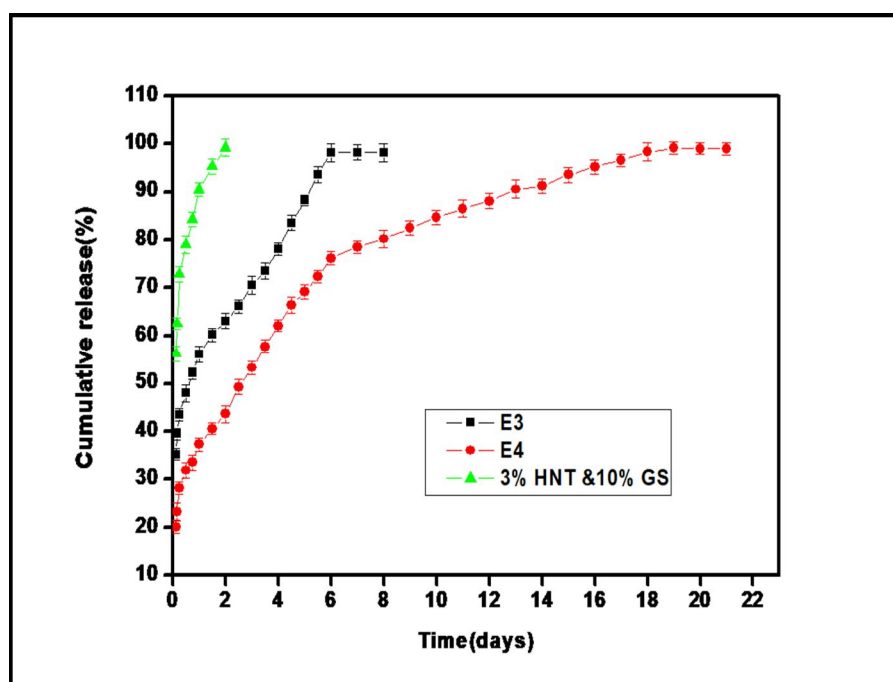


**Figure 5A.11:** Drug release from the nanofiber mats E3 and E4 and HNT containing GS.

The 10%GS entrapped into the lumen and on the surface of 3% HNT was completely released in PBS within 30 hours. In the nanofiber mats of EHEC/PVA/10GS (E3), burst release was observed initially for a period of two hours releasing 25% of the drug and then the release reached to 98.21%

for a period of 6 days. There was complete and slow release observed from the nanofiber mats containing the 3%HNT loaded 10%GS (E4) which was in a controlled and sustained manner for a period of 18 days and hence would help to prevent any bacterial infections in the wounds. HNT's are ideal candidates of biomaterials especially for controlled release of drugs. The gentamicin sulphate (GS) drug incorporated in the HNT is released slowly because it diffuses through the narrow lumen to reach the open ends of the nanotube. Halloysite retards the release rate up to several weeks, allowing protection against bacterial infection throughout the treatment. However, uneven distribution of the drug in nanofibers often results in initial burst effect for few minutes and then exhibiting slow and sustained release for several weeks to even months.[32]

### 5A.9.11 Cell Viability, growth and proliferation

The biocompatibility of nanofiber mats was examined by MTT assay using L929 cells over a period of 5 days. The toxicity of the halloysite nanotubes (HNT) and Gentamicin sulphate drug (GS) on the fibroblast cells was evaluated. **Fig 5A.12** shows the cell viability (%) of all the nanofiber mats along with the control. It can be seen from the figure, that the cells in the control group were 100% viable. The cells in E1, E2, E3 and E4 showed more than 100% cell viability over 5 days. These observations confirm that, HNTs and GS are non-toxic and having good cell viability.
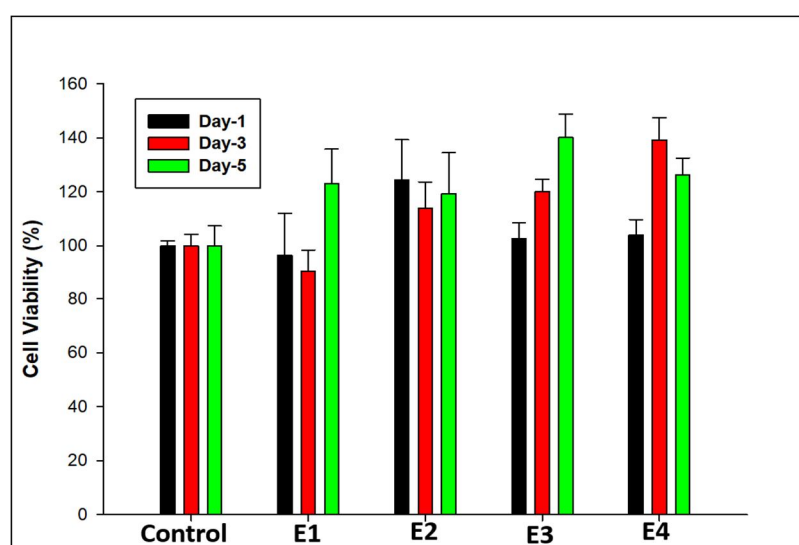


**Figure 5A.12:** MTT assay of E1, E2, E3 and E4 nanofiber mats.
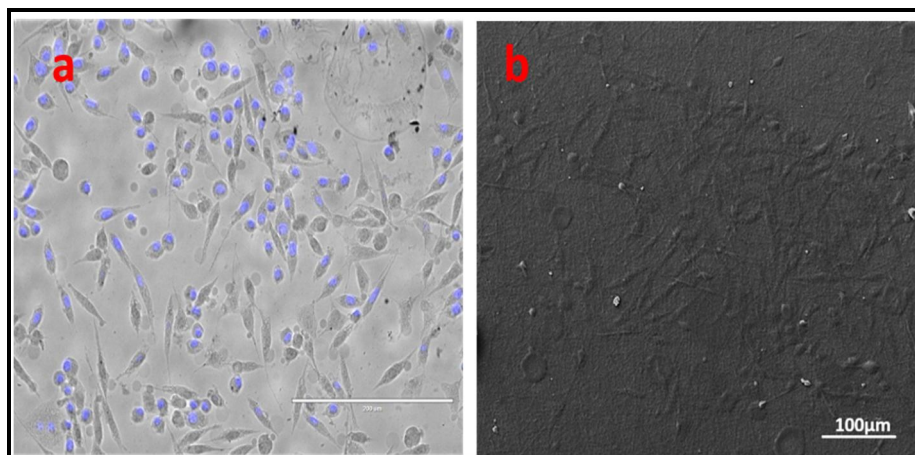
**Figure 5A.13:** Fluorescence image of E4 mat showing (a)nuclei of L929 cells by DAPI ; Scale bar : 200µm (b) SEM image of cell attachment and elongation; Scale bar :100µm.

The increased cell viability also suggests the good cyto-compatibility and promotes cell attachment, spreading and growth on the nanofibers. It can be seen that cells are attached to both the scaffold surface and the inner pores which suggests the cell growth and proliferation after 3 days of incubation. The results demonstrate that these nanofibers are biocompatible and have potential applications in tissue engineering. The spindle shaped L929 fibroblast cell growth and proliferation in the nanofiber mat (E4) was examined under fluorescence microscopy, where the blue colour indicates the nucleus of the cells as shown in **fig. 5A.13 (a)** and the SEM image was taken after 3 days of culture which confirms the cells are attached on the nanofiber mat are shown in **fig 5A.13 (b)**.

**5A.9.12 *In -vitro* Wound Migration Assay**

The wound migration assay is a simple and economical method to study cell migration *in- vitro*. One of the major advantages of this method is that it mimics to some extent migration of cells *in-vivo*. In our study, the assay was performed using L929 cell lines having control (only cells), E1, E2, E3, and E4.
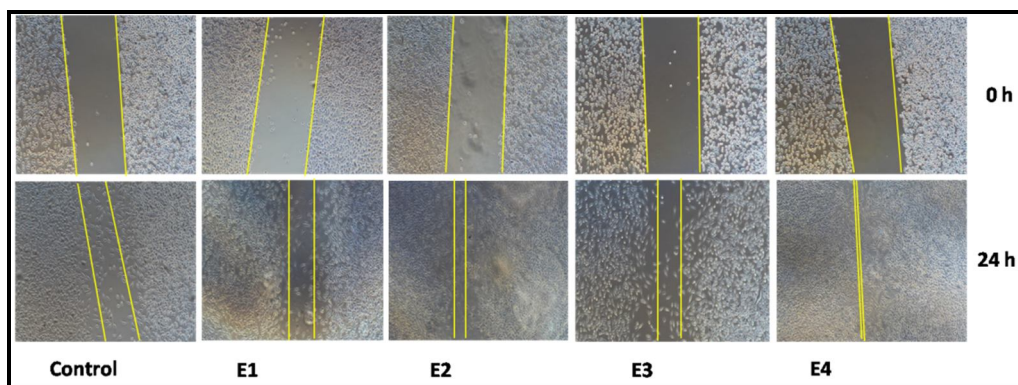
**Figure 5A.14:** Confocal microscopy images of L929 fibroblast cells of E1, E2, E3 and E4 nanofiber mats.
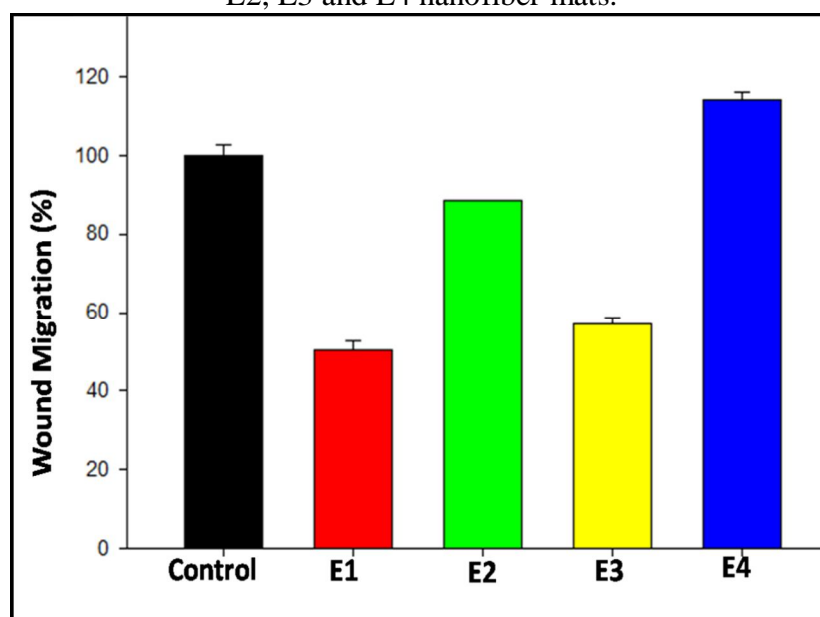


**Figure 5A.15:** Graphical representation of wound migration (%).

The cells having HNT showed good migration as compared to control and 0% HNT. The highest % of migration was seen in mats containing both HNT and GS which was almost 100% cell migration and confirmed cell viability as seen in **fig 5A.15**.

**5A.9.13 Hemocompatibility Assay**

Hemolysis is regarded as a significant screening test to perform its measurement of red blood cells in contact with materials and devices. In our study, we performed hemocompatibility test on four samples of nanofiber mats E1, E2, E3, and E4. It is known and reported that, if the hemolysis rate is below 5% then the medical materials are considered as non-hemolysis according to national biological safety protocol.[33] Hemolysis study

undertaken here showed the stability of red blood cells when in contact with the nanofiber mats and also HNT showed no toxicity effects.
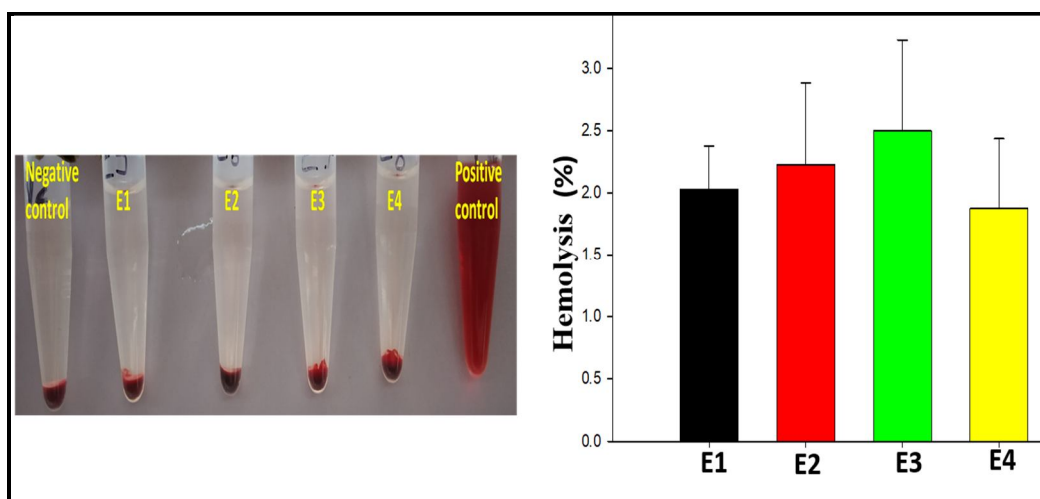


**Figure 5A.16:** Hemolysis assay of nanofiber mats (E1, E2, E3, and E4).

In **fig 5A.16** the results of all samples were less than 5%, conforming to the national biological material hemolysis rate security specified requirements.

### 5A.9.14 Antibacterial Studies

The antibacterial studies were done by Kirby Bauer disk diffusion method.[34] The zone of inhibition was observed for both gram positive and gram-negative bacteria are shown in **fig 5A.17**. There was no zone of inhibition for the negative control, i.e. the EHEC/PVA nanofiber mat (E1).
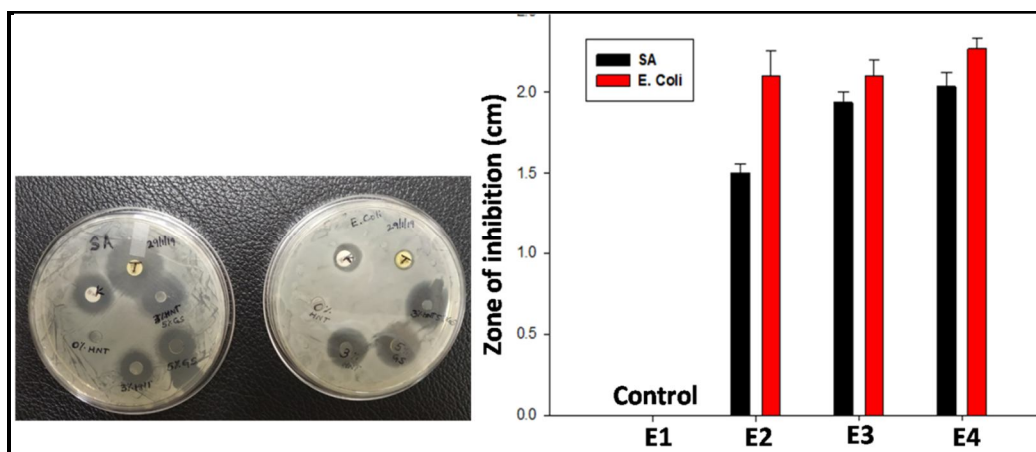


**Figure 5A.17:** Kirby Bauer disk diffusion method for gram-positive and gram-negative bacteria.

The zone of inhibition for EHEC/PVA/HNT (E2) was recorded as 1.5 cm for *S.aureus* and 2.1 cm for *E.coli*. The zones of inhibition for EHEC/PVA/GS (E3) and EHEC/PVA/GS/HNT (E4) was recorded as 1.8 and 1.9 cm for *S. aureus* and 2.1 and 2.2 cm for *E. coli* bacteria. In these experiments, we observed that the Halloysite nanoclay itself has an antibacterial property which was significantly observed. The zone of inhibition for the positive control antibiotic kanamycin and tetracycline were also observed and labelled as K and T respectively.

**5A.9.15 *In-vivo* Wound closure Assay**

The **table 5A.4** given below mentions the various groups which were used in the rat studies. Each group had three rats (n=3). The weight of the wistar rats used in the experiments was around 200-250 gm. The *in-vivo* studies were done using the nanofiber mats as per the code mentioned in **table 5A.4**, E1 to E4 and with a popular well known antibiotic ointment named povidone iodine. From the **fig 5A.18**, it was observed that there was not much significant difference in wound closure rate between the open wound (control) and with the marketed ointment (Povidone iodine).

**Table 5A.4:** The various groups used for *in-vivo* rat model studies.

| Group No. | Specifications | Code |
|-----------|----------------|------|
| I | Open wound (Control) | E |
| II | Marketed ointment (Povidone iodine) | E0 |
| III | EHEC/PVA nanofiber mat | E1 |
| IV | EHEC/PVA/3HNT nanofiber mat | E2 |
| V | EHEC/PVA/10GS nanofiber mat | E3 |
| VI | EHEC/PVA/3HNT/10GS nanofiber mat | E4 |
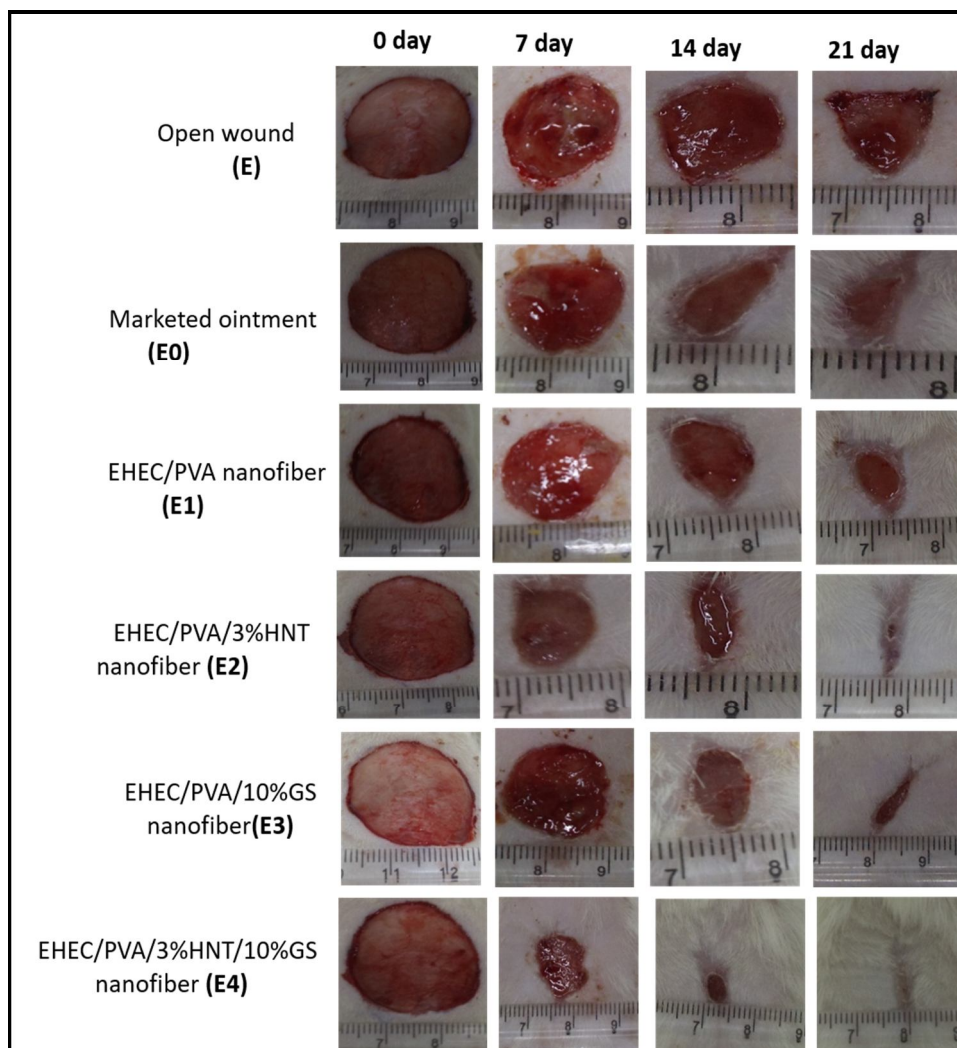
**Figure 5A.18:** Photographs of Wound healing of wistar rats and wound closure (%) from 0 to 21 days.

The closure rate of wounds for the control (open wound) and marketed ointment were 82% and 84%, and 90%, 95% for E1 and E2 mat on 14th day. The results demonstrated the ability of HNT loaded EHEC/PVA nanofiber mat to enhance the wound closure rate. The rats treated with E4 nanofiber mats showed more significant wound reduction compared to the rats treated with E3 nanofiber mat. The closure rates of wound treated with E3 and E4 nanofiber mats were 95% and 100% on the 14th day. A new layer of the skin with almost no scar was observed in E4 mats. Another notable observation was the results for HNT loaded nanofiber mats and the GS loaded nanofiber mats showed almost the same results.
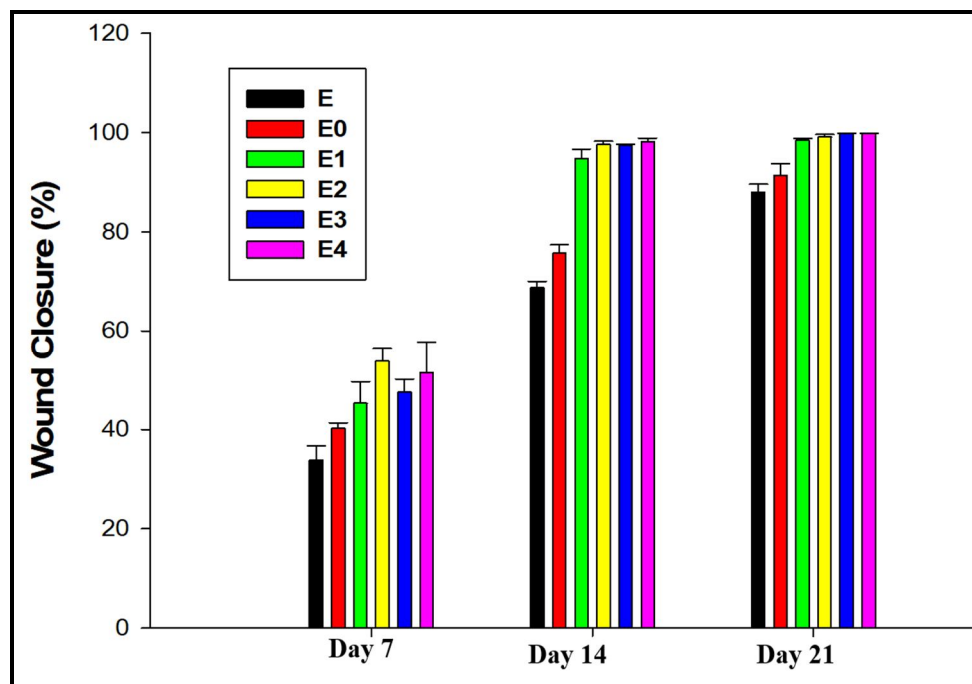
**Figure 5A.19:** Bar graph for Wound closure (%) from 0 to 21 days.

This implies that HNT alone could be used as a wound healing material and these results also are consistent with the antibacterial studies, scratch assay and cell attachment test. This indicates that the addition of HNT into GS-loaded EHEC/PVA nanofibers (E4) can not only improve the wound healing process but can also improve cell adhesion and proliferation of fibroblast cells. HNT also being hydrophilic in nature provide an adequate level of moisture to build up the exudates on the wound area for enhanced wound healing without scar formation.[35]

### 5A.9.16 Histopathology Study

The structural and functional regeneration of the skin depends mostly on the regulation of the extra cellular matrix(ECM) deposition.[36] We show in **fig 5A.20** the microscopic images of skin tissues of open wounds of rats (group E) for Hematoxylin and Eosin staining. It can be observed that there is no epidermal layer (Ep) formation (arrow shown). The small arrows in the figure indicate the mild to moderate ulceration (Ul), inflammation (In) and focal point (F). There is a focal minimal epidermal hyperplasia with epithelisation, minimal to mild collagen deposition and multifocal mild angiogenesis at dermis. Skin tissues of E0 and all the treated groups (E1 to E4) showed focal

mild to moderate epidermal hyperplasia with epithelisation, moderate collagen deposition and multifocal mild to moderate angiogenesis at dermis. In the group (E4 to E6), a thick and prominent epidermal layer and fibroblast cells were observed. In Masson's trichrome staining of the open wound (E) there was no deposition of collagen(Co) and angiogenesis(Ag) as shown in **fig 5A.20**.
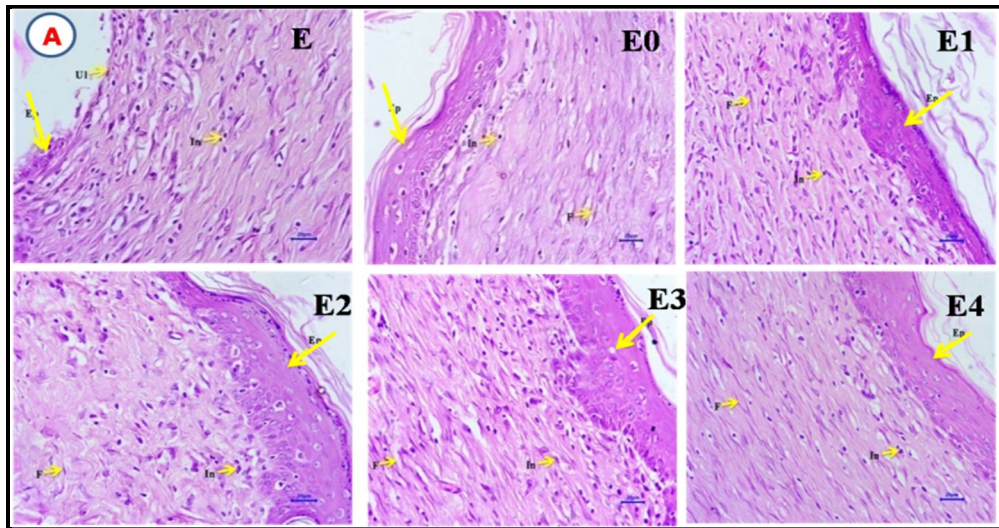


**Figure 5A.20:** Hematoxylin and Eosin staining.
Scale bar: 200µm and 400X magnification.
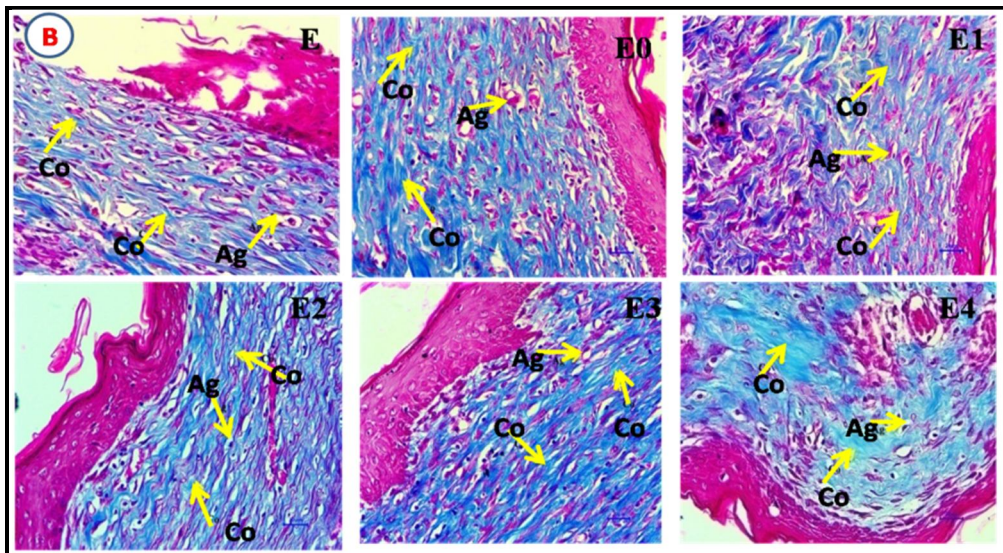


**Figure5A.21:** Masson's Trichrome for collagen staining.
Scale bar: 200µm and 400X magnification.
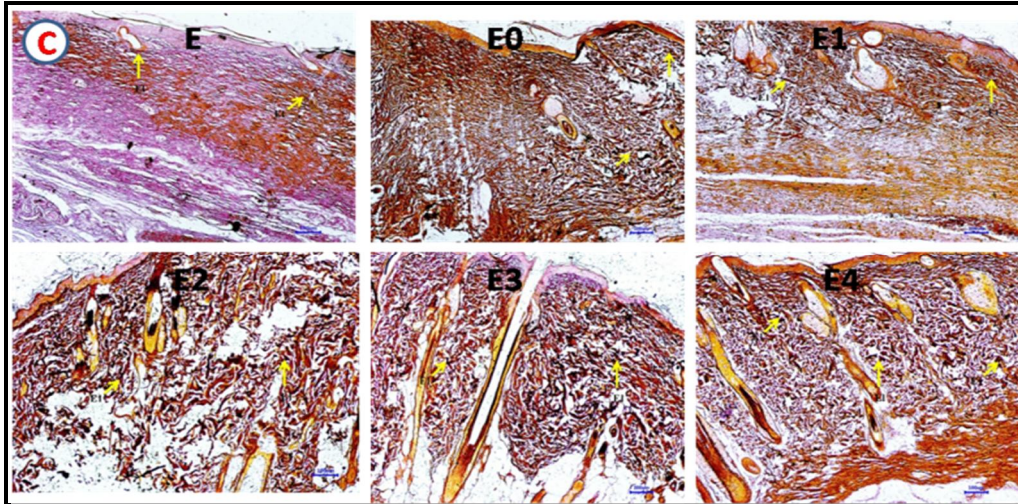
**Figure 5A.22:** Gomori's staining for reticular fibers.
Scale bar: 100µm and 400X magnification.
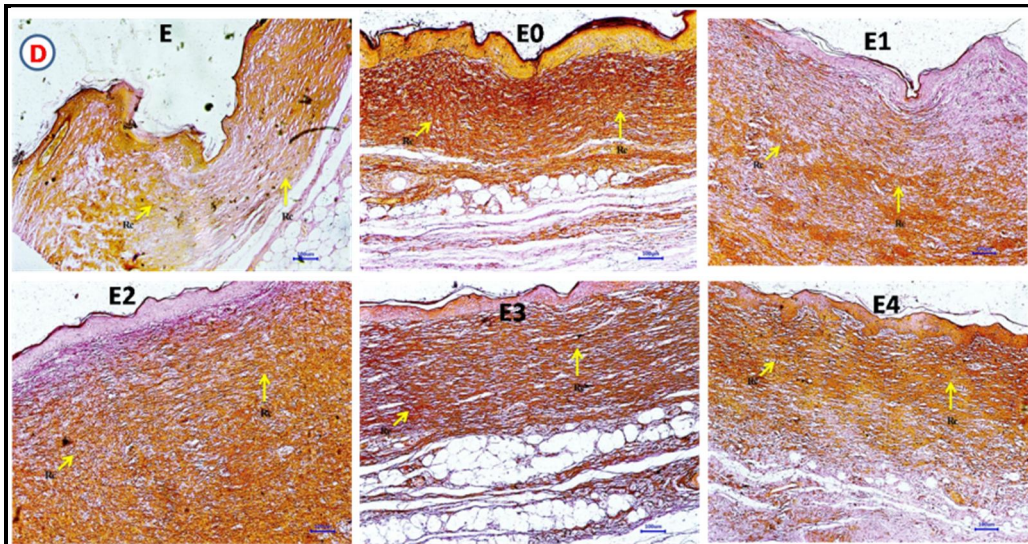


**Figure 5A.23:** Verhoeff's Van Gieson staining for elastin fibers.
Scale bar: 100µm and 400X magnification.

The formation of collagen is another remarkable signature of tissue generation which is essential for a healthy skin and normal functioning.[37] The groups E2 to E4, showed denser granulation tissue deposition and better collagen bundles indicated by dark blue staining along with significantly accelerated angiogenesis in full thickness dermal wounds as shown in **fig 5A.21**. Whereas E, E0 and E1 groups had poorly developed shattered collagen bundles.[38] Special stains are required for staining reticular and elastin fibers. Gomori's

staining technique of argyrophilic type using silver impregnation demonstrate the rectic fibers which are fine delicate fibers connected to coarser and stronger collagen fibers (type I) that provide framework to organs like skin, spleen, lymph etc. We observe in **fig 5A.22**, the reticulin fibers (black in colour) are found along with the fibroblastic and collagenous stroma, just below the epidermal layer. There was less number of reticulin fibers in case of open wound as the wounds were not completely re-reepithelialised, where as dense and mature reticular fibers were seen in all the groups at the end of 21 days.[39] The elastin fibers appeared brown in colour, thick, robust, mature and seen distributed all over the dermal tissue healed by nanofiber mats as shown in **fig 5A.23**. The elastin secretion was abundant in the dermal region of wounds treated with clay and gentamicin when compared with open wound due to faster wound healing. The overall healing progression in the open wound (control) and marketed ointment was slow as compared with group containing clay, gentamicin and combination of both. The treatment of nanofiber mat in combination with HNT and GS enhanced the recovery of wounded skin by increasing epithelisation, fibrous tissue proliferation, increased collagen deposition and angiogenesis. The results indicate that HNT accelerates skin wound healing by enhancing myofibroblast level and increasing wound contraction during the re-modeling phase of the wound healing process. Fibroblasts are responsible for new ECM formation and collagen deposition in the wound area.

## 5A.10 Conclusions

In conclusion, we have demonstrated the fabrication of electrospun nanofiber mats based on the natural polymer, EHEC and a biocompatible polymer PVA for wound healing applications. The solution properties like viscosity, conductivity and surface tension were studied to obtain good elctrospun fibers. The addition of HNT increased the mechanical strength to more than three folds from 5MPa to 19MPa. A mineral clay halloysite and an antibiotic drug, gentamicin were incorporated in the naonofiber mats for enhancing the mechanical strength and rapid wound healing process. *In-vitro* studies indicated that nanofiber mats were non-toxic and promoted rapid cell growth

and proliferation. The antibacterial studies also revealed that the halloysite nanoclay has antibacterial properties and helps to inhibit the gram positive and gram negative bacteria. There was no hemolysis observed for any of the mats, confirming the cytotoxicity. The *in- vivo* wound healing studies of mats on wistar rats for 21 days showed faster tissue regeneration in terms of re-epithelialisation and enhanced collagen deposition with almost no scar formation at the end of 21 days. These nanofiber mats show great potential in wound dressing materials.

## 5A.11 References

**1**. Rieger, K. A.; Birch, N. P.; Schiffman, J. D., Designing electrospun nanofiber mats to promote wound healing - a review. *Journal of Materials Chemistry.* B 2013, 1 (36), 4531-4541.

**2.** Sahana, T. G.; Rekha, P. D., Biopolymers: Applications in wound healing and skin tissue engineering. *Molecular Biology Reports.* 2018, 45 (6), 2857-2867.

**3.** Kumbar, S. G.; James, R.; Nukavarapu, S. P.; Laurencin, C. T., Electrospun nanofiber scaffolds: engineering soft tissues. *Biomedical Materials.* 2008, 3 (3),1-15.

**4.** Moura, D.; Mano, J. F.; Paiva, M. C.; Alves, N. M., Chitosan nanocomposites based on distinct inorganic fillers for biomedical applications. *Science and Technology of Advanced Materials.* 2016, 17 (1), 626-643.

**5.** Zhao, Y. L.; Wang, S. G.; Guo, Q. S.; Shen, M. W.; Shi, X. Y., Hemocompatibility of electrospun halloysite nanotube- and carbon nanotube-doped composite poly(lactic-co-glycolic acid) nanofibers. *Journal of Applied Polymer Science.* 2013, 127 (6), 4825-4832.

**6.** Xue, J. J.; Niu, Y. Z.; Gong, M.; Shi, R.; Chen, D. F.; Zhang, L. Q.; Lvov, Y., Electrospun Microfiber Membranes Embedded with Drug-Loaded Clay Nanotubes for Sustained Antimicrobial Protection. *Acs Nano.* 2015, 9 (2), 1600-1612.

**7.** Liu, M. X.; Shen, Y.; Ao, P.; Dai, L. B.; Liu, Z. H.; Zhou, C. R., The improvement of hemostatic and wound healing property of chitosan by halloysite nanotubes. *Rsc Advances.* 2014, 4 (45), 23540-23553.

**8.** PereswetoffMorath, L.; Bjurstrom, S.; Khan, R.; Dahlin, M.; Edman, P., Toxicological aspects of the use of dextran microspheres and thermogelling

ethyl(hydroxyethyl) cellulose (EHEC) as nasal drug delivery systems. *International Journal of Pharmaceutics.* 1996, 128 (1-2), 9-21.

**9.** Gaaz, T. S.; Sulong, A. B.; Akhtar, M. N.; Kadhum, A. A. H.; Mohamad, A. B.; Al-Amiery, A. A., Properties and Applications of Polyvinyl Alcohol, Halloysite Nanotubes and Their Nanocomposites. *Molecules.* 2015, 20 (12), 22833-22847.

**10.** Kataria, K.; Gupta, A.; Rath, G.; Mathur, R. B.; Dhakate, S. R., In vivo wound healing performance of drug loaded electrospun composite nanofibers transdermal patch. I*nternational Journal of Pharmaceutics.* 2014, 469 (1), 102-110.

**11**. Ghosh, S.; More, P.; Derle, A.; Kitture, R.; Kale, T.; Gorain, M.; Avasthi, A.; Markad, P.; Kundu, G. C.; Kale, S.; Dhavale, D. D.; Bellare, J.; Chopade, B. A., Diosgenin Functionalized Iron Oxide Nanoparticles as Novel Nanomaterial Against Breast Cancer. J*ournal of Nanoscience and Nanotechnology.* 2015, 15 (12), 9464-9472.

**12.** Wadhwani, S. A.; Gorain, M.; Banerjee, P.; Shedbalkar, U. U.; Singh, R.; Kundu, G. C.; Chopade, B. A., Green synthesis of selenium nanoparticles using Acinetobacter sp SW30: optimization, characterization and its anticancer activity in breast cancer cells. *International Journal of Nanomedicine.* 2017, 12, 6841-6855.

**13.** Liang, C. C.; Park, A. Y.; Guan, J. L., In vitro scratch assay: a convenient and inexpensive method for analysis of cell migration in vitro. *Nature Protocols.* 2007, 2 (2), 329-333.

**14.** Gui-Bo, Y.; You-Zhu, Z.; Shu-Dong, W.; De-Bing, S.; Zhi-Hui, D.; Wei-Guo, F. Study of the electrospun PLA/silk fibroin-gelatin composite nanofibrous scaffold for tissue engineering. *Journal of Biomedical Materials Research Part A.* 2010, 93A (1), 158-163.

**15.** Bui, H. T.; Chung, O. H.; Dela Cruz, J.; Park, J. S. Fabrication and characterization of electrospun curcumin-loaded polycaprolactone-polyethylene glycol nanofibers for enhanced wound healing. *Macromolecular Research.* 2014, 22 (12), 1288-1296.

**16.** Goldner, J. A modification of the masson trichrome technique for routine laboratory purposes. *Am. J. Pathol.* 1938, 14 (2), 237–243.

**17.** Bancroft J; Gamble M; Theory and Practice of Histological Techniques, 5th ed.;Churchhill Livingstone: New York, 2002; pp 155-159.

**18.** Lyanch M.J; Stanley S.R; Lyanch's Medical Laboratory Technology, 4th ed.;W.B.Saunders Company: Philadelphia,1983; pp 802-804.

**19.** A. Greiner.; and J. H. Wendorff. Electrospinning: a fascinating method for the preparation of ultrathin fibers. *Angewandte Chemie.* 2007, 46, 30, 5670–5703.

**20.** Doshi, J.; Reneker, D. H. Electrospinning Process and Applications of Electrospun Fibers. *J. Electrostat.* 1995, 35 (2), 151–160.

**21.** Salam, A.; Khan, M. Q.; Hassan, T.; Hassan, N.; Nazir, A.; Hussain, T.; Azeem, M.; Kim, I. S. In-Vitro Assessment of Appropriate Hydrophilic Scaffolds by Co-Electrospinning of Poly(1,4 Cyclohexane Isosorbide Terephthalate)/Polyvinyl Alcohol. *Sci. Rep.* 2020, 10 (1), 19751,1-9.

**22.** Qi, R. L.; Guo, R.; Zheng, F. Y.; Liu, H.; Yu, J. Y.; Shi, X. Y., Controlled release and antibacterial activity of antibiotic-loaded electrospun halloysite/poly(lactic-co-glycolic acid) composite nanofibers. *Colloids and Surfaces B-Biointerfaces.* 2013, 110, 148-155.

**23.** Tohidi, S.; Ghaee, A.; Barzin, J., Preparation and characterization of poly (lactic-co-glycolic acid)/chitosan electrospun membrane containing amoxicillin-loaded halloysite nanoclay. *Polymers for Advanced Technologies.* 2016, 27 (8), 1020-1028.

**24.**Wang, J.; Somasundaran, P., Mechanisms of ethyl(hydroxyethyl) cellulose-solid interaction: Influence of hydrophobic modification. *Journal of Colloid and Interface Science.* 2006, 293 (2), 322-332.

**25.** Lakdawala, M.; Hassan, P. A., Kothwala, D.; Malik, G. M., Poly (D, L-Lactide)-gentamicin composite coated orthopaedic metallic implant. *International journal of science and nature.* I.J.S.N., Vol. 4(3) 2013: 522-529. ISSN 2229 – 6441.

**26.** Liu, M. X.; Jia, Z. X.; Jia, D. M.; Zhou, C. R., Recent advance in research on halloysite nanotubes-polymer nanocomposite. *Progress in Polymer Science.* 2014, 39 (8), 1498-1525.

**27.**Yuan, P.; Southon, P.D.; Liu. Z.; Green, M.E.R.; Hook, J.M.; Antill, S.J.; Kepert, C.J., Functionalization of Halloysite Clay Nanotubes by Grafting with γ-Aminopropyltriethoxysilane. *J.Phys.Chem C.* 2008, 112-40, 15742-15751.

**28.** Maziyar, Makaremi.; Rangika Thilan De Silva.; and Pooria Pasbakhsh. Electrospun Nanofibrous Membranes of Polyacrylonitrile/Halloysite with Superior Water Filtration Ability *J. Phys. Chem. C* 2015**,** 119, 7949−7958**.**

**29.** Bordeepong, S.; Bhongsuwan, D.; Pungrassami, T.; Bhongsuwan, T. Characterization of halloysite from Thung Yai District, Nakhon Si Thammarat Province, in Southern Thailand. *Songklanakarin J. Sci. Technol.* 2011, 33 (5), 599-607.

**30.** Attia, G.; Abd El-kader, M. F. H. Structural, Optical and Thermal Characterization of PVA/2HEC Polyblend Films. *International Journal of Electrochemical Science.* 2013**,** 8 (4), 5672-5687.

**31.** Voon, H. C.; Bhat, R.; Easa, A. M.; Liong, M. T.; Karim, A. A. Effect of Addition of Halloysite Nanoclay and SiO2 Nanoparticles on Barrier and Mechanical Properties of Bovine Gelatin Films. *Food and Bioprocess Technology.* 2012**,** 5 (5), 1766-1774.

**32.** Sothornvit, R.; Hong, S. I.; An, D. J.; Rhim, J. W. Effect of clay content on the physical and antimicrobial properties of whey protein isolate/organo-clay composite films. *Lwt-Food Science and Technology.* 2010**,** 43 (2), 279-284.

**33.** Datta, S.; Rameshbabu, A. P.; Bankoti, K.; Maity, P. P.; Das, D.; Pal, S.; Roy, S.; Sen, R.; Dhara, S. Oleoyl-Chitosan-Based Nanofiber Mats Impregnated with Amniotic Membrane Derived Stem Cells for Accelerated Full -Thickness Excisional Wound Healing. *Acs Biomaterials Science & Engineering.* 2017**,** 3 (8), 1738-1749.

**34.** Contreras-Caceres, R.; Cabeza, L.; Perazzoli, G.; Diaz, A.; Lopez-Romero, J. M.; Melguizo, C.; Prados, J. Electrospun Nanofibers: Recent Applications in Drug Delivery and Cancer Therapy. *Nanomaterials.* 2019**,** 9 (656),1-24.

**35.** Zheng, F. Y.; Wang, S. G.; Wen, S. H.; Shen, M. W.; Zhu, M. F.; Shi, X.Y.Characterization and antibacterial activity of amoxicillin-loaded electrospun nano-hydroxyapatite/poly(lactic-co-glycolic acid) composite nanofibers. *Biomaterials.* 2013**,** 34 (4), 1402-1412.

**36.** Martin, P., Wound healing-aiming for perfect skin regeneration, *Science* .1997, 276 (5309) ,75–81.

**37.** Harel, Y.; Gerstenhaber, J.A.; Brodsky,R.; Huneke,R.B.; Lelkis,P.I., Electrospun soy protein scaffolds as wound dressings: Enhanced reepithelialization in a porcine model of wound healing. *Wound Medicine.* 2014, 5, 9–15.

**38.** Pal, P.; Das, B.; Dadhich, P.; Achar, A.; Dhara, S., Carbon nanodot impregnated fluorescent nanofibers for in vivo monitoring and accelerating full-thickness wound healing. *Journal of Materials Chemistry B.* 2017**,** 5 (32), 6645-6656.

**39.** Chouhan, D.; Chakraborty, B.; Nandi, S. K.; Mandal, B. B., Role of non-mulberry silk fibroin in deposition and regulation of extracellular matrix towards accelerated wound healing. *Acta Biomaterialia.* 2017, 48, 157-174.

# CHAPTER V(B)

## Design and Fabrication of EHEC Nanofibers with Nano-materials for Wound Healing Applications

### Part B: Silver Nanoparticles

*Science is a beautiful gift to humanity; we should not distort it.*

*Dr. APJ Abdul Kalam*

## 5B.1 Introduction

Nanomaterials exhibit outstanding physical and chemical properties, which include nanoparticles, quantum dots, nanowhiskers, nanorods, nanowires, nanofibers, nanosheets and nanotubes.[1] The nanomaterials have great potential in nano medicine, engineering, electronics, health care, energy generation, storage, filtration, environmental and in different biomedical applications.

Nanofibers particularly, are the ones which stand out among the rest of the nanomaterials due to their unique physicochemical properties and characteristics in nanometer size range. They are highly porous in nature with high surface area to volume ratios and are also capable of forming interconnectivity between the pores. Electrospinning technique is the best choice for large scale production of nanofibers. Electrospun nanofibers are easy and cost effective in production, easily stretchable and capable of surface modifications and therefore find variety of applications. The silver nanoparticles are of great interest these days due to their antibacterial, antimicrobial and antifungal properties against a wide range of fungi, bacteria and viruses.[2]

**Silver Nanoparticles (AgNPs**) are one of the most vital and fascinating nanomaterials among several other metallic nanoparticles that are used for biomedical applications. AgNPs play an important role, particularly in nanomedicine.[3] Ag-NPs have distinctive physico-chemical properties, with a high electrical and thermal conductivity, surface-enhanced Raman scattering, chemical stability, catalytic activity and non linear optical behaviour.[4] The Ag-NPs also exhibit broad spectrum bactericidal and fungicidal activity[5] which makes them popular in various consumer products, including food, soaps, pastes and textiles.[6,7]

## 5B.2 Antimicrobial Wound Dressings

A wound is defined as any disruption to the physiological of life and overall well-being. The number of patients suffering from all forms of chronic arrangement of the skin cells and a disturbance to its function in connecting and protecting the underlying tissues and organs in the human body.
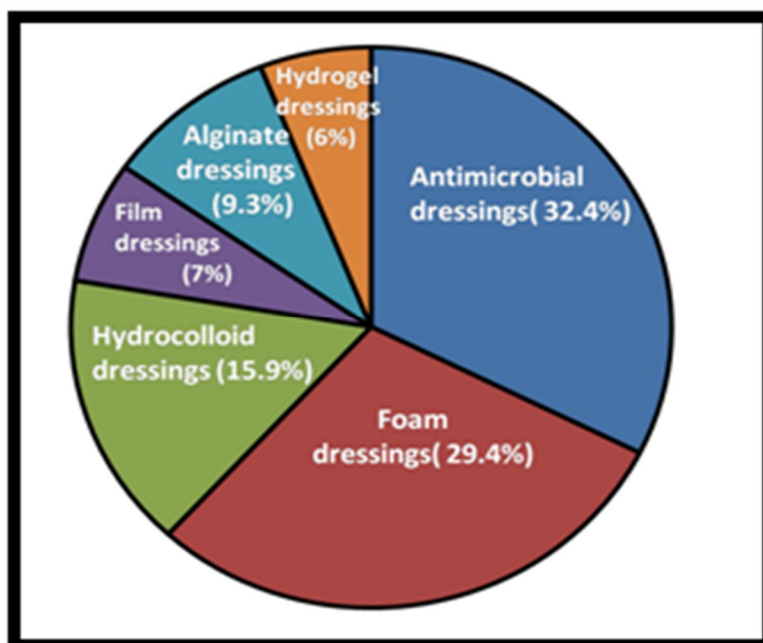
**Figure 5B.1:** Types of Wound care dressings.

[*Adapted from: Advanced wound care market forecast for the year 2016-2026*]
*www.visiongain.com*

The pie chart in **fig 5B.1** shows the percentage of different types of wound dressing materials available in the market and their demand. Antimicrobial wound dressings account for 32.4% of all the other wound dressings. Antimicrobial wound dressings play an important part in wound care prevention and management of infection. They also help to maintain a moist environment in the wound which helps in proliferation and migration of fibroblasts and keratinocytes.[8] The moist environment in the wound serves as a transporter for enzymes, growth factors, and hormones, which helps to induce cell growth and moist wound dressings promote collagen synthesis and decrease scar formation[9] which help wounds to heal faster[10]. Modern moist wound dressings can be classified depending on their materials (synthetic and natural polymers) and physical forms (hydrogels, hydrocolloids, films and foams).

### 5B.2.1 Properties of an Ideal Antimicrobial dressing

- ❖ Broad spectrum of activity against micro-organisms, including resistant strains of bacteria.
- ❖ Bactericidal not just bacteriostatic
- ❖ Rapid but sustained activity
- ❖ Suitable for use on broken skin/mucus membrane
- ❖ Non-irritant and non-toxic to tissue/environment
- ❖ Easily soluble in a non-toxic carrier
- ❖ Not inhibited by body fluids, wound exudates or biofilms
- ❖ Stable, easy to use and store
- ❖ Assists in wound bed preparation, e.g. debridement/ moisture management
- ❖ Cost-effective
- ❖ Reduces malodors
- ❖ Conforms to site and shape of the wound
- ❖ Patient satisfaction and clinician expectations. (*Vowden &Cooper, 2006)*[11]

### 5B.2.2 Bacterial Cell Death by Silver Nanoparticles (AgNPs)

Antimicrobial activity of silver dressings depends on the amount and rate of silver release and its toxicity to bacterial, fungal, and algal cells. Silver works by interacting with thiol groups present in the bacterial cells by stopping their respiration process. Silver nanoparticles prevent phosphate uptake and catalysation of disulfide bonds with silver tending to change the nature of protein structure in *E. coli.* The degenerative changes in cytosolic protein causes cell death.[12-14] Feng *et al* reported antibacterial mechanism of action of silver ions on gram positive *S. aureus* and gram negative *E. coli* bacteria showed that silver ions penetrate into bacterial cells and condense DNA molecules which inhibit their replication capabilities leading to cell death.[15] Silver nanoparticles show the most efficient antimicrobial activity amongst all forms of silver. The bactericidal effects of AgNPs depend on the size, shape, surface characteristics, and their dose.
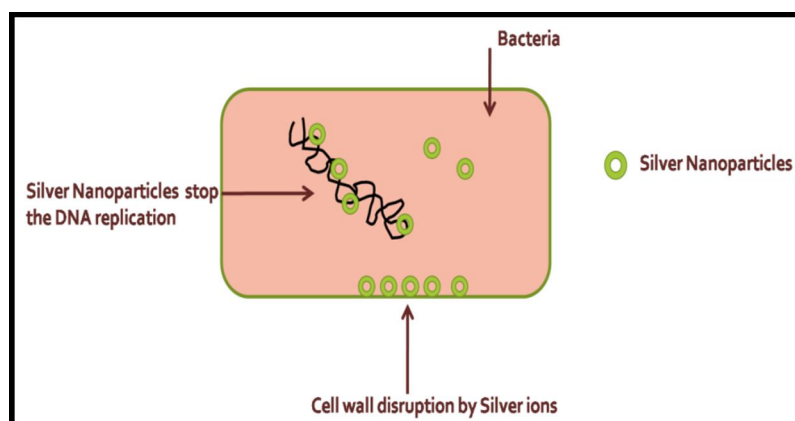
**Figure 5B.2:** Silver nanoparticles attack on mitochondria of bacterial cell.

It has also been reported that, nanoparticles having particle size ~ 1–10 nm have higher affinity of attaching to the surface of the cell membrane as compared to larger nanoparticles. The nanoparticles can attach to the larger surface area of bacterial cell membrane and cause cell death.[16]

**5B.2.3 Nanofibers with Silver Nanoparticles (Ag-NPs)**

The broad spectrum bactericidal efficacy of silver ions on microorganisms has long been recognised and utilised in the treatment of infected wounds. To protect the dressing material from oxidation and decolouration, and also have a steady and prolonged release of silver ions from the dressing materials, silver nanoparticles loaded nanofibers have been reported. In a research article by Damm *et al* 2007, the silver nanoparticles, embedded in a hydrophilic polymer, have long-term silver ion release behaviour.[17] One of the methods for synthesis of silver nanoparticles is that the silver salt like silver nitrate is mixed with a polymer solution and electropun into nanofibrous wound dressing mat and then expose to UV radiation to reduce the silver ions to silver nanoparticles *in situ*.[18] The synthetic polymers like polycaprolactone (PCL)[19] poly(vinyl alcohol)[20], polyacrylonitrile[21], poly(l-lactide)[22], poly(lactide-*co*-glycolide)[23] and polyvinyl pyrrolidone[24,25] and natural polymers such as gelatin[26], cellulose acetate[27,28] etc have been reported using this method in the literature.

## 5B.3 Material and Methods

Ethyl hydroxy ethyl cellulose (EHEC) was obtained from Akzo-Nobel Functional Chemicals AB, Sweden with trade name as Bermocoll E411 FQ. The molecular weight (MW) was 1200Kg/mol with about 7000 anhydro glucose units (AGU). Polyvinyl alcohol (PVA), molecular weight 1, 25000 g/mol, cold water soluble with degree of polymerization is 0.6 and 89% hydrolyzed was obtained from S.D Fine Chemicals, Boisar, India. Silver nitrate crystals, AR grade, molecular weight 169.87 g/mol, CAS No: 7761-88-8 was purchased from Thomas Baker Chemicals, Pvt Limited, India. Citric acid, anhydrous pure with mol wt 192.12 g/mol was purchased from Merck Limited, India. EHEC was purified as given in the procedure by Gupta *et al* [29] in 2015. Other materials were used directly without further purification. Distilled water was used throughout the experiments.

## 5B.4 Experimental Section

### 5B.4.1 Solution Preparation

The aqueous solution of EHEC and PVA was prepared in the ratio of 4:6 and the total polymer concentration was kept at 10 % (w/v). In order to post crosslink the nanofiber mats, citric acid (20 wt% of the total polymer) was added to the above solution. The silver nitrate ($AgNO_3$) salt was taken in 0.5, 1 and 2 wt% (w/w) with respect to the weight of EHEC/PVA blend.

### 5B.4.2 Electrospun EHEC/PVA Nanofiber mat embedded silver nanoparticles (Ag-NPs)

The antimicrobial EHEC/PVA nanofibrous mats were prepared by adding silver nitrate ($AgNO_3$) to an aqueous solution. The $AgNO_3$ salt was mixed with the polymer solution and subjected to UV radiation lamp at 25W/m$^2$ for a period of 10 minutes.[30] The milky white colour of the polymer solution turns light yellow to blackish brown in colour with increase in silver salt concentration from 0.5 to 2% and the size of nanopaticles[31] as shown in the **fig 5B.3**.

---
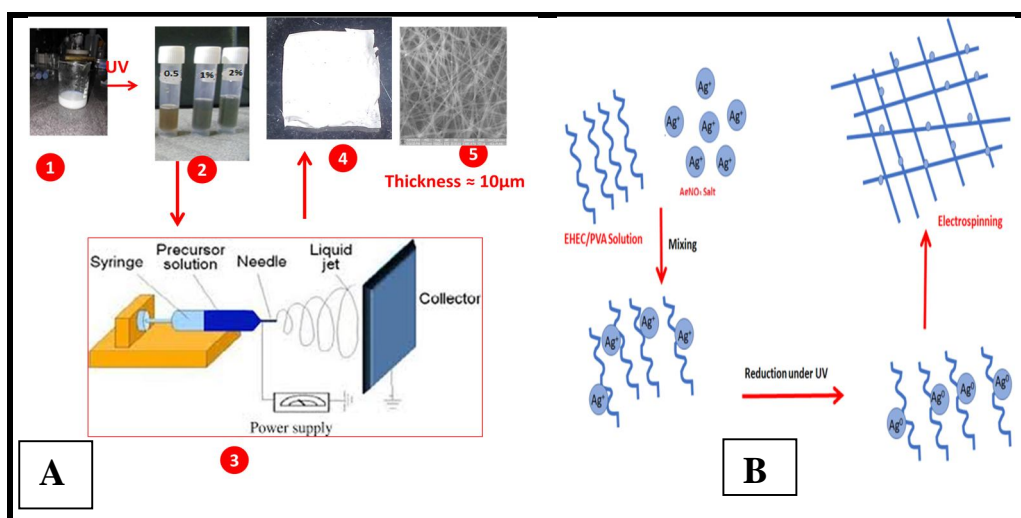
**Figure 5B.3: [A]**(1) EHEC/PVA solution (2) EHEC/PVA with 0.5, 1, 2% AgNO$_3$ salt after exposure to UV radiation (3) Electrospinning unit, (4) Nanofiber mat with 0.5% AgNPs, (5) SEM image of nanofiber mat containing 0.5% AgNPs. **[B]** AgNPs reduction from Ag$^+$ to Ag$^0$ using UV radiation is shown on right side.

The colour change of the polymer solution from white to blackish indicates the reduction of the AgNO$_3$ salt from Ag$^+$ ions to elemental silver Ag$^0$, which gives the primary confirmation for the formation of silver nanoparticles. The particles were uniformly dispersed on the fiber surface with the particle size ranging from 10 to 25 nm. The fibers containing silver nanoparticles showed very strong antimicrobial activity against gram positive and gram negative bacteria namely, *S. aureus* and *E. coli.*

## 5B.5 Characterization Techniques

The morphology of the nanofibers was studied using Scanning Electron Microscopy (SEM) quanta 200 3D dual beam ESEM FEI, Finland. The electron source was tungsten (W) filament with thermionic emission at 15 kV in high vacuum. The size and distribution of the electrospun fibers were analyzed using Image J analysis software (Image J, National Institutes of Health, USA). For each electrospun mat, 100 fibers were randomly selected from different regions of the SEM image and size of the fibers are reported as the average diameter. The size of the Ag-NPs was determined using TEM FEI, TECNAIG2 F30 instrument operated at an accelerated voltage of 200 kV.

The viscosity measurements were done on MCR 301, rheometer using cup and bob geometry. The electrical conductivities were measured using a conductometer, Toshniwal Instruments Mfg Pvt Ltd, Ajmer, SR No: 10J694. Conductivity cell: Type: TCC-1, K=0.98. All measurements were done at room temperature (27±2 $^0$C) in triplicates and the average values reported. Surface tension of the electrospinning solutions was carried out on the optical contact angle measurement system, Carl Zeiss, Jena, Japan.

Contact angle measurements were performed by using an optical contact angle apparatus (OCA 20, Data Physics Instruments, and Germany) equipped with a video measuring system having a high-resolution CCD camera and a high-performance digitizing adapter. SCA 20 software (Data Physics Instruments) was used for data acquisition. The fiber mats were fixed on top of a plane solid support and kept flat. The contact angle of water in air was measured by the sessile drop method. The water droplet volume was $6.0 \pm 0.5$ μL. Temperature was set at $25.0 \pm 0.1$ °C for the support and the injecting syringe as well. Images were collected 25 times per second, starting from the deposition of the drop to 40 s. From the data analysis, the contact angle, the volume, and the contact area of the drop were calculated. Five measurements at least were carried out on each fiber mat sample.

X-ray diffraction (XRD) measurements were performed on the Ag-NPs embedded nanofiber mats using a Philips X'pert pro powder X-ray diffractometer operating with CuKα radiation (λ=0.15406 nm, Ni filter) generated at 40 kV and 30 mA X-ray diffractometer.

The UV-Visible spectrometer UV-1601 PC Shimadzu, was used for the experimental analysis. The silver nanoparticles were scanned in the range 200–800 nm. The EDAX analysis was done on SEM-EDX machine, quanta 200 3D dual beam ESEM FEI, Finland.

The mechanical strength of the nano-matrices was measured using a dynamic mechanical analyzer (RSA3, TA Instruments, USA). The mat samples were cut into strips with dimensions of 20 cm × 0.5 cm and then mounted onto the tensile grips. The strain rate and gauge length were 10 mm min$^{-1}$ and 15 cm,

respectively. The mats were subjected to tensile force. Each sample was tested five times to authenticate its normal stress–strain curves.

The nitrogen adsorption desorption isotherm measurements were performed on a Quantachrome surface area analyser, the specific surface areas and pore size distribution of the samples were obtained by Brunauer-Emmett-Teller (BET) technique. The samples were weighed, dried in vacuum for 24 hours at the temperature of 30ºC to remove moisture. Pressure within the range of 0.01 to 1 P/P0; where P is relative pressure and P0 is saturation pressure and at temperature of 77 K was assumed for adsorption and desorption. Nitrogen with the purity of 5.0 was used as measuring gas.

Thermal analysis was performed in the temperature range from 30 to 900 °C at a controlled heating rate of 10 °C min$^{-1}$ with the nitrogen flushed at 50 mL min$^{-1}$ on the Thermal Analyzer (STA) 6000 (Perkin-Elmer, USA). The weight loss of various phases in the thermogram was correlated with the degradation of specific components of the AgNPs loaded nanofibers. The samples were analyzed in perforated and covered aluminium pans under nitrogen-purging conditions.

## 5B.6 Swelling Studies

The nanofiber mats weighting 5 mg each containing 0.0 0.5, 1, and 2% AgNPs were dipped in the phosphate buffer saline (PBS) solution (pH 7.4) at 37$^0$C. Excess surface water was blotted out with filter paper before weighing the samples and weights were taken at various time intervals starting from 30 minutes to 30 h. All the experiments were done in triplicates and average value was taken. The percent degree of swelling was calculated from the formula[32]:

$$\text{Degree of Swelling (\%)} = [(M_w - M_d)/ M_d] \times 100$$

Where the $M_w$ and $M_d$ are weights of wet and dry samples respectively.


## 5B.7 Release study of Silver ions in Phosphate Buffer Saline (PBS)

To evaluate the silver ions release from the electro spun nanofiber mats, the cut piece(1 cm x 1 cm) of nanofiber mat was immersed in 15 ml phosphate

buffer solution(PBS) taken in a covered test tube and kept in a shaker bath (Julabo SW 23) with gentle shaking at $37^0$C. At predetermined time intervals, 1 ml of PBS was taken and replenished with an equal volume of fresh PBS into the test tube. The amount of silver released was determined by UV-Vis spectrometer (UV-160 PC Shimadzu) at a $\lambda_{max}$ of 354 nm (obtained from the experimental calibration curve for silver). The percentage silver release was calculated using the calibration curve of silver in PBS at 7.4 pH. The release experiment of each sample was performed in triplicates and the average value is reported. The encapsulation efficiency was calculated as follows:

$$\text{Encapsulation efficiency } (\%) = \frac{\text{mass of maximum drug released}}{\text{mass of total drug released}} * 100$$

## 5B.8 Antibacterial Studies

The antibacterial studies were performed on the bare EHEC/PVA nanofiber mats with 0%AgNPs and nanofibers containing 0.5, 1 and 2 %AgNPs using the Kirby Bauer disk diffusion method. The gram-positive and gram-negative bacteria, *S. aureus* and *E. coli* were inoculated in 10 ml nutrient broth in culture tubes and kept at 37 $^0$C in an incubator. The nutrient agar petri plates were prepared. After overnight incubation of nutrient broth, 100ul from each (*E. coli* and *S. aureus*) were inoculated on the petriplates in triplets. The cultured broth (100ul) was spread on the nutrient agar plates by sterile spreader. All the nanofiber mats were cut into circular shape of equal size and placed on the agar plates along with negative control (antibiotic discs of kanamycin and tetracycline) at 37 $^0$C in the incubator. After overnight incubation, the zones of inhibition were measured and photographs taken.

## 5B.9 Biological Studies

### 5B.9.1 Cell Viability Study

The cytotoxicity of nanofiber mats was investigated using MTT assay. The L929 mouse fibroblast cell line used was obtained from National Centre for Cell Science (NCCS), Pune, India. The cells were cultured in DMEM medium, supplemented with 10% fetal bovine serum, streptomycin (10 g/ml) and penicillin (100 units/ml) and were maintained in a humidified atmosphere at $37^0$C under 5% $CO_2$.[33] Cells ($1\times10^4$) were seeded per well in 24-well, flat

bottom culture plate and incubated for 24 h, followed by the treatment using nanofiber mats 0, 0.5, 1 and 2 % AgNPs were kept for 1, 3 and 5 days. After incubation, the MTT solution (5 mg/ml of stock solution of which 20µl of MTT solution was added in 200µl of DMEM media) was added to each well followed by further incubation in darkness at $37^0$C for 4 h. The formazan crystals formed were dissolved by addition of acidified isopropanol. After 15 min, the amount of colored formazan derivative formed was determined by measuring the optical density (OD) using a microplate reader (Spectra Max, MS; Molecular Devices, LCC) at 570 nm. All the experiments were done in triplicate. The percentage cell viability was calculated as:

$$\% \text{ Cell viability} = \frac{(OD)sample - (OD)blank}{(OD)control - (OD)blank} * 100$$

## 5B.9.2 Hemolysis Study

Hemolysis study of electrospun mats containing 0%, 0.5%, 1% and 2% AgNPs were performed using method of indirect contact according to the requirements of ISO 10993.[34] About 3ml of rat blood was collected in EDTA coated vials and was diluted to 3 times in physiological saline. 1 ml of diluted blood was then centrifuged at 2000 rpm for 15 minutes at $4^0$C. 200µl of this diluted blood was taken in an eppendorf tube and made upto 1 ml. The nanofiber mats were immersed into the diluted blood and incubated for 1 h at $37^0$C and then centrifuged at 2000 rpm for 15 minutes. After centrifugation, the supernatant liquid was collected and absorbance was recorded at 540 nm. Triton-X (0.1%) was used as positive control and saline as negative control for the study. All the experiments were done in triplicates and average value was reported. The percent haemolysis was calculated using the following formula:

$$\% \text{ Hemolysis} = \frac{Sample\ (OD) - Negative\ control\ (OD)}{Positive\ control(OD) - Negative\ control(OD)} * 100$$

## 5B.9.3 In-vitro Cell growth and Proliferation

The nanofiber mat with 0.5% AgNPs was sterilized for 15 min inside a biosafety cabinet and placed in 24 sized flat bottom well plates. Approximately 4 x $10^4$ of L929 fibroblast cells were seeded with equal

number in each well plate. After 48 h incubation in 5% $CO_2$ at 37 °C, the cells were washed using PBS and fixed with 4% paraformaldehyde. The nanofiber mat was treated with 5% Bovine Serum Albumin (BSA) along with 0.1% Triton-X in PBS for 1 h, and further washed with PBS. The mats were then incubated with 3% glutaraldehyde in PBS for overnight at $4^0C$. The mat was again washed for 10 min using PBS and followed by ethanol at room temperature followed by gold sputtering for obtaining SEM images.

## 5B.9.4 *In-vivo* Wound Healing Assay

The macroscopic investigations of the treated and untreated groups were carried out for 21 days.The animal (wistar rats) experiments were performed in accordance with the guidelines for Institutional Animal Care and Use Committee (IACUC) at National Centre for Cell Science (NCCS), Pune, India, and approved by the Animal Ethics Committee of NCCS with approval number IEAF/2018/B-339, dated 13-03-2018, which follows the guidelines of the committee for the purpose of control and supervision of experimentation on animals (CPCSE, Govt. of India). Female white Wistar rats weighing around 200–250 g were anesthetized by intraperitoneal injection of ketamine and xylazine hydrochloride in the ratio(4:1).The dorsal hairs of the rats were shaved, depilated on their backs. A surgical wound of 2.5 cm diameter was created using a surgical scissor there-by removing the skin and subcutaneous tissue. The wounds were then washed with saline water. Five sets with three rats in each set (n=3) were used for the experiments. In set I, (**S0**) the wound was left open without applying any medication on the rats(control). In set II, (**S1**) marketed ointment povidine iodine was used. In set III **(S2)**, the nanofiber mats with 0%AgNPs (3cmx3cm) were applied on the wound of the rat and covered with a surgical adhesive tape. Similarly, in set IV **(S3)**, the nanofiber mats containing 0.5% AgNPs (3cmx3cm) were applied and covered. In set V **(S4)**, the nanofiber mats containing 1% AgNPs were applied and covered using the tape. These nanofibers mats were changed every once in two days and the reduction in wound size was monitored and measured using a scale. The images of the healing area were taken using a digital camera. The whole experiment was conducted for a period of 21 days and then the rats were

euthanized. The wounded area on the 21$^{st}$ day was cut using a scissor and stored in 10% neutral formalin solution for histopathology study. The percent wound closure was calculated using the formula[35]**:**

$$\text{Wound closure } (\%) = \frac{A0 - At}{A0} * 100$$

Where $A_0$ and $A_t$ are the wound sizes at day 0 and day $t$ respectively.

## 5B.9.5 Histopathology Study

The blood samples of the wistar rats were collected in tubes coated with EDTA anticoagulant. All the blood samples were analyzed by Beckman Coulter veterinary hematology analyzer. Formalin fixed skin tissue samples were trimmed and processed routinely. Tissue processing was done to dehydrate in ascending grades of alcohol, clearing in xylene and embedded in paraffin wax. Paraffin wax embedded tissue blocks were sectioned at 3 to 4 µm thickness with the Rotary Microtome. Slides of skin were stained with Hematoxylin and Eosin (H & E) and Masson Trichrome stains for morphological observations and collagen fibers.[36] The prepared slides were examined under microscope to note histopathological lesions if any. Severity of the observed lesions were recorded as 0= No abnormality detected, +1=Minimal (<1%),+2=Mild (1-25%), +3=Moderate (26-50%), +4=Marked/Moderately Severe (51-75%), +5= Severe (76-100%)and distribution was recorded as focal, multifocal and diffuse.

## 5B.9.6 Statistical Analysis

All the experiments were carried out for n = 3 samples, the data was analyzed using statistical software Origin Pro 8 (Origin lab Corporation, USA). The in-vitro, in-vivo experiments are represented in the form of bar and line graph respectively using Sigma Plot 10.0 software. The histological observations were done using Nikon E100 microscope along with Olympus DC-5 camera and software.

# 5B.10 Results and Discussion

## 5B.10.1 Scanning Electron Microscopy (SEM)

The SEM micrographs of electrospun nanofibers are shown in **fig 5B.4.** Morphology reveals the homogenous and uniform formation of nanofibers without any bead formation in all the cases. The fiber diameter is affected by

the viscosity and conductivity of the polymeric solution. The polymer solutions having high viscosity could prevent the fracturing of the ejected solution during the spinning process.
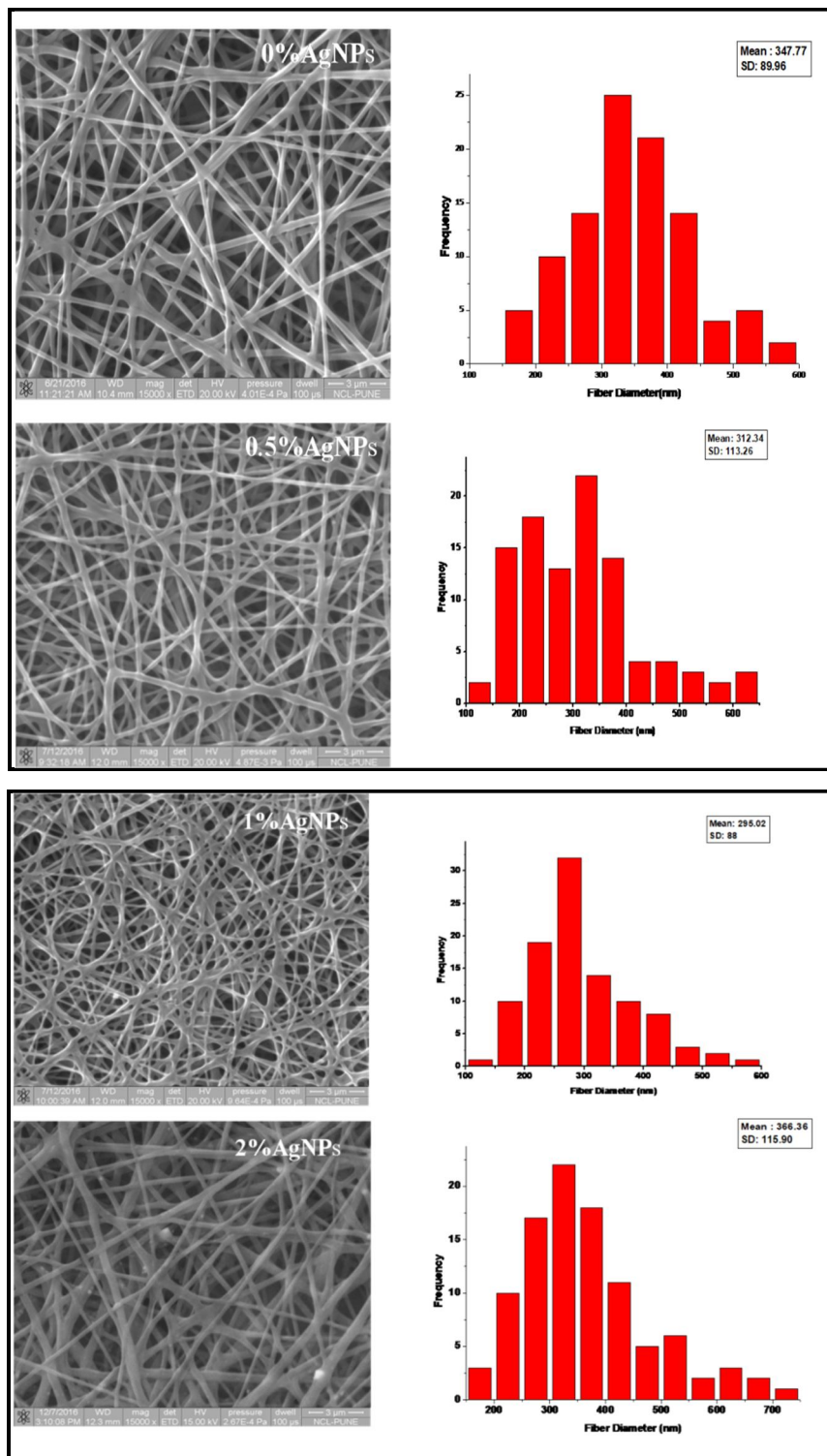


**Figure 5B.4:** SEM images of 0, 0.5,1 and2% AgNPs in the fiber matrix. All scale bars at 3µm and all magnification at 15000X.

The presence of longer stress relaxation time, increases the diameter of the nanofibers to a certain extent.[37] Here, due to high charge density, the high elongation forces are imposed on the fiber diameter which results in the decrease of the fiber diameter with increase in the concentration of AgNPs from 0 % to 1%. The synergic effect of viscosity and conductivity were responsible for decrease in the fiber diameters from 347 nm (0%AgNPs) to 312 nm for 0.5 % AgNPs and 295 nm for 1 % AgNPs respectively. However the diameter of the fibers increased to 366 nm for 2% AgNPs and this could be because of the formation of aggregates due to excess amount of AgNPs added in to the fiber matrix. The thickness of the nanofiber mat was measured using a screw gauge and reported as 11±1 μm.

**5B.10.2 Tunnelling Electron Microscopy (TEM)**

The **fig 5B.5** shows TEM micrographs of the AgNPs embedded into the EHEC/PVA nanofibers with different concentration of silver nanoparticles.
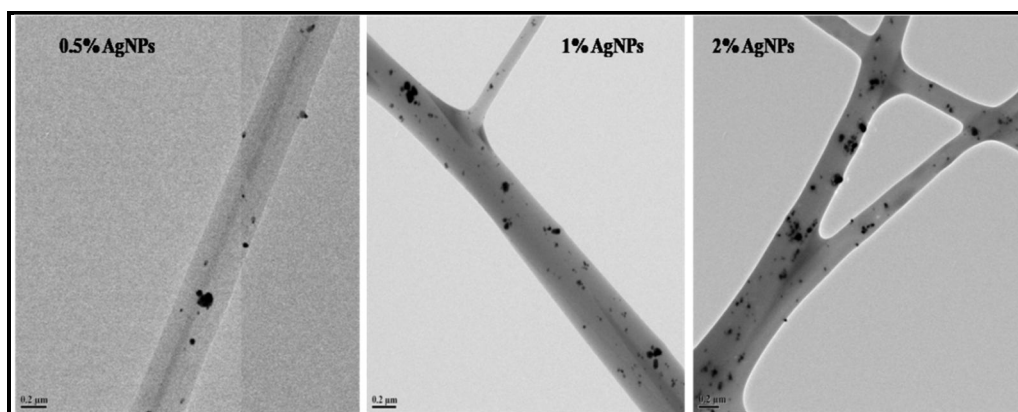


**Figure 5B.5:** 0.5, 1 and 2 % AgNPs in EHEC/PVA nanofibers. All scale bars at 0.2µm.

The AgNPs are observed on the surface of the nanofibers which are spherical in shape having even distribution with average size of the particles in the range of 10 to 25 nm. The density of the particles was more with the increase of the nanoparticles from 0.5 to 1 %. Some large size particles in the size range of 35 to 45 nm were observed on the nanofiber surfaces in the case of mat containing 2% AgNPs This could be attributed to the increased incidence of coalescence of silver atoms with the high concentration of silver content.[38]

## 5B.10.3 Solution properties and Nanofiber properties

The solution properties play an important role in the electrospinning process. The properties like viscosity, conductivity ad surface tension are essential parameters to get nanofibers and the polymer solution should have a minimum viscosity to form nanofibers without any bead formation[39,40] When the viscosity is low, the number of solvent molecules are higher with very few chain entanglements which show the tendency for bead formation along the nanofibers. With increase in viscosity there is gradual change in the shape of the beads from spherical to spindle like and with further increase in viscosity, the bead disappears and a fine fiber is obtained.[41]

It can be seen from the results in **table 5B.1**, that the viscosity of neat EHEC/PVA polymer solution gradually increased with the addition of the silver nanoparticles from 171 Pa.s for mats containing 0.5% AgNPs to 227 Pa.s for mats containing 2% AgNPs.

**Table 5B.1** Solution properties of the EHEC/PVA with silver nanoparticles.

| Sample Name 4/6 (w/w) | Solution Properties | | |
|---|---|---|---|
| | Conductivity (mS/cm) | Surface Tension (mN/m) | Viscosity (Pa-s) |
| EHEC/PVA 0% AgNPs | 3.68 | 45.84 | 166 |
| EHEC/PVA 0.5% AgNPs | 5.00 | 47.00 | 171 |
| EHEC/PVA 1%AgNPs | 5.42 | 49.27 | 185 |
| EHEC/PVA 2% AgNPs | 5.95 | 48.72 | 227 |

The conductivity of pure EHEC/PVA polymer solution was determined to be 3.68 mS/cm. The neat polymer solution without any silver nanoparticles contains very few free ions, and show lower conductivity. The addition of silver increases the conductivity of solution to 5.00 mS/cm for 0.5%AgNPs and 5.95 mS/cm for 2 %AgNPs. At high conductivity, more charges can be carried by the electrospinning solution which is expected to form bead free fiber deposition on the collector plate. The surface tension of the solution was

in the range of 45.84 mN/m to 48.72 mN/m and was in the optimum range 35 - 55 mnN/m for electrospinning.[42]

## 5B.10.4 Contact Angle (CA) measurements

The surface wettability of the material is an important parameter while designing materials for biomedical applications.[43] Water contact angle measurements provide hydrophilic or hydrophobic nature of the scaffold surface and further determines the wettability of the surface. The literature reports reveals that a nanofiber mat with good hydrophilicity and high porosity facilitates considerable wound healing in the early wound healing stage.[44] In this study, the bare EHEC/PVA polymeric nanofibers, and the EHEC/PVA embedded silver nanoparticles with various concentrations of AgNPs (0.5, 1, and 2, wt %) were studied to explore and understand the effect of the nanoparticles on the fiber wettability through contact angle measurements. The **fig 5B.6** reveals the contact angles of the plain nanofibers and AgNPs loaded nanofibers.
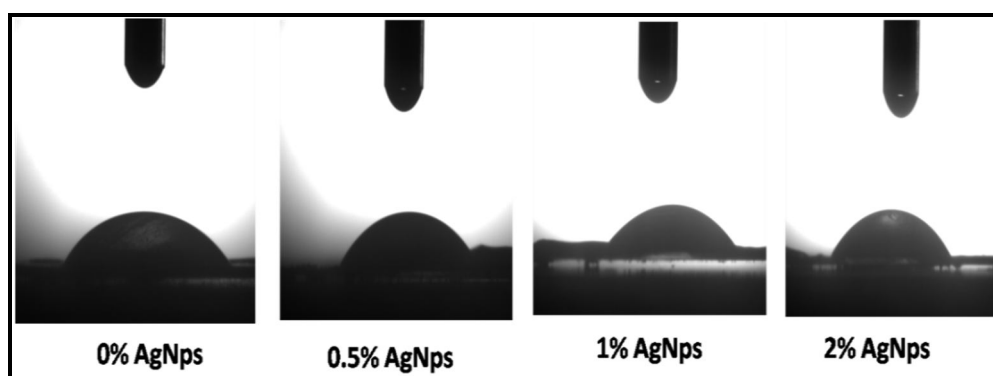


**Figure 5B.6** Contact angle measurements of nanofiber mats containing AgNPs.

From **fig 5B.6**, it can be seen that the contact angles measured in static mode, for EHEC/PVA samples were $60^0$ , and the addition of the AgNPs decreased the contact angle to 52, 48 and $45^0$ in case of 0.5,1 and 2% AgNPs respectively. This indicates that AgNPs were capable of significantly enhancing the surface hydrophilicity of the nanofiber mats. However, there was no significant decrease in the contact angle of mats containing 1 to 2% AgNPs which could be due to high chances of aggregation of AgNPs on the

nanofiber mats with the increase in concentration of AgNPs.[45] A recent report by Li *et al*, [46] explains the probable improvement in the hydrophilicity of the nanofiber mats due to the presence of Ag+ ions released by the oxidation process which adsorbs on the surface of nanoparticles thereby increasing the hydrophilicity.

**5B.10.5 Wide Angle X-ray Diffraction**

The XRD diffractograms of neat EHEC-PVA nanofibers along with silver nanoparticles embedded EHEC-PVA nanofibers are shown in **fig. 5B.7**. A number of Bragg reflections corresponding to the (111), (200), (101)  sets of lattice planes were observed.[47]
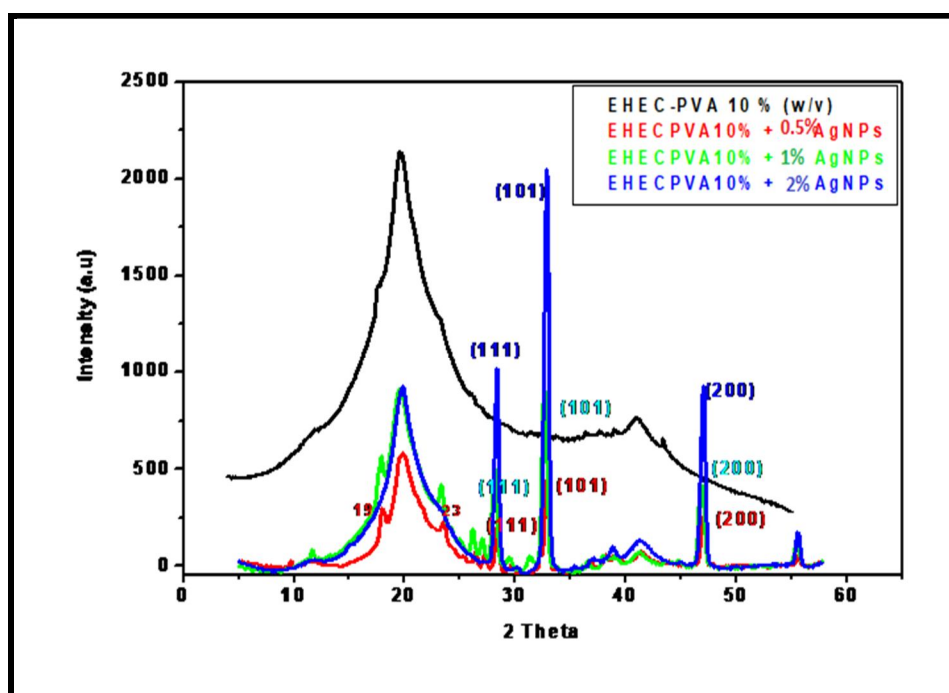


**Figure 5B.7:** XRD peaks of silver nanoparticles in EHEC/PVA nanofibers.

These characteristic peaks are matched with the face centered cubic (fcc) structure of silver. The neat EHEC/PVA nanofiber mat showed no peaks while the other nanofiber mats containing different concentration of AgNPs namely 0.5, 1, and 2 % AgNPs , showed prominent peaks at (111), (200) and (101) indicating the fcc structure of silver. The diffraction profiles of heat-treated silver are obviously broadened, as compared with bulk silver, revealing the formation of silver nanoparticles. The XRD patterns confirmed that the

polymeric blend was semicrystalline in nature and also confirmed the presence of Ag as AgNPs in the composite nanofibers, where the crystal structure of Ag was a surface cubic crystal structure.[48]

### 5B.10.6 UV-Visible Spectroscopy

The formation of AgNPs in electrospinning EHEC/PVA polymer solution can be detected by UV–visible spectrophotometer. The UV–visible spectra of the polymeric solution with different concentrations of AgNO$_3$ namely 0.5, 1 and 2 %(w/w) are shown in the **fig 5B.8**. The EHEC/PVA polymer solution without AgNPs was milky white in colour. The increase of AgNPs from 0.5 to 2%, the colour of the solution changed from light yellow to blackish brown in colour.
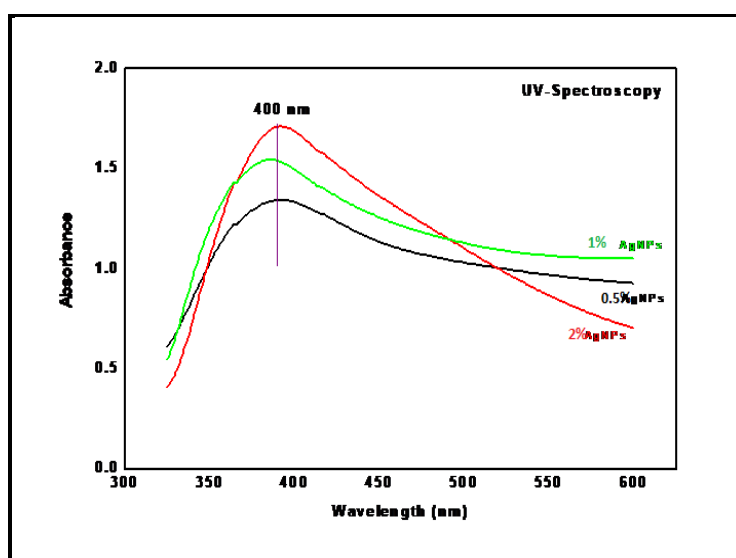


**Figure 5B.8:** UV-visible spectrum for 0.5, 1 & 2 % AgNPs.

The UV–visible spectrum exhibited an absorption band at around 390-400 nm, which is a typical surface plasmon absorption of AgNPs.[49] Furthermore, Polyvinyl Alcohol (PVA) stabilizes the silver nanoparticles due to its long pair electrons on the hydroxyl oxygen.[50] It is observed that a small amount of AgNPs could be formed during the preparation of EHEC/PVA/AgNO$_3$ electrospinning polymer solutions. This could be attributed to the reducing property of the EHEC.

**5B.10.7 Energy Dispersive X-Ray Analysis (EDX)**

EDX analysis was performed on the neat and AgNPs incorporated nanofiber mats to confirm the inclusion of Ag nanoparticles. The elemental energy dispersive x-ray analysis was done on the SEM-EDX instrument. The spectra are shown in **fig. 5B.9** which distinctly demonstrate the presence of Ag as the elemental component in the fiber matrix.
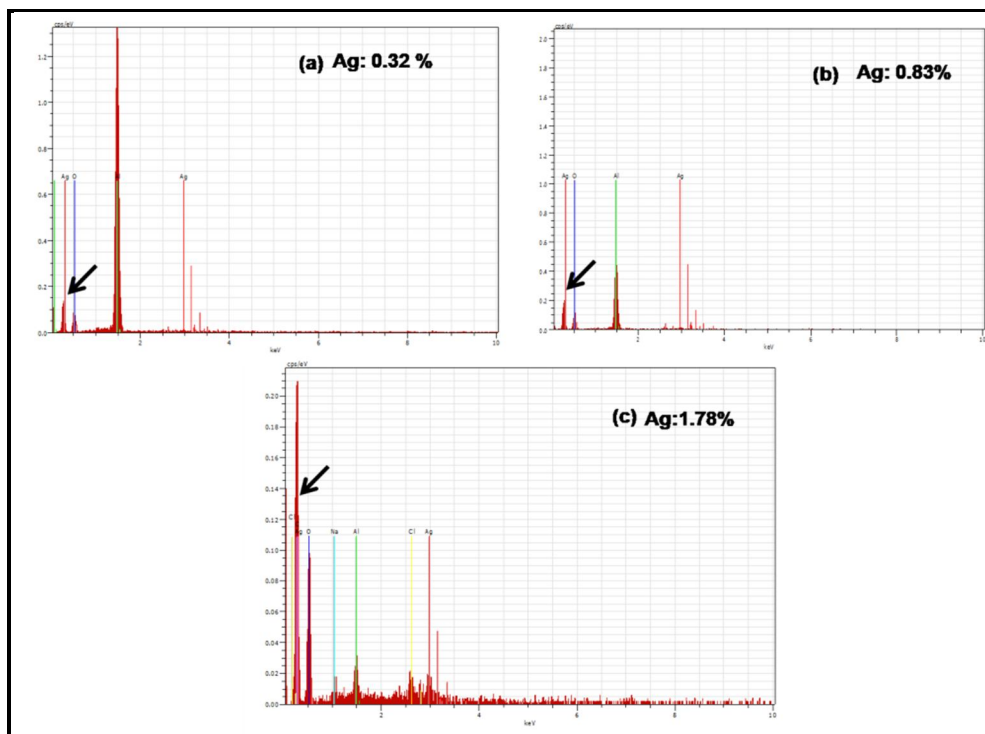


**Figure 5B.9:** Elemental EDX analysis for (a) 0.5%AgNPs (b) 1% AgNPs (c) 2%AgNPs.

The Ag percentage present in the fiber matrix was 0.32% for 0.5%AgNPs, 0.83% for 1%AgNPs and 1.78% for the 2%AgNPs, which is shown in the figure by arrow mark. The other peaks belonging to carbon, oxygen, nitrogen are generated from the biopolymer Ethyl hydroxy ethyl cellulose and the aluminium which is  are generated from the aluminium foil which was used for collecting the fibers from the electrospinning process. Therefore, it was confirmed from the EDX studies that the AgNPs are embedded into the fiber matrix and loaded without any chemical or structural modifications to form the composite matrix.

### 5B.10.8 Mechanical Properties

The effect of silver nanoparticles (AgNPs) on the mechanical properties of the EHEC/PVA nanofiber mats was investigated using the tensile stress-strain curves as shown in **fig 5B.10**. The mechanical properties of the non-woven mats depends on the geometrical structures of the fibers.[51] The EHEC/PVA nanofiber mats electrospun with AgNPs exhibited higher tensile strength and Young's modulus. The results are summarized in the **table 5B.2**. The tensile strength increased from 6.63MPa for 0%AgNPs to 11.3 MPa for 1%AgNPs.

**Table 5B.2:** Tensile strength, modulus and elongation at break for EHEC/PVA nanofibers with AgNPs.

| EHEC/PVA | Tensile Strength (MPa) | Young's Modulus (MPa) | Elongation at Break (%) |
|---|---|---|---|
| 0 % AgNPs | 6.63 | 0.11 | 105.00 |
| 0.5 % AgNPs | 8.71 | 0.16 | 108.00 |
| 1 % AgNPs | 11.3 | 0.19 | 151.95 |
| 2 % AgNPs | 10.89 | 0.23 | 119.86 |
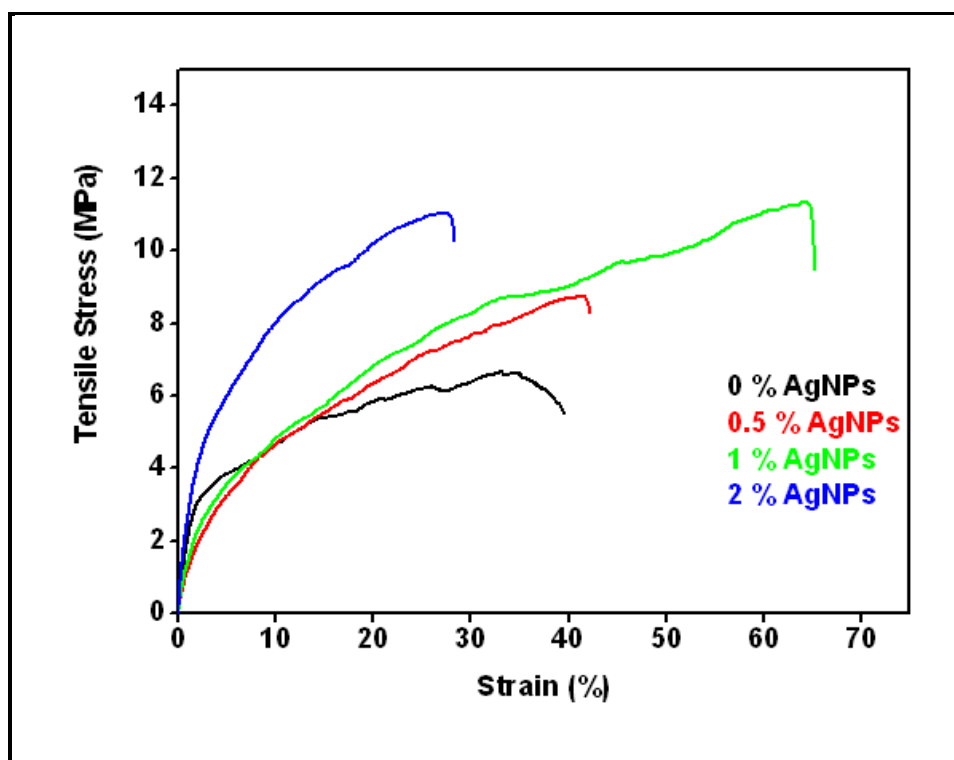
**Figure 5B.10:** Stress-Strain curves for the EHEC/PVA nanofiber mats with silver nanoparticles.

However, there was a slight decrease in the tensile strength to 10.89 MPa for 2% AgNPs and this may be due to the aggregation of the nanoparticles which causes the decrease in the tensile strength.[52] The increase in the Young's modulus can be attributed to the fact that nano sized AgNPs possessed higher modulus than the bulk silver.[53,54] Further, the packing density of the nanofibers contribute to the enhancement in the modulus. This observation is in line with the reports of Kwon *et al* [55], where it is shown that the electrospun poly (L-lactide-co-e-caprolactone) fibers exhibited high tensile modulus due to the smaller diameter fiber and better packing density.

**5B.10.9 Braunauer−Emmett−Teller (BET) Analysis**

The EHEC/PVA and EHEC/PVA/AgNPs electrospun nanofibers were degassed at 150 $^0$C for at least 12 h prior to surface area analysis and the experiments were done at 77 K. The specific surface areas of the nanofibers were calculated using the Braunauer−Emmett−Teller (BET) method and the pore size distribution was determined by Barrett−Joyner− Halenda (BJH) and

Density Function Theory (DFT) method. The results are summarised in **table 5B.3**. The average pore radius increased from 1.89 nm for 0%AgNPs to 1.93 nm for 2%AgNPs (data not shown in the table). The multi point BET specific surface area increased from 94.28 $m^2/g$ for bare EHEC/PVA nanofiber mat to 200.23 $m^2/g$ for 2%AgNPs.

**Table 5B.3** Multi point Surface area (BET) and pore size distribution (BJH & DFT) methods of EHEC/PVA nanofiber mats with AgNPs.

| AgNPs | BJH method pore size distribution | | | DFT method pore size distribution | | | Multipoint BET Surface area ($m^2/g$) |
|---|---|---|---|---|---|---|---|
| | Surface area ($m^2/g$) | Pore volume (cc/g) | Pore radius (Å) | Surface area ($m^2/g$) | Pore volume (cc/g) | Half pore width (Å) | |
| 0% | 46.97 | 0.082 | 16.30 | 31.01 | 0.072 | 15.85 | 94.22 |
| 0.5% | 18.72 | 0.037 | 15.65 | 13.72 | 0.031 | 13.85 | 24.01 |
| 1% | 49.43 | 0.082 | 14.85 | 31.02 | 0.065 | 15.85 | 114.87 |
| 2% | 104.13 | 0.072 | 15.70 | 70.80 | 0.064 | 15.85 | 200.23 |

The surface area increased with the increase in the silver nanoparticle concentration. There was an increase in the pore volume and pore radius by both methods for mats containing 0.5 % to 1% AgNPs, but gradually decreased when the silver nanoparticle concentration increased to mats containing 2% AgNPs.
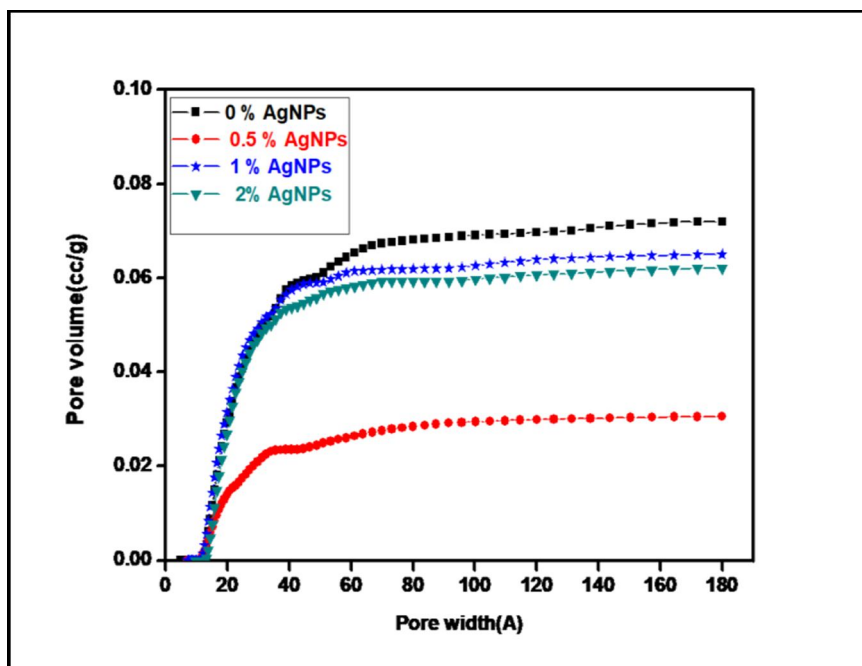
**Figure 5B.11** Graph from DFT method for pore volume Vs pore width of nanofiber mats with AgNPs.
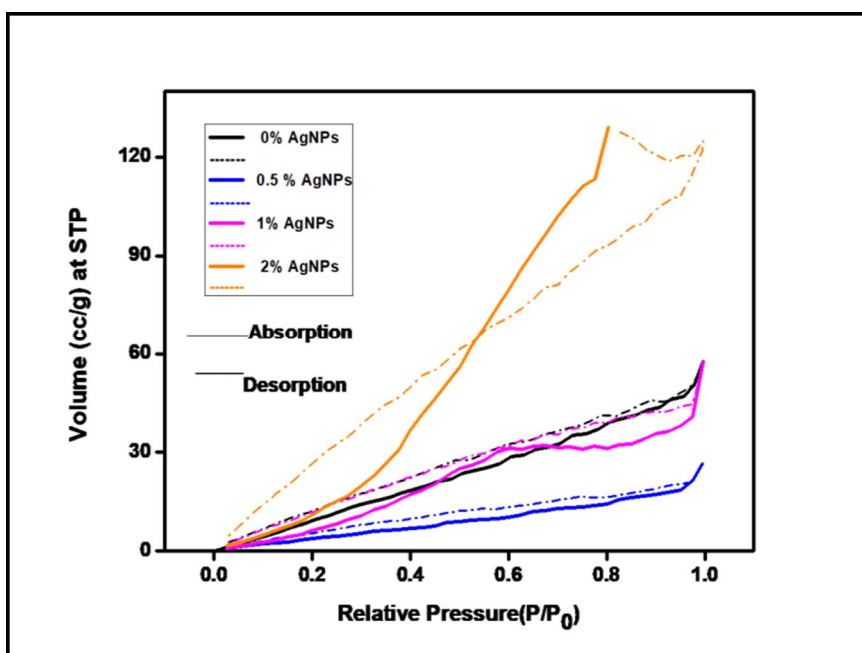


**Figure 5B.12** Nitrogen sorption isotherms of nanofiber mats with AgNPs.

This may be due to the excess of nanoparticles in the nanofiber mat leading to aggregation of particles and reduction in the pore size and volume. The **fig 5B.12** shows the nitrogen sorption isotherms of Ag nanoparticles embedded in the EHEC/PVA nanofiber mats. The experimental isotherms of the

investigated materials show typical adsorption behaviours for the IV type, with an H3 type hysteresis loop according to the IUPAC classification which is a characteristic of mesoporous structure and indicates the existence of narrow slit-like pores.[56, 57] It can be seen that electrospun EHEC/PVA mat containing 2% AgNPs has the highest volume adsorbed and widest desorption branch. This is attributed to increase in content of mesopores of fibers due to incorporation of AgNPs. Furthermore, during the adsorption and desorption process, existence of pores with complex shapes might trap the meniscus, leading to slower desorption process and wider desorption branch.[58]

## 5B.10.10 Thermogravimetric Analysis (TGA)

The TGA was done on the EHEC/PVA nanofibers and on the nanofibers loaded with different concentration of AgNPs (namely 1% and 2 %) The results shown in the **fig 5B.13** reveal that there is no weight loss up to 180 C. The weight loss is mainly occurred in the temperature range from $180^0$ to 270 $^0$C with a negligible change at temperatures higher than $320^0$ C.
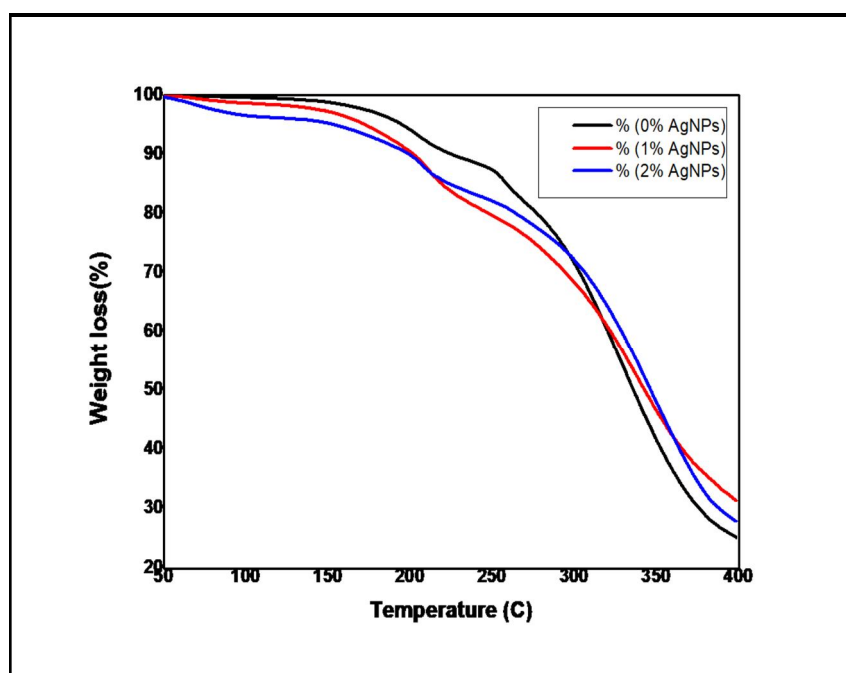


**Figure 5B.13** TGA of EHEC/PVA nanofiber mats with AgNPs.

The weight loss is attributed to the combustion of the organic EHEC/PVA in the matrix. The results of a sample containing 0.5% AgNPs are not shown in the above figure since there was negligible difference in the samples

containing 0.5% and 1% AgNPs. The TGA results also indicate that the degradation temperature of the composite nanofibers decreased and the weight loss is increased in the presence of AgNPs. This indicates that the thermal stability of the nanofibers decreased due tothe presence of AgNPs in the nanofibers which can be due to the high thermal conductivity of AgNPs compared to the polymeric nanofibers.[59]

## 5B.10.11 Swelling Studies

An ideal wound dressing material should be permeable and maintain a moist environment and help to prevent dehydration.[60] Therefore, the nanofiber mats should have high permeability, a high degree of swelling with lower weight loss. The results of the swelling studies on the EHEC-PVA nanofiber mats containing AgNPs are shown in **fig 5B.14.** It can be seen from the figure that, the water up take increased with the addition of the silver nanoparticles as compared to the neat nanofiber mats.
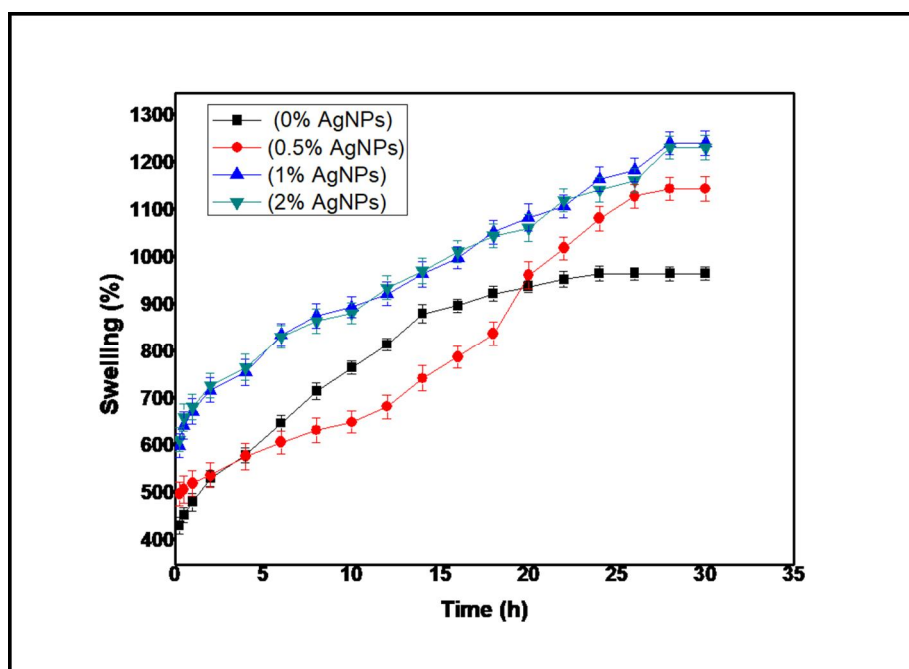


**Figure 5B.14: Swelling** studies of the EHEC/PVA nanofibers loaded silver nanoparticles.

The swelling percentage in case of EHEC/PVA nanofiber mats containing 0%AgNPs reached to 968% at the end of 24 hours and no increase in water up take was observed. In the case of say EHEC/PVA nano fiber containing 0.5%AgNPs the maximum water uptake reached to 1148% at the end of 28

hours and no more increase was seen. In case of EHEC/PVA nanofiber mats containing 1% AgNPs and 2% AgNPs the swelling percentage increased to 1245% and 1235% respectively. A slight decrease in swelling was observed for EHEC/PVA with 2% AgNPs in the swelling percentage. The silver nanoparticles loaded nanofiber mats exhibited good swelling thereby confirming the hydrophilicity of the mats and hence an ideal material for wound healing applications.

**5B.10.12 Release of Silver ions from the nanofiber mats**

The Ag ion release from the nanofiber mats is influenced by the dissolution and swelling behaviour of the matrix polymer.[61] The in-vitro cumulative percentage silver ions released from the nanofibers as a function of time in the phosphate buffer solution (PBS) is shown in **fig 5B.15**. The silver ions release was studied for a period of 11 days. It can be seen from the figure that, there is an initial burst release of 10% and 8% for the 0.5% and 1.0% AgNPs loaded mats respectively. Then the slow and continuous release was observed for the next 10 days. On the $10^{th}$ day (240 hours) ~ 16.0% and 20% release were observed for the mats containing 0.5% and 1.0% AgNPs.
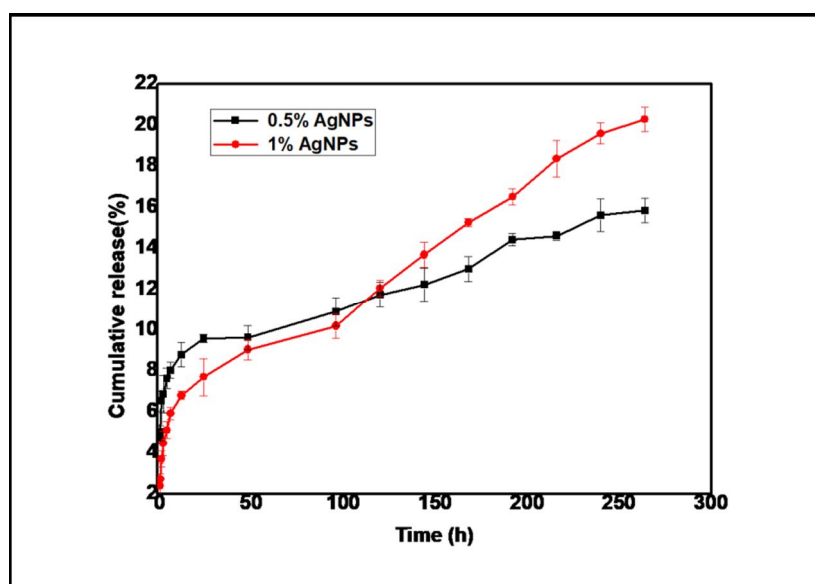


**Figure 5B.15:** Cumulative release (%) of silver ions in PBS.

The initial burst release of AgNPs was possibly due to the diffusion of AgNPs that were adsorbed at the surface of the polymeric nanofibers. However, the sustained release of Ag NPs in subsequent stages is due to the diffusion of

encapsulated AgNPs from the core region of the polymeric nanofibers or can be due to possible degradation of EHEC/PVA polymeric matrix. The results obtained were in agreement with Wu *et al* [62] which indicated that these nanofibers have a potential for sustained delivery of AgNPs with efficient and constant antimicrobial activity at the wound site for a longer period of time.

## 5B.11 Biological Studies

### 5B.11.1 Antibacterial Studies

Silver nanoparticles, due to their high ratio of surface area to volume and their unique chemical and physical properties have emerged as novel antimicrobial agents. They have high thermal stability, low volatility and low toxicity to human cells and therefore are used frequently in pharmaceuticals and medicine.[63] The antibacterial studies of EHEC/PVA nanofiber mats containing silver nanoparticles were done using the gram positive bacteria, *Staphylococcus aureus (S. aureus)* and gram negative bacteria, *Escherichia coli* (*E. coli*) procured from National Centre for Industrial Microorganism, NCL Pune having numbers (NCIM) No: 2079; and NCIM No: 2065. The positive control used here was Tetracycline antibiotic tablet. The antibacterial properties were measured using Kirby Bauer test, known as the disk diffusion method by calculating the zone of inhibition as shown in the images of **fig 5B.16 (A).** The results are summarised in the **table 5B.4**

**Table 5B.4** The zone of inhibition for *S. auerus* and *E. coli* bacteria.

| Zone of Inhibition in (cm) | | |
|---|---|---|
| | *S. aureus* | *E. coli* |
| EHEC/PVA/0.5% AgNPs | 1.25 | 1.30 |
| EHEC/PVA/1% AgNPs | 1.30 | 1.50 |
| EHEC/PVA/2% AgNPs | 1.35 | 1.56 |
| Positive control Tetracycline | 2.6 | 3.1 |
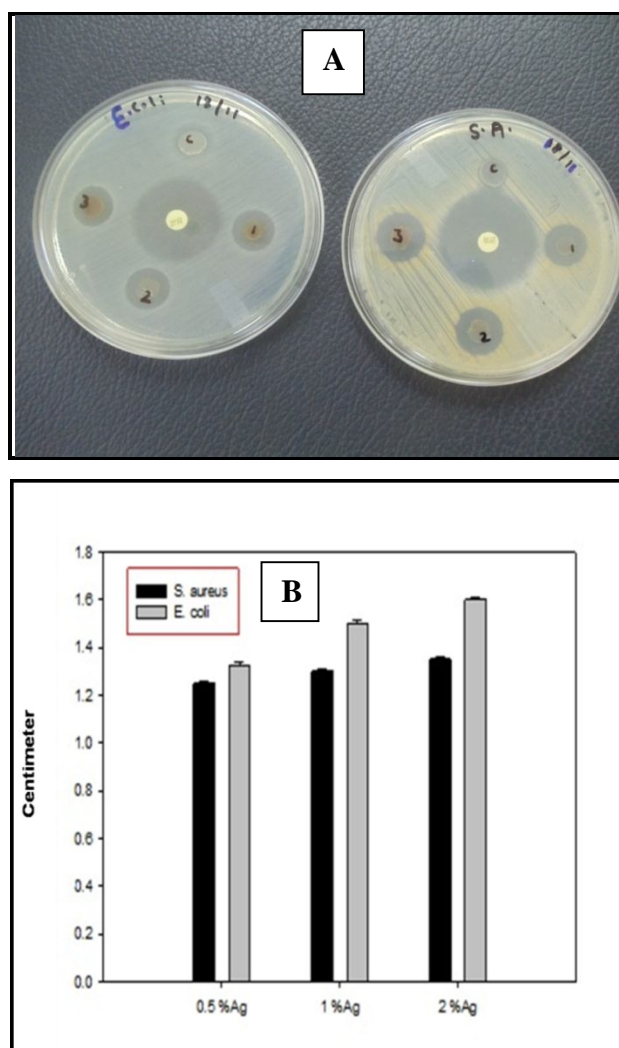
**Figure 5B.16 (A)** Photograph showing antibacterial activity of *S. auerus* and *E. coli* bacteria. **(B)** Bar graph showing the zone of inhibition of *S. auerus* and *E. coli* bacteria.

There was no zone of inhibition observed for bare EHEC/PVA nanofiber mats, which were used as negative control. The markings in the images were as follows. C indicated negative control that is the bare EHEC/PVA nanofiber mats, the numbers 1, 2 and 3 indicated EHEC/PVA nanofiber mats containing 0.5%, 1% and 2%AgNPs. The tetracycline tablet was used as positive control and was placed at the centre of the disc. The AgNPs embedded in the EHEC/PVA nanofiber mats demonstrated excellent bactericidal efficiency toward both gram positive and gram negative microorganisms. The presence of silver in the nanofiber mats, leads to death of the microorganism around the mats, which results in formation of clear circular zone. As the quantity of

AgNPs in the mats increased, the zone of inhibition was seen expanded. The larger surface area of the AgNPs provides a larger area for bacterial interactions, and therefore enhancing their antibacterial effect.[64,65] The zone of inhibition also increased in case of *E. coli* as compared to *S. aureus* which reveals that the AgNPs are more effective in case of the gram negative bacteria i.e. *E. coli.* It is evident that diameter of the inhibited area is a measure of the effectiveness or resistance of the bacteria toward organic antimicrobial agent.[66]

## 5B.11.2 Cell Viability Studies (MTT Assay)

The cell viability assay was done to measure the cytotoxicity of the silver containing EHEC/PVA nanofiber mats using the L929 fibroblast cell lines. The cell lines were procured from National centre for cell science, (NCCS) Pune. The in-vitro cytotoxicity studies were studied by the MTT (3-(4,5-dimethylthiazol-2-yl)- 2,5- diphenyl tetrazolium bromide) assay.
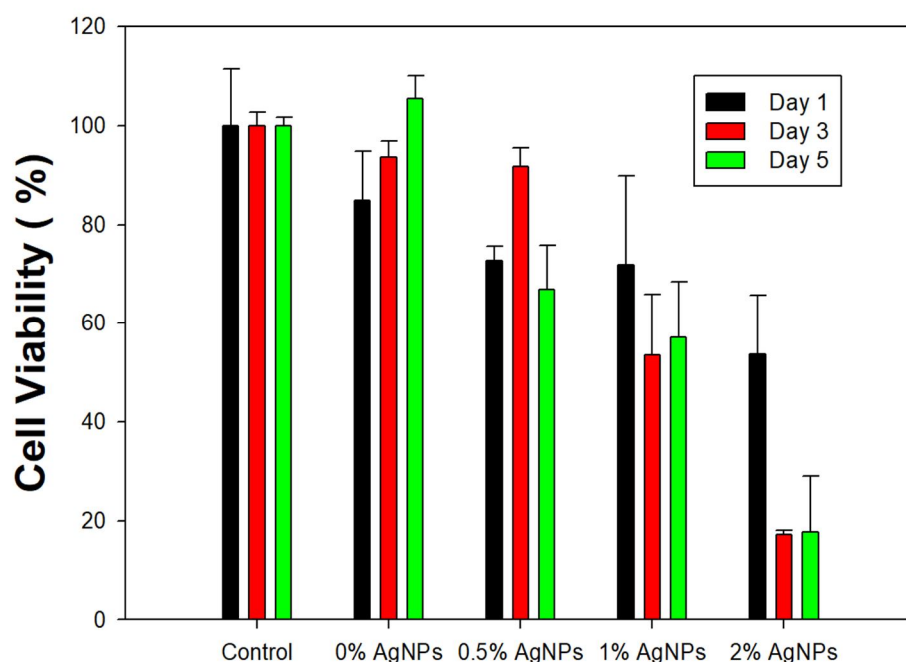


**Figure 5B.17:** Cell viability of L929 fibroblast cells by MTT assay.

The results of the assay are shown in **fig 5B.17.** The L929 fibroblast cells were cultured in a 96 well plate (positive control) and we observed that there was 100% cell growth from day 1 to day 5. The cells without any silver

nanoparticles (0%AgNPs, negative control) also showed good cell viability and was seen more that 100% on day 5.
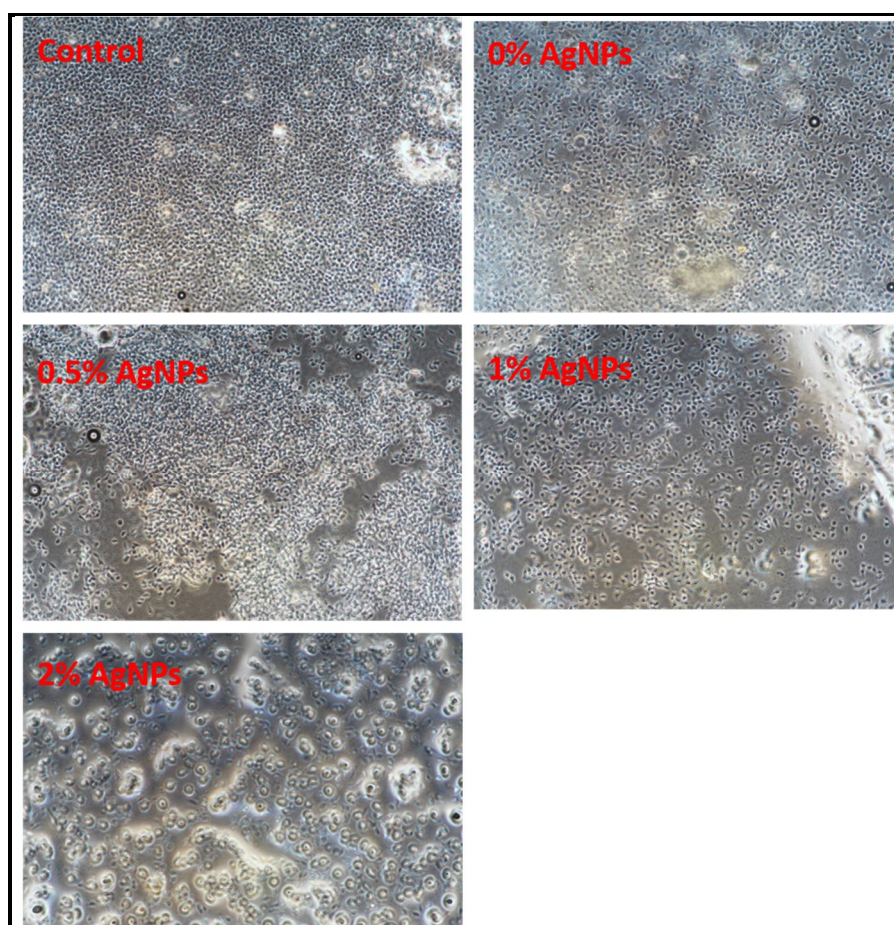


**Figure 5B.18**: Confocal images of the L929 fibroblast cells with different AgNPs concentration.

The cells were attached and growing. In case of EHEC/PVA nanofiber mats with 0.5% AgNPs, the cell viability increased from 75% to 95% from day 1 to day 3 and 75% on day 5 was observed.  In case of EHEC/PVA nanofiber mats with 1%AgNPs, the cell viability was 75% on day 1 but slightly decreased to 65 % on day 3 and day 5.  The cell viability drastically decreased in case of EHEC/PVA nanofiber mats with 2% AgNPs from 55% on day 1 to 20% on day 3 and day 5. This study revealed that EHEC/PVA nanofiber mats with 2% AgNPs possess toxic behaviour towards L929 fibroblast cells. The confocal images of the L929 fibroblast cells were as shown in the **fig 5B.18,** where the cell density in case of control was highest and in case was EHEC/PVA

nanofiber mats with 2% AgNPs, the cells were round in shape confirming the cell death.

### 5B.11.3 Cell growth and Proliferation

The cell viability results confirmed the cell growth of the L929 fibroblast cell lines. The L929 cells were evenly distributed over the nanofiber matrix and the morphological appearance of cells attached on nanofiber mats were investigated after 5 days of culturing the fibroblasts cells and is shown in the SEM image in **fig 5B.19**.
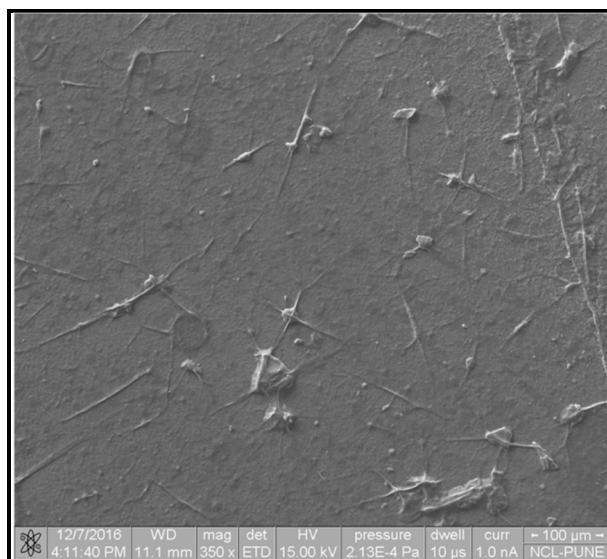


**Figure 5B.19:** SEM image showing L929 cell growth on the EHEC/PVA nanofiber mat containing 0.5% AgNPs.
Scale bar: 100µm; magnification: 350X.

The image reveals that the spindle shaped elongated cells attached on the fiber matrix with cell growth, spreading and proliferation which co-relates to the cell viability results. Further, cytotoxicity provides an accurate data for the use of the prepared nanofibers in various bio-medical applications.

### 5B.11.4 Hemolysis Study

The blood compatibility studies were undertaken on the EHEC/PVA nanofiber mats loaded with 0, 0.5 1, 2 % AgNPs. The wound dressings come in direct contact with the blood and therefore the evaluation of blood compatibility is very important.
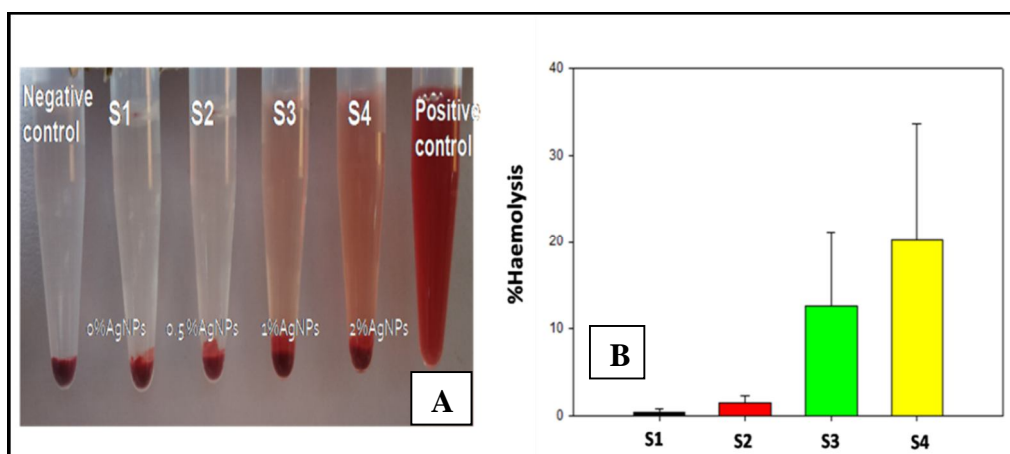
**Figure 5B.20:** **(A)** photographs of the haemolysis using RBC's; **(B)** %Hemolysis Vs concentration of the AgNPs. [S1= Nanofiber mats with 0%AgNPs, S2= Nanofiber mats with 0.5%aAgNPs, S3= Nanofiber mats with 1%AgNPs, S4= Nanofiber mats with 2%AgNPs]

Along with the development of AgNPs with potential use in the biomedical applications, the possible toxicity need to be examined. In our study, as shown in the **fig 5B.20(A),** and haemolysis graph in **fig 5B.20(B),** nanofiber mats containing 0%, and 0.5% AgNPs, the percentage haemolysis was 0.5 % and 1.2% and for nanofiber mats containing 1% and 2% AgNPs, the haemolysis % increased to 10.4 and 20%. From the data, we can say that as the concentration of nanoparticles increased, the red blood cells concentration decreased leading to higher percent of haemolysis. It is known and reported that, if the haemolysis rate is below 5% then the medical materials are considered as non-haemolysis according to national biological safety protocol.[67]

### 5B.11.5 *In-vivo* Wound Healing Experiments

The *in-vivo* wound healing assay was done for a period of 21 days and monitored and the nanofiber mats were changed every two days. The images were taken every week and the wound closure was measured using a scale and are as shown in the **fig 5B.21.** It was observed at the end of 21 days, that the average wound closure rate in case of open wound (S0) was 86% and the commercially used ointment (S1) was around 89%. The EHEC/PVA nanofiber mats (S2) also showed considerable closure of 91%.
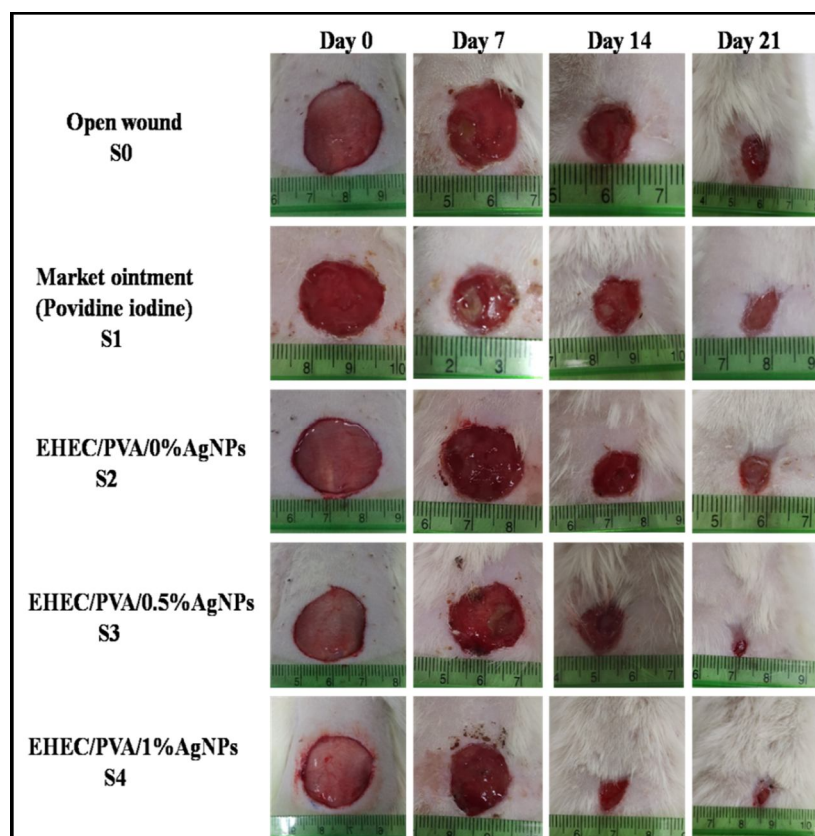
**Figure 5B. 21:** The 21 day wound healing assay for EHEC/PVA nanofiber mats.
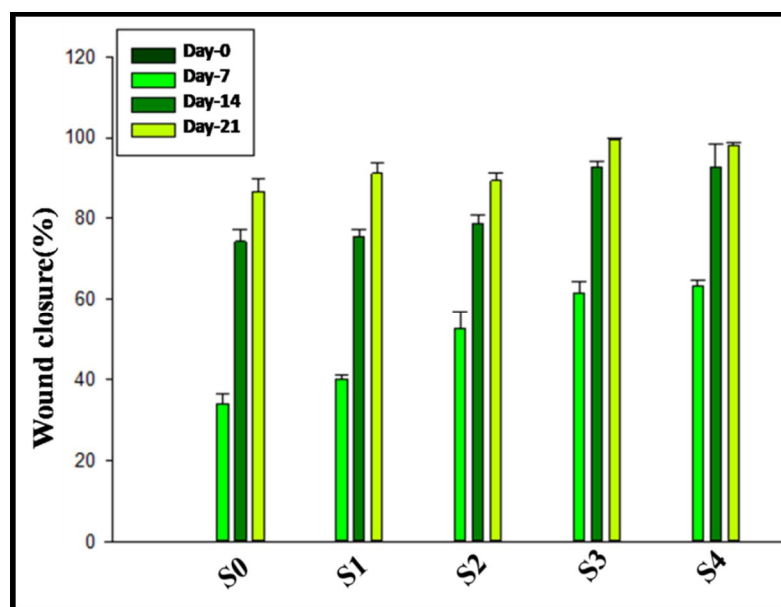


**Figure 5B. 22:** Bar graph of Wound closure (%) of rat skin after wound healing.

S0= open wound, S1= marketed ointment, S2= EHEC/PVA nanofiber mats S3= EHEC/PVA/0.5% AgNPs nanofiber mats, S4= EHEC/PVA/1% AgNPs nanofiber mats.

In case of EHEC/PVA with 0.5% AgNPs (S3) and EHEC/PVA with 1% AgNPs(S4),  the wound closure rates increased to 98 and 99% respectively showing complete closure of the wounds with any infection and complete closure of the area with new hair growth as shown in the images. The nanofiber mats containing 0.5 and 1% are suitable for wound healing applications was found from the wound healing assay experiments.

## 5B.11.6 Histopathology Studies

Microscopic examination of skin tissues of rats of open wound group revealed focal marked ulceration, multifocal mild epidermal hyperplasia with epithelisation, multifocal moderate dermal inflammation, focal minimal fibrous tissue proliferation, minimal collagen deposition and multifocal mild angiogenesis at dermis. The commercially used ointment showed focal ulceration, epidermis. Moderate multifocal hyperplasia, with epidermis and epithelisation and moderate multifocal inflammation.
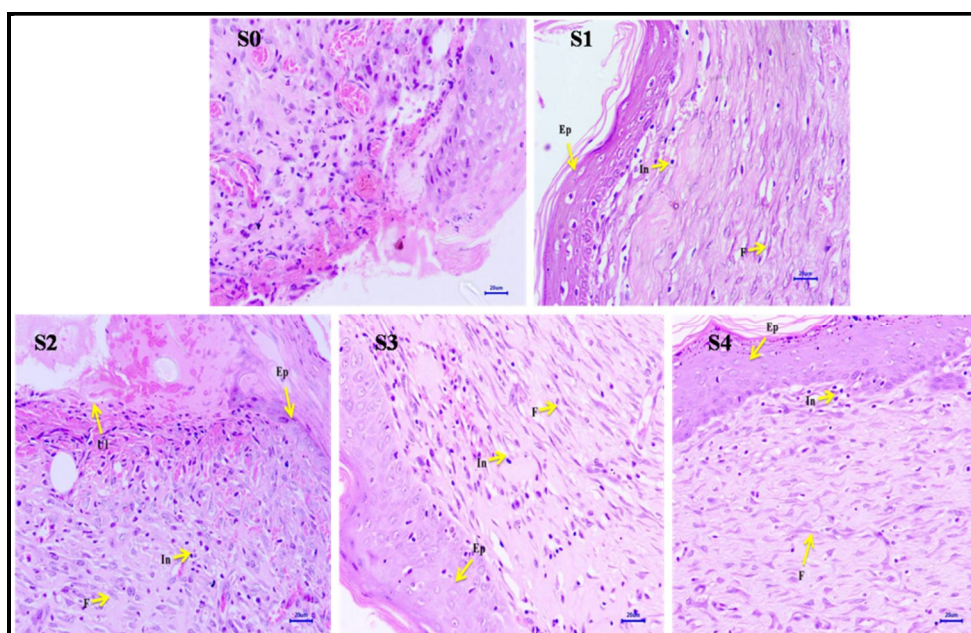


**Figure 5B. 23:** Hematoxylin and eosin(H&E) staining for the rat skin from S0 to S4. Yellow arrows showing the epidermis (Ep), Inflammation (In), Focal ulceration (F).All scale bars: 200µm.

The skin tissues of rats treated with 0% Silver nanoparticles showed focal mild ulceration, multifocal mild epidermal hyperplasia with epithelisation, multifocal mild dermal inflammation, focal mild fibrous tissue proliferation,

mild collagen deposition and multifocal minimal angiogenesis at the dermis. Skin tissues of rats treated with mats containing 0.5% silver nanoparticles revealed multifocal mild epidermal hyperplasia with epithelisation, multifocal mild dermal inflammation, multifocal mild fibrous tissue proliferation, moderate collagen deposition and multifocal mild angiogenesis at dermis. Microscopic examination of skin of rats treated with mats containing 1 % silver nanoparticles revealed multifocal mild epidermal hyperplasia with epithelisation, dermal inflammation, multifocal mild fibrous tissue proliferation, moderate collagen deposition and multifocal moderate angiogenesis at dermis.
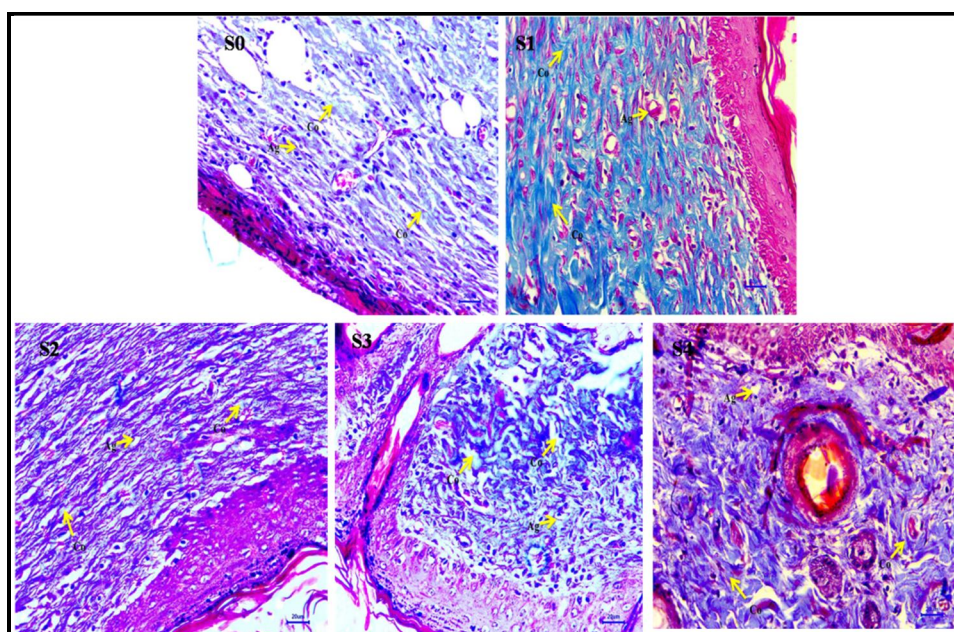


**Figure 5B. 24:** Masson's Trichrome (MT) staining for the rat skin from S0 to S4.Yellow arrows indicate Collagen deposition (Co), Angiogenisis (Ag). All scale bars: 200µm.

Patho-morphological observation of skin, in present report suggests that recovery of wounded skin is noted in all the groups including non-treated group. Treatment EHEC/PVA nanofibers with 0.5% silver nanoparticles and 1% silver nanoparticles enhance the recovery of wounded skin by increasing epithelisation, fibrous tissue proliferation, increased collagen deposition and angiogenesis.

## 5B.12 Conclusions

In this study, a novel and unique antibacterial wound dressing material with biodegradable and biocompatible Ethyl hydroxy ethyl cellulose polymer

incorporating silver nanoparticles was designed and developed using an electrospinning technique. The various physcio-chemical characterisations, revealed the size of the nanofibers and the nanoparticles. The average fiber diameter was in the range of 347 nm for neat EHEC/PVA nanofibers and increased to 366 nm for mat containing 2%AgNPs. The TEM images showed the nanoparticles are in the range of 10 to 25 nm. The polymer solution viscosities increased from166 Pa.s for mats with 0% AgNPs to 227 Pa.s for mats with 2%AgNPs. The solution conductivities increased from 3.68 to 5.95 mS/cm and surface tension increased 45.84 to 48.2 mN/m with increase in concentration of silver nanoparticles. This was in agreement with the electrospinning parameters for preparation of nanofibers. The contact angles decreased with addition of silver nanoparticles revealing the hydrophilic nature of the nanofiber mats. The XRD data significantly showed the crystal structure of silver as surface cubic. The UV-Visible spectroscopy data revealed the surface plasmon region by formation of silver nanoparticles in the region of 390-400 nm. The EDX data also proved the presence of silver in the nanofiber mats. The tensile strength increased from 6.63 MPa to 10.89 MPa for mat containing 2% AgNPs.The Young's modulus also increased from 0.11 to 0.23 MPa from nanofiber mats containing 0 to 2% AgNPs but the elongation increased initially from 105% to 152% for EHEC/PVA nanofiber mats with 1% AgNPs but gradually decreased to 120% for EHEC/PVA nanofiber mats with 2 % AgNPs. This was due to the excess silver nanoparticle aggregation. The BET isotherms revealed the adsorption behaviour of type IV with hysteresis loop. The thermo-gravimetric studies explain the thermal degradation temperature decreased from 250 to $180^0$ C by the addition of silver nanoparticles. The swelling characteristics revealed the nanofiber mats are hydrophilic in nature and the percent swelling in case of EHEC/PVA nanofiber mats containing 1% and 2% AgNPs was observed to be around 1245 and 1235 %. The silver ions were released in the phosphate buffer saline and we observed there was a slow and sustained release of 16% in case of EHEC/PVA nanofiber mats containing 0.5% AgNPs and 20% in case of EHEC/PVA nanofiber mats containing 1% AgNPs. The antibacterial

study revealed that these nanofiber mats showed good zone of inhibition done by the disk diffusion method and the circular zones increased with the increase in silver content. The zone of inhibition slightly increased for *E.coli* bacteria compared to the *S.auerus* bacteria. The MTT assay was done to check the cell viability and we observed the cell growth was more than 80% in case of EHEC/PVA nanofiber mats containing 0 and 0.5% AgNPs for a period of 5 days. In case of EHEC/PVA nanofiber mats containing 1% AgNPs and EHEC/PVA nanofiber mats containing 2% AgNPs they decreased to 55% and 20% for day 3 and day 5. In the SEM images of EHEC/PVA nanofiber mats containing 0.5% AgNPs, cell growth was observed with elongated spindle shaped L929 fibroblast cells attached on the surface of the nanofiber mats. The haemolysis study showed no toxicity in case of EHEC/PVA nanofiber mats containing 0 and 0.5% AgNPs, where as there was more RBC death observed in case of EHEC/PVA nanofiber mats containing 1 and 2% AgNPs loaded nanofiber mats. The in-vivo wound healing studies showed that there was around 98 to 99 % wound closure in case of EHEC/PVA nanofiber mats containing 0.5 and 1 % AgNPs as compared to marketed ointment and open wound which was around 91 and 86% closure rates. There was good epidermal layer growth and angiogenesis observed in the histopatological studies in case of the EHEC/PVA nanofiber mats containing 0.5 and 1 % AgNPs. The experiments for mats containing 2% AgNPs were not conducted due to the toxicity effects. All the above experimental data provides a good insight into the ethyl hydroxy ethyl cellulose nanofibers embedded silver nanoparticles for its use in wound dressings and as scaffolds in tissue regeneration applications.

## 5B.13 References

1. Kenry; Lim, C. T. Nanofiber Technology: Current Status and Emerging Developments. *Prog. Polym. Sci.* 2017, 70, 1–17.

2. Barani, H.; Montazer, M.; Samadi, N.; Toliyat, T. In Situ Synthesis of Nano Silver/Lecithin on Wool: Enhancing Nanoparticles Diffusion. *Colloids Surfaces B Biointerfaces.* 2012, 92, 9–15.

3. Zhang, X.F.; Liu,Z.G.; Shen, W.; Gurunathan, S. Silver Nanoparticles: Synthesis, Characterization, Properties, Applications, and Therapeutic Approaches. *Int J Mol Sci.* 2016, 13; 17(9):1534.

4. Krutyakov, Y. A.; Kudrinskiy, A. A.; Olenin, A. Y.; Lisichkin, G. V. Synthesis and Properties of Silver Nanoparticles: Advances and Prospects. *Russ. Chem. Rev.* 2008, 77 (3), 233–257.

5. Ahamed, M.; AlSalhi, M. S.; Siddiqui, M. K. J. Silver Nanoparticle Applications and Human Health. *Clin. Chim. Acta* 2010, 411 (23), 1841–1848.

6. García-Barrasa, J.; López-de-Luzuriaga, J.; Monge, M. Silver Nanoparticles: Synthesis through Chemical Methods in Solution and Biomedical Applications. *Open Chem.* 2011, 9 (1), 7–19.

7. Dallas, P.; Sharma, V. K.; Zboril, R. Silver Polymeric Nanocomposites as Advanced Antimicrobial Agents: Classification, Synthetic Paths, Applications, and Perspectives. *Adv. Colloid Interface Sci.* 2011, 166 (1), 119–135.

8. Omar Sarheed,; Asif Ahmed,; Douha Shouqair,; Joshua Boateng. Antimicrobial Dressings for Improving Wound Healing, *Wound Healing-New Insights into Ancient Challenges, INTECH*, 2016, chapter 17.

9. Moura, L I.; Dias AM.; Carvalho E.; de Sousa H C. Recent advances on the development of wound dressings for diabetic foot ulcer treatment--a review. *Acta Biomater.* 2013; 9(7):7093-7114.

10. Harding, K G.; Jones V.; Price P. Topical treatment: which dressing to choose. *Diabetes Metab Res Rev.* 2000, 16 Suppl 1:S47-S50.

11. Vowden, P.; Cooper R A. An integrated approach to managing wound infection. In: European Wound Management Association (EWMA) *Position Document: Management of Wound Infection*. London, MEP Ltd, 2006: 2–6.

12. Lansdown AB. Silver. I: its antibacterial properties and mechanism of action. *J Wound Care.* 2002, 11(4):125–130.

13. Leaper D.; Appropriate use of silver dressings in wounds: international consensus document. *Int Wound J.* 2012, 9 (5):461–464.

14. Rai M.; Yadav A.; Gade A. Silver nanoparticles as a new generation of antimicrobials. *Biotechnol Adv.* 2009**,** 27(1):76–83.

15. Feng Q L.; Wu J.; Chen G Q.; Cui FZ.; Kim TN.; Kim JO. A mechanistic study of the antibacterial effect of silver ions on

*Escherichia coli* and *Staphylococcus aureus*. *J Biomed Mater*. 2000, 52(4):662–668.

16. Rizzello, L.; Pompa, P. P. Nanosilver-Based Antibacterial Drugs and Devices: Mechanisms, Methodological Drawbacks, and Guidelines. *Chem. Soc. Rev.* 2014, 43 (5), 1501–1518.

17. Damm, C., Münstedt, H. & Rösch, A. Long-term antimicrobial polyamide 6/silver-nanocomposites. *J Mater Sci.* 2007 42, 6067–6073.

18. Hong, K. H. Preparation and Properties of Electrospun Poly(Vinyl Alcohol)/Silver Fiber Web as Wound Dressings. *Polym. Eng. Sci.* 2007, 47 (1), 43–49.

19. Jeon, H J.; Kim J S.; Kim T G, Kim J H.; Yu W R.; and Youk J H. Preparation of poly(epsilon-caprolactone)-based polyurethane nanofibers containing silver nanoparticles, *Appl Surf Sci.* 2008, 254, 5886–5890.

20. Hong, K. H.; Park, J. L.; Sul, I. H.; Youk, J. H.; Kang, T. J. Preparation of Antimicrobial Poly(Vinyl Alcohol) Nanofibers Containing Silver Nanoparticles. *J. Polym. Sci. Part B Polym. Phys.* 2006, 44 (17), 2468–2474.

21. Wang, Y.; Yang, Q.; Shan, G.; Wang, C.; Du, J.; Wang, S.; Li, Y.; Chen, X.; Jing, X.; Wei, Y. Preparation of Silver Nanoparticles Dispersed in Polyacrylonitrile Nanofiber Film Spun by Electrospinning. *Mater. Lett.* 2005, 59 (24), 3046–3049.

22. Xu, X.; Yang, Q.; Wang, Y.; Yu, H.; Chen, X.; Jing, X. Biodegradable Electrospun Poly(l-Lactide) Fibers Containing Antibacterial Silver Nanoparticles. *Eur. Polym. J.* 2006, 42 (9), 2081–2087.

23. Katti, D. S.; Robinson, K. W.; Ko, F. K.; Laurencin, C. T. Bioresorbable Nanofiber-Based Systems for Wound Healing and Drug Delivery: Optimization of Fabrication Parameters. *J. Biomed. Mater. Res. Part B Appl. Biomater.* 2004, 70B (2), 286–296.

24. Jin, W.-J.; Lee, H. K.; Jeong, E. H.; Park, W. H.; Youk, J. H. Preparation of Polymer Nanofibers Containing Silver Nanoparticles by Using Poly(N-Vinylpyrrolidone). *Macromol. Rapid Commun.* 2005, 26 (24), 1903–1907.

25. Jin M, Zhang X, Nishimoto S, et al. Large-scale fabrication of Ag nanoparticles in PVP nanofibres and net-like silver nanofibre films by electrospinning. *Nanotechnology*. 2007, 18(7):075605.

26. Rujitanaroj, P.; Pimpha, N.; Supaphol, P. Wound-Dressing Materials with Antibacterial Activity from Electrospun Gelatin Fiber Mats Containing Silver Nanoparticles. *Polymer.* 2008, 49 (21), 4723–4732.

27. Son, W. K.; Youk, J. H.; Lee, T. S.; Park, W. H. Preparation of Antimicrobial Ultrafine Cellulose Acetate Fibers with Silver Nanoparticles. Macromol. Rapid Commun. 2004, 25 (18), 1632–1637.

28. Son, W. K.; Youk, J. H.; Park, W. H. Antimicrobial Cellulose Acetate Nanofibers Containing Silver Nanoparticles. *Carbohydr. Polym.* 2006, 65 (4), 430–434.

29. Gupta, N. R.; Torris A. T, A.; Wadgaonkar, P. P.; Rajamohanan, P. R.; Ducouret, G.; Hourdet, D.; Creton, C.; Badiger, M. V. Synthesis and Characterization of PEPO Grafted Carboxymethyl Guar and Carboxymethyl Tamarind as New Thermo-Associating Polymers. *Carbohydr. Polym.* 2015, 117, 331–338.

30. Nadtoka, O., Kutsevol, N., Naumenko, A. et al. Photochemical synthesis and characterization of hydrogel–silver nanoparticle composites. *Res Chem Intermed.* 2019, 45, 4069–4080.

31. Pal, S.; Tak, Y. K.; Song, J. M. Does the Antibacterial Activity of Silver Nanoparticles Depend on the Shape of the Nanoparticle? A Study of the Gram-Negative Bacterium Escherichia Coli. *Appl. Environ. Microbiol.* 2007, 73 (6), 1712–1720.

32. Kataria, K.; Gupta, A.; Rath, G.; Mathur, R. B.; Dhakate, S. R. In Vivo Wound Healing Performance of Drug Loaded Electrospun Composite Nanofibers Transdermal Patch. *Int. J. Pharm.* 2014, 469 (1), 102–110.

33. Ghosh, S.; More, P.; Derle, A.; Kitture, R.; Kale, T.; Gorain, M.; Avasthi, A.; Markad, P.; Kundu, G. C.; Kale, S.; Dhavale, D. D.; Bellare, J.; Chopade, B. A., Diosgenin Functionalized Iron Oxide Nanoparticles as Novel Nanomaterial Against Breast Cancer. *Journal of Nanoscience and Nanotechnology.* 2015, 15 (12), 9464-9472.

34. Gui-Bo, Y.; You-Zhu, Z.; Shu-Dong, W.; De-Bing, S.; Zhi-Hui, D.; Wei-Guo, F., Study of the electrospun PLA/silk fibroin-gelatin composite nanofibrous scaffold for tissue engineering. *Journal of Biomedical Materials Research Part A.* 2010, 93A (1), 158-163.

35. Bui, H. T.; Chung, O. H.; Dela Cruz, J.; Park, J. S., Fabrication and characterization of electrospun curcumin-loaded polycaprolactone-polyethylene glycol nanofibers for enhanced wound healing. *Macromolecular Research.* 2014, 22 (12), 1288-1296.

36. Goldner, J., A modification of the masson trichrome technique for routine laboratory purposes. *Am. J. Pathol.* 1938, 14 (2), 237–243.

37. Li J, He A, Zheng J, Han, C C. Gelatin and gelatin-hyaluronic acid nanofibrous membranes produced by electrospinning of their aqueous solutions. *Biomacromolecules.* 2006, 7(7):2243-2247.

38. Saquing, C D.; Manasco J L.; Khan, S A. Electrospun nanoparticle-nanofiber composites via a one-step synthesis. *Small.* 2009, 5(8):944-951.

39. Megelski, S.; Stephens, J. S.; Chase, D. B.; Rabolt, J. F. Micro- and Nanostructured Surface Morphology on Electrospun Polymer Fibers. *Macromolecules.* 2002, 35 (22), 8456–8466.

40. Fong, H.; Chun, I.; Reneker, D. H. Beaded Nanofibers Formed during Electrospinning. *Polyme* . 1999, 40 (16), 4585–4592.

41. Mituppatham, M. Nithitanakul,; P. Supaphol. Ultrafine Electrospun Polyamide-6 Fibers: Effect of Solution Conditions on Morphology and Average Fiber Diameter, *Macromol. Chem. Phys.* 2004, 205, 2327–2338.

42. Doshi, J.; Reneker, D. H. Electrospinning Process and Applications of Electrospun Fibers. *J. Electrostat.* 1995, 35 (2), 151–160.

43. Ghosal, K.; Thomas, S.; Kalarikkal, N. *et al.* Collagen coated electrospun polycaprolactone (PCL) with titanium dioxide (TiO$_2$) from an environmentally benign solvent: preliminary physico-chemical studies for skin substitute. *J Polym Res.* 2014, 21**,** 410.

44. Liu, J.; Hurt, R. H. Ion Release Kinetics and Particle Persistence in Aqueous Nano-Silver Colloids. *Environ. Sci. Technol.* 2010, 44 (6), 2169–2175.

45. Yuliwati, E.; Ismail, A. F.; Matsuura, T.; Kassim, M. A.; Abdullah, M. S. Effect of Modified PVDF Hollow Fiber Submerged Ultrafiltration Membrane for Refinery Wastewater Treatment. *Desalination.* 2011, 283, 214–220.

46. Li, J.-H.; Shao, X.-S.; Zhou, Q.; Li, M.-Z.; Zhang, Q.-Q. The Double Effects of Silver Nanoparticles on the PVDF Membrane: Surface Hydrophilicity and Antifouling Performance. *Appl. Surf. Sci.* 2013, 265, 663–670.

47. Chou, H. L.; Wu, C. M.; Lin, F. D.; Rick, J. Interactions between Silver Nanoparticles and Polyvinyl Alcohol Nanofibers. *AIP Adv.* 2014, 4 (8), 87111.

48. Dubey, P.; Bhushan, B.; Sachdev, A.; Matai, I.; Uday Kumar, S.; Gopinath, P. Silver-Nanoparticle-Incorporated Composite Nanofibers for Potential Wound-Dressing Applications. *J. Appl. Polym. Sci.* 2015, 132 (35).

49. Huang, H. H.; Ni, X. P.; Loy, G. L.; Chew, C. H.; Tan, K. L.; Loh, F. C.; Deng, J. F.; Xu, G. Q. Photochemical Formation of Silver Nanoparticles in Poly(N-Vinylpyrrolidone). *Langmuir* 1996, 12 (4), 909–912.

50. Zhao, Y.; Zhou, Y.; Wu, X.; Wang, L.; Xu, L.; Wei, S. A Facile Method for Electrospinning of Ag Nanoparticles/Poly (Vinyl Alcohol)/Carboxymethyl-Chitosan Nanofibers. *Appl. Surf. Sci.* 2012, 258 (22), 8867–8873.

51. Lee, K. H.; Kim, H. Y.; La, Y. M.; Lee, D. R.; Sung, N. H. Influence of a Mixing Solvent with Tetrahydrofuran and N,N-Dimethylformamide on Electrospun Poly(Vinyl Chloride) Nonwoven Mats. *J. Polym. Sci. Part B Polym. Phys.* 2002, 40 (19), 2259–2268.

52. Ito, H.; Sakata, M.; Hongo, C.; Matsumoto, T.; Nishino, T. Cellulose Nanofiber Nanocomposites with Aligned Silver Nanoparticles. *Nanocomposites.* 2018, 4 (4), 167–177.

53. Guo, J.-G.; Zhou, L.-J.; Zhao, Y.-P. Size-Dependent Elastic Modulus And Fracture Toughness Of The Nanofilm With Surface Effects. *Surf. Rev. Lett.* 2008, 15 (05), 599–603.

54. Liang, L. H.; Li, J. C.; Jiang, Q. Size-Dependent Elastic Modulus of Cu and Au Thin Films. *Solid State Commun.* 2002, 121 (8), 453–455.

55. Keun Kwon, I.; Kidoaki, S.; Matsuda, T. Electrospun Nano- to Microfiber Fabrics Made of Biodegradable Copolyesters: Structural Characteristics, Mechanical Properties and Cell Adhesion Potential. *Biomaterials.* 2005, 26 (18), 3929–3939.

56. Zienkiewicz-Strzałka, M.; Deryło-Marczewska, A.; Skorik, Y.A.; Petrova, V.A.; Choma, A.; Komaniecka, I. Silver Nanoparticles on Chitosan/Silica Nanofibers: Characterization and Antibacterial Activity. *Int. J. Mol. Sci.* 2020, 21, 166.

57. Song K, Wu Q, Zhang Z, et al. Porous Carbon Nanofibers from Electrospun Biomass Tar/Polyacrylonitrile/Silver Hybrids as Antimicrobial Materials. *ACS Appl Mater Interfaces.* 2015, 7(27):15108-15116.

58. Makaremi, M.; De Silva, R. T.; Pasbakhsh, P. Electrospun Nanofibrous Membranes of Polyacrylonitrile/Halloysite with Superior Water Filtration Ability. *J. Phys. Chem. C* 2015, 119 (14), 7949–7958.

**59.** Almajhdi FN, Fouad H, Khalil KA, et al. In-vitro anticancer and antimicrobial activities of PLGA/silver nanofiber composites prepared by electrospinning. *J Mater Sci Mater Med.* 2014, 25(4):1045-1053.

**60.** Natarajan S, Williamson D, Stiltz AJ, Harding K. Advances in wound care and healing technology. *Am J Clin Dermatol.* 2000,1(5):269–275.

**61.** Abdelgawad, A. M.; Hudson, S. M.; Rojas, O. J. Antimicrobial Wound Dressing Nanofiber Mats from Multicomponent (Chitosan/Silver-NPs/Polyvinyl Alcohol) Systems. *Carbohydr. Polym.* 2014, 100, 166–178.

**62.** Wu, J.; Zheng, Y.; Song, W.; Luan, J.; Wen, X.; Wu, Z.; Chen, X.; Wang, Q.; Guo, S. In Situ Synthesis of Silver-Nanoparticles/Bacterial Cellulose Composites for Slow-Released Antimicrobial Wound Dressing. *Carbohydr. Polym.* 2014, 102, 762–771.

**63.** Shrivastava, S.; Bera, T.; Roy, A.; Singh, G.; Ramachandrarao, P.; Dash, D. Characterization of Enhanced Antibacterial Effects of Novel Silver Nanoparticles. *Nanotechnology* 2007, 18 (22), 225103.

**64.** Rai, M.; Yadav, A.; Gade, A. Silver Nanoparticles as a New Generation of Antimicrobials. *Biotechnol. Adv.* 2009, 27 (1), 76–83.

**65.** Martinez-Castanon GA, Nino-Martinez N, Martinez-Gutierrez F, Martinez-Mendoza JR, Ruiz F. Synthesis and antibacterial activity of silver nanoparticles with different sizes. *J Nanopart Res.* 2008, 10(8): 1343–1348.

**66.** Sheikh, F.A.; Ju H.W.; Moon, B M., et al. Facile and highly efficient approach for the fabrication of multifunctional silk nanofibers containing hydroxyapatite and silver nanoparticles. *J Biomed Mater Res A.* 2014, 102(10):3459-3469.

**67.** Datta, S.; Rameshbabu, A. P.; Bankoti, K.; Maity, P. P.; Das, D.; Pal, S.; Roy, S.; Sen, R.; Dhara, S., Oleoyl-Chitosan-Based Nanofiber Mats Impregnated with Amniotic Membrane Derived Stem Cells for Accelerated Full -Thickness Excisional Wound Healing. *Acs Biomaterials Science & Engineering.* 2017, 3 (8), 1738-1749.

# CHAPTER VI

# Design and Fabrication of Gelatin based Electrospun Filter Media for Bio-separation Applications

*One rule is important in Science- Only courageous people win.*

*Max Planck*

## 6.1 Introduction

The number of kidney disease patients are increasing by 6-7% globally with an estimated of 600 million suffering from chronic and acute kidney problems. The excess uremic toxin in the blood leads to severe side effects and thereby subjecting the patients to use of dialysis to prolong their life. The hemodialysis membrane market is steadily increasing annually to US$ one billion and is not cost effective and affordable treatment facility to many people.[1] Membrane based technologies have gained tremendous attention and popularity in recent years because there is a need to develop versatile and economic separation processes.[2] Researchers are trying to develop newer and affordable membrane based filter mediums using polymeric nanofiber technology. Specific nanofillers like nanoclays are incorporated to enhance the mechanical stability, decrease in pressure drop, increase the permeability and porosity of in the electrospun micro fibrous non-woven hybrid membranes. Therefore these electrospun fibers not only have biomedical applications, but also find applications in filtration, air and water purification, bio-separation of biological molecules and other waste products and uremic toxic molecules from the blood streams.[3]

Hemodialysis is often used for the treatment of kidney diseases where the synthetic commercial hollow fiber membranes are utilized for the blood purification. In haemodialysis, the unwanted low and medium molecular weight uremic toxins, uric acid, etc are removed by a membrane where the blood flows from a higher solute concentration to a lower solute concentration. Moreover it is a costly process and not affordable by common man. An alternative method to the commercial hollow fiber synthetic membranes could be utilizing the micro/nanofiber membrane systems for separating the unwanted uremic toxins from the blood. However, cost effective and environmental friendly filter media with less solvents and hazardous chemicals are required for bio-separation applications. Electrospinning based nano/micro fibrous membranes have high filtering efficiencies and therefore, find great demand in the separation based technologies.

There are reports where nanofibers are utilised in the bio-separation of small protein molecules like Bovine Serum Albumin (BSA) and bilirubin from urine from regenerated cellulose due to its compatibility and non toxicity features.[4] *Koki Namekawa et al* [5], in 2014 reported a simple efficient and cost effective filter mesh to separate the uremic toxins for blood purification using poly (ethylene co-vinyl alcohol) along with zeolites which would adsorb the uremic toxins selectively as shown in **fig 6.1**



**Figure 6.1:** Nanofiber filter media for separation of uremic toxins from blood.

*Adapted with permission from, Koki Namekawa et al ; Biomater. Sci., 2014.*[5]
*© The Royal Society of Chemistry, 2014.*

Gelatin is a natural biopolymer derived from partial hydrolysis of native collagen. It has also been reported that gelatin contains many integrin binding sites for cell adhesion, migration, and differentiation, which are found in natural collagen and other extracellular matrix proteins.[6] It is a cheap water soluble, biocompatible and biodegradable polymer. The polymer gelatin alone or a blend with other synthetic polymers are used in the fabrication of fibrous membranes for tissue regeneration, medical health care devices, wound healing and other biomedical applications.[7] Halloysite is an aluminosilicate clay mineral mined universally in many countries across the globe.[8] It is an elongated tubular shaped particle which varies from hundreds of nanometer to few micrometer in length. The rolled tubular structure contains varying number of alternative octahedral alumina and tetrahedral silica layers in the 1:1 ratio.[9] The literature on halloysite reveals its use in the traditional Chinese medicines for different ailments and healing the wounds.[10] It is also often used

in ceramic and pottery.[11] The halloysite nanoclay has also been studied extensively for drug delivery and nano bio-medicine in the recent times.[12-14]

In this work, the objective was to develop a simple cost effective biocompatible, biodegradable filter media, or a fiber mesh fabricated from natural polysaccharide namely gelatin for the effective separation of the uremic toxins like urea, phosphates, creatinine, virus, bacteria, and other smaller low molecular weight toxic biological molecules to aid in blood purification. The hydrophilic, non-toxic biocompatible Halloysite nanoclay was chosen as it would enhance the mechanical stability of the gelatine filter media and due to its long cylindrical tubular structure would further help to trap the small molecular weight uremic toxins within the layered cavities.

## 6.2 Material and Methods

Gelatin was obtained from Sigma-Aldrich, porcine skin having gel strength 300, Type A, G2500-100G, with CAS no: 9000-70-8 having water solubility 50mg/ml. Halloysite nanotubes (HNTs) were purchased from Sigma Aldrich, India with CAS No: 1332-58-7. The solvent 2, 2, 2 Trifluoroethanol (TFE) having molecular mass of 100.04g/mol was purchased from Loba Chemie, India, with CAS No: 75-89-8. The laboratory grade of 25% aqueous glutaraldehyde, CAS no 111-30-8, was purchased from S.D. Fine Chemicals Ltd, India and used as crosslinking agent. The L929 human fibroblast cell lines were procured from National Centre for Cell Science (NCCS) Pune. The hemolysis study was carried out using the rat's blood at NCCS, Pune.

## 6.3 Experimental Section

### 6.3.1 Solution preparation

The gelatin of type A, porcine skin was dissolved in the solvent 2,2,2 Tri fluro ethanol(TFE) at room temperature by stirring it for 1 hour to make transparent gelatin polymer solution. The gelatine polymer solution concentration was fixed at 20% (w/v) throughout the experiments. ie 1 gm of gelatine was dissolved in 5 ml of TFE solvent. The polymer and the solvent were used as provided and without any purification. Halloysite nanotubes (HNT) were

initially mixed with TFE solvent by sonication for 5 minutes and later the gelatin powder was added to the TFE solvent. The concentration of the nanotubes varied from 5 to 15 % (w/w) for the electrospinning process.

## 6.3.2 Electrospinning of Gelatin fibers

Even though gelatin is water soluble, it becomes difficult to electrospin into the required fiber dimensions due to its polyelectrolyte characteristics and strong hydrogen bond which results in a 3D macromolecular gel like network thereby reducing the mobility of the polymer molecules. The organic solvents are therefore used to improve the electrospinning of the solution. The fluorinated alcohols such as Tri fluoro ethanol (TFE) and hexa fluoro isopropanol (HFIP) are good solvents for polypeptide biopolymers such as gelatin and collagen . Collagen nanofibers were successfully electrospun using HFIP solvent by Matthews *et al* [15] The gelatin polymer is a denatured collagen, therefore fluorinated solvents would be more suitable in electrospinning process. The solvent 2,2,2 Tri fluro ethanol was selected for the experiments. Electrospinning was carried out on ESPIN NANO, Model No: V2C, S.No: 01062015, India. All the experiments were performed at ambient temperature.
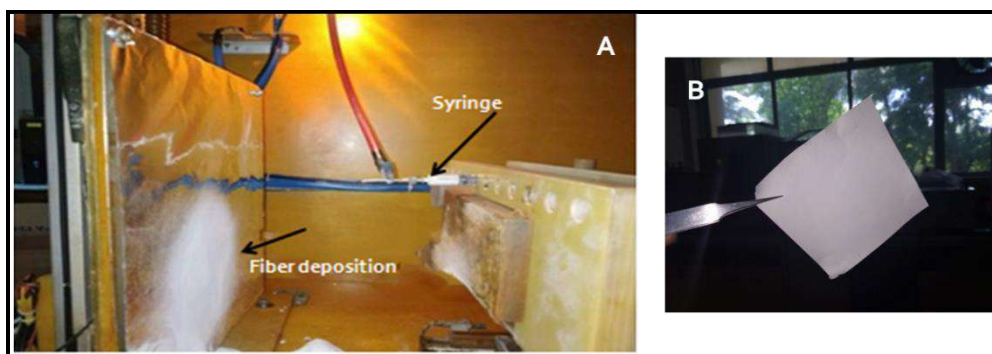


**Figure 6.2:** (A) Electrospinning set up showing Gelatin fiber deposition (B) Gelatin filter media.

The experimental setup for electrospinning is shown in **fig 6.2**(A). It consists of an adjustable DC power supply, a syringe pump on which a 5 ml plastic syringe was connected to a stainless steel needle having a diameter of 1.2 mm. The power supply was adjusted to 10 kV, and the polymer solution was ejected from the tip of the needle thus resulting in a non-woven fiber mesh

deposited on the collector plate covered with an aluminium foil, was connected to the ground (a negative polarity). A constant mass flow rate of 0.5 ml/h was maintained for all the experiments. The distance between the needle tip and the collector plate was kept at 10 cm. The aluminium foils were then removed and kept in desiccator for drying. The fiber mats after drying for two days were then crosslinked by 25% aqueous glutaraldehyde vapours for a period of 3 hours to ensure complete crosslinking. The obtained gelatin fiber mesh is shown in **fig 6.2**(B).

## 6.4 Characterization Techniques

### 6.4.1 Viscosity measurements

The viscosity measurements were done on Anton Paar, Germany Gmbh, Physica MCR 301, rheometer using cup and bob geometry. All experiments were done at $25^0$ C in triplicates and the average values reported.

### 6.4.2 Surface Tension measurements

Surface tension of the electrospinning solutions was carried out on the optical contact angle measurement system, Carl Zeiss, Jena, Japan.

### 6.4.3 Conductivity measurements

The electrical conductivities of the gelatin sample and gelatine containing halloysite nanotubes were measured using a conductometer, Toshniwal Instruments Mfg. Pvt Ltd, Ajmer, SR No: 10J694. Conductivity cell: Type: TCC-1, K=0.98. All measurements were done at $25^0$C in triplicates and average values reported.

### 6.4.4 Scanning Electron Microscopy (SEM)

The morphology of the microfibers was studied using Scanning Electron Microscopy quanta 200 3D dual beam ESEM FEI, Finland. The electron source was tungsten (W) filament with thermionic emission at 15 kV in high vacuum.

### 6.4.5 Transmission Electron Microscopy (TEM)

The size of HNTs in the gelain fiber mesh was determined using TEM FEI, TECNAIG2 F30 instrument operated at an accelerated voltage of 200 kV. The fibers were directly mounted on the copper grids during electrospinning, dried at room temperature and later examined under TEM.

## 6.4.6 Mechanical Properties

The mechanical strength of the gelatin fiber mesh was measured using a dynamic mechanical strain analyzer, RSA-3 (TA Instruments, USA). The samples were cut into dumble shaped strips with dimensions of 2 cm (length) x 0.5cm (width) and then mounted onto the tensile grips. The rate of pulling was 10mm/min and gauge length of 15 cm at 10 Hz was subjected to tensile force at $25^0$C. Each sample was repeated five times to authenticate its normal stress–strain curves. The material thickness (μm) was determined at five different places using a screw gauge and average values were taken for calculation.

## 6.4.7 3D X-ray micro-tomography

Gelatin filter media (GFM) were imaged using X-ray micro-tomography (Zeiss Xradia510Versa, Carl Zeiss, Pleasanton, USA) to study their micro-structure, morphology, pore-characteristics and permeability. GFMs were loaded on to the sample holder and kept in between the X-ray source and detector assembly. Detector assembly consisted of a scintillator, objective lens and a CCD camera. X-ray source was ramped up to 60 kV. The tomographic image acquisitions were completed by acquiring 3601 projections over 360° of rotation with a pixel size of approx 4 microns, for a sample size of 4 x 4 mm. In addition, projections without the samples in the beam (reference images) were also collected and averaged. Filtered back-projection algorithm was used for the reconstruction of the projections to generate two-dimensional (2D) virtual cross-sections of the specimens. Image processing software, Dragonfly Pro (Version 3.1) was used to generate volume-rendered three-dimensional (3D) images of specimens. Segmentation and further processing were performed using basic *GeoDict* software package (*GeoDict*2018, Math2Market GmBH, Germany). 2D images were trimmed down to a sub-volume (1.3 x 1.0 x 0.9 mm), filtered to remove noise and segmented after manual threshold selection based on local minima from the greyscale histogram. Resultant 3D reconstructed model was used to estimate the pore characteristics and the simulation of permeability using *PoroDict* and *FlowDict* software packages, respectively.

## 6.5 Biological studies

### 6.5.1 Cell viability studies (MTT Assay)

The cyto toxicity of gelatin filter media (GFM) was investigated using MTT assay. The L929 mouse fibroblast cell lines were obtained from National Centre for Cell Science (NCCS), Pune, India. The cells were cultured in DMEM medium, supplemented with 10% fetal bovine serum, streptomycin (10 g/ml) and penicillin (100 units/ml) and were maintained in a humidified atmosphere at $37^0$C under 5% $CO_2$. Cells ($1\times10^4$) were seeded per well in 24-well, flat bottom culture plate and incubated for 24 h, followed by the treatment using gelatine filter mats for a time period of 24 hours. After incubation, the MTT solution (5 mg/ml of stock solution of which 20µl of MTT solution was added in 200µl of DMEM media) was added to each well followed by further incubation in darkness at $37^0$C for 4 h. The formazan crystals formed were dissolved by addition of acidified isopropanol. After 15 min, the amount of coloured formazan derivative formed was determined by measuring the optical density (OD) using a microplate reader (Spectra Max, MS; Molecular Devices, LCC) at 570 nm. All the experiments were done in triplicate. The percentage cell viability was calculated as: [16]

$$\% \text{ Cell viability} = \frac{(OD)\text{sample} - (OD)\text{blank}}{(OD)\text{control} - (OD)\text{blank}} * 100$$

### 6.5.2 Hemocompatibilty Assay

Hemolysis study of the gelatin loaded HNTs were performed using method of indirect contact according to the requirements of ISO 10993.[17] About 3ml of rat blood was collected in EDTA coated vials and was diluted to 3 times in physiological saline. 1 ml of diluted blood was then centrifuged at 2000 rpm for 15 minutes at $4^0$C. 200µl of this diluted blood was taken in an eppendorf tube and made upto 1 ml. The nanofiber mats were immersed into the diluted blood and incubated for 1 h at $37^0$C and then centrifuged at 2000 rpm for 15 minutes. After centrifugation, the supernatant liquid was collected and absorbance was recorded at 540 nm. Triton-X (0.1%) was used as positive control and saline as negative control for the study. All the experiments were

done in triplicates and average value was reported. The percent hemolysis was calculated using the following formula:

$$\% \text{ Hemolysis} = \frac{\text{Sample (OD)} - \text{Negative control (OD)}}{\text{Positive control(OD)} - \text{Negative control(OD)}} * 100$$

## 6.6 Results and Discussion

### 6.6.1 Solution Properties of Gelatin polymer solution

The effect of viscosity and charged density of the electrospinning solution contribute to the change of diameter of electrospun nanofibers.[18] In this study, its observed that the incorporation of the HNT increases the viscosity of the gelatin polymer solution from 0.176 Pa.s (neat 20%Gelatin) to 0.268 Pa.s (20%Gelatin/10%HNT) but the viscosity lowered gradually to 0.202 Pa.s in case of (20%Gelatin/15%HNT).

**Table 6.1:** Properties of the Gelatin polymer solutions containing HNTs

| Parameter | Viscosity (Pa.s) | Conductivity (µs/cm) | Surface Tension (mN/m) |
|---|---|---|---|
| Gelatin_20% + 0_HNT | 0.176 | 4.03 | 42.31 |
| Gelatin_20% + 5_HNT | 0.238 | 4.18 | 43.65 |
| Gelatin_20% + 10_HNT | 0.268 | 4.24 | 45.37 |
| Gelatin_20% + 15_HNT | 0.202 | 4.35 | 47.14 |

The viscosity, conductivity and the surface tension of the polymer solution are summarised in **table 6.1**. The higher the viscosity, the liquid gets stretched and electrospun fibers are obtained with increased diameters.[19] The electrical conductivity showed an increasing trend with the increase in HNT concentration. The conductivity increased from 4.03 µS/cm for 20%Gelatin/0%HNT to 4.35 µS/cm for 20%Gelatin/15%HNT. This increase is due to the presence of negatively charged HNTs which increases the charge

density of the electrospinning solution thereby increasing the conductivity. The lower surface tension of the polymer solution determines bead free formation of the fibers by electrospinning. The surface tension data for the gelatin solution and gelatin/HNT solution values are in the range of 42.31mN/m to 47.14 mN/m and fall in the optimum range for electrospinning of polymer solutions.[20]

## 6.6.2 Scanning Electron Microscopy (SEM)

The characterization of gelatin fibers was done using the SEM analysis to know the surface morphology of the fibers and the halloysite nanotubes. The SEM images reveal that the fibers are in micron size range i.e in the range of 1 to 3µm. The fibers are non-woven and uniformly distributed throughout.
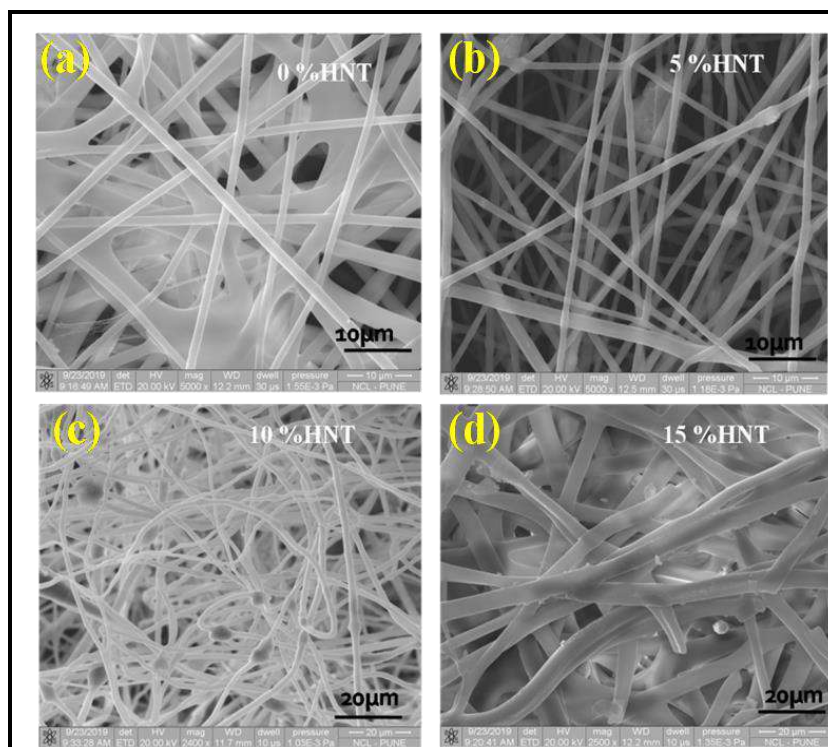


**Figure 6.3:** SEM images of Gelatin fibers with different loading of HNTs.
Scale bars**:** 10µm for (a) and (b); 20µm for (c) and (d)
5000X magnification for (a) and (b); 2500X magnification for (c) and (d).

The halloysite nanotubes (HNT) are also uniformly distributed throughout the fiber matrix. The HNTs possess tubular structure having length of 0.5 to 1.2µm and diameter of 50 to 100 nm. The fibers formed were having a smooth surface with no bead formation. The smooth surface was also seen at lower content of HNT. The fibers containing 10 and 15% HNT however

demonstrated rough surface.[21] The size of the fibers having HNT was slightly larger (few nanometres) than the fibres without HNT. In the images, it is clearly observed that the fibers with 5 and 10% HNT showed small hump which confirms the presence of halloysite within the matrix. In case of 15% HNT, the fibers appear darker due to excess HNT and the fiber diameter is also increased. The increasing concentration of HNT was also confirmed by Energy-dispersive X-ray spectroscopy, SEM-(EDX).

### 6.6.3 Transmission Electron Microscopy (TEM)

The pristine HNT nanotubes are bound together by Wander walls forces and therefore ultrasonication is done for 15 minutes for the Gelatin-TFE polymer solution for effective distribution of the HNT before the electrospinning process. The distribution of HNT was observed from the TEM images.
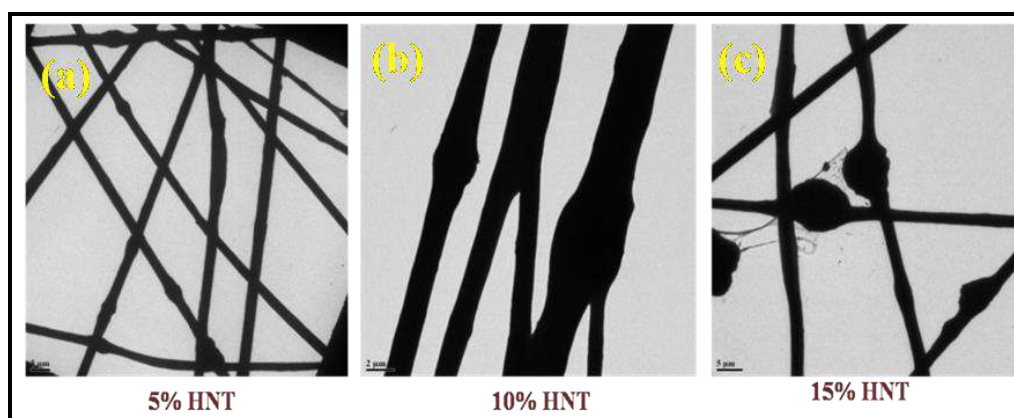


**Figure 6.4:** TEM images Gelatin fibers with different loading of HNTs
Scale bars**:** 5µm for (a) and (c); 2 µm for (b).

It was observed that the Halloysite nanotubes (HNT) were uniformly dispersed and distributed throughout the fiber matrix. There were small protrusions within the matrix as seen in **fig 6.4.** As the concentration of the HNTs increased (10 % HNT) the gelatin fibers were seen agglomerated in the form of small lumps and protruded outside the fibers. For the higher content of HNT (15%HNT), the agglomeration becomes evident. [21]

### 6.6.4 Mechanical Properties

The mechanical properties of the electrospun gelatin/HNT fiber mesh were investigated using the tensile studies. The obtained stress –strain curves are

shown in **fig 6.5**, and the tensile strength, Young's modulus and the elongation at break are measured and summarized in **table 6.2**.

**Table 6.2:** Mechanical properties of the Gelatin loaded HNT fibers.

| Parameter | Tensile Strength (MPa) | Young's Modulus (MPa) | Elongation at break (%) |
|---|---|---|---|
| Gelatin_0%HNT | 3.8 | 2.46 | 2.53 |
| Gelatin_5%HNT | 9.6 | 3.85 | 2.79 |
| Gelatin_10%HNT | 13.2 | 5.73 | 4.34 |
| Gelatin_15%HNT | 5.8 | 2.57 | 3.89 |
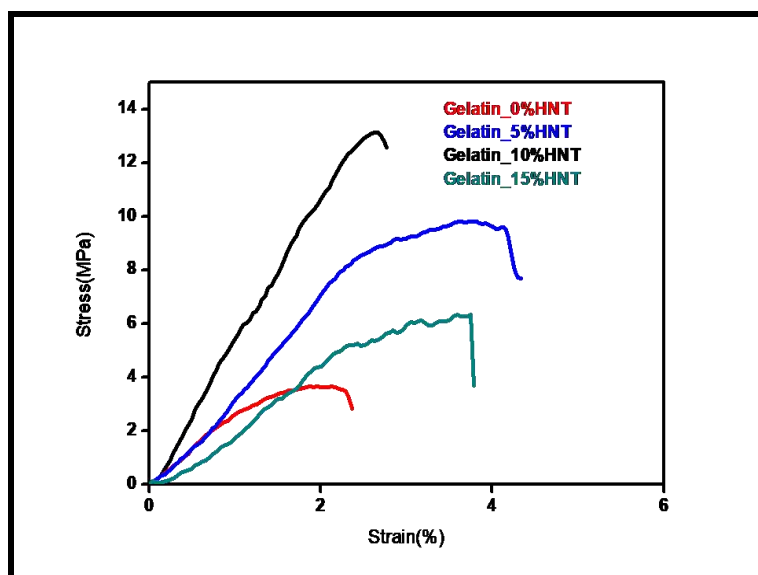


**Figure 6.5:** The stress-strain graph for Gelatin loaded HNT fibers.

The tensile strength and Young's modulus increased to 13.2 MPa (247%) and 5.73 MPa (132%) respectively with the addition of 10 wt% HNT. The gelatin filter media becomes stronger and stiffer. However, the extra addition of HNT (15wt %) no longer show any enhanced effects. The tensile strength and Young's modulus decreases with the increase in HNT from 10 to 15 wt%, as reported in **table 6.2**. The percent elongation at break increased from 2.53 to 4.34 % for 10%HNT. This may be due to the elastic nature of the gelatin fibers

but gradually decreased when the HNT concentration increased to 15%. The mechanical properties show strong interactions between the nanotubes and the fiber matrix which are due to hydrogen bonding between the nanotubes and gelatin matrix.[22]

## 6.6.5 *In- silico* Studies on Permeability of Gelatin Filter Media (GFM)

Computer-aided simulation experiments (*in-silico*) has attracted much attention in these decades, mostly due to the valuable insights it can provide, in understanding various underlying phenomena, across all subject disciplines and research. Direct numerical simulations on real 3D micro-structures of materials are one of the major approaches which has the potential to overcome various bottle necks related to hazardous and complex laboratory experiments.

In this study, the permeability characteristics of GFM, in filtering the uremic toxins were studied by performing direct numerical simulations on the real 3D micro-structure of GFM. Initially 3D micro-structure of GFM was reconstructed by 3D imaging of GFM by high-resolution X-ray micro-tomography. The pore-characteristics of the structure were estimated by segmentation of the reconstructed images using *PoroDict* image processing software. Segmented 3D model of GFM was further subjected to numerical simulations using *FlowDict* image processing software, to calculate the permeability of spherical particles through the tortuous path inside its micro-structure.

**GeoDict** is a software package which is a complete solution for 3D image processing (PoroDict module), modeling of materials visualization, material property characterization, simulation based material development (FlowDict) and process optimization. It helps to improve and design various filters for various applications such as air filtration, blood filtration, oil filtration etc.

### 6.6.5.1 3D imaging of non-woven GFM

X-ray projection images of GFM were reconstructed using back-projection algorithm to generate 2D virtual cross-sectional images, which were then later segmented to construct 3D images of GFM as shown in **fig 6.6**.
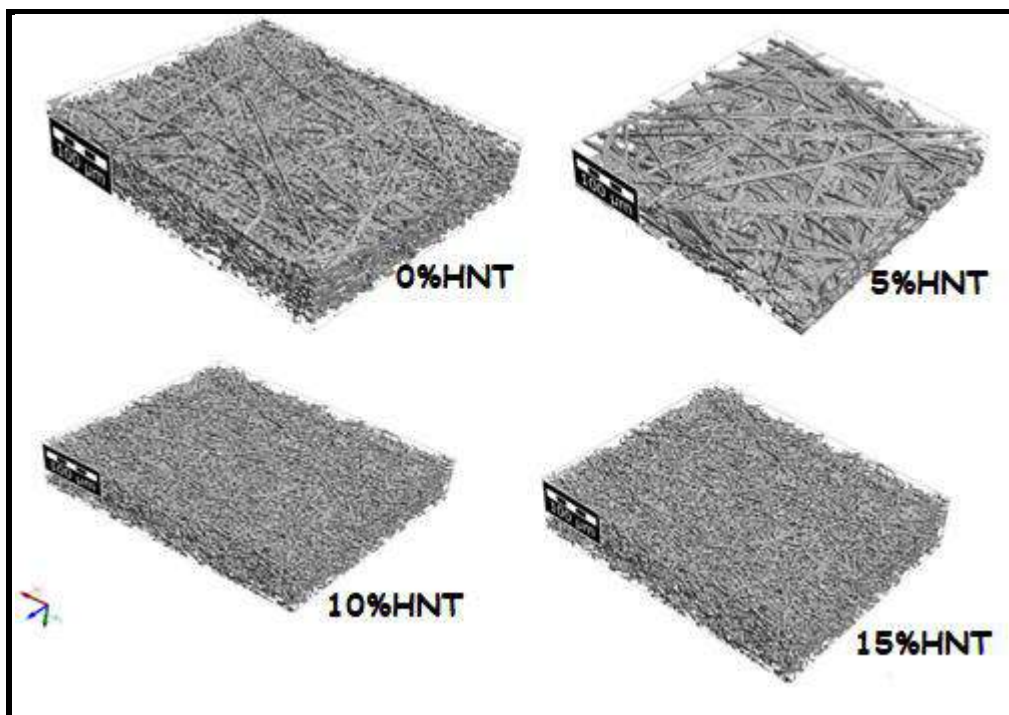
**Figure 6.6:** Segmented 3D images of non-woven GFM with various loading of HNTs.  Scale bars: 100 microns in all images.

From **fig 6.6**, we observe that with increase in HNT loading, the fibers are seemed to be tightly packed. Therefore tortuosity of the media varies with HNT loading and may regulate its pore-characteristics.

### 6.6.5.2 Pore characteristics of non-woven GFM

From the segmented datasets the pore space is differentiated by the image processing software by identifying the respective pixels in the image. Pixels in the 3D space are represented as voxels and the volume-based representation of pores aids in the accurate estimation of porosity in these media. 3D images of the colour-coded visualization of pores are shown in **fig 6.7**. As visualized in **fig 6.7**, with increase in the HNT loading, the pore diameter also increases. Increase in pore diameter can alter the porosity of these filters. Pore diameters were calculated by fitting spheres into the pore throat and thereafter calculating the diameter of the fitted spheres. Subsequently the number pores and their diameter can be calculated after the fitting process.

**Figure 6.7:** Colour-coded pore-size visualization in the 3D images of non-woven GFM with various loading of HNTs.
Scale bars: 100 microns in all images.
Red colour in the diameter scale denotes pores with larger diameter and blue denotes those with smaller diameter

The histogram of pore volume as a function of pore diameter is shown in **fig 6.8**.With increase in HNT loading the pore diameter range is increasing, as shown in **fig 6.8** Average pore diameters were 6, 10, 12 and 16 microns for 0, 5, 10 and 15 wt % HNT loading, respectively (**fig 6.9 b**). This increase in porosity with HNT loading (**fig 6.9 a**) may be resulting from the repulsive forces between HNT particles during the electro-spinning process or re-arrangement of HNT particles during the electro-spinning process by virtue of its high-aspect ratio.
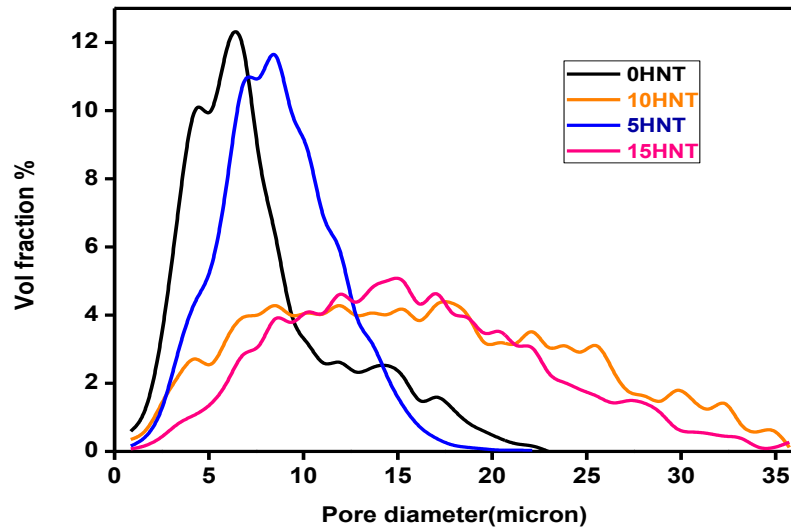
**Figure 6.8:** Histogram of pore diameter distribution as a function of pore volume in GFM with varying HNT loading.

Porosity of GFM are 78, 83, 87 and 95 % respectively for 0, 5, 10 and 15 wt % HNT loading (**fig 6.9 a**). At higher HNT loading pore diameter increases with relative reduction of pore volume. It shows the role of HNT enhancing the porosity of filter media.
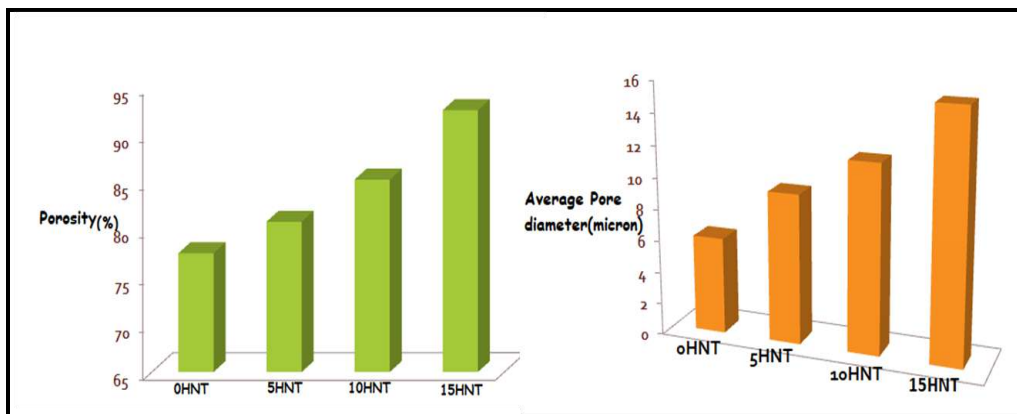


**Figure 6.9:** Histogram of (a) porosity and (b) average pore diameter as a function of HNT loading in GFM

## 6.6.5.3 Simulating velocity profiles through the micro-structure of non-woven GFM

Velocity in the movement of solutes through filter membranes depends on the porosity and average pore diameter of the membrane for a given pressure drop. **Figure 6.10** shows the color-coded velocity profile of water inside the micro-structure of GFM with 0, 5, 10 and 15 wt % HNT. In contrast with the

increasing rate of porosity and pore size with HNT loading, the velocity profile of GFM shows a different result. GFM 15 wt % HNT loading shows lower average flow velocity than 10 wt % loading. This observation may be due to the presence of bead-like structures inside the micro-structure of GFM with 15 wt % HNT. Bead-like structures are reported in the electrospun membranes with higher filler loading.
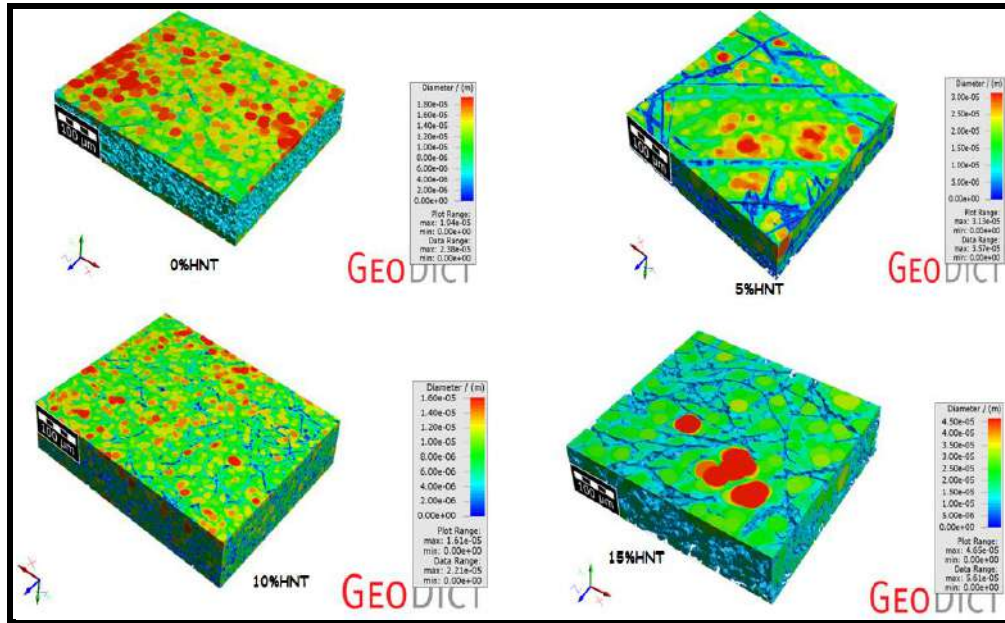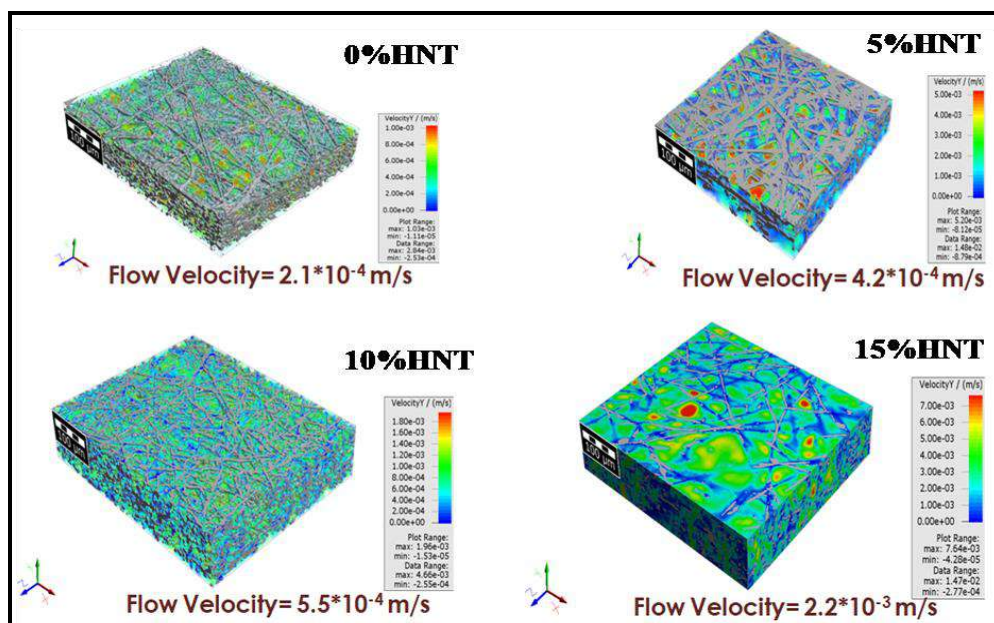


**Figure 6.10:** Colour-coded flow velocity visualization in the 3D images of non-woven GFM with various loading of HNTs.
Scale bars: 100 microns in all images.
Red colour in the velocity scale denotes flow domains with higher velocity and blue denotes those with lower velocity.

The color-coded velocity profiles of 0, 5 and 10 wt % HNT loading shows a homogeneous distribution of domains, whereas GFM with 15 wt % HNT exhibits velocity profile scattered in-homogeneously throughout the volume. Such distinct behaviour is observed in the mechanical behaviour of GFM (**table 6.2** and **fig 6.5**). Correlation of porosity and average flow velocity profiles are essential to understand the effect of HNT loading in GFM histogram (**fig 6.11**) shows the plot of both porosity and velocity profile as a function of HNT loading in GFM. It is evident that a drastic difference is observed in the velocity profile of GFM with 15 wt % HNT, whereas the

porosity of GFM with the same HNT loading does not exhibit similar behaviour.
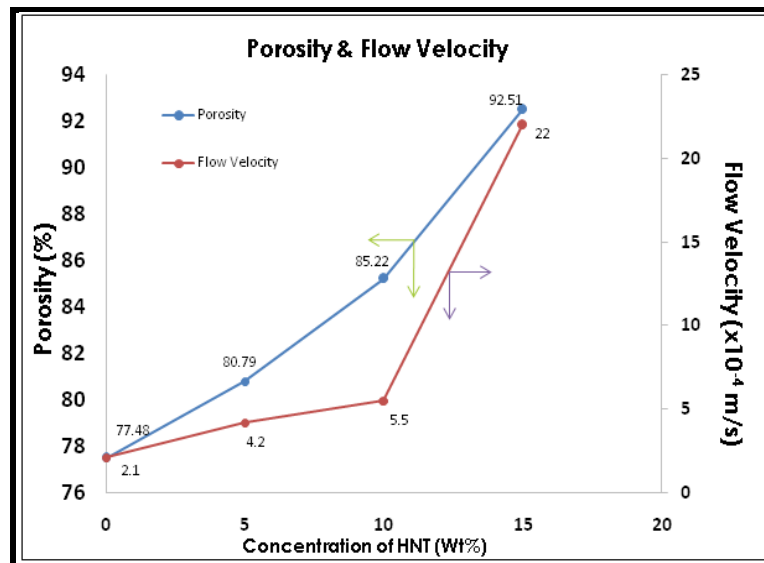


**Figure 6.11:** Histogram of porosity and average flow velocity as a function of HNT loading in GFM.

### 6.6.5.4 Simulation of permeability studies on non-woven GFM *in-silico* model

Numerical simulations studies are done to predict the diameter of spheres that can permeate through the tortuous paths inside the micro-structure of GFM's with various HNT loading ends up in a trajectory profile shown in **fig 6.12**.
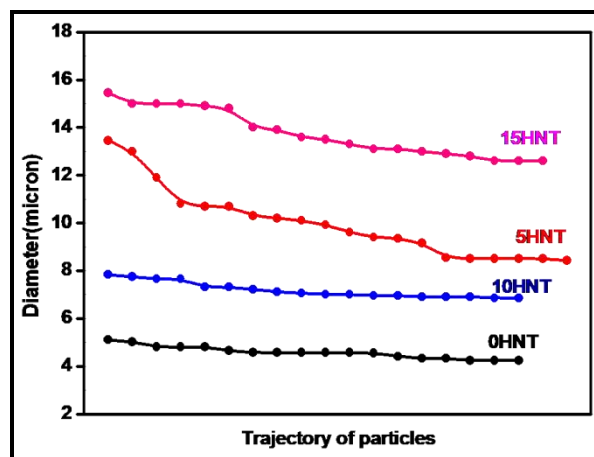


**Figure 6.12:** Histogram of predicted sphere diameters permeated in GFM with different HNT loading.

The trajectory paths for 0 and 10% HNT were in a same direction and followed a straight path as seen in the figure. There path of trajectory for 5 and 15% HNT loaded gelatine filter media were in slightly curved initially and later followed a straight line.

In the **fig 6.13** a schematic representation of small and middle molecule uremic toxins and excess water are separated/filtered through the gelatin filter media thereby purifying the blood in our body.
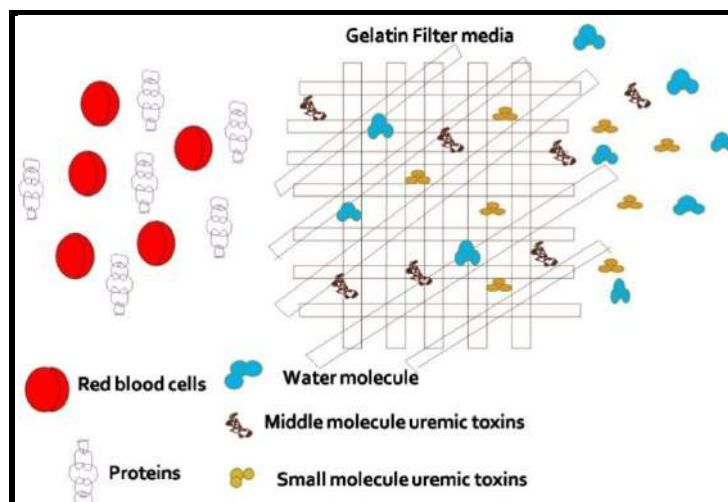


**Figure 6.13:** Schematic representation for separation of uremic toxins from blood using gelatin filer media.

**Table 6.3: Sizes of biological materials**

| Material | Size( microns) |
|---|---|
| Chloride ion | $9.9 \times 10^{-5}$ |
| Urea | $1.6 \times 10^{-4}$ |
| Glucose | $8.6 \times 10^{-4}$ |
| Insulin | $4 \times 10^{-3}$ |
| Human serum albumin | $7.2 \times 10^{-3}$ |
| Dextran | $1 \times 10^{-3}$ to $15 \times 10^{-3}$ |
| Immunoglobulin G | $11.1 \times 10^{-3}$ |
| Virus particle | 0.004 to 0.1 |
| Bacteria | 0.2 to 2.0 |
| Yeast cells | 2 to 30 |
| Mammalian cell in culture | 2-10 |

*Source: Principles of Bio-separations; Raja Ghosh ;
World Scientific Publishing Company,2006.* [23]

This cheap handy gelatin based filter media would serve its purpose and also save lot of time and heavy costly instruments required in the hospitals during

the blood purification. Spheres with diameter of 5, 8, 13 and 15 microns can permeate through the micro-structure of GFM's with 0, 5, 10 and 15 wt% of HNT loading respectively. Such information about the size distribution of spheres can aid in the differentiation of these membrane filters for the partitioning or separation of bio-molecules such as creatine, RBC, proteins, etc (**fig 6.13**). Thus GFM with tunable micro-structure may be employed for the bio-separation process such as artificial dialysis, oxygen enrichment unit, etc (**table 6. 3**).

### 6.6.6 Cytocompatibility Studies

The MTT assay is a standard colorimetric assay which measures the activity of enzymes that reduces the MTT to formazan, giving a purple color. The yellow MTT (3-(4,5-dimethylthiazol-2-yl)-2,5-diphenyltetrazolium bromide, a tetrazole) is reduced to purple formazan in the mitochondria of living cells.[24] The cytocompatibilty test of the gelatine/HNT fiber mats were evaluated using the L929 human fibroblast cells by the MTT Assay. The bar graph results suggest that  the gelatin/5% HNT fiber mesh showed more than 100%  cell growth and proliferation which only means that the halloysite nanotubes are favouring the cell attachment , proliferation and growth.
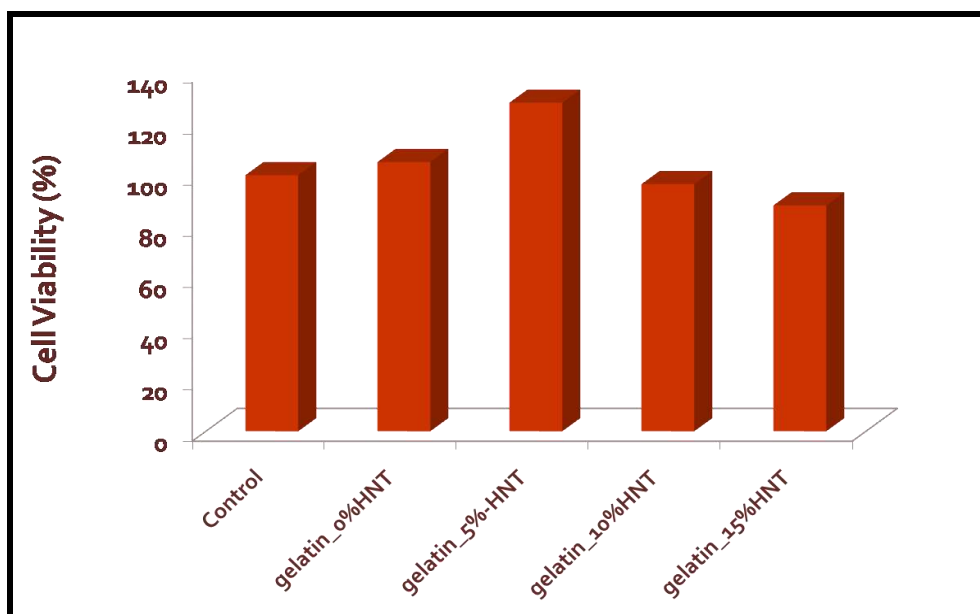


**Figure 6.14:** Cell Viability of HNT loaded Gelatin filter media using L929 fibroblast cell line.

The increase in the halloysite concentration also favours good cell adhesion and cell growth seen was around 95 to 98% in gelatin loaded 10% and 15% HNTs. The experimental study was carried out for 24 hours.  The experiment confirms the non-toxicicity of the nalloysite nanotubes to the L929 fibroblast cells.

### 6.6.7 Hemocompatibility Study

The blood compatibility study plays a significant role in deciding the application of developed implants for their use in biomedical applications. When the blood comes in contact with an implant, the plasma proteins tend to get adsorbed by enhancing the platelet surface interaction, leading to thrombus formation and thereby resulting in the failure of an implant.[25] Hemolysis was performed to investigate the safety of red blood cells on the electrospun gelatine/HNT fiber mats. The **fig 6.15** shows the % hemolysis of  the gelatin fiber mat was 0.5, and the gelatin fiber mats with 5, 10 and 15% HNT were 1.2, 1.7 and 1.9 respectively.
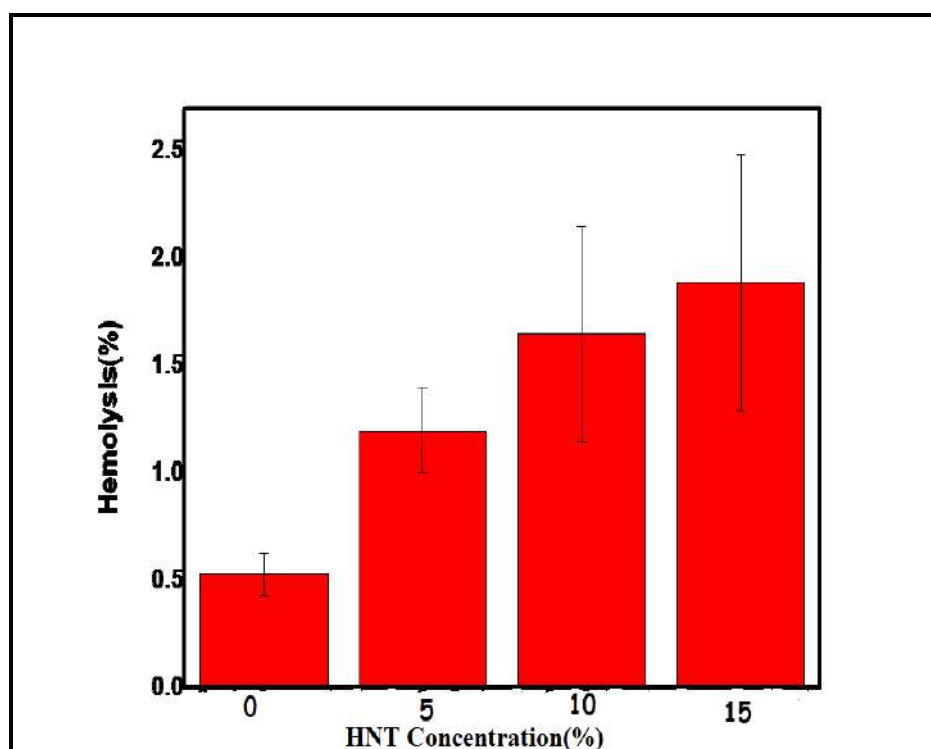


**Figure 6.15:** Bar graph showing Hemolysis(%) for Gelatin filter media with different loading of HNTs.

The reports from literature reveal, that if the percentage of hemolysis is less than 5%, then the material is non-hemolytic.[26] Huang *et al* in 2003 reported that that the blood compatibility is influenced by several factors such as surface area, surface tension, surface roughness, surface energy, fiber diameter and wettability characteristics.[27] Manikandan *et al* reported hydrophilic Polyurathene blended with murivennai oil for tissue engineering applications which exhibited god surface wettability.[28] In this study, the gelatine being hydrophilic and when blended with hydrophilic halloysite nanotubes increases the surface wettability for the gelatin/HNT fibers and hence might have attributes to enhanced blood compatibility. The results obtained in our studies reveal that the hemolysis percentage is less than 2 percent and therefore our filter media from gelatine fibers are most suitable for bio-separation of small uremic toxins and also other smaller toxic molecules from the blood.

## 6.7 Conclusions

Polymeric fibrous membranes fabricated through electrospinning technique have great potential due to the high surface area to volume ratios, high porosity, and interconnected porous structures and find variety of applications in oil/water separations, distillation, bio-separations micro, ultra and nano filtration technologies. In this study, we designed and fabricated a new electrospun filter media using gelatin and halloysite nanoclay which could be useful for separation of smaller bio molecules like urea, uric acid, creatinine, uremic toxins having sizes in the range of 0.5 -20 KDa. The gelatin and clay solution concentration was optimised and the solution properties like viscosity, conductivity and surface tension were determined and were in the optimum range of the electrspinning. The fiber morphology revealed bead free non woven fibers with average fiber diameter of 1 to 2 microns. In the TEM images, the halloysite nanoclay was seen as small humps in case of 15%HNTs. The addition of nanoclay enhanced the mechanical properties of the gelatin filter media upto 10% wt of HNT, but gradually decreased with excess of HNT addition. This was attributed to the formation of aggregates which reduces the strength of the gelatin fibers. The *in-silico* permeation studies, pore size, porosity and flow velocity studies

were done using micro-tomography experiments. The average pore size and porosity increased with the increase in HNT concentration. The flow velocity decreased with the increase in the HNT concentration and this may be due to the beaded structure because of excess HNT deposition within the gelatin fibers. The biological studies were done to know the material compatibility with blood cells. The MTT assay showed good cell adhesion, growth of L929 fibroblast cells and the gelatin loaded halloysite filter media was not showing any toxicity. The hemolysis study also confirmed that the percentage hemolysis was within the acceptable range (<5%) and no RBC death observed. The fabricated filter media would serve as a bio-separation device to remove the toxic uremic toxins and other smaller mad lower molecular weight molecules from the blood and help in purification with an affordable cost. This preliminary study will help to carry forward the research to develop a sustainable and cost effective bio-separating membrane in future.

## 6. 8 References

**1.** Striemer, C., Gaborski, T., McGrath, J. et al. Charge- and size-based separation of macromolecules using ultrathin silicon membranes. *Nature.* 2007, 445, 749–753.

**2.** Nagarale, R. K.; Gohil, G. S.; Shahi, V. K. Recent Developments on Ion-Exchange Membranes and Electro-Membrane Processes. *Adv. Colloid Interface Sci.* 2006, 119 (2), 97–130.

**3.** Yu, X.; Shen, L.; Zhu, Y.; Li, X.; Yang, Y.; Wang, X.; Zhu, M.; Hsiao, B. S. High Performance Thin-Film Nanofibrous Composite Hemodialysis Membranes with Efficient Middle-Molecule Uremic Toxin Removal. *J. Memb. Sci.* 2017, 523, 173–184.

**4**. Ma, Z.; Kotaki, M.; Ramakrishna, S. Electrospun Cellulose Nanofiber as Affinity Membrane. *J. Memb. Sci*. 2005, 265 (1), 115–123.

**5.** Namekawa, K.; Tokoro Schreiber, M.; Aoyagi, T.; Ebara, M. Fabrication of Zeolite–Polymer Composite Nanofibers for Removal of Uremic Toxins from Kidney Failure Patients. *Biomater. Sci.* 2014, 2 (5), 674–679.

**6.** Hajiali, H., Shahgasempour, S.,Naimi-Jamal, M. R., & Peirovi, H. Electrospun PGA/gelatin nanofibrous scaffolds and their potential application in vascular tissue engineering. *International journal of nanomedicine,* 2011, 6, 2133–2141.

**7.** Giusti P, Barbani N, Lazzeri L, Polacco G, Cristallini C, Cascone MG. Gelatin-poly(vinyl alcohol) blends as bioartificial polymeric materials. *Proceedings of the Fourth International Conference on Frontiers of Polymers and Advanced Materials*, 4–9 January, Cairo, Egypt; 1997.

**8.** Du, M.; Guo, B.; Jia, D. Newly Emerging Applications of Halloysite Nanotubes: A Review. *Polym. Int.* 2010, 59 (5), 574–582.

**9.** Lvov, Y. M.; Shchukin, D. G.; Möhwald, H.; Price, R. R. Halloysite Clay Nanotubes for Controlled Release of Protective Agents. *ACS Nano* 2008, 2 (5), 814–820.

**10.** Chi Shi Zhi (Halloysite, Kaolin)—Chinese Herbal Medicine, in: Yin Yang House, 2014.

**11.** S.R. Levis, P.B. Deasy, Characterisation of halloysite for use as a microtubulardrug delivery system*, Int. J. Pharm.* 2002, 243, 125–134.

**12.** K. Krejcova, P.B. Deasy, M. Rabiskova, Optimization of diclofenac sodiumprofile from halloysite nanotubules, *Ceska Slov. Farm.* 2013, 62, 71–77.

**13.** S.R. Levis, P.B. Deasy, Use of coated microtubular halloysite for the sustained release of diltiazem hydrochloride and propranolol hydrochloride, *Int. J.Pharm.* 2003, 253, 145–157.

**14.** J. Forsgren, E. Jamstorp, S. Bredenberg, H. Engqvist, M. Stromme, A ceramicdrug delivery vehicle for oral administration of highly potent opioids, *J.Pharm. Sci.* 2010, 99, 219–226.

**15.** Matthews JA, Wnek GE, Simpson DG, Bowlin GL. Electrospinning of collagen nanofibers. *Biomacromolecules* 2002; 3: 232–238.

**16.** Ghosh, S.; More, P.; Derle, A.; Kitture, R.; Kale, T.; Gorain, M.; Avasthi, A.; Markad, P.; Kundu, G. C.; et al. Diosgenin Functionalized Iron Oxide Nanoparticles as Novel Nanomaterial Against Breast Cancer. *Journal of Nanoscience and Nanotechnology.* 2015**,** 15 (12), 9464-9472.

**17.** Gui-Bo, Y.; You-Zhu, Z.; Shu-Dong, W.; De-Bing, S.; Zhi-Hui, D.; Wei-Guo, F., Study of the electrospun PLA/silk fibroin-gelatin composite nanofibrous scaffold for tissue engineering. *Journal of Biomedical Materials Research Part A.* 2010**,** 93A (1), 158-163.

**18.** Liu L, Ren Y, Li Y, Liang Y .Effects of hard and soft components on the structure formation, crystallization behaviour and mechanical properties of electrospun poly (L-lactic acid) nanofibers. *Polymer. 2013,* 54: 5250–5256.

**19.** Thompson, C. J.; Chase, G. G.; Yarin, A. L.; Reneker, D. H. Effects of Parameters on Nanofiber Diameter Determined from Electrospinning Model. *Polymer*. 2007, 48 (23), 6913–6922.

**20.** Doshi, J.; Reneker, D. H. Electrospinning Process and Applications of Electrospun Fibers. *J. Electrostat.* 1995, 35 (2), 151–160.

**21.**Cai, N.; Dai, Q.; Wang, Z.; Luo, X.; Xue, Y.; Yu, F. Toughening of Electrospun Poly(l-Lactic Acid) Nanofiber Scaffolds with Unidirectionally Aligned Halloysite Nanotubes. *J. Mater. Sci.*2015, 50 (3), 1435–1445.

**22.** Schadler LS, Giannaris SC, Ajayan PM. Load transfer in carbon nanotube epoxy composites. *Appl Phys Lett.* 1998, 73:3842– 3844.

**23.** Ghosh, R. *Principles Of Bioseparations Engineering*; World Scientific Publishing Company, 2006.

**24.** F. L. Mi, H. W. Sung, and S. S. Shyu, *J. Polym. Sci. Part A: Polym. Chem.* 2000, 38, 2804 (2000).

**25.** Dhandayuthapani B, Varghese SH, Aswathy RG, Yoshida Y, Maekawa T, Kumar DS. Evaluation of antithrombogenicity and hydrophilicity on zein-SWCNT electrospun fibrous nanocomposite scaffolds. *Int J Biomater*. 2012, 345029:1–10.

**26**. Datta, S.; Rameshbabu, A. P.; Bankoti, K.; Maity, P. P.; Das, D.; Pal, S.; Roy, S.;  Sen, R.; Dhara, S., Oleoyl-Chitosan-Based Nanofiber Mats Impregnated with Amniotic Membrane Derived Stem Cells for Accelerated Full -Thickness Excisional Wound Healing. *ACS Biomaterials Science & Engineering*. 2017**,** 3 (8), 1738-1749.

**27**. Huang N, Yang P, Leng YX, et al. Hemocompatibility of titanium oxide films. *Biomaterials*. 2003, 24: 2177–2187.

**28.** Manikandan A, Mani MP, Jaganathan SK, Rajasekar R, Jagannath M. Formation of functional nanofibrous electrospun polyurethane and murivenna oil with improved haemocompatibility for wound healing. *Polym Test*. 2017, 61: 106–113.

# CHAPTER VII

## Summary and Conclusions

*This is not the end, it is not even the beginning of the end,  But it is the end of the beginning.*

*Winston Churchill*

The thesis comprises of two parts namely polymeric gels and electrospun fibers for applications in the biomedical area. The objective of the thesis was to develop and synthesize newer microgels for drug delivery applications and also to design and fabricate electrospun fibers from the least explored polysaccharides for human health care applications. Polysaccharides are non-toxic, stable, biodegradable and biocompatible in nature. These polysaccharides can be easily modified by various chemical routes due to their reactive functional groups present on their backbone and therefore they find applications in food, cosmetic, pharmaceutical and biomedical industry. The polysaccharides selected in this work, were the non-ionic cellulose ethers namely Ethyl hydroxy ethyl cellulose (EHEC), and hydrophobically modified Ethyl hydroxy ethyl cellulose (HM-EHEC) and Gelatin for the study.

In the first introduction chapter, the broad area of biomaterials, its classification and their use in human health care are discussed. The polymeric gels, properties, their source are further discussed. More emphasize was given on microgels, their importance, synthesis routes and applications are discussed. Then the electrospun fibers, their fabrication techniques with electrospinning, along with their applications in biomedical field are discussed. Apart from some standard characterization techniques like SEM, TEM, FTIR, XRD, EDX, and UV used in the thesis, some special characterization techniques like AFM and micro-computed tomography are discussed.

In second chapter, the scope and objectives of the thesis are discussed.

In third chapter, reports on the synthesis of microgels using hydrophobically modified ethyl hydroxy ethyl cellulose (HM-EHEC) by emulsion polymerization technique using Divinyl sulphone (DVS) as crosslinking agent. The synthesized microgels were characterised using SEM which revealed spherical flower like morphology of the microgels in the size range of 5 to 8µm. The FTIR analysis confirmed the presence of the anti-cancer drug into the microgel particles. The release studies of 5-Flurouracil were done in PBS for a period of 72 hours and it was observed 56% of 5-Flurouracil (5-FU) was released in slow and sustained manner upto 72 hours. The cell viability was

done using human breast cancer cell lines MDA MB -231 also confirmed the cell death with increase in the concentration of the microgel particles containing 5-FU.

In the fourth chapter, the high molecular weight, Ethyl hydroxy ethyl cellulose (EHEC) polymer was blended using Poly vinyl alcohol (PVA) for the fabrication of electrospun nanofibers. The solution properties namely viscosity, conductivity and surface tension of the polymer solutions were measured before electrospinning. The characterizations were done using SEM, AFM, FTIR and contact angles. The average fiber diameter sizes of the nanofibers were in the range of 250-325 nm. The contact angles revealed that the mats are hydrophilic in nature. The slow and sustained release of Chlorhexidene Digluconate (ChD) from the nanofiber mats were 45, 56 and 86% for 5, 10 and 15% ChD for a period of 60 hours. The cell viability (MTT assay), the cell growth and proliferation also showed that the EHEC nanofiber mats have great potential as scaffolds in tissue engineering applications.

The fifth chapter is divided into two parts. In the first part, Halloysite nanoclay, (HNT), (tubular form) was incorporated to study its effects on mechanical properties and their activity as a wound dressing material. The SEM morphology of halloysite incorporated EHEC/PVA nanofibers, showed smooth and bead free surface with an average fiber diameters in the range of 325 ±30 nm. The FTIR and XRD studies also confirmed the presence of halloysite and gentamicin, an antibacterial drug within the nanofibers. The BET isotherms revealed the pore size distribution of the nanofibers and showed typical adsorption behaviours for the IV type, with an H3 type hysteresis loop. The mechanical properties improved with an increase of HNT concentration in the nanofiber mats. With excess HNT above 3%, the tensile strength decreased and that could be due to the aggregation of halloysite nanotubes within the nanofibers. The nanofiber mats showed good thermal stability in the range of 200-250$^0$C. The swelling studies for all the mats showed equilibrium swelling in the range of 1000-1200%, which confirmed the hydrophilic nature of the mats. There was a controlled and sustained release observed from the nanofiber mats containing the HNT and gentamicin drug for a period of 18 days. The cell viability and wound migration studies

showed that the halloysite nanoclay was non-toxic in nature and the L929 fibroblast cells showed good cell adhesion o the nanofiber mats. The hemolysis study also confirmed that the nanoclay did not harm the RBCs and was compatible with blood. The antibacterial studies were done using the Kirby disk diffusion method on the gram positive, *S.aureus* and gram negative, *E.coli* bacteria's which showed zone of inhibition which confirmed the bacterial death by the nanofiber mats. Finally, the *in-vivo* wound healing was done using wistar rats and was observed that the nanofiber mat containing halloysite and gentamicin drug showed faster wound healing with deposition of collagen fibers and angiogenesis without any scar formation. The results demonstrated that these nanofiber mats show a potential as wound dressing material for acute and chronic wounds.

In the second part reports on the incorporation of the silver nanoparticles (AgNPs) into the EHEC/PVA nanofibers and their characterization. The fiber dia was in the range of ~345-370 nm. The Ag nanoparticles were in the range of 10 to 45 nm. The size increased with the in case of silver nanoparticles. The mechanical properties also improved with addition of silver nanoparticles and gradually decreased with increase in silver. The FT-IR, XRD, UV experiments confirmed the presence of silver into the nanofibers. The BET isotherms also were done to study the pore size distribution and specific surface area. The surface area increased with increase in nanoparticles. The antibacterial studies was done on the gram positive and gram negative bacteria and the results showed there was bacterial inhibition due to the nanoparticles. The cell viability studies showed good cell growth and proliferation but as the silver nanoparticles increased, the cell viability reduced and the death of L929 fibroblast cells were confirmed using confocal microscopy which revealed the rounded shape of the dead cells. The hemolysis study showed there was less than 2% lysis for EHEC/PVA mats containing 0.5%AgNPs but there was cell lysis (cell death) observed for 1 and 2% AgNPs containing nanofiber mats. The wound healing assay was done only for nanofiber mats containing 0.5 and 1%AgNPs. In both the cases the wound healing was 98 to 99 % at the end of 21 days. The collagen deposition was observed on the epidermal layer with no scar formation and with angiogenesis. Both HNT and AgNPs incorporated

EHEC/PVA nanofiber mats showed great potential as wound dressing materials.

The sixth chapter reports on the design and fabrication of a cost effective filter media from natural polysaccharide for the separation of uremic toxins present in the blood. The biodegradable gelatin polysaccharide was used along with the nanofiller, halloysite to enhance the porosity and mechanical properties. The gelatine solution was prepared using tri fluro ethanol and further cross linked the electrospun fibers using glutaraldehyde vapours. The simulation studies using micro tomography were conducted and the pore size and porosity were measured. The average pore size and porosity increased with an increase in halloysite concentration. The cyto-toxicity and hemocompatibilty studies were done using L9292 fibroblast cells and no toxic effects were observed. The percent hemolysis was also very negligible and showed no toxic effect on the RBCs.

To conclude, the thesis was designed into 1) Gels-microgels 2) Electrospun fibers for their use in biomedical area. Here, three natural polysaccharides such as Ethyl hydroxy ethyl cellulose (EHEC), hydrophobically modified ethyl hydroxy ethyl cellulose (HM-EHEC) and Gelatin were utilized. The biocompatible synthetic polymer, polyvinyl alcohol (PVA) was used to blend the EHEC polymer to improve the spinnability of electrospun nanofibers. The EHEC/PVA nanofiber mats fabricated by utilizing the nanomaterials were found to be effective wound dressing materials for acute and chronic burns and also helpful for diabetic patients for faster healing of the wounds. These unexplored polysaccharides have a great potential as future biomaterials in human health care applications.

## I.     List of Publications

- **Ashwini Wali,** Mahadeo Gorain, Satish Inamdar,Gopal Kundu, Manohar V. Badiger, *In-vivo wound healing performance of Halloysite clay and Gentamicin incorporated Cellulose ether-PVA electro-spun nanofiber mats". **ACS Applied Biomaterials,** 2019,* DOI: 10.1021/acsabm.9b00589

- **Ashwini Wali**, Yucheng Zhang, Poulomi Sengupta, Yuji Higaki, Atsushi Takahara, Manohar V. Badiger*,"Electrospinning of non-ionic cellulose ethers/polyvinyl alcohol nanofibers: Characterization and applications", **Carbohydrate Polymers** 181, **2018,** 175–182.* DOI: org/10.1016/j.carbpol.2017.10.070

## II.     List of Publications under Preparation

- **Ashwini Wali**, Mahadeo Gorain, Satish Inamdar, Gopal Kundu, Manohar V. Badiger, *"Fabrication of cellulose ether nanofiber membranes with silver nanoparticles",* (***Acta Biomaterlia, Elsevier***)

- **Ashwini Wali,** Arun Torris A T, Manohar V. Badiger, *"Gelatin based filter media for Bio-separation of uremic toxins",* (***Material Science and Engineering C, Elsevier)***

- **Ashwini Wali**, Satish R. Inamdar, Manohar V. Badiger, *"HM-EHEC microgels for topical delivery of 5-Flurouracil",* (***International Journal of Biological Macromolecules, Elsevier***)

## III.    List of Conference Proceedings

1. **Ashwini Wali**, Mahadeo Gorain, Satish Inamdar, Gopal Kundu, Manohar V. Badiger, *"Electro-spinning of Cellulose Ether based nanofiber mats for wound healing Applications",* International Carbohydrate Conference on Emerging Trends in Carbohydrate Chemistry and Glycobiology, (CARBOXXXIV), 5-7th December

2019, University of Lucknow, **INDIA.**

2. **Ashwini Wali**, Mahadeo Gorain, Satish Inamdar, Gopal Kundu, Manohar V. Badiger, *"Fabrication and characterization of electrospun cellulose ether-PVA nanofiber mat loaded with halloysite nanotubes and antibiotics for enhanced wound healing applications",* International Conference on Advances in Polymeric materials and Health care, (APA), 16-18th October 2019, Goa, **INDIA.**

3. **Ashwini Wali**, Satish Inamdar, Manohar V. Badiger, *"Silver Nanoparticles (AgNPs) in Cellulose Ether Nanofibers: An effective wound dressing material".* 15th International Conference on Polymer Science and Technology, (SPSI MACRO), 19-22nd December 2018, IISER Pune, **INDIA.**

4. **Ashwini Wali,** Satish Inamdar, Manohar V. Badiger, *"Electrospinning of Non-Ionic Cellulose ether Nanofibers with Silver nanoparticles having antibacterial Activity",* 4th International Conference on Biomedical Polymers and Polymeric Biomaterials, (ISBPPB), 15 -18th July **2018**, Krakow, **POLAND**.

5. **Ashwini Wali**, Yucheng Zhang, Yugi Higaki, Atsushi Takahara, Manohar V. Badiger, *"Electro-spinning of Non-ionic Cellulose Ethers for Biomedical Applications",* International Conference on Advances in Polymer Science and Technology, (APA), 23-25th December **2017**, New- Delhi,**INDIA**.

6. **Ashwini Wali**, Yucheng Zhang, Yugi Higaki, Atsushi Takahara, Manohar V. Badiger *"Electro-spinning of Non-ionic Cellulose Ethers and Characterization by Atomic Force Microscopy, Scanning Electron Microscopy and Contact Angle Measurements",* 14th International Conference on Polymer Science and Technology, (SPSI MACRO), 8-11th January **2017**, Kerala, **INDIA.**

7. **Ashwini Wali**, Manohar V. Badiger *"Synthesis and Characterization of Modified and Unmodified EHEC Microgels",* International Conference on Polymeric Biomaterials, Bio-engineering and Bio-diagnostics, (APA), 27-30th October **2014**, New Delhi, **INDIA.**

# ASHWINI WALI

Senior Research Fellow
 Lab No 936, Dr. M.V. Badiger's Research Group
Polymer Science and Engineering Division
CSIR- National Chemical Laboratory,
Dr. Homi Bhabha Road, Pune, INDIA
ashwiniwali@gmail.com ; ac.wali@ncl.res.in,
+91 9767985821(M)Group Web:
http://academic.ncl.res.in/mv.badiger/group-members

## Professional Summary

- Strong academic background with over **6 years** of teaching and **8 years** of research experience on polysaccharides, polymeric gels and electrospun nanofibers for drug delivery and tissue engineering applications.

- Hands on experience on Electrospinning Techniques.

- Extensive experience on nanofiber membrane modification techniques and their characterization using SEM, TEM, TGA, DSC, FT-IR, XRD, DLS and pore-size analysis.

- Author of peer-reviewed manuscripts, various internal technical documents.

- Experienced with timely documentation of research, and compilation of progress reports.

- Gained modest knowledge in design of experiments and setting-up equipment's for research labs.

- Strong verbal and written communication skills. Effective working in interdisciplinary groups and individual settings.

## Education

- **PhD:** Chemical Engineering, Pune University, India.
  Dissertation: "**Gels and Electro spun fibers for Bio-medical Applications**"
  **2017-2020**
- **M.Tech:** Chemical Engineering, National Institute of Technology, Surathkal, Karnataka, India**.**  **2005-2007**

- **B.E:** Chemical Engineering, Visvesvaraya Technological University, Karnataka, India.  **1999-2003**

## Research Experience

- **Senior Research Fellow:**  CSIR- National Chemical Laboratory, Pune, India.  **2013 – 2017**
- **Research Fellow:** Center for Excellence in Polymer Science, Karnataka University, Dharwad, India.  **2004-2005**

# ASHWINI WALI

## Teaching Experience

- **Assistant Professor:** K.L.E College of Engineering and Technology, Belgaum, Karnataka, India.                                                              **2007-2010**

- **Assistant Professor:** B.M.S College of Engineering, Bangalore, Karnataka, India.                                                                  **2010-2013**

**Subjects Handled:** Industrial Waste Water Treatment, Environmental Science, Pollution Prevention and Control, Solid Waste Management, Biochemical Engineering, Transport Phenomena, Process Equipment Drawing, Energy Technology, Chemical Technology, Food Technology, Instrumental Methods of Analysis, Chemical Plant Utility and Safety, Process Equipment Design.

**Laboratory Courses Handled:** Heat Transfer, Instrumental Methods of Analysis.

**Number of Projects Handled (UG):** 06

**Other Duties:** Counseling and Mentoring of Undergraduate students. Classes taken for MBA students on Presentation and Communication skills.

## List of Publications

- **Ashwini Wali,** Mahadeo Gorain, Satish Inamdar, Gopal Kundu, Manohar V. Badiger, In-vivo wound healing performance of Halloysite clay and Gentamicin incorporated Cellulose ether-PVA electro-spun nanofiber mats". **ACS Applied Biomaterials, 2019,** 2, 10, 4324-4334.  DOI: 10.1021/acsabm.9b00589

- **Ashwini Wali**, Yucheng Zhang, Poulomi Sengupta, Yuji Higaki, Atsushi Takahara, Manohar V. Badiger, "Electrospinning of non-ionic cellulose ethers/polyvinyl alcohol nanofibers: Characterization and applications", **Carbohydrate Polymers** 181, **2018,** 175–182.  DOI: org/10.1016/j.carbpol.2017.10.070

- **Ashwini Wali**, M.B.Saidutta, "Defluoridation of fresh water using the process of Electro-coagulation combined with Adsorption", **International Journal of Earth Science and Engineering,** Vol 6, Issue 4, 122-131 , **2013**. ISSN 0974-5904.

- Venkatesh Mutalik, Lata S. Manjeshwar, **Ashwini Wali**, Malladi Sairam, Bojja Sreedhar, K. V. S. N. Raju, Tejraj M. Aminabhavi, "Aqueous-Solution and Solid-Film properties of Poly(vinyl alcohol), Poly(vinyl pyrrolidone), Gelatin, Starch, and Carboxy methyl cellulose Polymers", **Journal of Applied Polymer Science**, Vol. 106, 765–774, **2007**. DOI 10.1002/app.25427

- Venkatesh Mutalik , Lata S. Manjeshwar , **Ashwini Wali** , Malladi Sairam ,K.V.S.N. Raju , Tejraj M. Aminabhavi, "Thermodyanamics, Hydrodynamics of aqueous polymer solutions and mechanical characterization of solid films of chitosan, sodium alginate, guar gum, hydroxyl ethyl cellulose and hydroxypropyl methyl cellulose at different temperatures", **Carbohydrate Polymers**, Vol 65, Issue 1, 9-21, **2006**. DOI:10.1016/j.carbpol.2005.11.018

- B. Vijaya Kumar Naidu, S. D. Bhat, M. Sairam, **A. C. Wali**, D. P. Sawant, S. B. Halligudi,N. N. Mallikarjuna, T. M. Aminabhavi, " Comparison of the Pervaporation separation of water Acetonitrile mixture with zeolite filled sodium alginate and poly aniline semi-interpenetrating polymer network membranes**", Journal of Applied Polymer Science**, Vol. 96, 1968–1978, **2005**. DOI 10.1002/app.21653

- **A.C. Wali**, B. Vijaya Kumar Naidu, N. N. Mallikarjuna, S. R. Sainkar, S. B. Halligudi,T. M. Aminabhavi,"Miscibility of chitosan, hydroxyethyl cellulose blends in a aqueous acid solutions at 35 $^0$C**", Journal of Applied Polymer Science**, Vol. 96, 1996–1998, **2005**. DOI 10.1002/app.21421

## In preparation - Publications

- **Ashwini Wali**, Manohar V. Badiger,"Hydrophobically modified HM-EHEC Microgels for release of anti-cancer drug 5-Flurouracil",(***International Journal of Biological Macromolecules, Elsevier***)

- **Ashwini Wali**, Mahadeo Gorain, Satish Inamdar, Gopal Kundu, Manohar V. Badiger, "Fabrication of cellulose ether nanofiber membranes with silver nanoparticles" (***Acta Biomaterlia, Elsevier***)

- **Ashwini Wali,** Arun Torris A T, Manohar V. Badiger, "Gelatin based filter media for Bio-separation of uremic toxins" (***Material Science and Engineering C, Elsevier***)

## Selected Presentations

- "Electro-spinning of Cellulose Ether based nanofiber mats for wound healing Applications".(CARBOXXXIV) International Carbohydrate Conference on Emerging Trends in Carbohydrate Chemistry and Glycobiology, 5-7th December 2019, University of Lucknow, **INDIA. (ORAL AND POSTER)**

- "Fabrication and characterization of electrospun cellulose ether-PVA nanofiber mat loaded with halloysite nanotubes and antibiotics for enhanced wound healing applications". International Conference on Advances in Polymeric materials and Health care, 16-18th October 2019, Goa, **INDIA**. (**ORAL**)

- "Silver Nanoparticles (AgNPs) in Cellulose Ether Nanofibers: An effective wound dressing material". 15th International Conference on Polymer Science and Technology, SPSI MACRO, 19-22nd December 2018, IISER Pune, **INDIA.** (**POSTER**)

- "Electrospinning of Non-Ionic Cellulose ether Nanofibers with Silver nanoparticles having antibacterial Activity", 4th International Conference on Biomedical Polymers and Polymeric Biomaterials, ISBPPB, 15 -18th July **2018**, Krakow, **POLAND**. (**ORAL**)

- "Electro-spinning of Non-ionic Cellulose Ethers for Biomedical Applications", International Conference on Advances in Polymer Science and Technology, APA, 23-25th December **2017**, New- Delhi,**INDIA**. (**POSTER**)

- "Electro-spinning of Non-ionic Cellulose Ethers and Characterization by Atomic Force Microscopy, Scanning Electron Microscopy and Contact Angle Measurements". 14th International Conference on Polymer Science and Technology, SPSI MACRO, 8-11th January **2017**, Kerala, **INDIA**. (**POSTER**)

- "Synthesis and Characterization of Modified and Unmodified EHEC Microgels". International Conference on Polymeric Biomaterials, Bio-engineering and Bio-diagnostics, 27-30th October **2014**, New Delhi, **INDIA**. (**POSTER**)

- "Defluoridation of fresh water using the process of Electro-coagulation combined with Adsorption".3rd International Engineering Symposium, 4-6th March **2013**, Kumamoto University, **JAPAN**. (**ORAL**)

## Selected Workshops/Seminars

- Attended one week exclusive "Induction Training for Fresh Teachers in Technical Institutions" held at NITK, Surathkal, June 9-15th 2008.
- Workshop "Women in Science Administration Management" at IISER Pune, February 15-17th 2017.
- Preparatory course for Patent Agent Examination: (Patent Act, Procedure and Drafting) at IPFACE Venture center, Pune, February 17 to March 1st 2014.
- Training program on "Safety & Health Issues in Industrial Environment" at BMS College of Engineering, Bangalore, April 17- 22nd 2013.
- Faculty development program on "Advances in Chemical Engineering" Maharashtra Academy of Engineering, Pune, December 3-5th 2012.
- Staff Development Programme on "Research Scenario in Nanotechnology", at NIT Surat, January 18– 22nd 2010.
- Workshop on "Emerging Trends in Environmental Biotechnology", Dept. of Chemical Engineering, NITK Surathkal, January 12-14th 2009.

## Leadership Skills

- Mentored undergraduate, graduate students and research trainees, assistants.

- Organized technical events, guest lectures, and industrial visits for undergraduate students.

- Organized Staff day for the college staff and faculty in 2010 at KLE Engineering College and at BMS Engineering College in 2012.

- Compeered various technical and non-technical events/programmes in different languages in colleges.

## Awards and Affiliations

- Best Poster Award at CARBOXXXIV, International Conference on Carbohydrate Chemistry and Glycobiology, University of Lucknow, India, **2019.**

- Travel grant from DST- SERB (Govt of India) to attend International conference at AGH University of science and technology, Krakow, Poland, **2018.**

- Best Safety video award at NCL Pune, **2017.**

- Sports women of the year at Research Scholars Meet at NCL Pune, **2016.**

- CSIR-Senior Research Fellowship by MHRDG (Govt of India) **2013.**

- Indian Institute of Chemical Engineers (Life Member), Membership No: 46904.

- Member of American Chemical Society, (Regular Member), Membership No: 31425334.

- Member of Society of Polymer Science, Pune chapter, (Life Member) Membership No: 588.

- Member of Organization for Women in Science for the Developing World.

## References

**1) Dr Satish R. Inamdar (Guide)**
Professor, Department of Chemical Engineering
Vishwakarma Institute of Technology, Pune, India.
E-mail: satish.inamdar@vit.edu

**2) Dr Manohar V. Badiger (Co-Guide)**
Chief Scientist, Polymer Science and Engineering Division
CSIR-National Chemical Laboratory, Pune, India.
E-mail: mv.badiger@ncl.res.in

**3) Dr Gopal C. Kundu (Collaborator)**
Chief Scientist and Ex-Director
Laboratory of Tumor Biology, Angiogenesis and Nanomedicine Research
National Centre for Cell Science, Pune, India.
E-mail: kundu@nccs.res.in